

University of Alberta

A comprehensive assessment of peroxisome biology: ER-dependent peroxisome proliferation control, evolution of organelle inheritance in yeast and a *Drosophila* model system of Zellweger syndrome.

by

Fred David Mast

A thesis submitted to the Faculty of Graduate Studies and Research in partial fulfillment of the requirements for the degree of

Doctor of Philosophy

Department of Cell Biology

©Fred David Mast

Fall 2013

Edmonton, Alberta

Permission is hereby granted to the University of Alberta Libraries to reproduce single copies of this thesis and to lend or sell such copies for private, scholarly or scientific research purposes only. Where the thesis is converted to, or otherwise made available in digital form, the University of Alberta will advise potential users of the thesis of these terms.

The author reserves all other publication and other rights in association with the copyright in the thesis and, except as herein before provided, neither the thesis nor any substantial portion thereof may be printed or otherwise reproduced in any material form whatsoever without the author's prior written permission.

Dedication

For Eric and Evan.

Abstract

The modern eukaryotic cell is a meshwork of encapsulating membranes that compartmentalize many distinct biochemical processes. It is complex. This complexity facilitates the many unique and diverse processes that aid the eukaryote in its growth, division and adaptation to its environment. A comprehensive understanding of this complexity is benefited by the integration of knowledge from cell biological and molecular mechanisms, from the evolution of the factors involved in these processes and from studying how these mechanisms in cells are integrated into tissues and organisms. This thesis attempts to achieve this for a particular organelle, the peroxisome.

We studied the mechanisms of peroxisome biogenesis and proliferation in the yeast *Saccharomyces cerevisiae*. We found that peroxisome proliferation takes cues from the growth cycle of the cell and that the endoplasmic reticulum is involved in regulating this process. Searching deeper, we discovered the presence of a reticulon-peroxin complex composed of Pex30p, Pex29p, Rtn1p and Yop1p that regulates peroxisome proliferation from the endoplasmic reticulum. We identified homologs of one of the complex members, Pex30p, in metazoans and implicate the involvement of the *Drosophila* homolog of Pex30p, *DmelPex23*, in regulating peroxisome proliferation. We next addressed the evolutionary question of how adaptability is generated in a system composed of interacting cellular machineries, each with a separate and functionally critical job to perform. Using the machinery for organelle inheritance mechanisms present in budding yeasts as a model system we propose an evolutionary model whereby the emergence of myosin V-based organelle inheritance results from mechanisms of paralogy, mutation, and the appearance of pliable evolutionarily novel adaptor proteins. We also demonstrate the relevance of *Drosophila* as a genetic model for early developmental defects associated with human peroxisome biogenesis disorders. Mutation of the *PEX1* gene is the most common cause of peroxisome biogenesis disorders and is one of the causes of the most severe form of the disorders, Zellweger syndrome.

Inherited mutations in *Drosophila Pex1* correlate with reproducible defects during early development. A microarray analysis defined several clusters of genes whose expression varied significantly between wild-type and mutant larvae, implicating peroxisomal function in neuronal development, innate immunity, lipid and protein metabolism, gamete formation, and meiosis.

Acknowledgements

First and foremost, I owe a debt of gratitude to my supervisor, Professor Richard A. Rachubinski. It has been a pleasure to be a member of your laboratory and to share in the exciting research of peroxisome biology. You exemplify, both professionally and personally, the qualities of a gentleman and scientist that I admire and wish to emulate in my own life. Thank-you for the many opportunities you afforded me to enrich my research training and thank-you for continuing to uphold a high standard of excellence that has been worthy of pursuit and something I will continue to strive for.

I am also grateful for the friendship of Andrei Fagarasanu and Ryan Perry; who as coworkers taught me many of the finer aspects of our trade, who as scientists expanded my understanding and challenged my preconceptions, and who as friends enlivened and enriched my experience as a graduate student.

During my time in the Rachubinski laboratory it has been the scientific home to a culturally diverse and unique group of people, many of whom I have had the pleasure of collaborating with or, just simply, have come to know as friends. This list includes: Hiren Banerjee, Jinlin (Jenny) Chang, Melissa Dobson, Monica Fagarasanu, Mary Klute, David Lancaster, Sandrine Lepine, Nina Novak, Mafer (Maria) Padilla, Dorian Rachubinski, Yuen Yi (Chris) Tam, Robert Tower, and Maninder Virk. I owe a special shout-out to the team of technicians in the Rachubinski laboratory: Hanna Kroliczak, Rick Poirier, Elena Savidov and Dwayne Weber. Thank-you for your contributions to making the day-to-day operation of the lab a smooth one. I would like to particularly acknowledge Rick Poirier, who was my coconspirator in efforts to take the imaging capabilities of our lab towards the cutting edge of the field.

Joel Dacks, thank-you for lighting the intellectual spark that opened up my universe to the exciting field of evolutionary cell biology. It has been a helluva good time collaborating with you and I admire and respect how you have setup your laboratory and made it a congregating place for

exploring exciting ideas, whether they are of a scientific nature or not. To the many members of the Dacks lab, particularly Lael Barlow, Emily Herman, Mary Klute, and Alex Schlacht, thank-you for welcoming a “squatter” like me and for help and discussion on comparative genomic and phylogenetic questions I had.

I would also like to thank my supervisory committee members, Charles F.B. Holmes and Richard Lehner for their enthusiastic support of my graduate program. In addition, I would like to thank Thomas Simmen, I. Robert Nabi, Joel Dacks for serving on my defense committee.

I would like to acknowledge the strong financial support I have received over the course of graduate studies from the Department of Cell Biology, Faculty of Medicine and Dentistry, Alberta Innovates Health Solutions, the Canadian Institutes of Health Research and the Government of Canada.

The Department of Cell Biology has been a great place and over the past decade, first as an undergraduate and then as a graduate student, I have come to really enjoy working with the many faculty, office staff, and fellow students here. In particular, I would like to thank Gary Eitzen for being a congenial repository of all things biochemistry related. Also, thank-you to Paul Melancon for hosting many internationally acclaimed scientists and inviting students to meet with them over dinner. Those dinners were one of the highlights of my graduate student career. Sarah Hughes and Andrew Simmonds, thank-you for being the best students in the microscopy course and taking home the “Chocolate Salmon” award. I also very much enjoyed our collaboration on the *Drosophila* PBD project and appreciated the exposure to a multicellular model system that offered almost the same degree of freedom as experimentation with yeast affords.

Over the years, many members of the Wozniak laboratory have been hospitable neighbors and have shared a passion for discussing science and drinking beer. Thank-you in particular to David van de Vosse, Lucas Cairo, Chris Neufeld, Chris Ptak and Neil Adames.

My success as a microscopist can be traced to the training and mentorship I received from Jim Pawley, Glen MacDonald and Mark Cannell. It was a pleasure working with you at the Live Cell Microscopy course, first as a student, and then as a group leader for two years.

Finally, I would like to acknowledge the love and support of my wife, Christina, and our two boys, Eric and Evan. It's been a long journey getting to this point, but we now have a whole new world to explore together. I'm looking forward to exploring it with you.

Technical Acknowledgements

My deepest thanks are extended to my co-authors on the publications included in my thesis. In particular, I wish to acknowledge the contributions of Lael Barlow and Joel Dacks to the thoughts and ideas dealing with eukaryotic evolution in Chapter 1. Lael also contributed to the making of Figures 1-6 and 1-7. Joel also contributed to the research presented in Chapter 5 and performed an initial phylogenetic analysis of the Pex3 family that served as a blueprint for the more extensive analysis presented in Figures 5-2 and 5-3. Arvind Jamakhandi, Ramsey Saleem, and David Dilworth in the laboratory of John Aitchison at the Institute for Systems Biology and Seattle Biomedical Research Institute performed the immunoprecipitation experiments described in Chapter 3 and Arvind also performed the de novo biogenesis experiment reported in Figure 3-15. Elena Savidov raised the antibodies against Pex29p and Pex30p. For the characterization of a *Drosophila* model for the Zellweger spectrum of peroxisome biogenesis disorders presented in Chapter 6, I would like to acknowledge the contributions of Maninder Virk, Jing Li, Sarah Hughes and Andrew Simmonds for assistance with the RNAi experiments and characterization of the *pex1* mutant fly embryos and larvae and the contribution of Anna Hutton who performed the microarray experiment.

Table of Contents

I	Introduction.....	1
I.1	Overview.....	2
I.2	The peroxisome concept	3
I.3	PEX genes are required for peroxisome biogenesis.....	7
I.4	Peroxisomal matrix protein import	7
I.5	Peroxisomal membrane protein trafficking.....	11
I.6	Peroxisome growth and division	13
I.7	De novo peroxisome biogenesis.....	21
I.8	Model of peroxisome biogenesis in yeast.....	22
I.9	Peroxisomes are all not equal	26
I.10	Origins and diversity of eukaryotes.....	27
I.11	Mechanisms for the evolution of organelles	30
I.12	Endosymbiosis and horizontal gene transfer	30
I.13	Non-endosymbiotic (autogenous) organelles	36
I.14	Evolution of peroxisomes.....	39
I.15	The role of peroxisomes in lipid metabolism	41
I.16	Focus of this thesis	47
I.16.1	Specific Aim 1. A molecular characterization of peroxisome proliferation	47
I.16.2	Specific Aim 2. An evolutionary analysis of mechanisms that facilitate emergent complexity in eukaryotes.	47
I.16.3	Specific Aim 3. Develop a model system for studying peroxisome biogenesis disorders	48
2	Materials and methods.....	50
2.1	Materials for molecular and cellular biology	51
2.2	Microorganisms and culture conditions	60
2.2.1	Bacterial strains and culture conditions.....	60
2.2.2	Yeast strains and culture conditions.....	61
2.2.3	Mating of <i>S. cerevisiae</i>	65
2.3	DNA manipulation and analysis	66
2.3.1	Amplification of DNA by the polymerase chain reaction (PCR)	66
2.3.2	Digestion of DNA by restriction endonucleases.....	66
2.3.3	Dephosphorylation of 5'-ends	67
2.3.4	Separation of DNA fragments by agarose gel electrophoresis.....	67
2.3.5	Purification of DNA fragments from agarose gel.....	67
2.3.6	Purification of DNA from solution	67
2.3.7	Ligation of DNA fragments	68
2.3.8	DNA sequencing.....	68
2.4	Introduction of DNA into microorganisms	69
2.4.1	Chemical transformation of <i>E. coli</i>	69
2.4.2	Chemical transformation of <i>S. cerevisiae</i>	69
2.4.3	Electroporation of <i>S. cerevisiae</i>	70
2.4.4	Electroporation of <i>Y. lipolytica</i>	71
2.5	Isolation of DNA from microorganisms	72
2.5.1	Isolation of plasmid DNA from bacteria.....	72
2.5.2	Isolation of chromosomal DNA from yeast.....	72
2.6	Protein manipulation and analysis	73
2.6.1	Preparation of yeast whole cell lysates.....	73

2.6.2	Precipitation of proteins	73
2.6.3	Determination of protein concentration	74
2.6.4	Separation of proteins by electrophoresis	75
2.6.5	Detection of proteins by gel staining	75
2.6.6	Detection of proteins by immunoblotting	75
2.7	Polyclonal antibody production	76
2.7.1	Production of antisera directed against <i>S. cerevisiae</i> Pex30p and Pex29p	78
2.8	Affinity purification of polyclonal antibodies	78
2.9	Subcellular fractionation of <i>S. cerevisiae</i> cells	79
2.9.1	ER-mobility shift assay	80
2.10	Immunoprecipitation of protein complexes and identification by mass spectrometry	81
2.10.1	Isotopic determination of differentiation of interactions as random or targeted	83
2.11	In vitro vesicle budding assay	85
2.11.1	Preparation of permeabilized yeast cells	85
2.11.2	Preparation of a concentrated yeast cytosol	86
2.11.3	In vitro ER-budding assay	86
2.12	Microscopy	87
2.12.1	Acquisition of a point spread function (PSF)	87
2.12.2	Confocal microscopy of peroxisome proliferation in yeast	88
2.12.3	3D confocal microscopy of living yeast	88
2.12.4	3D confocal microscopy of yeast strains encoding doxycycline regulated genes	89
2.12.5	3D confocal microscopy of temperature-sensitive yeast strains	90
2.12.6	2D confocal video microscopy of yeast	90
2.12.7	3D immunofluorescence widefield microscopy of yeast	90
2.12.8	3D fluorescence microscopy of <i>Drosophila</i> S2 cell culture	91
2.12.9	3D immunofluorescence microscopy of <i>Drosophila</i> embryos	91
2.13	Deconvolution and image processing	92
2.14	Quantification of colocalization	92
2.15	Quantification of peroxisome number, volume and intensity	93
2.16	<i>Drosophila</i> cell culture	93
2.17	RNAi Knockdown of DmelPex Homologs and Semi-quantitative PCR	93
2.18	Preparation of Antibodies to DmelPex I Protein and Immunoblotting	95
2.19	<i>Drosophila</i> Stocks	95
2.20	Larval Survival, Growth and Mobility Assays	95
2.21	Microarray Analysis	96
2.22	Comparative Genomic Survey	98
2.22.1	Comparative genomic survey of Pex30p homologs	100
2.22.2	Comparative genomic survey of organelle inheritance machinery	102
2.23	Alignment and Phylogenetic Analysis	103
3	A reticulon-peroxin complex regulates peroxisome biogenesis from the ER	105
3.1	Peroxisome biogenesis in <i>S. cerevisiae</i>	106
3.2	The regulation of peroxisome proliferation is independent of cell cycle regulation	114
3.3	The ER is involved in regulating peroxisome proliferation in yeast	118
3.4	Identification of peroxins involved in regulating peroxisome biogenesis and proliferation ..	121
3.5	The subcellular localization of Pex30p shares commonalities with both the ER and peroxisomes	127
3.6	Pex30p associates with peroxisomes when yeast are grown in the presence of oleic acid ..	132
3.7	Identification of a reticulon-peroxin complex	135

3.8	Pex30p and Pex29p are ER resident proteins even when cells are grown in the presence of oleic acid.....	143
3.9	In vivo redistribution of members of the reticulon-peroxin complex.....	149
3.10	Peroxisome biogenesis is altered in cells lacking <i>RTN1</i> , <i>RTN2</i> and <i>YOP1</i>	152
3.11	Egress of preperoxisomal vesicles is enhance in deletion mutants of the reticulon-peroxin complex.....	160
3.12	Discussion.....	163
3.12.1	The ER in peroxisome biogenesis.....	163
3.12.2	Regulation of peroxisome proliferation: the role of the ER.....	164
3.13	A conserved mechanism for reticulon proteins in ER-derived organelle biogenesis?	166
4	The evolution of the Pex23p/Pex30p family of peroxins.....	168
4.1	Overview.....	169
4.2	A comparative genomic analysis of the Pex23p/Pex30p family in Opisthokonts	169
4.3	<i>Drosophila</i> Pex23 is involved in peroxisome biogenesis.....	174
4.4	A phylogeny of the Pex23p family in Saccharomycotina.....	177
4.5	Pex23p localizes to the ER	177
4.6	A sensitive search algorithm identifies a putative Pex23 homolog outside of the Opisthokonta	185
5	Emergent complexity in myosin V-based organelle inheritance.....	188
5.1	Overview.....	189
5.2	A comparative genomic survey of the organelle inheritance machinery in budding yeast... ..	193
5.3	Pex3 proteins in the Saccharomycotina share common ancestry with the myosin V adaptor Pex3Bp	196
5.4	Evolution and conservation of class V myosins in opisthokonts.....	201
5.5	Recent emergence and lineage-specific novelty is a common feature of myosin V adaptors.	204
5.6	Discussion.....	209
6	A <i>Drosophila</i> model for the Zellweger spectrum of peroxisome biogenesis disorders	217
6.1	Overview.....	218
6.2	RNAi analysis in S2 cells confirms that the majority of the known genes required for peroxisome assembly are conserved in <i>Drosophila</i>	219
6.3	Mutation of <i>DmelPex1</i> leads to tissue-specific defects in developing embryos.....	225
6.4	Developing <i>DmelPex1</i> homozygous mutant embryos do not show obvious muscle defects	235
6.5	<i>DmelPex1</i> homozygous mutants exhibit malformed central and peripheral nervous systems	235
6.6	Loss of <i>DmelPex1</i> causes disorganization in specific subsets of CNS and PNS neurons	240
6.7	<i>DmelPex1</i> homozygous mutant embryos also show disorganized glia	243
6.8	Tissue defects correlate with genome-wide changes in gene expression in <i>DmelPex1</i> mutant embryos	243
6.9	Discussion.....	260
6.9.1	Peroxisome assembly in <i>Drosophila</i> is mechanistically similar to human peroxisome assembly	260
6.9.2	<i>DmelPex1</i> Mutants Mirror the Early Developmental Defects Associated with Human PBDs	264

7	Perspectives	267
7.1	Synopsis	268
7.2	Future directions for studies on the reticulon-peroxin complex.....	268
7.3	Future directions for studies of de novo peroxisome biogenesis.....	270
7.4	Future directions for the study of peroxisome evolution	271
7.5	Future directions for study of the widget hypothesis	272
7.6	Future directions for studying Zellweger Syndrome in <i>Drosophila</i>	272
7.7	Concluding remarks	273
8	References	275

List of Tables

Table 1-1. Peroxisomal proteins lacking overall homology in prokaryotic genomes as identified by Schluter and colleagues (2006).....	41
Table 2-1. Chemicals and reagents.....	51
Table 2-2. Enzymes.....	53
Table 2-3. Molecular size standards.....	53
Table 2-4. Multicomponent systems for molecular biology	54
Table 2-5. Plasmids	54
Table 2-6. Primary antibodies	55
Table 2-7. Secondary antibodies.....	56
Table 2-8. Oligonucleotides	56
Table 2-9. Common solutions	60
Table 2-10. Bacterial culture media	61
Table 2-11. <i>S. cerevisiae</i> and <i>Y. lipolytica</i> strains.....	61
Table 2-12. Yeast culture media	65
Table 2-14. Primers for RT-PCR confirmation of RNAi knockdown of <i>DmelPex</i> genes	94
Table 2-15. Organisms whose genomes were surveyed in this study.	98
Table 2-16. Organisms in the Saccharomycotina whose genomes were surveyed for Pex30 family orthologs.....	101
Table 3-1. Proteins identified by mass spectrometry of Pex30p-pA, Pex29p-pA, Rtn1p-pA and Yop1p-pA immunisolations	141
Table 6-1. Genes upregulated more than 3-fold in <i>DmelPex I</i> homozygous mutant larvae	250
Table 6-2. Genes downregulated more than 3-fold in <i>DmelPex I</i> homozygous mutant larvae	258

List of Figures and Illustrations

Figure 1-1 The peroxisome concept	5
Figure 1-2 Schematic of the planar lipid bilayer used to demonstrate the induction of an expandable and transient peroxisomal translocon channel by cargo-laden Pex5p.....	10
Figure 1-3 Five hypothetical ways to achieve peroxisomal membrane protein insertion	15
Figure 1-4 A model comparing asymmetrical versus symmetrical division of peroxisomes	19
Figure 1-5 The growth and division cycle of peroxisomes	25
Figure 1-6 Retracing the evolutionary emergence of modern eukaryotes	29
Figure 1-7 Mechanisms of cellular evolution.....	33
Figure 1-8 Peroxisomes rely on the endoplasmic reticulum and mitochondria, and vice versa, to properly carry out their role in the metabolism of lipids in cells	43
Figure 3-1 Peroxisome biogenesis in <i>Saccharomyces cerevisiae</i>	109
Figure 3-2 Peroxisome morphology in cells in the presence of oleate and glucose.....	112
Figure 3-3 The number of Pex3p-GFP puncta per cell is growth state dependent.....	117
Figure 3-4 Pex3p-GFP labeled peroxisomes proliferate in cells repressed for <i>SEC61</i>	120
Figure 3-5 Peroxisomes proliferate in a temperature sensitive mutant of <i>SEC61</i>	123
Figure 3-6 Screening for candidate peroxins involved in regulating peroxisome biogenesis and proliferation	126
Figure 3-7 An unbiased colocalization analysis shows Pex30p to partially colocalized with Pex3p and Sec13p.....	129
Figure 3-8 Pex30p dynamically localizes to the ER or peroxisomes depending on the carbon source utilized.	134
Figure 3-9 Pex29p and Pex30p copurify with the ER resident proteins, Rtn1p and Yop1p	137
Figure 3-10 Pex30p and Pex29p cofractionate with Sec61p in an ER-shift assay	145
Figure 3-11 Pex30p, and to a lesser extent Pex29p, associates with peroxisomes under peroxisome proliferating conditions as part of a peroxisome-associated ER membrane	148
Figure 3-12 Colocalization analysis between members of the reticulon-peroxin complex	151
Figure 3-13 The stability of the peroxin-reticulon complex is dependent on the presence of peroxisomes.	154
Figure 3-14 Triple deletion of <i>RTN1</i> , <i>RTN2</i> , and <i>YOP1</i> does not abrogate the ability of cells to grow on medium containing oleic acid as a sole carbon source.....	157
Figure 3-15 Deletion of <i>RTN1</i> , <i>RTN2</i> , and <i>YOP1</i> increases peroxisome formation and the prevalence of cells containing peroxisomes	160
Figure 3-16 Egression of preperoxisomal vesicles is enhanced in reticulon-peroxin deletion strains as shown by a cell-free in vitro budding assay.....	162
Figure 4-1 Comparative genomic survey of the Pex23p/Pex30p family in opisthokonts.....	172
Figure 4-2 <i>Drosophila</i> Pex23 (<i>DmelPex23</i>) is involved in peroxisome biogenesis.....	176
Figure 4-3 Comparative genomic survey and phylogenetic analysis of the Pex23p/Pex30p family in the Saccharomycotina	179
Figure 4-4 Subcellular localization of Pex30 paralogs in <i>S. cerevisiae</i>	182
Figure 4-5 The <i>Y. lipolytica</i> Pex23p also localizes to the ER.....	187

Figure 5-1 Comparative genomic survey of the machinery for organelle inheritance in opisthokonts	191
Figure 5-2 Phylogeny of Pex3 proteins found in opisthokonts	199
Figure 5-3 Phylogeny of Pex3 proteins found in opisthokonts	200
Figure 5-4 Phylogeny of class V myosins found in opisthokonts	203
Figure 5-5 Conservation of receptor binding sites on class V myosins	206
Figure 5-6 Evolutionary history for the emergence of the organelle inheritance machinery in ascomycete fungi	208
Figure 5-7. A model for the evolution of myosin V-based organelle inheritance	213
Figure 6-1 Peroxins and their putative homologs in <i>Drosophila</i>	221
Figure 6-2 Peroxisomes are absent or exhibit altered morphology in S2 cells treated with dsRNA to putative <i>DmelPex</i> genes	224
Figure 6-3 Detection of <i>DmelPex I</i> transcripts by RT-PCR and <i>DmelPex I</i> protein by immunoblotting	227
Figure 6-4 <i>DmelPex I^{s4868}</i> homozygous larvae exhibit defects in growth	230
Figure 6-5 <i>DmelPex I^{s4868}</i> homozygous flies have reduced lifespan	232
Figure 6-6 <i>DmelPex I^{s4868}</i> homozygous larvae are smaller in size and fail to show coordinated movement toward food	234
Figure 6-7 <i>DmelPex I^{s4868}</i> homozygous embryos exhibit an essentially wild-type musculature	237
Figure 6-8 The overall pattern of CNS and PNS development is abnormal in <i>DmelPex I^{s4868}</i> homozygous embryos	239
Figure 6-9 CNS and PNS neurons are disorganized in <i>DmelPex I^{s4868}</i> homozygous embryos	242
Figure 6-10 Glial cells are disorganized in <i>DmelPex I^{s4868}</i> homozygous embryos	245
Figure 6-11 Systems level view of changes in gene expression in <i>DmelPex I^{s4868}</i> homozygous embryo	248

List of symbols and abbreviations

ATP	adenosine triphosphate
AP	adaptin
BCFA	branched chain fatty acid
BLAST	basic local alignment search tool
CNS	central nervous system
CPT	carnitine palmitoyltransferase
C-terminal	carboxyl terminal
Da	Dalton
DmelPexI	<i>Drosophila melanogaster</i> peroxin I
DNA	deoxyribonucleic acid
dNTP	deoxyribonucleoside triphosphate
dsRNA	double-stranded ribonucleic acid
ECL	enhanced chemi-luminescence
EGT	endosymbiotic gene transfer
ER	endoplasmic reticulum
F	farad
FECA	first eukaryotic common ancestor
g	gram
g	gravitational acceleration
GFP	green fluorescent protein
GO	gene ontology
GTP	guanosine triphosphate
h	hour
HGT	horizontal gene transfer
HRP	horse radish peroxidase
HMM	hidden Markov model
IgG	immunoglobulin G
IRD	infantile refsum disease
LECA	last eukaryotic common ancestor
M	molar concentration
min	minute
mPTS	peroxisomal membrane protein targeting signal
mRFP	monomeric red fluorescent protein
mRNA	messenger ribonucleic acid
NALD	neonatal adrenoleukodystrophy
NADH	reduced form of nicotinamide adenine dinucleotide
NPC	nuclear pore complex
N-terminal	amino terminal
OD	optical density
OPH	organelle paralogy hypothesis
pA	protein A

PBD	peroxisome biogenesis disorder
PCR	polymerase chain reaction
PEX	peroxin
PI4P	phosphatidyl inositol 4 phosphate
PMP	peroxisomal membrane protein
PNS	postnuclear supernatant or peripheral nervous system
PTS	peroxisomal targeting signal
PYC	permeabilized yeast cell
RCDP	rhizomelic chondrodysplasia punctata
RNAi	ribonucleic acid interference
ROS	reactive oxygen species
RT-PCR	real time-polymerase chain reaction
SDS-PAGE	sodium dodecyl sulfate polyacrylamide gel electrophoresis
sec	second
SM	simplified media
UTR	untranslated region
V	volt
v/v	volume to volume ratio
VLCFA	very-long chain fatty acid
VNC	ventral nerve cord
w/w	weight to weight ratio
w/v	weight to volume ratio
ZS	Zellweger syndrome
Ω	ohm

I Introduction

A version of this chapter has been published:

Mast, F.D., A. Fagarasanu, B. Knoblach, and R.A. Rachubinski. 2010. Peroxisome biogenesis: something old, something new, something borrowed. *Physiology*. 25:347–356. doi:10.1152/physiol.00025.2010.

A version of this chapter has been submitted for publication:

Mast, F.D., L.D. Barlow, R.A. Rachubinski, and J.B. Dacks. 2013. Evolutionary mechanisms for establishing eukaryotic cellular complexity. *Trends Cell Biol.*

I.1 Overview

The cell is the basic building block of life. Albert Claude, a Nobel laureate and pioneer of the discipline of Cell Biology, defined the cell as an “autonomous and all-contained unit of living matter, which has acquired the [ability and the means] to reproduce; the capacity to store, transform and utilize energy, and the capacity to accomplish physical works and to manufacture practically unlimited kinds of products.” This description is apt, if a bit teleological, for conveying the excitement and challenge of discovering the mechanisms underlying cellular processes. It is amazing that despite the pace of scientific understanding, we still know so little about the basic mechanisms that enable cells to grow, survive and interact with their environment. This knowledge is imperative for understanding human health and physiology and plays a strong role in the diagnosis and treatment of human disease. It is also necessary for placing our evolutionary trajectory within the context of the rest of eukaryotes.

One set of membrane-bound, usually spherical compartments are commonly grouped together under the term, “peroxisomes”. Peroxisomes function in regulating the synthesis and availability of many diverse lipids by harnessing the power of oxidative reactions and contribute to a number of metabolic processes essential for cellular differentiation and organismal development. Although peroxisomes are a ubiquitous constituent of eukaryotic cells, they also display cell-type/organismal specific characteristics that can aid in producing this diversity. Peroxisomes are remarkably plastic in both their metabolic functions and their response to environmental stimuli, and they display properties that position them as key regulators of many biochemical pathways.

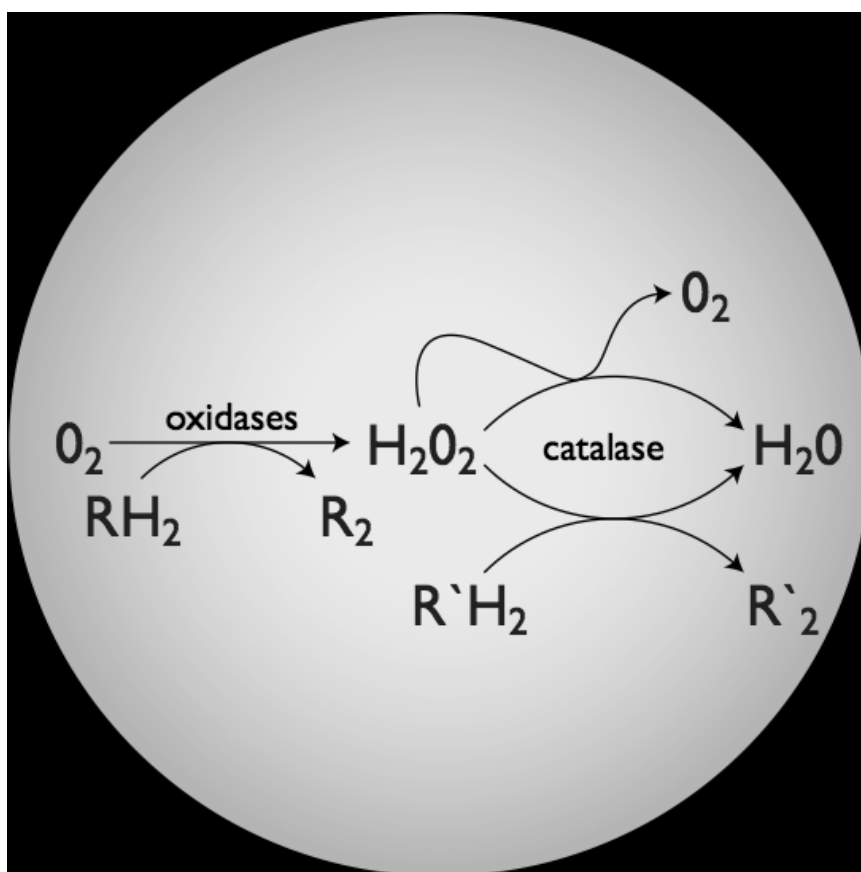
This thesis presents the results of studies on three different facets of peroxisome biology. The first is a molecular analysis of the regulation of peroxisome proliferation in the budding yeast *Saccharomyces cerevisiae*. This is followed by an assessment of the evolution of one of the protein families implicated in regulating peroxisome proliferation. Next, an exploration of the evolution of organelle inheritance in yeast helps to answer the question of how adaptability is generated in a

system composed of essential cellular machineries, each with a separate and functionally critical job to perform. Finally, an assessment is made of the utility of *Drosophila* as a model system for studying the most prominent peroxisome biogenesis disorder, Zellweger syndrome.

1.2 The peroxisome concept

Christian de Duve coined the term “peroxisome” to help explain the observed cosedimentation of a group of hydrogen peroxide-producing oxidases and catalase in equilibrium density gradient centrifugation (Baudhuin et al., 1965; de Duve and Baudhuin, 1966; de Duve et al., 1960). The functional coupling of these two enzymes creates an environment in which the oxidase-mediated production of hydrogen peroxide is harnessed by catalase to oxidize a second substrate through mediated peroxidation, resulting in the controlled decomposition of hydrogen peroxide into water and molecular oxygen (Figure 1-1). The substrate specificity of the peroxisomal oxidases is narrow (van Veldhoven et al., 1992; Wanders et al., 1993), and in humans, depending on the cell type, peroxisomes contain oxidases specific for, among others, fatty acyl-CoAs, *D*- and *L*-amino acids, spermidine and *L*-pipecolic acid (Wanders and Waterham, 2006). Substrates for catalase exhibit a much broader range and include alcohols like ethanol and methanol, certain phenols, formaldehyde, formic acid and the nitrite ion. In the absence of a suitable substrate, catalase can mediate the direct peroxidation of hydrogen peroxide using another hydrogen peroxide molecule. In this way, multiple oxidases are coupled to a single catalase. Irrespective of the substrates involved, the net oxygen consumption of oxidase/catalase-coupled reactions can be positive, negative or neutral depending on the availability of substrate for catalase and the specific oxidases coupled to it, which may be cell type-specific. Oxygen consumption by peroxisomes is high, reaching levels of 20% of the total oxygen consumed by the liver of rat (Boveris et al., 1972). Several groups have proposed that this high level of oxygen consumption by peroxisomes

Figure I-1. The peroxisome concept. Adapted from de Duve and Baudhuin (1966).



positions them to serve as both a generator and buffer of reactive oxygen species (ROS) (Angermüller et al., 2009; Schrader and Fahimi, 2006).

Curiously, oxidases and catalase do not need to colocalize for a coupled reaction to occur. For example, catalase in peroxisomes may assist in degrading hydrogen peroxide produced by NADPH oxidase, which is found at the plasma membrane and has been implicated in the generation of ROS for the respiratory burst of neutrophils (Maitra et al., 2009; Zmijewski et al., 2009). Therefore, it is the combination of an oxidase and catalase enclosed by the distinct lipid bilayer of peroxisomes that forms the basis of what de Duve labeled the “peroxisome concept” (de Duve and Baudhuin, 1966) (Figure 1-1). The peroxisomal membrane represents an essential part of this concept, forming a selectivity barrier that provides an important level of regulation for the transport of substrates and metabolites as well as the peroxisomal enzymes themselves. In addition to catalase and the oxidases, peroxisomes also contain over 50 other enzymes that enable them to metabolize both very-long chain fatty acids and branched-chain fatty acids, which in their turn makes peroxisomes an important site for the synthesis of bile acids and plasmalogens (Wiese et al., 2007) (see (Wanders and Waterham, 2006) for a thorough discussion of peroxisome biochemistry). Peroxisomes also act as cellular detoxifiers. In the liver, peroxisomes can couple the β -oxidation of fatty acids and bile acid precursors with the oxidation of ingested ethanol to acetaldehyde to account for as much as 50% of the total metabolism of ethanol when substrates for the H_2O_2 -producing oxidases are present in excess (Bradford et al., 1993; Orellana et al., 1998; Thurman and McKenna, 1975). In the kidney, peroxisomes couple the oxidation of *L*- and *D*-amino acids to the oxidation of harmful molecules filtered from the blood, such as lipid-based xenobiotics. And in glial cells, peroxisomes are thought to regulate ROS availability together with plasmalogen synthesis (Kassmann et al., 2007).

1.3 *PEX* genes are required for peroxisome biogenesis

Peroxisomes are formed and maintained through the concerted efforts of a group of proteins called peroxins that are encoded by *PEX* genes and have roles in the formation and maintenance of peroxisomes (Distel et al., 1996). The finding that the products of a distinct collection of genes function in the biogenesis of peroxisomes refines de Duve's classical definition of a peroxisome to include the essential contribution of these *PEX* genes. Our understanding of the specific roles of individual peroxins in both peroxisome biogenesis and in other aspects of cell biology is still at a rather rudimentary level, and the proposed roles of many peroxins still rely heavily on the pleiotropic phenotypes of peroxisomes and cells that result from their mutation. Peroxisome biogenesis is also stimulated by the expression of genes that encode peroxisomal enzymes and whose transcription is regulated by changes in the metabolic requirements of cells (Gurvitz and Rottensteiner, 2006; Smith et al., 2002).

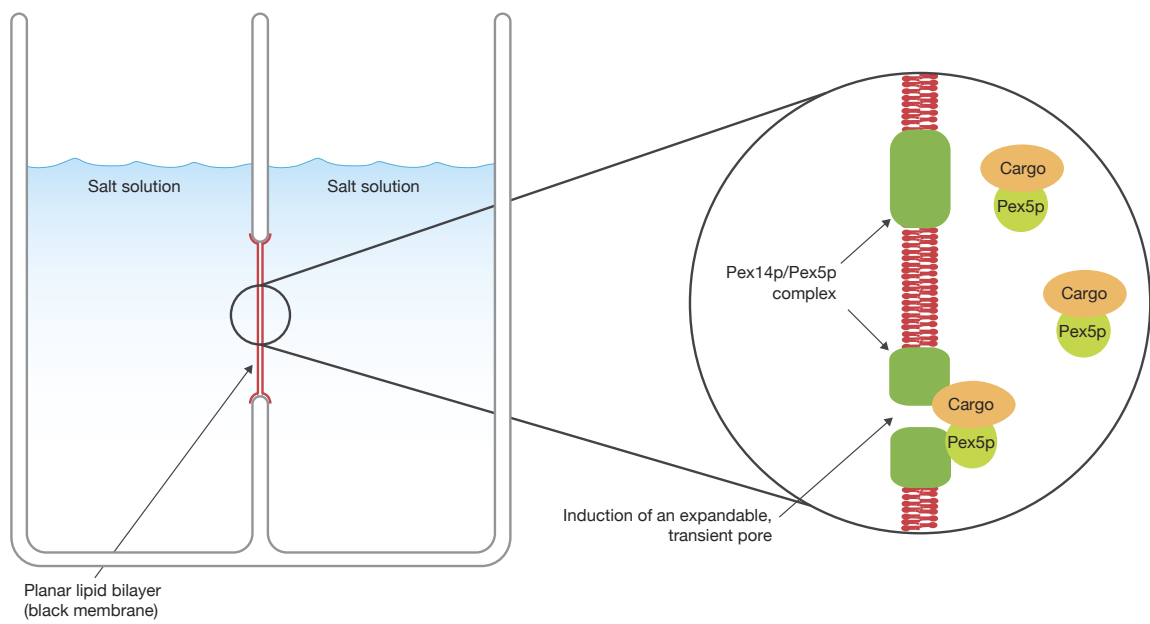
1.4 Peroxisomal matrix protein import

Two types of sequences that target proteins to the peroxisomal matrix have been described: a C-terminal serine-lysine-leucine variant known as peroxisomal targeting signal (PTS) I (Gould et al., 1987; 1989) and a N-terminal nonapeptide known as PTS2 (Swinkels et al., 1991). Each sequence is recognized in the cytosol by its own cognate receptor, Pex5p for PTSI and Pex7p for PTS2 (Marzioch et al., 1994; Platta and Erdmann, 2007; Rehling et al., 1996; Terlecky et al., 1995; Zhang and Lazarow, 1996). Receptor-cargo complexes then dock at the peroxisomal membrane and cross the lipid bilayer. This process has been termed an "extended shuttle" because the receptor translocates together with its cargo into the peroxisomal matrix (Rachubinski and Subramani, 1995). The receptors are then monoubiquitinated or polyubiquitinated and exit the peroxisome to be recycled for another round of cargo import or to be degraded by the proteasomal system, respectively (Léon et al., 2006; Ma and Subramani, 2009; Platta et al., 2005; 2007). The PTSI and

PTS2 import pathways converge at the peroxisomal membrane through docking to Pex13p and Pex14p. In yeast, PTS2 import has been shown to favor docking to Pex13p, while PTS1 cargo-laden Pex5p can bind directly to Pex14p (Grunau et al., 2009; Meinecke et al., 2010). It has been observed that peroxisomes can differ in their concentrations of Pex13p and Pex14p within an individual cell and between cell types (Karnati and Baumgart-Vogt, 2009; Nenicu et al., 2007), and therefore peroxisomes may specialize for particular metabolic functions by their different capacities for PTS1 and PTS2 import. However, the ability of peroxisomes to specialize based on differential PTS1 and PTS2 import is probably limited, as most peroxisomal matrix proteins contain PTS1s (Subramani, 1993).

The ability of a soluble protein to gain access to the peroxisomal matrix is not dependent on its having a PTS, and proteins have been shown to interact with the peroxisomal matrix protein receptors in a non-PTS-dependent fashion (van der Klei and Veenhuis, 2006). Even more striking is the ability of peroxisomes to import proteins that lack a PTS but which can piggyback on a protein containing a PTS via protein-protein interaction (Glover et al., 1994; Thoms et al., 2008; Yang et al., 2001). Indeed, peroxisomes are unique in their ability to import fully folded and even very large oligomeric protein complexes into their matrix. The capacity of the peroxisome to accommodate large oligomeric protein structures and translocate them into the matrix is due to the proposed ability of Pex14p to associate with cargo-laden Pex5p to form a highly dynamic and expandable pore called the peroxisomal importomer (Meinecke et al., 2010) (Figure 1-2). In theory, the unique properties of the peroxisomal importomer position the peroxisome as a central regulator of a cell's metabolic potential through its ability to modulate the distribution of key metabolic enzymes between the cytosol and the peroxisome. For example, in *S. cerevisiae*, Gpd1p and Pnc1p, two proteins that modulate chromatin remodeling and NADH levels in the cell, are differentially regulated in their subcellular location among the nucleus, cytosol and peroxisomes (Anderson et al., 2003; Jung et al., 2010). In mammalian cells, malonyl-CoA decarboxylase localizes to both the

Figure 1-2. Schematic of the planar lipid bilayer assay used to demonstrate the induction of an expandable and transient peroxisomal translocon channel by cargo-laden Pex5p. The peroxisomal matrix protein importomer can be reconstituted when membrane anchored Pex14p/Pex5p complex encounters soluble Pex5p bound to cargo (Meinecke et al. 2010). To account for the variety that exists in the types of cargoes destined for the peroxisome matrix, the importomer can expand up to 9 nm in diameter. These findings explain how the peroxisome can import the fully folded and even oligomeric protein complexes *en route* to its lumen.



cytosol and peroxisomes depending on metabolic need (Sacksteder et al., 1999). A key challenge in interpreting the proteomes of mammalian peroxisomes has been the apparent contamination of enriched peroxisomal fractions with proteins that have other well characterized subcellular localizations (Saleem et al., 2006). However, are these proteins actually contaminants of peroxisomes or are they true peroxisomal residents? An answer to this question is important for understanding how peroxisomes can influence cellular metabolism by regulating their protein complement through regulated protein import.

1.5 Peroxisomal membrane protein trafficking

To understand how proteins are inserted into the peroxisomal membrane, it is important to consider that all peroxisomal proteins are acquired posttranslationally by the peroxisome (Fujiki et al., 1984; 1985; 2006; Fujiki and Lazarow, 1985; Goldman and Blobel, 1978; Imanaka et al., 1996; Rachubinski et al., 1984; Sacksteder et al., 2000; van der Zand et al., 2010). However, a conundrum remains as to how peroxisomal membrane proteins (PMPs) are inserted into and anchored within the peroxisomal membrane. Membrane proteins of the secretory pathway rely on the Sec61p translocon to passage certain portions of their sequence through the endoplasmic reticulum (ER) membrane and also to imbed their hydrophobic transmembrane domains within the membrane (Rapoport, 2007). Similarly, mitochondria have translocons in their inner and outer membranes to aid in the insertion of the hydrophobic segments of proteins into these membranes (Chacinska et al., 2009). As for peroxisomes, Pex3p and Pex19p have been shown to be essential for targeting membrane proteins to peroxisomes (Hettema et al., 2000). siRNA-mediated knockdown of Pex19p impairs the import of membrane proteins into peroxisomes and decreases their half-lives (Jones et al., 2004a; Sacksteder et al., 2000). PMPs contain a poorly defined divergent hydrophobic sequence known as the membrane peroxisomal targeting sequence (mPTS) that is bound by Pex19p in the cytosol (Halbach et al., 2005; Rottensteiner et al., 2004). Pex19p

bound to a cargo PMP docks to Pex3p on the peroxisomal membrane (Fang et al., 2004) and, in a poorly understood process, facilitates the insertion and orientation of the PMP into the peroxisomal membrane (Heiland and Erdmann, 2005). Pex16 in mammalian cells has been proposed to substitute for Pex3 as the Pex19 docking site of a second class of PMPs that do not rely on Pex3 for their targeting (Matsuzaki and Fujiki, 2008). Surprisingly, the entire process of protein integration into the peroxisomal membrane does not require ATP or GTP hydrolysis (Pinto et al., 2006).

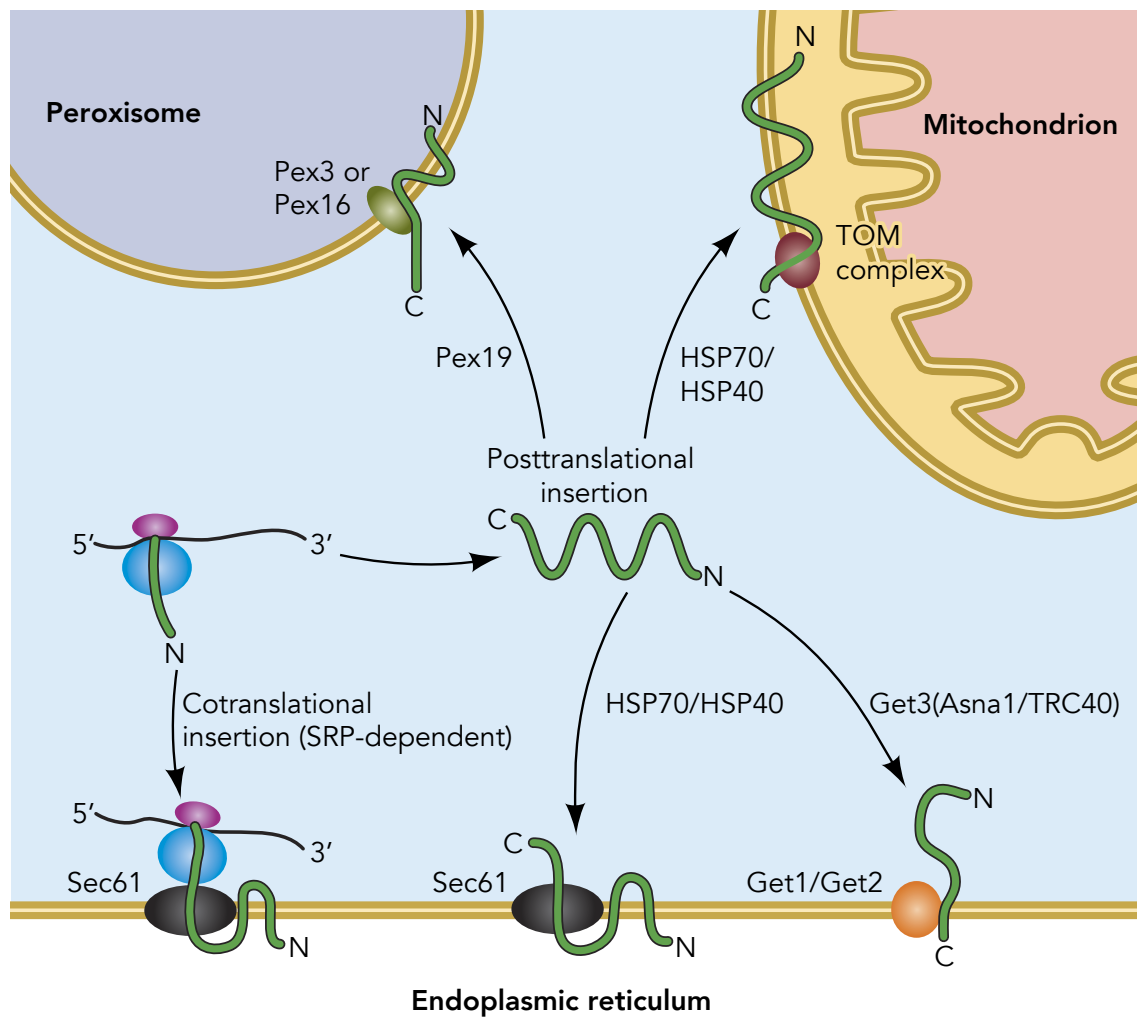
Is it possible Pex3p, Pex16p and Pex19p associate to form a translocon that would help in overcoming the energy barrier to insertion expected both for a protein that spans a membrane once and especially for a protein that spans the membrane multiple times and requires the passage of alternating hydrophobic and hydrophilic regions across a lipid bilayer? Pex19p is farnesylated at its C-terminus, which could aid in disrupting the membrane lipid bilayer and/or stabilizing the hydrophobic transmembrane domain of a nascent PMP (Götte et al., 1998). But farnesylation is dispensable for Pex19p function (Vastiau et al., 2006). Pex19p is also dispensable for peroxisomal protein import in the yeast *Yarrowia lipolytica* (Lambkin and Rachubinski, 2001). Moreover, there is no evidence that Pex3p or Pex16p can form channels in membranes either alone or in combination with each other. Alternative strategies for the incorporation of PMPs into membranes include use of the ER translocation apparatus and/or the mitochondrial outer membrane translocase, followed by a trafficking event from these membranes to the membranes of peroxisomes. There is an ever lengthening list of PMPs that have been shown to traffic through the ER (Agrawal et al., 2011; Baerends et al., 1996; Geuze et al., 2003; Halbach et al., 2009; Hoepfner et al., 2005; Kim et al., 2006; Kragt et al., 2005; Lam et al., 2010; Tam et al., 2005; Titorenko and Rachubinski, 1998; van der Zand et al., 2010; 2012; Yan et al., 2008). As previously mentioned, Pex16p is a glycosylated protein in *Y. lipolytica* (Titorenko and Rachubinski, 1998) that is cotranslationally inserted into the ER (Kim et al., 2006). The N-termini of several PMPs, including

notably Pex3p, have been demonstrated to be sufficient both for their targeting to and insertion into the ER and for their subsequent travel from the ER to peroxisomes (Thoms et al., 2012). Interestingly, the demonstration of a distinct insertion pathway for proteins with a transmembrane domain at their extreme C-termini revealed that the tail-anchored PMP, Pex15p, also relies on this system for its insertion into membranes (Schuldiner et al., 2008). What is currently unknown is whether the guided entry of tail-anchored protein (GET) system is an exclusive resident of the ER or if it is also present on the peroxisomal membrane. Using mitochondria for PMP biogenesis is a particularly attractive alternative with regards to the mitochondrial metabolite transporters that have been localized to the peroxisome membrane (Antonenkov and Hiltunen, 2006). One transporter, carnitine palmitoyltransferase (CPTI), has been shown to localize to the ER, mitochondria and peroxisomes (Fraser et al., 1999). The CPTI in mitochondrial and peroxisomal membranes but not the CPTI in ER membranes appears to have undergone an N-terminal cleavage, suggesting that mitochondria may be able to modify peroxisome function in cells by equipping peroxisomes with key metabolite transporters. The recent discovery of a vesicular mode of communication from mitochondria to peroxisomes provides a mechanism for the routing of these transporters between the two organelles (Neuspiel et al., 2008; Andrade-Navarro et al., 2009). Thus, a complex model of PMP biogenesis has emerged (Figure 1-3) that will require extensive and careful analysis to define the actual sequence of events involved in the targeting and insertion of the different and varied PMPs.

1.6 Peroxisome growth and division

Cells expand their peroxisomal population by growth and division of peroxisomes (Lazarow, 2003; Motley and Hettema, 2007). This observation played a crucial role in rejecting a contribution of other organelles to peroxisome biogenesis in early models of peroxisome biogenesis (Fujiki et al., 1985; Lazarow and Fujiki, 1985). Peroxisomes are homeostatic organelles that monitor the

Figure 1-3. Five hypothetical ways to achieve peroxisomal membrane protein insertion. The translation of all PMPs begins in the cytosol where the pathway diverges into those proteins destined for cotranslational insertion into the ER, which is mediated by the signal recognition particle (SRP) pathway, and those relying on the following posttranslational insertion pathways: HSP70/HSP40 chaperones can maintain membrane proteins in an insertion competent state and can direct proteins to either the ER translocon or the translocase of the outer mitochondrial membrane (TOM) complex, C-terminal anchored proteins rely on the guided entry of tail-anchored proteins (GET) pathway for entry into the ER. Import into both the ER and mitochondria necessitates the existence of a trafficking mechanism to bring these PMPs to peroxisomes, which is not depicted here. PMPs can also use the PMP targeting system that consists of the cytosolic chaperone Pex19 and its two docking partners Pex3 and Pex16. PMPs range in size from ~20 kDa to ~100 kDa.

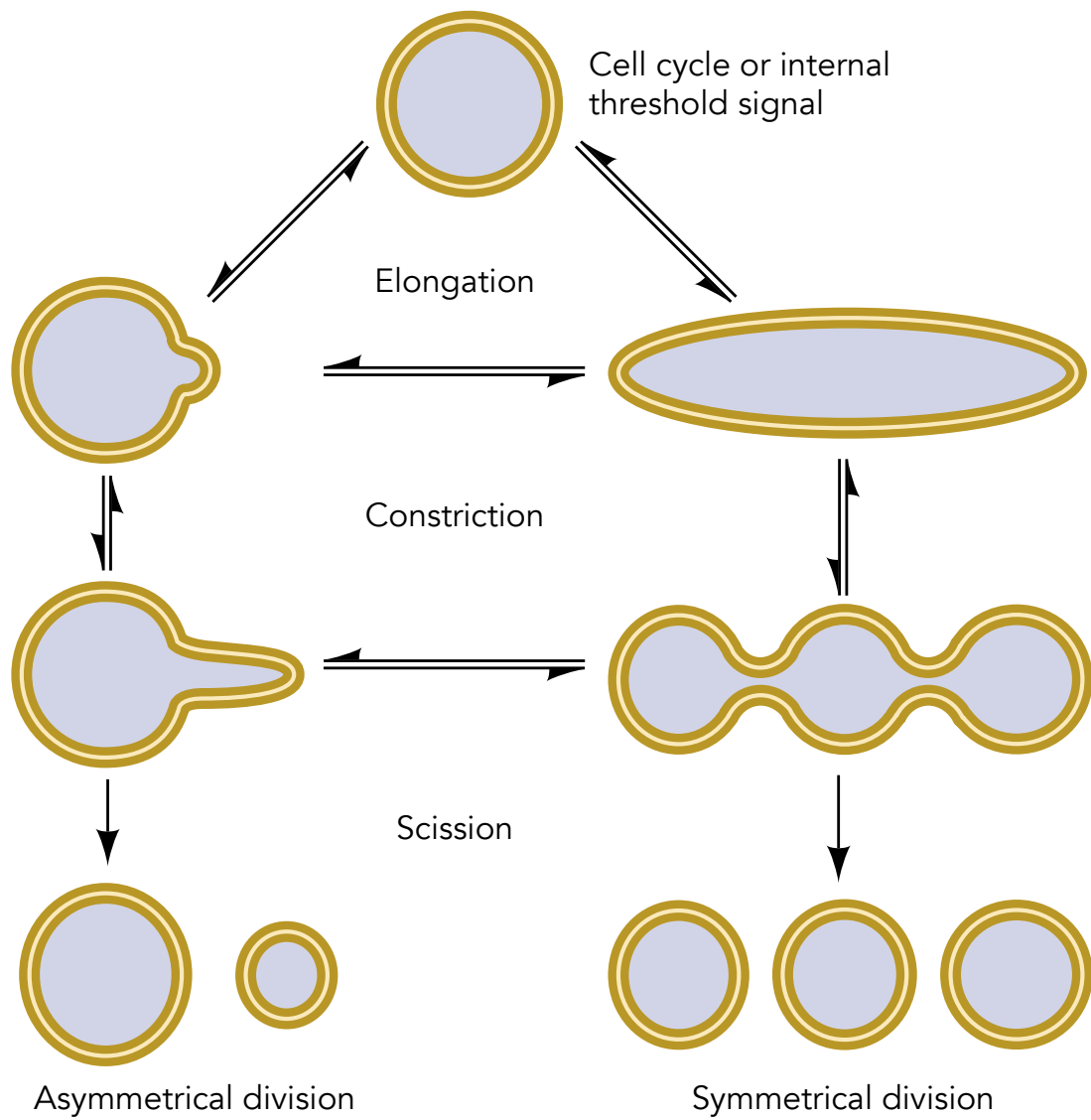


levels of their matrix proteins and divide only after a particular threshold has been reached (Guo et al., 2003). In *Y. lipolytica*, sequestration of the PMP Pex16p by the matrix enzyme fatty acyl-CoA oxidase results in a cascade of events that leads to the production of diacylglycerol, which promotes positive membrane curvature and the recruitment of peroxisome division factors (Guo et al., 2003; 2007). Threshold appears to be relative, because the diameter of individual peroxisomes ranges from 0.1 to 1 μm . Several factors involved in peroxisome division are shared with other organelles. These factors, which include dynamin-like proteins and their associated recruitment factors, may function to coordinate the division of peroxisomes with other cellular processes (Schrader, 2006). In *S. cerevisiae*, the dynamin-related proteins Dnm1p and Vps1p were shown to differentially regulate peroxisome division because their recruitment to peroxisomes is mediated by nonoverlapping factors (Guo et al., 2007; Motley and Hettema, 2007; Motley et al., 2008; Vizeacoumar et al., 2006). In the case of Dnm1p, its recruitment factors, i.e. Fis1p, Mdv1p and Caf4p, are shared between peroxisomes and mitochondria (Motley et al., 2008). Cells of a patient deficient in the dynamin-like protein, Dlp1, the human homolog of Dnm1p, also exhibited defects in both mitochondrial and peroxisomal division (Waterham et al., 2007). Fis1 appears to recruit Dlp1 to both compartments (Koch et al., 2005). Together these findings suggest that more than one mechanism can signal and execute organelle division. Studies in *S. cerevisiae* showed that abrogation of peroxisome division occurred only in cells lacking the two dynamin-related proteins, Dnm1p and Vps1p, together with Inp2p, which is the peroxisome-specific receptor for the molecular motor, Myo2p, and a key regulator of peroxisome inheritance in this yeast (Motley and Hettema, 2007). These findings support a contribution of mechanical forces to the final scission of peroxisomes and implicate cell cycle cues in linking the growth of peroxisomes to overall cell growth and division. Currently, two modes of peroxisome division are envisioned, one guided by the need to proliferate peroxisomes in response to environmental stimuli, i.e. a diet rich in substances requiring metabolism by peroxisomes, and one guided by a cell's need to replicate its

organelle population in response to cell division (Fagarasanu et al., 2007; Hettema and Motley, 2009). Peroxisome division appears also to be required for proper metabolic function, although this requirement is not absolute. Mice lacking *PEX1* β , which is involved in regulating peroxisome division, exhibit the classic hallmarks of Zellweger syndrome but, surprisingly, are normal in their ability to metabolize very-long chain fatty acids, suggesting that the lack of *PEX1* β results in a defect in some yet uncharacterized metabolic function of peroxisomes (Li et al., 2002). In *S. cerevisiae*, *pex1* Δ cells display defects in β -oxidation, particularly of medium-chain fatty acids (Erdmann and Blobel, 1995; van Roermund et al., 2000); however, the mechanism underlying these defects remains controversial (Li and Gould, 2002). Recently, a *pex1* Δ mutant of the yeast *Pichia pastoris* was shown to have a defect in the unconventional secretion of acyl-CoA binding protein (Manjithaya et al., 2010a), but this was shown to be due to a defect in peroxisomal metabolism rather than a direct contribution of Pex1 β to the secretion of the protein.

One undetermined aspect of peroxisome division is whether it is symmetrical, asymmetrical, or both (Figure 1-4). Evidence for asymmetrical division has come from electron micrographs showing dimples or tubules emanating from the body of the peroxisome (Erdmann and Blobel, 1995; Fujiki et al., 1982). Also, in the yeast *Hansenula polymorpha*, peroxisomes were observed to divide asymmetrically with the formation of a prominent tubule emanating from the body of the peroxisome (Nagotu et al., 2008). Asymmetry is not restricted to the peroxisome body but is also seen in constituents of the peroxisomal membrane. The membrane protein Inp2p is polarized towards the leading edge of peroxisomes in yeast cells lacking the dynamin-related protein, Vps1p (Fagarasanu et al., 2009). Matrix proteins can also show an asymmetrical distribution, as in the case of rat acyl-CoA oxidase, which is often asymmetrically distributed between the two peroxisomes arising from peroxisome division (Wilcke et al., 1995). The asymmetrical distribution of lipids within the peroxisomal membrane is an important aspect of the current model of peroxisome

Figure 1-4. A model comparing asymmetrical versus symmetrical division of peroxisomes. This flow diagram highlights the two potential mechanisms of peroxisome division. After receiving a signal to divide, peroxisomes undergo physical changes that elongate and constrict the peroxisome into divisible units, making them competent for the final scission event. Whether symmetric or asymmetric division represents the primary mode of peroxisome division is still a matter awaiting detailed analysis. Furthermore, it remains unresolved if peroxisome division could lead to membrane or matrix protein asymmetry, regardless of the physical method of cleavage.



division in *Y. lipolytica* (Boukh-Viner et al., 2005; Guo et al., 2003; 2007). Studies have shown that Pex11p may oligomerize (Marshall et al., 1996; Rottensteiner et al., 2003; Tam et al., 2003) to form a tubule by elongating a portion of the peroxisome in an asymmetrical manner (Kuravi et al., 2006). However, contrarily, overexpressed Pex11p/PEX11 β constricts peroxisomes symmetrically, giving rise to peroxisomes with a dumbbell or beads-on-a-string appearance (Erdmann and Blobel, 1995; Koch et al., 2003). Yeast cells lacking Vps1p also have peroxisomes with a beads-on-a-string appearance, with constrictions regularly spaced along the elongated axis (Hoepfner et al., 2001).

The importance of peroxisome division is reflected in another prominent aspect of peroxisomes, their heterogeneous nature. Liver peroxisomes isolated from rats treated with the hypolipidemic drug clofibrate showed the presence of a distinct population of peroxisomes that were less dense than mature peroxisomes but still import competent for the matrix enzyme, acyl-CoA oxidase (Heinemann and Just, 1992). Similar observations were made in individual cells of a human hepatoblastoma cell line (Schrader et al., 1994). Erdmann and Blobel provided a temporal justification for the conversion of peroxisomes of light density to peroxisomes of heavy density as a response of yeast to growth on oleate, which activates the transcription of oleate-responsive genes and increases the import of matrix proteins so that peroxisomes “mature” (Erdmann and Blobel, 1995). Remarkably, Titorenko and Rachubinski demonstrated six biochemically and morphologically distinct peroxisomal populations in *Y. lipolytica* (Titorenko et al., 2000). Together, these findings show that although peroxisomes behave essentially as individual entities that form and function in relative seclusion to one another, they can be timed for synchronous development depending on environmental factors, e.g. nutrient availability. These findings also support the concept that mature peroxisomes do not fuse with each other, although the fusion of immature, precursor peroxisomes may play a role in their development (Titorenko et al., 2000). Therefore, organellar fusion apparently does not help maintain the metabolic functionality of peroxisomes as it does for mitochondria (Hermann and Shaw, 1998). Also, in contrast to mitochondria (Hermann et

al., 1998), mature peroxisomes were not observed to fuse in yeast mating assays (Hettema and Motley, 2009; Motley and Hettema, 2007).

1.7 De novo peroxisome biogenesis

Peroxisomes rely on essential contributions from the ER to support their growth and division. This reinterpretation of the growth and division model of peroxisomes is significant because it now positions peroxisomes as a specialized branch or extension of the secretory system (Schekman, 2005). The first mechanistic support for an ER contribution to peroxisome biogenesis came from studies in *Y. lipolytica* showing that mutations in the signal recognition particle constituent, Srp54p, or deletion of another gene required for secretion, *SEC238*, resulted in defective peroxisome biogenesis and the accumulation of the PMPs, Pex2p and Pex16p, in the ER (Titorenko and Rachubinski, 1998; Titorenko et al., 1997). In addition, Pex2p and Pex16p were shown to normally contain *N*-linked core glycosylation, unequivocally demonstrating that the branch point to peroxisomes in the secretory system was at the level of the ER. It has been proposed that this contribution of the ER underlies the reemergence of peroxisomes in cells from PBD patients upon complementation of the defective gene (Kim et al., 2006; Matsuzono et al., 1999; South and Gould, 1999). The contribution of the ER to peroxisome biogenesis was also demonstrated by studies of the peroxins Pex3p and Pex19p. Absence of Pex3p or Pex19p results in a complete mislocalization of peroxisomal matrix and membrane proteins (Hettema et al., 2000). Working in yeast, Hoepfner and colleagues asked the simple question, “What happens when Pex3p and Pex19p are added back?” They showed that when Pex3p was reintroduced into *pex3Δ* cells, it first sampled the ER and then sequestered into distinct subdomains that went on to become functional peroxisomes (Hoepfner et al., 2005). This ability of Pex3p to sort through and exit the ER was shown to depend on Pex19p, and an ER-localized pool of Pex3p that accumulated in *pex19Δ* cells could form peroxisomes upon reintroduction of Pex19p (Hoepfner et al., 2005).

These results were taken as evidence that peroxisomes form de novo from the ER. Further support for the de novo synthesis of peroxisomes came from work in mammalian cells. Kim and colleagues observed that cells lacking peroxisomes because of mutation of the *PEX16* gene could form peroxisomes upon reintroduction of the gene (Kim et al., 2006). In an elegant experiment employing photoactivatable GFP, they showed that peroxisomes appeared to form de novo rather than by division (Kim et al., 2006).

It must be said that all the aforementioned findings cannot unequivocally exclude division as the sole or principal mechanism underlying the maintenance or growth of the peroxisome population in wild-type cells. Indeed, the contribution of central players in the secretory pathway, such as COPI and COPII (Lay et al., 2005; Passreiter et al., 1998; Perry et al., 2009; South et al., 2000; Voorn-Brouwer et al., 2001) and the ER translocon channel protein, Sec61p (Perry et al., 2009; South et al., 2001), to peroxisome biogenesis remains uncertain, although components of the DSL1 complex involved in retrograde transport between the Golgi complex and the ER have been shown to be involved in peroxisome biogenesis in yeast (Perry et al., 2009). In effect, it has been uncharitably argued that de novo peroxisome biogenesis is an anomalous yet fortunate response to a complete and catastrophic loss of peroxisomes from cells and not a normally occurring event in nature (Lazarow, 2003). It remains for investigators to provide an unequivocal demonstration of the role of de novo peroxisome biogenesis in “normal” cells under “normal” conditions.

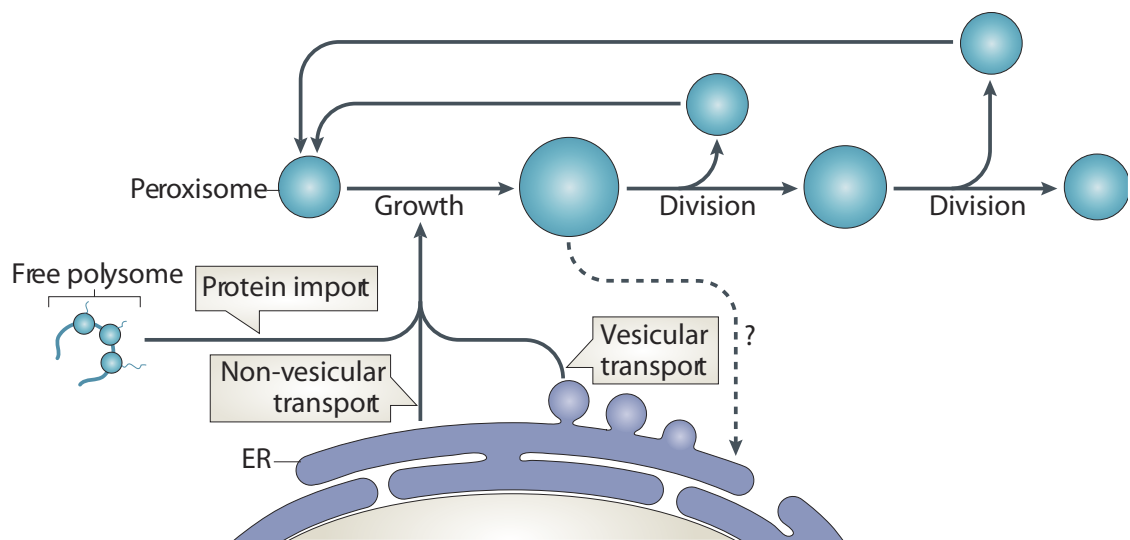
1.8 Model of peroxisome biogenesis in yeast

Peroxisomes are unique intracellular entities in yeast cells because a population of peroxisomes is formed and organized by a common complement of proteins, the products of *PEX* genes, but yet each peroxisome retains an individual characteristic. The steady state number of peroxisomes in a cell is controlled by the emergence of new peroxisomes from preexisting ones and also the

selective turnover, or degradation, of certain peroxisomes by a specialized form of autophagy, termed pexophagy (Manjithaya et al., 2010b). The existence of a de novo pathway for peroxisome formation has been demonstrated to exist (Hoepfner et al., 2005; Tam et al., 2005; van der Zand et al., 2012) but its contribution to maintaining peroxisome populations in yeast appears to be minor (Hettema and Motley, 2009; Motley and Hettema, 2007). Many PMPs sample the ER membrane en route to mature peroxisomes (van der Zand et al., 2010). The transfer of proteins and lipids from the ER to peroxisomes is envisioned to occur both by vesicles that bud from specialized regions of the ER (Agrawal et al., 2011; Lam et al., 2010) and by a nonvesicular pathway acting principally in the transfer of lipids (Raychaudhuri and Prinz, 2008). However, all matrix proteins, together with some PMPs, are imported into peroxisomes directly after being synthesized in the cytosol (Figure I-5).

With each round of cell division, peroxisomes follow an orchestrated sequence of events that result in their equitable distribution between mother and daughter cells at cytokinesis (Fagarasanu et al., 2005; 2006b; Hoepfner et al., 2001): In unbudded cells, peroxisomes are scattered over the entire cell cortex, where they assume static positions. The anchoring and retention of peroxisomes in the mother cell is mediated by Inp1p, a peripheral membrane protein of peroxisomes with an essential role in immobilizing peroxisomes at the cell cortex (Fagarasanu et al., 2005). Concomitant with the emergence of a bud from the mother cell, peroxisomes detach one-by-one from their anchored cortical positions to travel toward and populate the nascent bud. This recruitment of peroxisomes, from mother cell to bud, continues until an equivalent density of peroxisomes between both mother cell and bud has been achieved (Fagarasanu et al., 2006b). Small peroxisomes are often observed to detach from larger, cortically anchored peroxisomes in the mother cell and then migrate to the bud. Division of peroxisomes is not confined to the mother cell cortex, since travelling peroxisomes are also observed to divide both en route to the

Figure 1-5. The growth and division cycle of peroxisomes. Peroxisome membrane expansion is achieved mainly by material coming from the ER, presumably via both vesicular and nonvesicular pathways. A retrograde pathway, yet to be demonstrated, could retrieve escaped ER proteins and recycle factors involved in the assembly of vesicles destined for the peroxisome (dashed arrow). In contrast, all matrix proteins and some PMPs are acquired by the peroxisome by posttranslational import from the cytosol after synthesis on free polysomes. The division of mature peroxisomes is needed to maintain peroxisome numbers during cell proliferation. In contrast to the prevailing view of peroxisome division as being the simultaneous severing of peroxisomal tubules at multiple regular intervals, it is more likely that peroxisomes divide asymmetrically, with small daughter peroxisomes pinching off from larger parental ones.



bud and even inside it (Chang et al., 2009; Fagarasanu et al., 2006b). This implies a loose connection between peroxisome division and peroxisome inheritance into buds. Loose in the sense that while peroxisome division is needed to maintain peroxisome numbers in a growing cell population, the two processes are neither sequentially coupled nor inextricably linked. A class V myosin, Myo2p, is the actin-based motor responsible for moving most organelles, including peroxisomes, to the bud (Hoepfner et al., 2001; Weisman, 2006). Inp2p is a PMP required for the localization of peroxisomes to buds and is the adaptor molecule that connects Myo2p to the peroxisomal membrane (Fagarasanu et al., 2006b).

1.9 Peroxisomes are all not equal

Although all peroxisomes share common mechanisms guiding their biogenesis, division and protein import, peroxisomes in different cell types and in different organisms host different metabolic pathways and perform different functions. As mentioned earlier, mammalian peroxisomes have been shown to vary in their enzymatic compositions in the different organs, which helps them to perform their specific metabolic roles. Peroxisomes have also specialized to help organisms adapt to their specific environmental niches. One example is found in the *Trypanosomatidae*, which contain specialized peroxisomes called glycosomes that house enzymes of the glycolytic cycle for energy production in the oxygen-poor environment of the bloodstream (Michels et al., 2006). In plants, three specialized peroxisomes have been described that have distinct roles in fatty acid β -oxidation, the formation of succinate by the glyoxylate cycle, or photorespiratory glycolate metabolism (Hayashi and Nishimura, 2006). Peroxisomes can also specialize to perform nonmetabolic functions. In some filamentous fungi, a specialized peroxisome plugs the septal pore between cells when the cell wall has been damaged and cytoplasm begins to bleed through it. Called Woronin bodies, these specialized peroxisomes form by the asymmetric division of a small

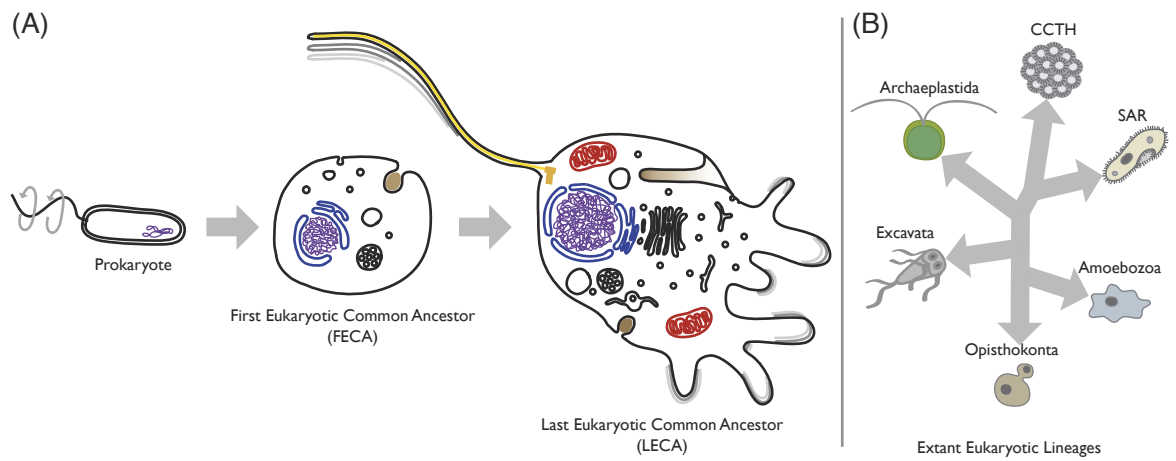
number of peroxisomes that have imported the protein HexIp, which is essential for the formation of Woronin bodies (Liu et al., 2008).

1.10 Origins and diversity of eukaryotes

There is general agreement from both molecular phylogenetic analyses (Gribaldo and Cammarano, 1998; Iwabe et al., 1989) and evidence from the fossil record (Javaux et al., 2001; Schopf, 1999) that prokaryotes predate eukaryotes. Consequently, eukaryotes must have arisen from a prokaryotic-like ancestor. This does not imply that there has not been evolution in modern prokaryotic lineages (Penny and Poole, 1999) or that we can treat extant prokaryotes as primitive states. However, it does mean that the acquisition of organelles and complex cellular machines in eukaryotes must be explained from a cellular state lacking these features.

The transition from prokaryote to eukaryote can be divided into, at least, three successive evolutionary stages (Figure 1-6). These include: 1) transition from a prokaryotic-like starting point to an organism that would possess some arguable set of cellular features that would define it as eukaryotic, i.e. a first eukaryotic common ancestor (FECA), 2) transition from FECA to a last eukaryotic common ancestor (LECA), and 3) radiation after LECA, of which six extant lineages of eukaryotes are known today (Adl et al., 2012; Walker et al., 2011). The prokaryote to eukaryote transition has generally focused on the transition through the first two stages to the LECA. Based on comparative genomics, the LECA was complex with a well established actin/tubulin cytoskeleton, a sophisticated endomembrane system, nucleus, mitochondria, and machinery for intron splicing, meiosis and more (Cavalier-Smith, 2010; Dacks and Doolittle, 2001; Field and Dacks, 2009; Koonin, 2010; Roger, 1999). There has been at least one additional major cellular innovation impacting post-LECA increases in complexity: the acquisition of plastids.

Figure 1-6. Retracing the evolutionary emergence of modern eukaryotes. (a) The emergence of eukaryotes can be divided into at least three successive evolutionary stages. These include: 1) transition from a prokaryotic-like starting point to a first eukaryotic common ancestor (FECA), i.e. an organism that would possess some arguable set of cellular features that would define it as eukaryotic (a nucleus, membrane-bound organelles, a cytoskeleton); 2) transition from FECA to a last eukaryotic common ancestor (LECA). Based on comparative genomics, the LECA was complex with a well established actin/tubulin cytoskeleton, a sophisticated endomembrane system, nucleus, mitochondria, and machinery for intron splicing, meiosis and more. The acquisition of plastids, again transformative in certain lineages, occurred post-LECA; and 3) evolution and divergence after LECA to form the major lineages of eukaryotes as we know them today.



I.11 Mechanisms for the evolution of organelles

Before 1974, the null hypothesis for the evolution of internal membrane-bound compartments (organelles) within the eukaryotic cell had been via autogenous processes, i.e. eukaryotic cells are built up in a stepwise manner from individual building blocks present in the pre-eukaryotic ancestor (Cavalier-Smith, 1975). For example, de Duve and Wattiaux (de Duve and Wattiaux, 1966) proposed an autogenous origin for lysosomes based on their work identifying and characterizing this organelle. However, the dominance of the autogenous theory shifted when Lynn Margulis revived and championed the idea of endosymbiosis (Sagan, 1967), which had been first proposed as early as 1882 (reviewed in (Hagemann, 2007)). When Bonen, Gray and Doolittle (Gray and Doolittle, 1982) presented the first strong molecular evidence for bacterial origins for both mitochondria and chloroplasts, the theoretical basis of the eukaryotic evolutionary field was shifted such that both endosymbiotic and autogenous origins were now equally viable alternatives to entertain when beginning to address the origins of a given eukaryotic organelle. Importantly, both models were shown to be consistent with the mechanisms of protein targeting, sorting and topogenesis (Blobel, 1980). Günter Blobel elegantly summarized in his Nobel address this continuity of cellular membranes by reformulating Virchow's dictum, 'all cells come from cells,' to 'all membranes come from membranes'. Our scientific understanding of endosymbiosis and autogeny is maturing, with endosymbiosis being the far better understood.

I.12 Endosymbiosis and horizontal gene transfer

Endosymbiosis is the incorporation and residence of one organism, the endosymbiont, inside another, the host. The process progresses from an initial state of mutual coexistence to eventual assimilation and reduction of the endosymbiont by the host (Sagan, 1967). Endosymbiosis can be classified into various types depending on the nature of the host and of the endosymbiont. The simplest form, or primary endosymbiosis, involves a eukaryotic host and a bacterial endosymbiont.

Two such primary endosymbiotic events have been transformative in the history of eukaryotes and involved the incorporation of an α -proteobacterium and a cyanobacterium to give rise to what are today known as the mitochondrion- and plastid-derived organelles, respectively. Both events are known to have occurred early in eukaryotic history, with the mitochondrial event now convincingly shown to have pre-dated the LECA, as all currently known eukaryotes have possessed a mitochondrion at some point in their evolutionary histories (Müller et al., 2012). Exactly how early in eukaryogenesis mitochondria were acquired is still unknown and remains hotly debated. A primary plastid endosymbiosis very likely occurred at the base of the Archaeplastidae lineage, conferring photosynthetic capacity and giving rise to all red algae, green algae and land plants (Gould et al., 2008). The ability to photosynthesize was clearly advantageous, enough so that it spawned the subsequent evolution of complex plastids (Palmer, 2003) through secondary and tertiary endosymbioses (Figure I-7A).

As a mechanism, the process of endosymbiosis can be divided into initiation and integration. Theoretically, either party can initiate endosymbiosis but with different implications for the nature of the host-endosymbiont interaction, i.e. either the endosymbiont is an undigested meal or the host has been subverted, at least initially, for the benefit of the endosymbiont. Plastids likely arose from an undigested meal, whereas the driver for the establishment of mitochondria is less clear (Gould et al., 2008; Müller et al., 2012). Regardless, after initiation, the success of the resulting chimera depends on the ability to synchronize successfully the cell growth and division cycles of the host and endosymbiont. In all cases, this synchronization has been achieved by gradual transfer of genetic material from the endosymbiont genome to the host genome (Figure I-7B). This ratchet-like mechanism is referred to as endosymbiotic gene transfer (EGT) and drives the enslavement of the endosymbiont by its host (Doolittle, 1998). A protein essential for organelle function must subsequently be retargeted to that organelle before loss of the gene encoding it in the endosymbiont genome can occur. This is not a trivial event, as it requires the emergence of

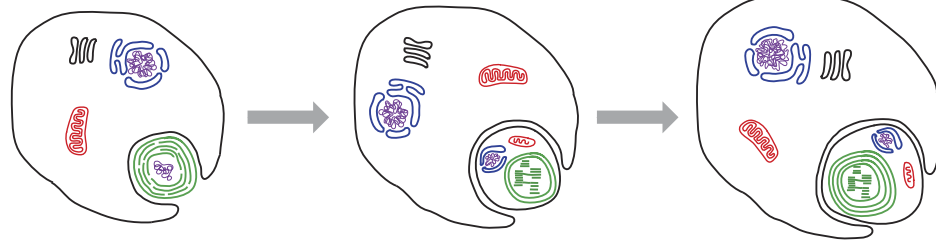
Figure 1-7. Mechanisms of organellar evolution. (a) Complex plastids arise from iterative acquisition of photosynthetic endosymbionts. (i) Primary endosymbiosis is established following engulfment of a cyanobacterium (green) by a eukaryotic host cell. A similar primary endosymbiotic process would also have produced the mitochondrion from a proteobacterium (not depicted here). (ii) In secondary endosymbiosis, a green or red algal cell is engulfed by a new host cell. (iii) This process is repeated in tertiary endosymbiosis. (b) Endosymbiotic gene transfer (EGT) is a mechanism of endosymbiont enslavement by the host. (i) After acquiring an endosymbiont, the organism has two genomes, one in the nucleus and one in the endosymbiont. (ii) Whether by lysis or improper fission and fusion events of the endosymbiont during replication, endosymbiont DNA released into the cytoplasm can be integrated into the host genome. (iii) With an endosymbiont gene now encoded and expressed by the host, it must successfully retarget back to the endosymbiont. (iv) When successful retargeting occurs, the endosymbiont copy is redundant and sustains mutational decay, and the endosymbiont genome is reduced. (v) The directionality imposed by this transfer results in a ratchet-like mechanism that is repeated. (vi) The window of opportunity permitting EGT remains open until only a single endosymbiont genome remains. (c) Organelle paralogy hypothesis (OPH). (i) Different protein families interact cooperatively to specify organelle-defining properties, such as tethering, docking, fission or fusion. (ii) Specificity-encoding protein families evolve by gene duplication and divergence as represented by this hypothetical phylogeny. (iii) Increases in the complexity of specificity encoding protein families is mirrored by increases in the complexity of the membrane trafficking system. Paralogs of the specificity-encoding protein family reside and have their effect on distinct compartments.

(a) endosymbiosis

(i) primary

(ii) secondary

(iii) tertiary



(b) EGT and transfer window hypothesis

(i)

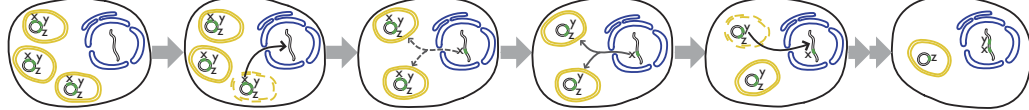
(ii)

(iii)

(iv)

(v)

(vi)

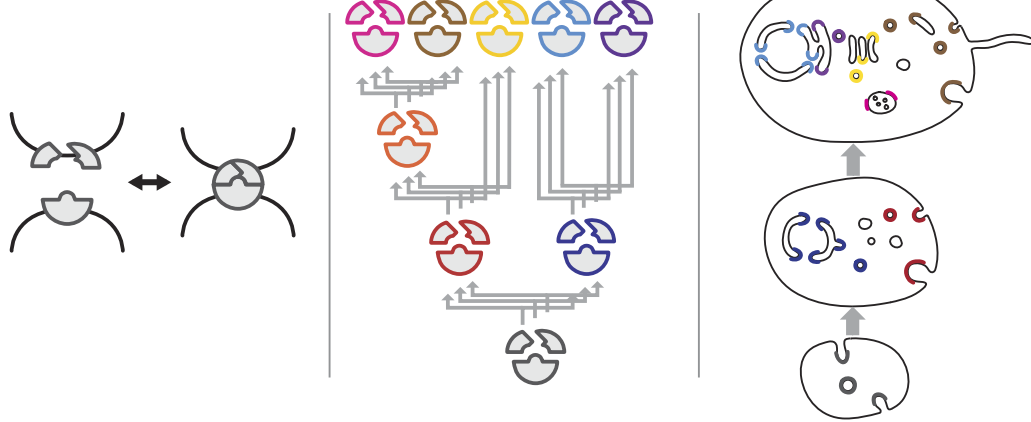


(c) organelle paralogy hypothesis

(i)

(ii)

(iii)



recognition sequences added to the amino acid coding region of the protein being retargeted and of a set of recognition, chaperone and transport machineries in the organelle itself (Gould et al., 2008; Müller et al., 2012).

Although endosymbiosis as an evolutionary mechanism results in overall increased complexity for the eukaryotic cell, as a process it is principally about decreasing complexity! The system is at its most complex immediately after the initiation stage, with integration progressing principally via EGT or gene loss. We know this to be the case because our exploration of eukaryotic diversity has revealed examples of ongoing endosymbioses at various stages (Keeling, 2010; Keeling and Archibald, 2008). There are examples of recent and independent instances of both primary, e.g. *Paulinella* (Marin et al., 2005), and secondary endosymbioses (Okamoto and Inouye, 2005). Even more useful for studying the process of endosymbiosis are the organisms possessing nucleomorphs, which are secondary plastids that have retained not only their plastid genomes but remnant nuclear genomes as well (Moore and Archibald, 2009). Examples of organelles at the other extreme include the non-photosynthetic apicoplasts of the parasitic apicomplexans, which have been retained for their roles in biosynthesizing metabolites (Gould et al., 2008; Müller et al., 2012), and hydrogenosomes and mitosomes, which derive from mitochondria. These organelles in many cases no longer possess organellar genomes (Müller et al., 2012).

The range of degeneracy found for endosymbiotically derived organelles clearly raises the question of what mechanism determines and limits the extent of this reductive trend in any given lineage. It is more than the simple passage of time, since we see a range of reduction in organelles clearly derived from the same founding event, e.g. mitochondria. The best supported idea is the 'transfer window hypothesis' (Barbrook et al., 2006). This proposes that because the main mechanism of DNA transfer to the host nucleus comes from lysed organelles, the rate of transfer is proportional to the copy number of the endosymbiont in the cell (Figure 1-7B). Importantly, the hypothesis implies that transfer cannot continue once the number of organelles has stabilized at a

single copy. This idea has now been supported by experimental (Lister et al., 2003) and comparative (Smith et al., 2011) genomic analyses showing far fewer transfers from plastids to nuclear genomes in organisms possessing low plastid copy number. The nuclear genomes of two organisms possessing a single nucleomorph have also recently been sequenced (Curtis et al., 2012). This analysis revealed a lack of recent DNA transfer from either the plastid or nucleomorph genomes despite evidence of transfer from mitochondria, consistent with the idea that it is reduction to a single organelle that freezes EGT and hence organelle reduction.

Interestingly, EGT appears to have played a role in shaping other organelles in addition to those originating endosymbiotically and has thus provided capabilities to the eukaryotic cell beyond the capacity for energy generation. One landmark study demonstrated that as much as 18% of the proteins encoded in the genome of the model plant, *Arabidopsis*, are of cyanobacterial origin and involved in diverse cellular processes beyond photosynthesis (Martin et al., 2002). As more organellar and nuclear genomes of diverse eukaryotes are sequenced, the chimeric, i.e. both host-derived and endosymbiont-derived, nature of metabolic pathways (e.g. heme biosynthesis, fatty acid biosynthesis, aromatic amino acid metabolism) is also being revealed. These findings explain in part why plastids and mitochondria are retained in some lineages that have lost the original energy-generating function of the organelle (Gould et al., 2008; Müller et al., 2012).

EGT can be viewed as a special case of horizontal gene transfer (HGT), the transmission of genetic material horizontally across phylogenetic lines rather than vertically to progeny. This phenomenon is a powerful evolutionary driver in prokaryotes (Doolittle and Bapteste, 2007), and there are well supported examples of HGT in eukaryotes that have shaped metabolism (Keeling and Palmer, 2008) and enhanced pathogenesis (Richards et al., 2006; Slot and Rokas, 2011). However, the overall extent and impact of HGT on eukaryotic evolution, in particular cellular evolution, are unclear and await systematic investigation.

I.13 Non-endosymbiotic (autogenous) organelles

While endosymbiosis has undoubtedly been a powerful force in shaping eukaryotic cellular complexity, there are many features of eukaryotic gene complexity that it does not explain. An alternative and simpler explanation for the origin of organelles delimited by a single lipid bilayer and devoid of genetic material is that they are autogenous, i.e. derived from component parts already present in the lineage giving rise to eukaryotes. The organelles most commonly proposed to have an autogenous origin are those of the membrane-trafficking system and include the endoplasmic reticulum, Golgi apparatus, endosomes, and plasma membrane (de Duve, 2007). Although these endomembrane organelles are dynamically connected to one another, they are maintained as distinct compartments through the action of membrane trafficking machineries, which include Rabs, SNAREs, coatomer, and adaptin (AP) complexes, among others (Bonifacino and Glick, 2004; Robinson, 2004). These “specificity-encoding” protein families have different members that perform the same essential function, e.g. inducing membrane curvature or facilitating membrane fusion, at a unique location within the membrane trafficking system (Bonifacino and Glick, 2004). Clearly, each specificity-encoding protein family could therefore play a role in encoding specificity in membrane-trafficking, but part of that specificity-encoding information also appears to result from combinatorial interactions between different protein families (Cai et al., 2007). Comparative genomic and phylogenetic analyses of these various protein families revealed the families’ primary diversification occurs via gene duplication (Dacks and Field, 2007; Elias et al., 2012). Surprisingly, the timing of the duplications giving rise to major paralogs of the various specificity-encoding proteins associated with each cellular location occurred prior to the LECA (Field and Dacks, 2009). Moreover, when endocytic paralogs of the SNAREs, Rabs and AP families were examined, a pattern emerged whereby some organelle-specific paralogs had duplicated prior to the LECA, while others had not (Dacks and Field, 2007; Dacks et al., 2008). Subsequently, patterns of parallel duplications in lineages after the LECA were also found. These patterns have not only provided a

sense of the timing of events but also hinted at a process for the events, which has been formalized in the organelle paralogy hypothesis (OPH) (Dacks and Field, 2007; Dacks et al., 2009).

In the OPH, a set of specificity-encoding proteins, with complementary functions that together define the properties of a distinct organelle, undergoes duplications to produce sets of interacting paralogs (Figure 1-7C). Through co-evolution, these sets of specificity-encoding proteins accumulate mutations that fix their specific functional binding, thus defining separate organelles (Dacks et al., 2009). Iterations of this process could therefore account for the array of organelles in the endomembrane systems of extant eukaryotes that arose via differentiation from an original prototypical internal compartment in the FECA (Figure 1-7C).

Although based on observed evolutionary patterns in gene families, the OPH has recently been tested by computer simulation. Mathematical modeling of specificity-encoding genes in populations of vesicles showed that gene duplication and differential interactions between paralogs produced novel vesicular compartments (Ramadas and Thattai, 2013). Crucially, under the OPH, it follows that the order of evolutionary emergence for each member of a specificity-encoding protein family should correspond to the order of emergence of the different organelles they define and on which they have effect. Although testing this aspect of the theory has not been methodologically tractable until recently, two studies have now reported phylogenetic resolution for important specificity-encoding protein families. Thus statements, or at least hypotheses, regarding an order of evolutionary emergence beyond simply establishing extensive complexity in membrane trafficking in the LECA can now be made. The first example involves the recent discovery of the enigmatic fifth AP complex (Hirst et al., 2011). AP complexes aid in sorting the vesicular traffic between organelles found between and including the plasma membrane and the trans-Golgi network (Robinson, 2004). Comparative genomic and phylogenetic analysis of the AP complexes, including AP5, allowed for a resolution of the order in which the members of the AP complex family emerged, with the sequence of AP3 splitting from the rest of the AP complexes

first, followed by AP5, AP4 and AP1/2 (Hirst et al., 2011). This order was interpreted to suggest that the adaptins were first involved in creating an interface between the secretory system and the phagocytic system and, subsequently, a full-fledged trans-Golgi network, based on the known location of action for the AP complexes. The second example deals with the Rab family of GTPases, which are molecular switches involved in specifying organelle identity in the membrane trafficking system (Grosshans et al., 2006). It has been well established that Rab GTPases are ancient and that the LECA possessed a large complement of such proteins (Pereira-Leal and Seabra, 2001). The question was “How large?”. Recent efforts using rigorous methods based on homology-searching expanded the Rab complement in LECA to as high as 15 (Diekmann et al., 2011). However, the development of a new phylogenetic technique allowing for robust phylogenetic resolution between the many paralogs of the Rab gene families further increased the estimated number of Rab subfamilies in LECA to between 19 and 23 (Elias et al., 2012). Surprisingly, this analysis showed one ancient set of Rabs involved in exocytosis and one involved predominantly in endocytosis, potentially harkening back to the earliest establishment of these pathways. As improved comparative and phylogenetic methods are applied to other trafficking families, it will be important to compare the evolutionary patterns that emerge and to delve further into the events pre-LECA.

The OPH is a mechanism for evolving increased organelle complexity but currently encompasses only the organelles of the membrane trafficking system. However, an idea that complements the OPH is the protocoatome hypothesis, which makes a strong statement of homology between the membrane deformation components of vesicular trafficking and the nuclear pore based on protein structural evidence (Field et al., 2011). Specifically, proteins integrated into the COP I, COP II, clathrin and nuclear pore complexes share the structure of a β -propeller followed by an α -solenoid. These proteins were deemed as being homologous and thus

derived from a single ancestral proto-coatomer protein (Devos et al., 2004). Recent analyses also firmly established proteins of the intra-flagellar complex as being related as well (van Dam et al., 2013). The protocoatomer-derived proteins, which are dispersed throughout the cell and are essential for organelle-specific functions, appear to have expanded along with their organelles via the process described in the OPH, and so the overlap between the two hypotheses extends a mechanism of autogenous organelle evolution to many, and potentially all, of the organelles for which a non-endosymbiotic origin appears likely.

1.14 Evolution of peroxisomes

There are examples that blur the divisions of autogenous and endosymbiotic organellar evolution. A case in point is the peroxisome, whose origin has been contentiously explained by both mechanisms (de Duve, 2007). While the evidence, both functionally (Hoepfner et al., 2005; Tam et al., 2005; Titorenko et al., 2000) and evolutionarily (Gabaldón and Capella-Gutiérrez, 2010; Gabaldón et al., 2006; Schluter et al., 2006), strongly favors an autogenous origin for peroxisomes, there has undoubtedly been some interaction and cross talk between peroxisomes and organelles of endosymbiotic origin (Andrade-Navarro et al., 2009; Neuspiel et al., 2008). This is true evolutionarily, with genes acting at peroxisomes being of bacterial origin (Gabaldón et al., 2006), and functionally, with pathways shared between peroxisomes and mitochondria, e.g. fatty acid oxidation (Wanders and Waterham, 2006). Indeed, the question of how endosymbiotic organelles have become integrated within the cell and interact with non-endosymbiotically derived systems is still a very open question both functionally and evolutionarily.

Peroxisomes are ancient and likely present in the LECA, as organisms possessing peroxisomes have been found in all extant lineages of eukaryotes (Gabaldón, 2010). However, there are notable exceptions including the parasitic apicomplexan *Plasmodium falciparum* and the excavate *Giardia lamblia* (de Souza et al., 2004; Schluter et al., 2006), causative agents of malaria

and giardiasis respectively. Furthermore, the colocalization of catalase and at least one oxidase in organisms from across the diversity of eukaryotes also suggests that the biochemical function of peroxisomes is ancient (de Duve, 2007). The metabolic diversity of peroxisomes has been a confounding variable in considering its evolution. Recently, a potential mechanism driving metabolic diversity in peroxisomes was discovered in fungi (Freitag et al., 2012). Cryptic PTS1 targeting sequences are encoded in the 3' untranslated region of genes for many metabolic enzymes and can be activated by alternative splicing or stop codon suppression. Therefore the adaptability and ease of accommodation of peroxisomal matrix protein import may have a strong influence on the evolutionary trajectory of these organelles in diverse eukaryotic lineages.

A comprehensive comparative genomic analysis of the peroxisome proteome demonstrated that while most of the peroxisomal matrix proteins could be traced to prokaryotic ancestry, many of constituents of the peroxisomal membrane, and the peroxins (Pex proteins) themselves, were of eukaryotic origin (Schluter et al., 2006) (Table I-1). Notably absent from this list was Pex14p, Pex5p and Pex7p, which are essential for peroxisomal matrix protein import, and Pex1p and Pex6p, which are essential for the recycling of the PTS receptors as well as peroxisome biogenesis at the ER. Additionally, Schluter and colleagues. (2006) proposed four peroxins, Pex3p, Pex19p, Pex10p and Pex12p served as “peroxisomal markers” for in silico assessment of peroxisome presence or absence. In contrast to this, a similar study by Galbadón and colleagues (2006) proposed a minimal ancestral peroxisome peroxin complement consisting of Pex1p, Pex2p, Pex4p, Pex5p, Pex10p and Pex14p. Because of these discrepancies and the fact that several important peroxins cannot be excluded to have prokaryotic origins, debate remains as to the evolutionary origin of peroxisomes (de Duve, 2007).

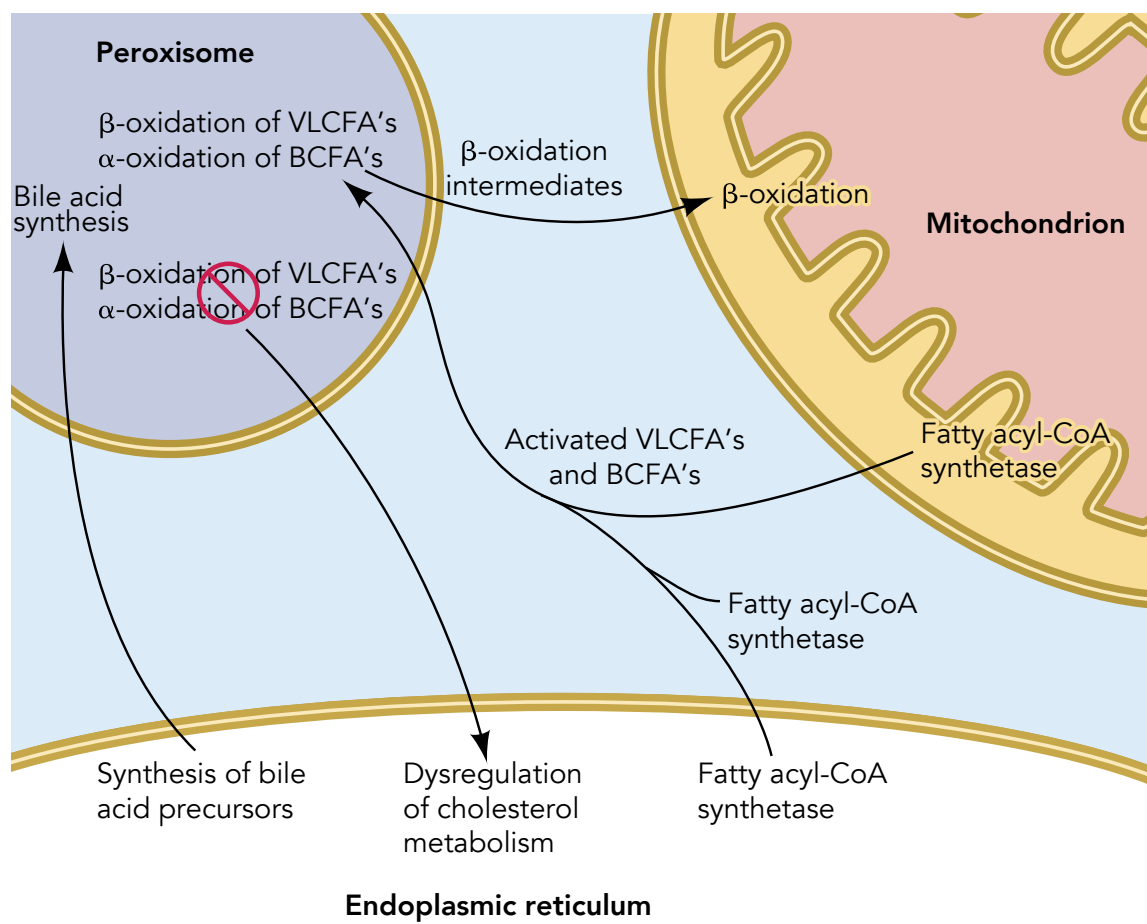
Table I-1. Peroxisomal proteins lacking overall homology in prokaryotic genomes as identified by Schluter and colleagues (2006).

Protein	Domain	Function	Compartment	Protein type
Pex2	Zn-RING	protein import	membrane	peroxin
Pex3	-	membrane assembly	membrane	peroxin
Pex4	ubiquitin ligase	protein import	cytosol and membrane	peroxin
Pex8	-	matrix protein import	membrane	peroxin
Pex9	-	matrix protein import	membrane	peroxin
Pex10	-	protein import	membrane	peroxin
Pex11, Pex11 β , Pex11 γ	-	division proliferation	membrane	peroxin
Pex12	Zn-RING	protein import	membrane	peroxin
Pex13	SH3	docking of receptors	membrane	peroxin
Pex15	phosphorylation	membrane assembly, docking of Pex1 and Pex6	membrane	peroxin
Pex16	-	membrane assembly	membrane	peroxin
Pex17	-	docking of receptors	membrane	peroxin
Pex18	-	PTS targeting	cytosol and membrane	peroxin
Pex19	farnesylation	membrane assembly	cytosol and membrane	peroxin
Pex20	-	PTS targeting	cytosol and membrane	peroxin
Pex21	-	PTS targeting	cytosol and membrane	peroxin
Pex22	-	protein import	membrane	peroxin
Pex23	dysferlin	proliferation	membrane	peroxin
Pex24	-	membrane assembly	membrane	peroxin
Pex25	-	proliferation	membrane	peroxin
Pex26	-	docking of Pex1 and Pex6	membrane	peroxin
Pex27	-	proliferation	membrane	peroxin
Pex28	-	proliferation	membrane	peroxin
Pex29	-	proliferation	membrane	peroxin
Pex30	dysferlin	proliferation	membrane	peroxin
Pex31	dysferlin	proliferation	membrane	peroxin
Pex32	dysferlin	proliferation	membrane	peroxin
Mpv17, Pmp2	Mpv17	unknown	membrane	PMP
Pxmp4	-	unknown	membrane	PMP
Pmp34	-	ATP transporter	membrane	PMP

I.15 The role of peroxisomes in lipid metabolism

Peroxisomes, together with the ER and mitochondria, function as important sites of lipid metabolism in the cell (Figure I-8). The interdependence of these organelles is illustrated by the requirement for the transfer of the activated variants of branched and very-long chain fatty acids from the mitochondria or ER to peroxisomes (Wanders et al. 2006). For example, phytanic acid, a branched-chain fatty acid present in the human diet and requiring a round of α -oxidation before subsequent rounds of β -oxidation, can be activated in the ER, mitochondria or peroxisomes by fatty acyl-CoA synthetases found in all three compartments.

Figure I-8. Peroxisomes rely on the ER and mitochondria, and vice versa, to properly carry out their role in the metabolism of lipids in cells. For example, peroxisomes import the activated (acyl-CoA) variants of very-long chain fatty acids (VLCFA), and branched chain fatty acids (BCFA), from the ER, cytosol and mitochondria. Intermediate metabolites from peroxisomal β oxidation are subsequently transferred to the mitochondria for the remaining rounds of β oxidation. Bile acid precursors are synthesized in the ER using cholesterol as a backbone before they are transferred to peroxisomes for the final steps in forming mature bile acids. When peroxisomes are non-functional, the buildup of VLCFAs results in the dysregulation of cholesterol metabolism in the ER, and cells accumulate VLCFAs esterified to cholesterol.



Activation of phytanic acid requires its transfer across the membranes of the ER or mitochondria to peroxisomes where its catabolism occurs. Furthermore, disrupting peroxisome formation alters the metabolism of cholesterol in the ER and results in the accumulation of cholesterol esterified to very-long chain fatty acids, as observed in mutant mice that fail to assemble functional peroxisomes (Kovacs et al., 2004; 2009). Conversely, peroxisomal β -oxidation of very-long chain fatty acids does not proceed to completion in the peroxisome, and partially oxidized fatty acyl-CoA intermediates are shuttled to the mitochondria to generate energy (reviewed in (Poirier et al., 2006)).

The contribution of peroxisome function for normal human development and physiology is underscored by the severity and lethality of the peroxisome biogenesis disorders (PBDs). The PBDs are a heterogeneous group of fatal autosomal recessive diseases that includes Zellweger syndrome (ZS), rhizomelic chondrodysplasia punctata (RCDP), neonatal adrenoleukodystrophy (NALD), and infantile Refsum disease (IRD). These four disorders are classified based on the severity of the clinical phenotypes. In addition to these broad biogenic disorders there are additional single-enzyme peroxisome diseases that share many of the same traits as these more serious disorders. In general, PBD patients suffer from profound neurological abnormalities, muscular hypotonia, cataracts, cardiac defects, dysmorphic features, and growth and mental retardation (for reviews, see (Shimozawa et al., 2005; Steinberg et al., 2006)). ZS is the most severe, and patients typically present with severe hypotonia, such that children with ZS are sometimes initially misdiagnosed with various forms of developmental, mental and physical retardation including Down syndrome, Prader-Willi syndrome, or spinal muscular dystrophy. Patients with ZS typically die in the first year of life (Wilson et al., 1986; Yik et al., 2009). The overall incidences of the PBDs vary widely among different population groups but are invariably infrequent enough to be classified as rare genetic diseases. ZS has an estimated incidence of 1 in 50,000 in North America but approximately 1 in 500,000 in Japan (Steinberg et al., 2004).

Thirteen *PEX* genes functionally complement the defects in peroxisome assembly of all the known complementation groups of the PBDs (Shimozawa et al., 2005; Steinberg et al., 2006). These 13 *PEX* genes function in a variety of different steps in the peroxisome biogenic pathway, including peroxisomal membrane assembly and peroxisomal protein targeting. An unexpected complication in the assignment of PBD phenotypes to any particular complementation group is the fact that different complementation groups share similar clinical phenotypes (Moser et al., 1995; Steinberg et al., 2006). This is most likely due to the fact that a defect in any aspect of the peroxisome biogenic program results in the same functional loss of the organelle. As a result, clinical diagnosis of the cause of any one PBD has required an in-depth and tedious biochemical characterization followed by sequencing efforts to pinpoint the source of the mutation (Shimozawa 2011; Steinberg et al., 2004). Advances in sequencing technology have improved the speed of diagnosis and there is currently an undertaking to fully annotate and catalogue the range of mutations present along the PBD continuum (<http://dbpex.org/home.php>). In addition, model systems have greatly aided in the identification and characterization of peroxisomal genes (Titorenko and Rachubinski, 2001)

Table 1-2. Complementation groups and *PEX* gene defects in PBDs. Adapted from Steinberg et al. (2006).

Gene	CG-Dutch	CG-Japan	CG-KKI	Clinical phenotype	Proportion of ZSS
<i>PEX1</i>	2	E	1	ZS NALD IRD	70%
<i>PEX2</i>	5	F	10	ZS IRD	3%
<i>PEX3</i>	4	G	12	ZS	<1%
<i>PEX5</i>	3		2	ZS NALD	<2%
<i>PEX6</i>	1	C	4 and 6	ZS NALD IRD	10%
<i>PEX7</i>		R	11	RCDP	-
<i>PEX10</i>		B	7	ZD NALD	3%

PEX12		3	ZS NALD IRD	5%
PEX13	H	13	ZS IRD	<1%
PEX14	K		ZS	<1%
PEX16	D	9	ZS	<1%
PEX19	J	14	ZS	<1%
PEX26	A	8	ZS NALD IRD	5%

CG: complementation group, Dutch:University of Amsterdam; KKI:Kennedy Krieger Institute; Japan: Gifu University School of Medicine

^aEstimate of CG frequency from KKI;

ZSS: Zellweger syndrome spectrum; NALD: neonatal adrenoleukodystrophy; IRD: infantile Refsum disease; RCDP: rhizomelic chondrodysplasia punctata

Defects in peroxisome function usually result in the accumulation of unused peroxisomal metabolites. In assaying the plasma of patients with a PBD for increased levels of the bile acid precursors di- and trihydroxycholestanoic acid, Wanders and colleagues also identified a C₂₉-dicarboxylic acid that is not present at significant levels in the serum of normal individuals (Ferdinandusse et al., 2009). They and others have postulated that the accumulation of this compound results from an aberrant reaction involving C₂₇, trihydroxycholestanoic acid (Ferdinandusse et al., 2009; Janssen et al., 1982; Parmentier et al., 1979). The accumulation of these and other lipid molecules typically metabolized by peroxisomes is thought to contribute to the many and pleiotropic defects exhibited by individuals with peroxisome dysfunction (reviewed in (Steinberg et al., 2006)). In an original description of ZS cells of patients were reported to have reduced capacity for mitochondrial respiration (Goldfischer et al., 1973). This observation may also explain the phenotypic diversity exhibited by patients within the same complementation group of a PBD, as the ability of cells to withstand stress resulting from the accumulation of peroxisomal metabolites depends to a greater or lesser extent on the different genetic makeups of individuals and the environments in which they live (Moser et al., 1995; Roscher et al., 1989).

I.16 Focus of this thesis

The goal and aim of this thesis is the significant advancement of our fundamental knowledge of peroxisomes. Towards that end, I had three specific aims:

I.16.1 Specific Aim 1. A molecular characterization of peroxisome proliferation

Two modes of peroxisome proliferation have been described: de novo biogenesis from the ER and the growth and division of existing peroxisomes. In chapter 3 of this thesis I present initial evidence showing that peroxisome proliferation is regulated by the growth cycle of the cell and that the ER was implicated in this regulation. This led to the hypothesis that peroxins involved in regulating peroxisome size and number localized to the ER. A fluorescence microscopy screen identified Pex30p as being an ER protein that exists in a complex with Pex29 and the reticulon proteins Rtn1p and Yop1p. This led to the hypothesis that this reticulon-peroxin complex was regulating peroxisome proliferation by regulating the egress of preperoxisomal vesicles from the ER and the sorting of peroxisomal membrane proteins within the ER. This hypothesis was tested with an in vitro budding assay and microscopy experiments that demonstrated an involvement of the reticulon-peroxin complex in negatively regulating peroxisome proliferation. In chapter 4 of this thesis I present additional evidence to support the conclusion that this is a conserved mechanism within the Opisthokont supergroup and suggest that it may be common mechanism in across the broad diversity of eukaryotes.

I.16.2 Specific Aim 2. An evolutionary analysis of mechanisms that facilitate emergent complexity in eukaryotes.

How is adaptability generated in a system composed of interacting cellular machineries, each with a separate and functionally critical job to perform? In chapter 5 of this thesis I address this question with a comparative genomic and phylogenetic analysis of organelle inheritance factors from *S.*

cerevisiae. I found that while some factors are retained widely across the animals and fungi, others are limited primarily to the Saccharomycetaceae family of budding yeast, with the emergent pattern of a conserved biogenic and inheritance factor often paired with an evolutionarily novel inheritance adaptor. This led to the proposal of the widget hypothesis, which states that a propensity exists for the utilization of evolutionarily novel adaptors to bridge and facilitate contact between conserved cellular modules. I tested this hypothesis with a comparative genomic analysis of an adaptor from metazoans, which confirmed the use of novel adaptors is a conserved evolutionary mechanism in Opisthokonts.

1.16.3 Specific Aim 3. Develop a model system for studying peroxisome biogenesis disorders

The underlying cause of pathophysiology of the PBDs remains poorly understood and would benefit from a disease model that recapitulates aspects of the patient phenotype, enables functional characterization of disease mechanisms and increases understanding of the contribution of peroxisomes to normal physiology. In chapter 6, I present the results of an investigation into the use of *Drosophila melanogaster* as a model in which to study the pathophysiology of PBDs. An in silico interrogation of the *Drosophila* genome identified 15 putative homologs (Pex genes) of known human and yeast *PEX* genes. RNAi-mediated knockdown confirms that 13 of these putative Pex genes are required for peroxisome assembly in *Drosophila* S2 cells. For example, the *Pex1* gene encodes an AAA-ATPase, which, when mutated in humans, causes the most severe PBD, ZS. I show that knockdown of *Pex1* in S2 cells results in mislocalization of a peroxisome-targeted chimeric protein consisting of GFP and PTS1 (GFP-SKL) to the cytosol. Furthermore, analysis of flies carrying a mutant form of the *Pex1* gene shows that *Pex1* is required for normal fly development, as is its homolog required for normal human development. Furthermore, mutant flies exhibit abnormalities characteristic of ZS patients, including developmental delay, poor feeding,

severe structural abnormalities in the peripheral and central nervous systems, and early death. Finally, microarray analysis defines several clusters of genes whose expression varies significantly between wild-type and *Pex1*-mutant larvae, and that implicate peroxisomal function as a requirement for normal neuronal development, innate immunity, lipid and protein metabolism, gamete formation, and meiosis.

2 Materials and methods

2.1 Materials for molecular and cellular biology

Table 2-1. Chemicals and reagents

Reagent	Source
1-butanol	Fisher
2-(N-Morpholino)ethanesulfonic acid (MES)	Sigma-Aldrich
2-propanol	Fisher
5-bromo-4-chloro-3-indolyl- β -D-galactoside (X-gal)	Rose Scientific
5-(N-2,3-dihydroxypropylacetamido)-2,4,6-tri-iodo-N-N'-bis(2,3-dihydroxypropyl)isophthalamide (Nycodenz)	BioLynx/Axis-Shield POC
acetone	Fisher
acrylamide	Roche
adenosine 5'-triphosphate (ATP) disodium salt hydrate	Sigma-Aldrich
agar	Difco
agarose, UltraPure	Invitrogen
albumin, bovine serum (BSA)	Roche
ammonium bicarbonate (NH_4HCO_3)	Sigma-Aldrich
ammonium chloride (NH_4Cl)	EM Science
ammonium persulfate	BDH
ammonium sulfate ($(\text{NH}_4)_2\text{SO}_4$)	BDH
ampicillin	Sigma-Aldrich
anhydrous ethyl alcohol	Commercial Alcohols
boric acid	EM Science
Brij 35	EM Science
bromophenol blue	BDH
calcium pantothenate	Sigma-Aldrich
chloroform	Fisher
cOmplete, Mini, protease inhibitor cocktail tablets	Roche
cOmplete, Mini, EDTA-free protease inhibitor cocktail tablets	Roche
complete supplement mixture (CSM)	BIO 101
complete supplement mixture, leucine dropout (CSM-LEU)	BIO 101
complete supplement mixture, uracil dropout (CSM-URA)	BIO 101
Coomassie Brilliant Blue R-250	ICN
copper sulphate pentahydrate	Invitrogen
D-(+)-glucose	EM Science
D-(+)-galactose	EM Science
D-(+)-raffinose	Sigma-Aldrich
deoxycycline	Sigma-Aldrich
deoxyribonucleotide triphosphate mixture (dNTPs)	Invitrogen
diethylpolycarbonate (DEPC)	Sigma-Aldrich
dithiothreitol (DTT)	Fisher
estradiol	Sigma-Aldrich
ethidium bromide	Sigma-Aldrich
ethylenedinitrilo-tetraacetic acid (EDTA)	EM Science
fetal bovine serum	Invitrogen
Folin-Ciocalteu phenol reagent	Sigma-Aldrich

galactose	EMD
Geneticin (G418)	Invitrogen
glacial acetic acid, 17.4 M	Fisher
glass beads, acid washed	Sigma-Aldrich
glycerol	EM Science
glycine	Roche
guanosine 5'-triphosphate sodium salt hydrate	Sigma-Aldrich
isoamyl alcohol	Fisher
isopropyl β -D-thiogalactopyranoside (IPTG)	Roche
hygromycin	Sigma-Aldrich
lanolin	Alfa Aesar
L-histidine	Sigma-Aldrich
lithium acetate	Sigma-Aldrich
L-leucine	Sigma-Aldrich
L-lysine	Sigma-Aldrich
magnesium sulfate (MgSO_4)	Sigma-Aldrich
methanol	Fisher
methyl salicylate	Sigma
maltose	Sigma-Aldrich
neosourthricin (NAT)	HKI
N,N,N',N'-tetramethylethylenediamine (TEMED)	EM Science
N,N'-dimethyl formamide (DMF)	BDH
N,N'-methylene bisacrylamide	Sigma-Aldrich
N-propyl gallate	Sigma-Aldrich
oleic acid	Fisher
paraffin	Fisher
paraformaldehyde	Sigma-Aldrich
penicillin	Invitrogen
phenol, buffer saturated	Invitrogen
phosphocreatine disodium salt	Sigma-Aldrich
poly L-lysine	Sigma-Aldrich
polyethylene glycol, M.W. 3350 (PEG)	Sigma-Aldrich
Ponceau S	Sigma-Aldrich
potassium acetate	BDH
potassium chloride	BDH
potassium permanganate (KMnO_4)	BDH
potassium phosphate, dibasic (K_2HPO_4)	EM Science
potassium phosphate, monobasic (KH_2PO_4)	EM Science
potassium tartrate	Sigma-Aldrich
raffinose	EMD
salmon sperm DNA, sonicated	Sigma-Aldrich
Sephadex G25	Amersham
skim milk	Carnation
sodium acetate	EM Science
sodium azide	Sigma-Aldrich
sodium carbonate (Na_2CO_3)	BDH

sodium chloride	EM Science
sodium deoxycholate	Sigma-Aldrich
sodium dithionite ($\text{Na}_2\text{S}_2\text{O}_4$)	BDH
sodium dodecyl sulfate (SDS)	Bio-Rad
sodium fluoride (NaF)	Sigma-Aldrich
sodium phosphate, dibasic (Na_2HPO_4)	BDH
sodium sulphite (Na_2SO_3)	Sigma-Aldrich
sorbitol	EM Science
streptomycin sulphate	Invitrogen
sucrose	EM Science
thiamine-HCl	Sigma-Aldrich
trichloroacetic acid (TCA)	EM Science
tris(hydroxymethyl)aminomethane (Tris)	Roche
Triton X-100	VWR
Trizol	Invitrogen
tryptone	Difco
Tween 20	Sigma-Aldrich
Tween 40	Sigma-Aldrich
uracil	Sigma-Aldrich
vaseline	Vaseline
xylene cyanol FF	Sigma-Aldrich
yeast extract	Difco
yeast nitrogen base without amino acids (YNB)	Difco
2-mercaptoethanol	BioShop

Table 2-2. Enzymes

Enzyme	Source
CIP (calf intestinal alkaline phosphatase)	NEB
creatine phosphokinase	Sigma-Aldrich
DNaseI ("DNA free")	Ambion
Easy-A high-fidelity polymerase	Stratagene
Platinum Pfx DNA polymerase	Invitrogen
Quick T4 DNA ligase	NEB
restriction endonucleases	NEB
RNase A (ribonuclease A), bovine pancreas	Sigma-Aldrich
T4 DNA ligase	NEB
Zymolyase 20T	ICN
Zymolyase 100T	ICN

Table 2-3. Molecular size standards

Molecular Size Standard	Source
1 kb DNA ladder (500-10,000 bp)	NEB
100 bp DNA ladder (100-1,517 bp)	NEB
prestained protein marker, broad range (6-175 kDa)	NEB

Table 2-4. Multicomponent systems for molecular biology

Multicomponent System	Source
BigDye Terminator Cycle Sequencing Ready Reaction Kit	Applied Biosystems
pGEM-T Easy Vector System	Promega
pMAL Protein Fusion and Purification System	NEB
QIAprep Spin Miniprep Kit	Qiagen
QIAquick Gel Extraction Kit	Qiagen
QIAquick PCR Purification Kit	Qiagen
T7 RiboMAX kit	Promega
Ready-To-Go PCR Beads	Amersham Biosciences

Table 2-5. Plasmids

Plasmid	Description	Source
pBS34/ <i>hph</i>	source of <i>hphNT1</i> cassette for targeted gene deletion in <i>S. cerevisiae</i>	Shaner et al., 2004
pCM159- <i>tet₀₇-tata</i>	source of Tet promoter for regulatable gene expression in <i>S. cerevisiae</i>	Gari et al., 1997
pFA6a- <i>kanMX</i>	source of <i>KanMX4</i> cassette for targeted gene deletion in <i>S. cerevisiae</i>	Longtine et al., 1998
pFA6a- <i>natNT2</i>	source of <i>natNT2</i> cassette for targeted gene deletion in <i>S. cerevisiae</i>	Longtine et al., 1998
pGEM-T Easy	multipurpose cloning vector for amplifying PCR generated DNA in <i>E. coli</i>	Promega
pGFP/ <i>HIS5</i>	source of <i>GFP-HIS5</i> cassette for genomic integration of a C-terminal GFP tag for targeted genes of interest	Dilworth et al., 2001
pMAL-c2	expression vector for purification of MBP fusion proteins from <i>E. coli</i>	NEB
pMAL-c2- <i>PEX3</i>	expression vector for protein purification of a fusion protein consisting of MBP and the C-terminal 301 amino acids of Pex3p from <i>S. cerevisiae</i>	Tam et al., 2005
pMAL-c2- <i>PEX29</i>	expression vector for protein purification of a fusion protein consisting of MBP and the C-terminal 246 amino acids of Pex29p from <i>S. cerevisiae</i>	this study
pMAL-c2- <i>PEX30</i>	expression vector for protein purification of a fusion protein consisting of MBP and the C-terminal 241 amino acids of Pex30p from <i>S. cerevisiae</i>	this study

pmRFP-SKL/URA3	mRFP-SKL expression vector for visualizing peroxisomes in <i>S. cerevisiae</i> by fluorescent microscopy	Fagarasanu et al., 2005
pProtA/HIS5	source of pA-HIS5 cassette for genomic integration of a C-terminal GFP tag for targeted genes of interest	Aitchison et al., 1995
pRS415	source of LEU2 cassette for targeted gene deletion in <i>S. cerevisiae</i>	ATCC
pRS426	source of URA3 cassette for targeted gene deletion in <i>S. cerevisiae</i> and parental plasmid for pRS426-mRFP, pRS426-mRFP-HDEL, and pRS426-mRFP-SKL	ATCC
pRS426-mRFP	source for mRFP (URA3) cassette for the in frame genomic integration of mRFP into the 3'-end of a gene of interest	this study
pRS426-mRFP-HDEL	source for mRFP-HDEL (URA3) cassette for the in frame genomic integration of mRFP into the 3'-end of a gene of interest	this study
pRS426-mRFP-SKL	source for mRFP-SKL (URA3) cassette for the in frame genomic integration of mRFP into the 3'-end of a gene of interest	this study
pTC3	expression vector for <i>Y. lipolytica</i> with exogenous gene expression regulated by the promoter and terminator of the <i>Y. lipolytica</i> POT1 gene	Chang et al., 2008
pTC3-PEX23-mCherry	PEX23-mCherry expression vector for visualizing a fusion of PEX23 and mRFP in <i>Y. lipolytica</i>	this study

Table 2-6. Primary antibodies

Specificity	Type	Name	Dilution ^a	Reference
<i>S. cerevisiae</i> Kar2p	rabbit	P42	IB 1:5,000 IF 1:1,000	Tam et al., 2005
<i>S. cerevisiae</i> Pex3p, affinity purified	rabbit	P84	IB 1:1,000	Tam et al., 2005, this study
<i>S. cerevisiae</i> Pex29p, affinity purified	guinea pig	W3 & W6	IB 1:10,000	this study
<i>S. cerevisiae</i> Pex30p, affinity purified	guinea pig	V4	IB 1:10,000 IF 1:1,000	this study
<i>S. cerevisiae</i> G6PDH	rabbit		IB 1:10,000	Invitrogen
<i>S. cerevisiae</i> Sdh2p	rabbit	P87	IB 1:5,000	Perry et al., 2009

<i>S. cerevisiae</i> Sec6Ip	rabbit		IB 1:5,000	gift from R. Schekman, University of California, Berkeley
<i>Y. lipolytica</i> thiolase	guinea pig	N-3°	IB 1:10,000	Eitzen et al., 1996
<i>D. melanogaster</i> DmelPex I	guinea pig		IB 1:1,000	this study
<i>D. melanogaster</i> CNS axons	mouse	BP102	IF 1:100	Developmental Studies Hybridoma Bank
<i>D. melanogaster</i> neuroglian	mouse	BP104	IF 1:100	Developmental Studies Hybridoma Bank
<i>D. melanogaster</i> fasciclin 2	mouse	1D4	IF 1:100	Developmental Studies Hybridoma Bank
<i>D. melanogaster</i> repo	mouse	8D12	IF 1:100	Developmental Studies Hybridoma Bank
<i>D. melanogaster</i> wrapper	mouse	10D3	IF 1:100	Developmental Studies Hybridoma Bank
<i>D. melanogaster</i> futsch	mouse	22C10	IF 1:100	Developmental Studies Hybridoma Bank
<i>D. melanogaster</i> even skipped	mouse	2B8	IF 1:100	Developmental Studies Hybridoma Bank
<i>D. melanogaster</i> cut	mouse	2B10	IF 1:100	Developmental Studies Hybridoma Bank
GFP	rabbit		IF 1:1000	Invitrogen

IB: immunoblot

IF: immunofluorescence

Table 2-7. Secondary antibodies

Specificity	Type	Dilution	Source
horseradish peroxidase (HRP)-conjugated anti-rabbit IgG	donkey	1:20,000	GE Healthcare UK Limited
HRP-conjugated anti-guinea pig IgG	goat	1:20,000	Sigma-Aldrich
AlexaFluor 488-conjugated IgG	goat	1:2,000	Invitrogen
AlexaFluor 568-conjugated IgG	goat	1:2,000	Invitrogen
Cy-2-conjugated IgG	goat	1:2,000	Jackson ImmunoResearch Laboratories
Cy-5-conjugated IgG	goat	1:2,000	Jackson ImmunoResearch Laboratories

Table 2-8. Oligonucleotides

Name	Sequence	Application
1316-DW-YIL160c	ggggttgtagtatgtgtatcggtactggtatgggtgccgcccatctttattaaagaa ggcgggtggcggggaagctcaaaaacttaaat	<i>POT1-GFP+</i> construction, fwd
1317-DW-YIL160c	aaatattgaaaatggaaaattataaacaattgataaaactacgtaatagcttttacaaa gacggtatcgataagctt	<i>POT1-GFP+</i> construction, rev
1664-FM1	gaattcatggtgagcaagggcgag	pRS426- <i>mRFP</i> , fwd
1665-FM2	ctcgagttactgtacagctcgtccat	pRS426- <i>mRFP</i> , rev

1678-FM5	tccatagtgttagagtctcta	checking oligo for <i>PEX3</i> gene
1679-FM6	tcacgcgctcccacttgaa	checking oligo for <i>mRFP</i> gene
1692-FM7	gatctgagcgccagcgatatacagcaacttggcgctctccagctcgttttccttcaagcc	<i>PEX3-mRFP</i> construction, fwd
1693-FM8	tcaatatatcaacctattttctccctttctctttttctccaagcgcctgtaaatcttg	<i>PEX3-mRFP</i> construction, rev
2121-FM21	tctaataattgaagaaaagtacaaaaacttgcaaatgaattggaaaaaacaac	<i>RTN1-mRFP</i> construction, fwd
2122-FM22	gctggaggcggtggcgagtgagcaaggcgaggat	<i>RTN1-mRFP</i> construction, rev
2183-RY-WebA-YOPI	gcacttttaactgcaatgggttaactgtagcaatgttgtaaaaaagcagggaagttc	<i>YOPI-mRFP/YOPI-pA</i> construction, fwd
2184-RY-WebB-YOPI	agtgatgaaattagagcttcctcaatgaggcttctaaggctacaggtgcttctgttca	<i>YOPI-mRFP/YOPI-pA</i> construction, rev
2300-FM71	gctatcttctgggacaccataaacgactccaaaatattttatgttaagtagcgatata	checking oligo for <i>PEX1</i> gene
2301-FM72	ctgacagctgtggtcacaat	checking oligo for <i>PEX5</i> gene
2302-FM73	ggagacgttgatctctctt	checking oligo for <i>PEX6</i> gene
2303-FM74	cgtcgctggttgataagatt	checking oligo for <i>PEX7</i> gene
2304-FM75	acctgtcgaatatggagagat	checking oligo for <i>PEX19</i> gene
2305-FM76	agcttggtgatagccctatta	checking oligo for <i>PEX30</i> gene
2460-RY-rtn1	tgccgaagcatcaaacatcaa	checking oligo for <i>RTN1</i> gene
2461-RY-rtn2	gcttggtgatcttctgtttcctat	checking oligo for <i>RTN2</i> gene
2462-RY-yop1	gagcaaaataattacgaaaagtgga	checking oligo for <i>YOPI</i> gene
2578-FM122	gtaagtaggttatatggctgctgga	checking oligo for <i>PEX29</i> gene
2579-FM123	aagtagttaatccattgaggga	checking oligo for <i>PEX31</i> gene
2580-FM124	agtaacaacaacgtatgacgat	checking oligo for <i>PEX32</i> gene
2697-FM129	taaccatgaggagtggtttgc	checking oligo for <i>PEX3</i> gene
2749-FM143	atactagtcacgtaaaagcag	checking oligo for <i>LEU2</i> gene
2750-FM144	aaatggaatatgttcattagggt	checking oligo for <i>LEU2</i> gene
2904-FM154	ttagtcatgaacgcttctct	<i>PEX30-GFP+/PEX30-pA</i> construction, fwd
2905-FM155rev	gatactgaagagaaagagcaatcaaatccaaccattggctcgcatagcaagaaggcc	<i>PEX30-GFP+/PEX30-pA</i> construction, rev
2966-FM158	gtaggcgggtggcggtgaagctcaaaaactta	checking oligo for <i>PEX30</i> gene
2967-FM159	attttaaaagtcataacgttgtagttaataaaaaaattggattactattcattgaagg	checking oligo for <i>PEX30</i> gene
2968-FM160	ctgacggtatcgataagctt	checking oligo for <i>PEX30</i> gene
	ctcttttctggttctttcatcag	
	tcgtatcactttttagtagtattgcca	
	agcctacaacagaagagacaaaaga	

2969-FM161	aaaactaagaatactttcccatcgc	checking oligo for <i>PEX30</i> gene
3052-BK826	gataataagtgaagaagaattacaaattgtgggaaccgaagtattgacggaagaa gaacatcgatgaattcgagctcg	<i>PEX19</i> deletion
3053-BK827	tctaggataatgaactacttttttttttttttactgttatcataaatatataaccgct gcaggctgcacggatc	<i>PEX19</i> deletion
3244-FM190	aattctagaccgtccaatcgtgaatattg	pMAL- <i>PEX29</i> , fwd
3245-FM188	aataagcttttatatagtgaattgagagtg	pMAL- <i>PEX29</i> , rev
3246-ES-ScPEX30	attctcgagtcatacggccttctgctatcgc	pMAL- <i>PEX30</i> , fwd
0094-324-RN	attcctgcagagtcatacggccttctgctatc	pMAL- <i>PEX30</i> , rev
3247- Cherry200bp	agccgtacatgaactgaggg	checking oligo for <i>mCherry</i> gene
3798-MDH2 3WebA	cagttaaagaaaaatcgcataagggttggaattcgtgcatcgagatcgcacatc tggtgaagctcaaaaactaat	<i>MDH2-GFP+</i> or <i>MDH2-mRFP</i> construction, fwd
3799-MDH2 3WebB	gactggcttaacgggaatattatcaattgtcgtcattcttgcttcgggccgatgctca gctgacggtatcgataagctt	<i>MDH2-GFP+</i> or <i>MDH2-mRFP</i> construction, fwd
3800-MDH2- CheckingC	gtccaattgtttctttgtattgg	checking oligo for <i>MDH2</i> gene
4017-FM252	ctgtctagtgatcctccggagtgtaaaaactgattttcaagattgtactgagagtgac	<i>PEX30</i> deletion
4018-FM253	tagagattatattatgtaaaggtaaaaacgggagcgcgactgtgctggtatttcacacc g	<i>PEX30</i> deletion
4019-FM254	acgtagcaaaatttcagtcctactgtatatacgtctagagattgtactgagagtgca c	<i>PEX29</i> deletion
4020-FM255	actgaacctttgacaatcgtacaacaaaaggatcccaaaactgtgcggtatttcacac cg	<i>PEX29</i> deletion
4216-RTN1webA	tctaataaattgaagaaaagtacaaaaaacttgcaaaatgaattggaaaaaacaac gctggtgaagctcaaaaactaat	<i>RTN1-pA</i> construction, fwd
4217-RTN1webB	gcacttttaactgcaatgggttaactgtagcaatgttggtaaaaaagcagggaaagttc agctgacggtatcgataagctt	<i>RTN1-pA</i> construction, rev
4313-FM281	gagtggtgaatcgatatctcttgaa	checking oligo for <i>PEX31</i> gene
4314-FM282	aaaatagcctcttgatcttcctcat	checking oligo for <i>PEX31</i> gene
4400-FM287	agatagcttgtagggtttggcttat	checking oligo for <i>PEX29</i> gene
4401-FM288	tatccaggttaattgcttgaattgt	checking oligo for <i>PEX29</i> gene
4971-FM418	attgaattcatgtcggataaggagaagaaaa	<i>YIPEX23-mCherry</i> construction
4972-FM419	tatatctcctctctcttagagtcctcctcg	<i>YIPEX23-mCherry</i> construction
4973-FM420	gactctaagagagaaggagatatacatggcgg	<i>YIPEX23-mCherry</i> construction
5241-FM430	caagcgtatatatatataatataattcacacacgcaaatagattgtactgagagtgca c	<i>RTN1</i> deletion
5242-FM431	aagttagctattcttgtttgaaatgaaaaaaaaaagcacctgtgcggtatttcacacc g	<i>RTN1</i> deletion
5243-FM432	ttcaattgctgtctcaacttgccacaaactatcatcaacagattgtactgagagtgca c	<i>RTN2</i> deletion
5244-FM433	ctactagctagaagaagagagaaaaaaaaaactagactgtgcggtatttcaca ccg	<i>RTN2</i> deletion
5245-FM434	agtgaaaacaaataacaaagacataaccgcactccaatcagattgtactgagagtg cac	<i>YOP1</i> deletion
5246-FM435	aaaacgagagtttgatttgaggataggtgagttgcctcctgtgcggtatttcacaccg	<i>YOP1</i> deletion
0753-CT/KAR2-f	atgctgctaacgatgttttag	checking oligo for <i>KAR2</i> gene

0754-CT/KAR2-r	cgcaaaattagcatattgatga	checking oligo for KAR2 gene
I008-BK-BK184	gggtttagtatgtgtatcg	checking oligo for <i>POT1</i> gene
0775-RP-GFP+200bp5'out	cgggaaaagcattgaacacca	checking oligo for <i>GFP+</i> gene
0776-RP-GFP+520bp3'out	aattcgccacaacattgaagat	checking oligo for <i>GFP+</i> gene
AA1295-479GFP-F	gacgcggatgcatcttatccgtcaatgaagactaacagacactctcaattcaacta taggtgaagctcaaaaacttaat	<i>PEX29-GFP+ / PEX29-pA</i> construction, fwd
AA1296-479GFP-R	ctcacttacaaaccttttatcgaaaagaatcaagagaaaaaatggaaaagaagaa aaggctgacggatcgataagctt	<i>PEX29-GFP+ / PEX29-pA</i> construction, rev
AA1339-YGR004w-CFP-F	ccttcctcggacagtagcaaattaatacaaatatctgatgtttcaatgtctccttctcta ggtgaagctcaaaaacttaat	<i>PEX31-GFP+</i> construction, fwd
AA1340-YGR004w-CFP-R	aacttgccataaccgcgcagatactttaagcacaagattgaattgtgtccatgcag cgctgacggatcgataagctt	<i>PEX31-GFP+</i> construction, rev
AA1341-YBR168w-CFP-R	attatgaaataacatacacaaagtcacatgatctataaagttttactgtctctatgtt gctgacggatcgataagctt	<i>PEX32-GFP+</i> construction, fwd
AA1342-YBR168w-CFP-F	tacagttctttgaaagttttaccaggtcaagaaaatggaaacgacgcctcttcatt gggtgaagctcaaaaacttaat	<i>PEX32-GFP+</i> construction, rev
AA1398-YDR-479-F	gggagcaccgactgttatgatct	checking oligo for <i>PEX29</i>
AA1399-YHR150W-R	gtcgtttacttgatgtattgaggg	checking oligo for <i>PEX28</i>
AA1400-YHR150wF	gccttactgccgaacgactgg	checking oligo for <i>PEX28</i>
AA1401-YDR479C-R	gggtactccgcgaacttggcggc	checking oligo for <i>PEX29</i>
AA1405-YBR168W-R	gggcacgcgctgcaagtgatgatagcg	checking oligo for <i>PEX32</i>
AA1406-YBR168W-F	ggcgtcaataaggagtggttctggca	checking oligo for <i>PEX32</i>
AA1441-YGR004W-A	gagtgggtaatcgatatctcttgaa	checking oligo for <i>PEX31</i>
AA1442-YBR168W-A	attattcaaccatattgagctggac	checking oligo for <i>PEX32</i>
AA1443-YLR324W-A	ctcttttctggttctttcatcag	checking oligo for <i>PEX30</i>
AA1444-YDR479C-A	tgtatgtatacgctctaattgtccga	checking oligo for <i>PEX29</i>
AA1445-YHR150W-A	tcttttcgatgaactttcctatttg	checking oligo for <i>PEX28</i>
AA1446-KANB	ctgcagcaggagccgtaat	checking oligo for <i>KanMX</i>
AA1447-KANC	tgattttgatgacgagcgaat	checking oligo for <i>KanMX</i>
0522-Thiol-C	gaagcgaagaatgtctaataccaa	checking oligo for <i>POT1</i>
0523-Thiol-D	tgaagaagtttctcttcatggac	checking oligo for <i>POT1</i>
0524-Thiol-A	agttttgaacctatgccacaaatag	checking oligo for <i>POT1</i>
0625-URA3Rev	ccaatgtcagcaaatctctg	checking oligo for <i>URA3</i>
0921-CT-PEX19PrA	cagaatgtaagcataaaaggag	checking oligo for <i>PEX19</i>
0922-CT-PEX19PrB	ttaacctgtctagcgtattgg	checking oligo for <i>PEX19</i>
0923-CT-URA3r	catccacgggtctatactgtt	checking oligo for <i>URA3</i>
I796-FM16	ctcgagttatagtttagactgtacagctcgtccatg	pRS426- <i>mRFP-SKL</i>

I200-CT- templatePCR	taatacgactcactatagggagaccacgggcgggt	To make template for dsRNA production
I298-CT- templatePCR2	taatacgactcactatagggga	To make template for dsRNA production

Table 2-9. Common solutions

Solution	Composition	Reference
1 × PBS	137mM NaCl, 2.7 mM KCl, 8 mM Na ₂ HPO ₄ , 1.5 mM K ₂ HPO ₄ , pH 7.3	Pringle et al., 1991
1 × TBST	20 mM Tris-HCl, pH 7.5, 150 mM NaCl, 0.05% (w/v) Tween 20	Huynh et al., 1988
1 × transfer buffer	20 mM Tris-HCl, 150 mM glycine, 20% (v/v) methanol	Towbin et al., 1979; Burnette, 1981
5 × SDS-PAGE running buffer	0.25 M Tris-HCl, pH 8.8, 2 M glycine, 0.5% SDS	Ausubel et al., 1989
10 × TBE	0.89 M Tris-borate, 0.89 M boric acid, 0.02 M EDTA	Maniatis et al., 1982
2 × sample buffer	20% (v/v) glycerol, 167 mM Tris-HCl, pH 6.8, 2% SDS, 0.005% bromophenol blue	Ausubel et al., 1989
6 × DNA loading dye	0.25% bromophenol blue, 0.25% xylene cyanol, 30% (v/v) glycerol	Maniatis et al., 1982
breakage buffer, yeast	2% (v/v) Triton X-100, 1% SDS, 100 mM NaCl, 10 mM Tris-HCl, pH 8.0, 1 mM EDTA, pH 8.0	Ausubel et al., 1989
disruption buffer	20 mM Tris-HCl, pH 7.5, 0.1 mM EDTA, pH 7.5, 100 mM KCl, 10% (w/v) glycerol	Eitzen, 1997
Ponceau stain	0.1% Ponceau S, 1% TCA	Szilard, 2000
solution B	100 mM KH ₂ PO ₄ , 100 mM K ₂ HPO ₄ , 1.2 M sorbitol	Pringle et al., 1991
TE	10 mM Tris-HCl, pH 7.0-8.0 (as needed), 1 mM EDTA	Maniatis et al., 1982

2.2 Microorganisms and culture conditions

2.2.1 Bacterial strains and culture conditions

Cells of *Escherichia coli* strain DH5 α (F, Φ 80dlacZ Δ M15, Δ (lacZYA-argF), U169, *recA*¹, *endA*¹, *hsdR*¹7(r_k⁻, m_k⁺), *phoA*, *supE*44, λ ⁻, *thi*-1, *gyrA*96, *relA*¹) were grown at 37°C. Cultures of 5 mL or

less were grown in culture tubes in a rotary shaker at 200 rpm. Cultures greater than 5 mL were grown in flasks in a rotary shaker at 250 rpm. Culture volumes were approximately 20% of flask volumes. For short term storage, cultures were maintained on agar plates at 4°C for 1 week. For longer term storage, glycerol was added to liquid culture at a 30% (v/v) final concentration and the suspension frozen and stored at -80°C.

Table 2-10. Bacterial culture media

Medium	Composition	Reference
LB ^a	1% tryptone, 0.5% yeast extract, 1% NaCl	Maniatis et al., 1982
SOB	2% tryptone, 0.5% yeast extract, 10 mM NaCl, 2.5 mM KCl	Maniatis et al., 1982

^aFor solid media, agar was added to 2%.

2.2.2 Yeast strains and culture conditions

The *S. cerevisiae* and *Y. lipolytica* strains used in this study are listed in Table 2-11. Yeast culture media are described in Table 2-12. Yeasts were grown at 30°C, unless otherwise indicated. Cultures of 10 mL or less were grown in 16 × 150-mm glass tubes in a rotating wheel. Cultures greater than 10 mL were grown in flasks in a rotary shaker at 250 rpm. Culture volumes were approximately 20% of flask volumes. For short term storage cultures were maintained on agar plates at 4°C for 1-6 months. For longer term storage, glycerol was added to liquid culture at a 30% (v/v) final concentration and the suspension frozen and stored at -80°C.

Table 2-11. *S. cerevisiae* and *Y. lipolytica* strains

Strain	Genotype	Reference
<i>S. cerevisiae</i>		
BY4741	<i>MATα, his3Δ1, leu2Δ0, met15Δ0, ura3Δ0</i>	Giaever et al., 2002
BY4742	<i>MATα, his3Δ1, leu2Δ0, lys2Δ0, ura3Δ0</i>	Giaever et al., 2002
RSY521	<i>MATα, ura3-52, trp1-1, his4-401, leu2-3, 112, HOL1-1</i>	Randy Schekman, University of California, Berkeley

RSY1132	<i>MATα, leu2-3,-112, ura3-52, trp1-1, sec61-3</i>	Stirling et al., 1992
R1158	<i>MATα, his3Δ1, leu2Δ0, met15Δ0, URA3::CMV-tTa</i>	Hughes et al., 2000
POT1-GFP+	<i>MATα, his3Δ1, leu2Δ0, lys2Δ0, ura3Δ0, pot1::POT1-GFP (HIS5)</i>	this study
pex3 Δ /POT1-GFP+	<i>MATα, his3Δ1, leu2Δ0, lys2Δ0, ura3Δ0, pex3::KanMX4, pot1::POT1-GFP (HIS5)</i>	this study
PEX3-GFP+/POT1-mRFP	<i>MATα, his3Δ1, leu2Δ0, lys2Δ0, ura3Δ0, pex3::PEX3-GFP (HIS5), pot1::POT1-mRFP (URA3)</i>	this study
PEX1-GFP	<i>MATα, his3Δ1, leu2Δ0, lys2Δ0, ura3Δ0, pex1::PEX1-GFP (HIS3MX6)</i>	Huh et al., 2003
PEX5-GFP	<i>MATα, his3Δ1, leu2Δ0, lys2Δ0, ura3Δ0, pex5::PEX5-GFP (HIS3MX6)</i>	Huh et al., 2003
PEX6-GFP	<i>MATα, his3Δ1, leu2Δ0, lys2Δ0, ura3Δ0, pex6::PEX6-GFP (HIS3MX6)</i>	Huh et al., 2003
PEX11-GFP	<i>MATα, his3Δ1, leu2Δ0, lys2Δ0, ura3Δ0, pex11::PEX11-GFP (HIS3MX6)</i>	Huh et al., 2003
PEX13-GFP	<i>MATα, his3Δ1, leu2Δ0, lys2Δ0, ura3Δ0, pex13::PEX13-GFP (HIS3MX6)</i>	Huh et al., 2003
PEX15-GFP	<i>MATα, his3Δ1, leu2Δ0, lys2Δ0, ura3Δ0, pex15::PEX15-GFP (HIS3MX6)</i>	Huh et al., 2003
PEX25-GFP	<i>MATα, his3Δ1, leu2Δ0, lys2Δ0, ura3Δ0, pex25::PEX25-GFP (HIS3MX6)</i>	Huh et al., 2003
PEX29-GFP	<i>MATα, his3Δ1, leu2Δ0, lys2Δ0, ura3Δ0, pex29::PEX29-GFP (HIS3MX6)</i>	Huh et al., 2003
PEX30-GFP	<i>MATα, his3Δ1, leu2Δ0, lys2Δ0, ura3Δ0, pex30::PEX30-GFP (HIS3MX6)</i>	Huh et al., 2003
R1158/PEX3-GFP+	<i>MATα, his3Δ1, leu2Δ0, met15Δ0, URA3::CMV-tTa, pex3::PEX3-GFP+ (HIS5)</i>	Perry et al., 2009
THCSEC61/PEX3-GFP+	<i>MATα, his3Δ1, leu2Δ0, met15Δ0, URA3::CMV-tTa, pSEC61::tet07-TATA(KanMX6), pex3::PEX3-GFP+ (HIS5)</i>	Perry et al., 2009
THCSEC14/PEX3-GFP+	<i>MATα, his3Δ1, leu2Δ0, met15Δ0, URA3::CMV-tTa, pSEC61::tet07-TATA(KanMX6), pex3::PEX3-GFP+ (HIS5)</i>	Perry et al., 2009
RSY521/PEX3-GFP+	<i>MATα, ura3-52, trp1-1, his4-401, leu2-3, 112, HOL1-1, pex3::PEX3-GFP (HIS5)</i>	this study
RSY1132/PEX3-GFP+	<i>MATα, leu2-3,-112, ura3-52, trp1-1, sec61-3</i>	this study
PEX30-GFP+	<i>MATα, his3Δ1, leu2Δ0, lys2Δ0, ura3Δ0, pex30::PEX30-GFP (HIS5)</i>	this study
MDH2-GFP+	<i>MATα, his3Δ1, leu2Δ0, lys2Δ0, ura3Δ0, mdh2::MDH2-GFP (HIS5)</i>	this study
pex3 Δ /MDH2-GFP+	<i>MATα, his3Δ1, leu2Δ0, lys2Δ0, ura3Δ0, pex3::KanMX4, mdh2::MDH2-GFP (HIS5)</i>	this study
pex5 Δ /MDH2-GFP+	<i>MATα, his3Δ1, leu2Δ0, lys2Δ0, ura3Δ0, pex5::KanMX4, mdh2::MDH2-GFP (HIS5)</i>	this study
pex7 Δ /MDH2-GFP+	<i>MATα, his3Δ1, leu2Δ0, lys2Δ0, ura3Δ0, pex7::KanMX4, mdh2::MDH2-GFP (HIS5)</i>	this study
PEX3-GFP+/MDH2-mRFP	<i>MATα/a, his3Δ1/his3Δ1, leu2Δ0/leu2Δ0, lys2Δ0/LYS2, MET15/met15Δ0, ura3Δ0/ura3Δ0, pex30::PEX30-GFP (HIS5)/PEX30, mdh2::MDH2-mRFP (URA3)/MDH2</i>	this study
PEX30-GFP+/CHC1-mRFP	<i>MATα/a, his3Δ1/his3Δ1, leu2Δ0/leu2Δ0, lys2Δ0/LYS2, MET15/met15Δ0, ura3Δ0/ura3Δ0, PEX30/pex30::PEX30-GFP (HIS5), chc1::CHC1-mRFP (KanMX4)/CHC1</i>	this study

PEX30-GFP+/COP1-mRFP	MAT α /a, his3 Δ 1/his3 Δ 1, leu2 Δ 0/leu2 Δ 0, lys2 Δ 0/LYS2, MET15/met15 Δ 0, ura3 Δ 0/ura3 Δ 0, PEX30/pex30::PEX30-GFP (HIS5), cop1::COP1-mRFP (KanMX4)/COP1	this study
PEX30-GFP+/ERG6-mRFP	MAT α /a, his3 Δ 1/his3 Δ 1, leu2 Δ 0/leu2 Δ 0, lys2 Δ 0/LYS2, MET15/met15 Δ 0, ura3 Δ 0/ura3 Δ 0, PEX30/pex30::PEX30-GFP (HIS5), erg6::ERG6-mRFP (KanMX4)/ERG6	this study
PEX30-GFP+/NIC96-mRFP	MAT α /a, his3 Δ 1/his3 Δ 1, leu2 Δ 0/leu2 Δ 0, lys2 Δ 0/LYS2, MET15/met15 Δ 0, ura3 Δ 0/ura3 Δ 0, PEX30/pex30::PEX30-GFP (HIS5), nic96::NIC96-mRFP (KanMX4)/NIC96	this study
PEX30-GFP+/PEX3-mRFP	MAT α /a, his3 Δ 1/his3 Δ 1, leu2 Δ 0/leu2 Δ 0, lys2 Δ 0/LYS2, MET15/met15 Δ 0, ura3 Δ 0/ura3 Δ 0, PEX30/pex30::PEX30-GFP (HIS5), pex3::PEX3-mRFP (KanMX4)/PEX3	this study
PEX30-GFP+/SAC6-mRFP	MAT α /a, his3 Δ 1/his3 Δ 1, leu2 Δ 0/leu2 Δ 0, lys2 Δ 0/LYS2, MET15/met15 Δ 0, ura3 Δ 0/ura3 Δ 0, PEX30/pex30::PEX30-GFP (HIS5), sac6::SAC6-mRFP (KanMX4)/SAC6	this study
PEX30-GFP+/SEC13-mRFP	MAT α /a, his3 Δ 1/his3 Δ 1, leu2 Δ 0/leu2 Δ 0, lys2 Δ 0/LYS2, MET15/met15 Δ 0, ura3 Δ 0/ura3 Δ 0, PEX30/pex30::PEX30-GFP (HIS5), sec13::SEC13-mRFP (KanMX4)/SEC13	this study
PEX30-GFP+/SNF7-mRFP	MAT α /a, his3 Δ 1/his3 Δ 1, leu2 Δ 0/leu2 Δ 0, lys2 Δ 0/LYS2, MET15/met15 Δ 0, ura3 Δ 0/ura3 Δ 0, PEX30/pex30::PEX30-GFP (HIS5), snf7::SNF7-mRFP (KanMX4)/SNF7	this study
PEX30-GFP+/PEX3-mRFP	MAT α , his3 Δ 1, leu2 Δ 0, lys2 Δ 0, ura3 Δ 0, pex30::PEX30-GFP (HIS5), pex3::PEX3-mRFP (URA3)	this study
PEX30-GFP+/POT1-mRFP	MAT α , his3 Δ 1, leu2 Δ 0, lys2 Δ 0, ura3 Δ 0, pex30::PEX30-GFP (HIS5), pot1::POT1-mRFP (URA3)	this study
PEX30-GFP+/MDH2-mRFP	MAT α , his3 Δ 1, leu2 Δ 0, lys2 Δ 0, ura3 Δ 0, pex30::PEX30-GFP (HIS5), mdh2::MDH2-mRFP (URA3)	this study
PEX30-GFP+/KAR2-mRFP-HDEL	MAT α , his3 Δ 1, leu2 Δ 0, lys2 Δ 0, ura3 Δ 0, pex30::PEX30-GFP (HIS5), kar2::KAR2-mRFP-HDEL (URA3)	this study
pex3 Δ	MAT α , his3 Δ 1, leu2 Δ 0, lys2 Δ 0, ura3 Δ 0, pex3::KanMX4	Giaever et al., 2002
pex19 Δ	MAT α , his3 Δ 1, leu2 Δ 0, lys2 Δ 0, ura3 Δ 0, pex19::KanMX4	Giaever et al., 2002
PEX30-pA	MAT α , his3 Δ 1, leu2 Δ 0, lys2 Δ 0, ura3 Δ 0, pex30::PEX30-pA (HIS5)	this study
PEX29-pA	MAT α , his3 Δ 1, leu2 Δ 0, lys2 Δ 0, ura3 Δ 0, pex29::PEX29-pA (HIS5)	this study
RTN1-pA	MAT α , his3 Δ 1, leu2 Δ 0, lys2 Δ 0, ura3 Δ 0, rtn1::RTN1-pA (HIS5)	this study
YOP1-pA	MAT α , his3 Δ 1, leu2 Δ 0, lys2 Δ 0, ura3 Δ 0, yop1::YOP1-pA (HIS5)	this study
PEX30-GFP+/MDH2-mRFP	MAT α /a, his3 Δ 1/his3 Δ 1, leu2 Δ 0/leu2 Δ 0, lys2 Δ 0/LYS2, MET15/met15 Δ 0, ura3 Δ 0/ura3 Δ 0, pex30::PEX30-GFP (HIS5)/PEX30, mdh2::MDH2-mRFP (URA3)/MDH2	this study
PEX30-GFP+/POT1-mRFP	MAT α /a, his3 Δ 1/his3 Δ 1, leu2 Δ 0/leu2 Δ 0, lys2 Δ 0/LYS2, MET15/met15 Δ 0, ura3 Δ 0/ura3 Δ 0, pex30::PEX30-GFP (HIS5)/PEX30, pot::POT1-mRFP (URA3)/POT1	this study
PEX29-GFP+/MDH2-mRFP	MAT α /a, his3 Δ 1/his3 Δ 1, leu2 Δ 0/leu2 Δ 0, lys2 Δ 0/LYS2, MET15/met15 Δ 0, ura3 Δ 0/ura3 Δ 0, pex29::PEX29-GFP (HIS5)/PEX29, mdh2::MDH2-mRFP (URA3)/MDH2	this study
PEX29-GFP+/POT1-mRFP	MAT α /a, his3 Δ 1/his3 Δ 1, leu2 Δ 0/leu2 Δ 0, lys2 Δ 0/LYS2, MET15/met15 Δ 0, ura3 Δ 0/ura3 Δ 0, pex29::PEX29-GFP (HIS5)/PEX29, pot::POT1-mRFP (URA3)/POT1	this study
PEX30-	MAT α , his3 Δ 1, leu2 Δ 0, lys2 Δ 0, ura3 Δ 0, pex30::PEX30-GFP	this study

GFP+ /pmRFP-SKL	(HIS5), pmRFP-SKL (URA3)	
PEX30-GFP/RTN1-mCherry	MATa/a, his3Δ1/his3Δ1, leu2Δ0/leu2Δ0, lys2Δ0/LYS2, MET15/met15Δ0, ura3Δ0/ura3Δ0, pex30::PEX30-GFP (kanMX4)/PEX30, rtn1::RTN1-mCherry (hphNT1)/RTN1	this study
PEX30-GFP/YOPI-mCherry	MATa/a, his3Δ1/his3Δ1, leu2Δ0/leu2Δ0, lys2Δ0/LYS2, MET15/met15Δ0, ura3Δ0/ura3Δ0, pex30::PEX30-GFP (kanMX4)/PEX30, yop1::YOPI-mCherry (hphNT1)/YOPI	this study
PEX29-GFP/PEX30-mCherry	MATa/a, his3Δ1/his3Δ1, leu2Δ0/leu2Δ0, lys2Δ0/LYS2, MET15/met15Δ0, ura3Δ0/ura3Δ0, pex29::PEX29-GFP (kanMX4)/PEX29, pex30::PEX30-mCherry (hphNT1)/PEX30	this study
PEX29-GFP/RTN1-mCherry	MATa/a, his3Δ1/his3Δ1, leu2Δ0/leu2Δ0, lys2Δ0/LYS2, MET15/met15Δ0, ura3Δ0/ura3Δ0, pex29::PEX29-GFP (kanMX4)/PEX29, rtn1::RTN1-mCherry (hphNT1)/RTN1	this study
PEX29-GFP/YOPI-mCherry	MATa/a, his3Δ1/his3Δ1, leu2Δ0/leu2Δ0, lys2Δ0/LYS2, MET15/met15Δ0, ura3Δ0/ura3Δ0, pex29::PEX29-GFP (kanMX4)/PEX29, yop1::YOPI-mCherry (hphNT1)/YOPI	this study
ptetO7-TATA-Pex19/GFP1-GFP+	MATa, his3Δ1, leu2Δ0, met15Δ0, URA3::CMV-tTa, pPEX19::KanMX4-tetO7-TATA, gpd1::GPD1-GFP (HIS5)	this study
ptetO7-TATA-Pex19/GFP1-GFP+/rtn1Δ/rtn2Δ/yop1Δ	MATa, his3Δ1, leu2Δ0, met15Δ0, URA3::CMV-tTa, pPEX19::KanMX4-tetO7-TATA, gpd1::GPD1-GFP (HIS5), rtn1::natNT2, rtn2::hphNT1, yop1::leu2	this study
PEX3-GFP	MATa, his3Δ1, leu2Δ0, lys2Δ0, ura3Δ0, pex3::PEX3-GFP (HIS3MX6)	this study
pex29Δ/pex30Δ/PEX3-GFP	MATa, his3Δ1, leu2Δ0, ura3Δ0, pex29::KanMX4, pex30::KanMX4, pex3::PEX3-GFP (HIS3MX6)	this study
rtn1Δ/rtn2Δ/yop1Δ/PEX3-GFP	MATa, his3Δ1, leu2Δ0, ura3Δ0, rtn1::KanMX4, rtn2::KanMX4, yop1::KanMX4, pex3::PEX3-GFP (HIS3MX6)	this study
vps1Δ/PEX3-GFP	MATa, his3Δ1, leu2Δ0, lys2Δ0, ura3Δ0, pex3::PEX3-GFP (HIS3MX6), vps1::hphNT1	this study
pex19Δ/PEX3-GFP	MATa, his3Δ1, leu2Δ0, lys2Δ0, ura3Δ0, pex19::URA3, pex3::PEX3-GFP (HIS3MX6)	this study
pex19Δ/pex29Δ/pex30Δ/PEX3-GFP	MATa, his3Δ1, leu2Δ0, ura3Δ0, pex29::KanMX4, pex30::KanMX4, pex3::PEX3-GFP (HIS3MX6), pex19::URA3	this study
pex19Δ/rtn1Δ/rtn2Δ/yop1Δ/PEX3-GFP	MATa, his3Δ1, leu2Δ0, ura3Δ0, rtn1::KanMX4, rtn2::KanMX4, yop1::KanMX4, pex3::PEX3-GFP (HIS3MX6), pex19::URA3	this study
PEX29-GFP+/POT1-mRFP	MATa, his3Δ1, leu2Δ0, lys2Δ0, ura3Δ0, pex29::PEX29-GFP (HIS5), pot1::POT1-mRFP (URA3)	this study
PEX29-GFP+/RTN1-mRFP	MATa, his3Δ1, leu2Δ0, lys2Δ0, ura3Δ0, pex29::PEX29-GFP (HIS5), rtn1::RTN1-mRFP (URA3)	this study
PEX30-GFP+/POT1-mRFP	MATa, his3Δ1, leu2Δ0, lys2Δ0, ura3Δ0, pex30::PEX30-GFP (HIS5), pot1::POT1-mRFP (URA3)	this study
PEX30-GFP+/RTN1-mRFP	MATa, his3Δ1, leu2Δ0, lys2Δ0, ura3Δ0, pex30::PEX30-GFP (HIS5), rtn1::RTN1-mRFP (URA3)	this study
PEX31-GFP+/POT1-mRFP	MATa, his3Δ1, leu2Δ0, lys2Δ0, ura3Δ0, pex31::PEX31-GFP (HIS5), pot1::POT1-mRFP (URA3)	this study
PEX31-GFP+/RTN1-mRFP	MATa, his3Δ1, leu2Δ0, lys2Δ0, ura3Δ0, pex31::PEX31-GFP (HIS5), rtn1::RTN1-mRFP (URA3)	this study
PEX32-GFP+/POT1-mRFP	MATa, his3Δ1, leu2Δ0, lys2Δ0, ura3Δ0, pex32::PEX32-GFP (HIS5), pot1::POT1-mRFP (URA3)	this study
PEX32-	MATa, his3Δ1, leu2Δ0, lys2Δ0, ura3Δ0, pex32::PEX32-GFP	this study

GFP+/RTN1-mRFP (HIS5), *rtn1* I::RTN1-mRFP (URA3)

Y. lipolytica

E34	<i>MATα</i> , <i>ura3-302</i> , <i>leu2-270</i> , <i>lys8-11</i> , <i>pot1</i> :: <i>POT1-GFP</i> (LEU2)	Chang et al., 2007
E34 pTC3-PEX23-mCherry	<i>MATα</i> , <i>ura3-302</i> , <i>leu2-270</i> , <i>lys8-11</i> , <i>pot1</i> :: <i>POT1-GFP</i> (LEU2), pTC3-PEX23-mCherry (URA3)	this study

Table 2-12. Yeast culture media

Medium	Composition ^a	Reference
nonfluorescent medium ^c	6.61 mM KH ₂ PO ₄ , 1.32 mM K ₂ HPO ₄ , 4.06 mM MgSO ₄ ·7H ₂ O, 26.64 mM (NH ₄)SO ₄ , 1 × CSM, 2% glucose	Fagarasanu et al., 2006
nonfluorescent, nonfermentative medium ^c	6.61 mM KH ₂ PO ₄ , 1.32 mM K ₂ HPO ₄ , 4.06 mM MgSO ₄ ·7H ₂ O, 26.64 mM (NH ₄)SO ₄ , 1 × CSM, 0.6 M sorbitol, 1% glycerol	this study
SCIM	0.67% YNB, 0.5% yeast extract, 0.5% peptone, 0.5% Tween (w/v) 40, 0.3% glucose, 0.3% (v/v) oleic acid, 1 × CSM	Fagarasanu et al., 2006
SM	0.67% YNB, 2% glucose, 1 × CSM without histidine, leucine, lysine, methionine or uracil as required	Tam et al., 2005
YEPA	1% yeast extract, 2% peptone, 2% sodium acetate	Brade, 1992
YEPD	1% yeast extract, 2% peptone, 2% glucose, supplemented with 400 mg/mL geneticin, 125 mg/mL hygromycin, or 100 mg/mL nourseothricin as required	Rose et al., 1988
YEPR	1% yeast extract, 2% peptone, 2% raffinose	Rose et al., 1988
YPBO	0.3% yeast extract, 0.5% peptone, 0.5% K ₂ HPO ₄ , 0.5% KH ₂ PO ₄ , 0.2% (w/v) Tween 40 or 1% (v/v) Brij 35, 1% (v/v) oleic acid	Kamiryo et al., 1982

^aFor solid media, agar was added to 2%.

2.2.3 Mating of *S. cerevisiae*

S. cerevisiae strains were mated according to the method of Rose et al. (1988). Haploid strains of opposite mating types were streaked in single straight lines on separate YEPD agar plates (Table 2-12) and incubated overnight. They were then replica-plated onto a fresh YEPD agar in such a way that streaks of cells of opposite mating types were perpendicular to each other and incubated overnight. Cells on this plate were then replica-plated onto SM agar (Table 2-12) supplemented for the auxotrophic requirements of the diploid strain. Diploid cells appeared after overnight incubation.

2.3 DNA manipulation and analysis

Unless otherwise indicated, reactions were carried out in 1.5-mL microcentrifuge tubes, and microcentrifugation was performed in an Eppendorf microcentrifuge at $16,000 \times g$.

2.3.1 Amplification of DNA by the polymerase chain reaction (PCR)

PCR was used to amplify specific DNA sequences from chromosomal or plasmid DNA, which sometimes also introduced modifications in the amplified DNA sequence including recognition sites for restriction endonucleases or intracellular targeting sequences for the encoded proteins. Primer design, reaction components and cycling conditions were performed following standard protocols (Innis and Gelfand, 1990; Saiki, 1990). A reaction usually contained 0.1 to 0.5 μ g of yeast genomic DNA or 0.1 to 0.2 μ g of plasmid DNA to act as a template for the reaction. Each reaction also contained 20 pmol each of a forward and reverse primer, 0.25 mM of each dNTP, 1 mM Mg_2SO_4 , and 1.25 U of Easy-A high-fidelity polymerase in 50 μ l of the supplied reaction buffer (Stratagene). Reactions were performed in 0.6-ml microcentrifuge tubes in a Robocycler 40 with a Hot Top attachment (Stratagene) or in 0.2 mL microfuge tubes in a 2720 Thermocycler (Applied Biosystems). Alternatively, when fidelity of the reaction was not important, Ready-to-Go PCR Beads were used as recommended by the manufacturer (Amersham Biosciences) or 1.25 U of Taq polymerase in the supplied reaction buffer (NEB).

2.3.2 Digestion of DNA by restriction endonucleases

In general, 1 to 2 μ g of plasmid DNA or purified DNA was digested by restriction endonucleases for 1 to 3 h according to the manufacturer's instructions (NEB). Digestion was immediately terminated by agarose gel electrophoresis of the DNA fragments, except for plasmid DNA linearized by a single restriction endonuclease, which required dephosphorylation.

2.3.3 Dephosphorylation of 5'-ends

Plasmid DNA linearized by a single restriction endonuclease was subjected to dephosphorylation at its 5'-ends to prevent spontaneous intramolecular (and intermolecular) ligations. After digestion of plasmids, reactions were mixed with 10 U of CIP and incubated at 37°C for 30 min. The dephosphorylation reaction was terminated by agarose gel electrophoresis of the DNA fragments.

2.3.4 Separation of DNA fragments by agarose gel electrophoresis

DNA fragments in solution were mixed with 0.2 volume of 6 × DNA loading dye (Table 2-4) and separated by electrophoresis in 1% agarose gels in 1 × TBE (Table 2-4) containing 0.5 µg of ethidium bromide/ml. Gels were subjected to electrophoresis at 10 V/cm in 1 × TBE, and DNA fragments were subsequently visualized on an ultraviolet transilluminator (Photodyne, Model 3-3006).

2.3.5 Purification of DNA fragments from agarose gel

When a DNA fragment required purification, e.g. after a digestion reaction, it was separated by electrophoresis in an agarose gel and the desired band was excised with a razor blade. DNA was extracted from the excised agarose slice using the QIAquick Gel Extraction Kit according to manufacturer's instructions (Qiagen). This method is based on the dissolution of agarose gel and subsequent selective adsorption of DNA to a silica membrane in the presence of a high concentration of chaotropic salts, followed by washing and elution of DNA in the presence of low salt. DNA was eluted in 20 to 50 µL of the supplied elution buffer.

2.3.6 Purification of DNA from solution

Contaminants (small oligonucleotides, salts, enzymes, etc.) were removed from a DNA solution using the QIAquick PCR Purification Kit as described by the manufacturer (Qiagen). Again, the principle of this method is the selective adsorption of DNA to a silica membrane in the presence

of chaotropic salts, followed by washing and elution of DNA in the presence of low salt. DNA was eluted in 20 to 50 μL of the supplied elution buffer.

2.3.7 Ligation of DNA fragments

DNA fragments treated with restriction endonucleases and purified as described in Section 2.5.5 were ligated using ~ 400 U of T4 DNA ligase in the buffer supplied by the manufacturer (NEB). Reactions were typically conducted in a volume of 20 μL , with the molar ratio of plasmid to insert varying between 1:1 and 1:10, and incubated overnight at 16°C. Occasionally, PCR products after purification by agarose gel electrophoresis were ligated with the vector pGEM-T Easy using the pGEM-T Easy Vector System according to the manufacturer's instructions (Promega).

2.3.8 DNA sequencing

DNA sequencing was performed using the BigDye Terminator v1.1/3.1 Cycle Sequencing Ready Reaction Kit as described by the manufacturer (Applied Biosystems). This method is based on the method of Sanger et al. (1977) and involves the random incorporation of fluorescent dideoxy terminators during the elongation of DNA sequences with a modified version of *Taq* DNA polymerase. Essentially, a reaction contained 1 ng of plasmid DNA, 3.2 pmol of primer, 3 μL of Terminator Ready Reaction Mix, and 2.5 μL of the supplied 5 \times buffer in a total volume of 20 μL . The reaction was subjected to cycle sequencing using the Robocycler 40 with a Hot Top attachment, or the 2720 Thermocycler (Applied Biosystems), and the following conditions: 1 cycle at 96°C for 2 min; 25 cycles at 96°C for 46 sec, 50°C for 51 sec and 60°C for 4 min 10 sec; 1 cycle at 6°C to hold until ready to purify. Reaction products were precipitated with 80 μL of 75% (v/v) isopropanol for 20 min at room temperature, subjected to microcentrifugation at 16,000 $\times g$ for 20 min, washed twice with 250 μL of 75% isopropanol, dried in a rotary vacuum dessicator and resuspended in 15 μL of Template Suppression Reagent. They were then heated at 95°C for 2 min

and immediately cooled on ice. Finally, they were separated by capillary electrophoresis, and fluorescence was detected and recorded by an ABI 310 Genetic Analyzer (Applied Biosystems).

2.4 Introduction of DNA into microorganisms

2.4.1 Chemical transformation of *E. coli*

Plasmid DNA was introduced into Subcloning Efficiency, chemically competent *E. coli* DH5 α cells, as recommended by the supplier (Invitrogen). Chemically competent *E. coli* DH5 α cells were prepared by growing a cell culture in 200 mL of LB liquid to an OD₆₀₀ of ~0.35. Cells were harvested by centrifugation for 20 min at 4000 \times g at 4°C. The supernatant was poured off and the pellet resuspended in 100 mL of ice-cold, sterile 100 mM CaCl₂ and incubated on ice for 30 min. The cells were harvested by centrifugation, resuspended in 5 mL of ice-cold, sterile solution of 100 mM CaCl₂ and 20% (v/v) glycerol. 25 μ L aliquots of this suspension were flash frozen using dry ice and ethanol and subsequently stored at -80°C until needed. For chemical transformation, 1 to 2 μ L of ligation reaction (Section 2.5.7) or 0.25 μ g of plasmid DNA was added to 25 μ L of cells. The mixture was incubated on ice for 30 min, subjected to a 90 sec heat shock at 42°C, and chilled on ice for 2 min. 500 μ L of LB medium (Table 2-6) was added, and the cells were incubated in a rotary shaker for 45 to 60 min at 37°C. Cells were spread onto LB agar plates (Table 2-6) containing ampicillin and incubated overnight at 37°C. 100 μ L of 2% X-gal in DMF and 50 μ L of 100 mM IPTG were added to agar plates to allow for blue/white selection of colonies carrying recombinant plasmids, when necessary.

2.4.2 Chemical transformation of *S. cerevisiae*

Plasmid DNA for self-replication, integration via homologous recombination or DNA fragments generated by PCR for homologous recombination was introduced into yeast according to the procedure of Gietz and Woods (2002). Essentially, yeast cells were grown overnight in 5

mL of YEPD and subcultured the following morning in 10 mL of fresh YEPD to a starting OD₆₀₀ of ~0.2. After 4 to 5 h, or until the culture reached an OD₆₀₀ of ~1.0, cells were harvested by centrifugation for 3 min at 2,000 × g, the supernatant was poured off and the pellet of cells resuspended in 10 mL of water by brief vortex. Cells were harvested by centrifugation, resuspended in 1 mL of 100 mM lithium acetate, and incubated at 30°C for 5 min. Cells were harvested by microcentrifugation, the supernatant aspirated and the following components were added to the cell pellet in this order: 10 µL of 5 mg/mL sheared salmon sperm, 10 pg of self-replicating plasmid DNA or 100 pg of linearized plasmid DNA for integration or 1 ng of DNA fragments for homologous recombination, 600 µL of 50% PEG containing 100 mM lithium acetate. The cell pellet was resuspended in the mixture by use of a pipet. After a 15 min incubation period at room temperature 50 µL of DMSO was added and mixed by inversion before the cells were subjected to a 20 min heat shock at 42°C. Cells were collected by microcentrifugation and washed by gentle resuspension in 1 mL of water before being harvested by microcentrifugation and resuspended in 200 µL of water. The cells were plated onto SM agar plates, or on YEPD agar plates supplemented with appropriate antibiotics (Table 2-12). Plates were incubated at 30°C for 3 days for colony formation.

2.4.3 Electroporation of *S. cerevisiae*

S. cerevisiae cells were made electrocompetent as recommended by Ausubel *et al.* (1989), and Thompson *et al.* (1998). Essentially, yeast cells were grown overnight in 5 mL of YEPD and subcultured the following morning in 10 mL of fresh YEPD to a starting OD₆₀₀ of ~0.2. After 4 to 5 h, or until the culture reached an OD₆₀₀ of ~1.0, cells were harvested by centrifugation for 3 min at 2,000 × g, the supernatant was poured off and the pellet resuspended in 10 mL of water by brief vortex. Cells were then harvested by centrifugation again at 2,000 × g, resuspended in 10 mL of a freshly prepared TE buffer, pH 7.5 (Table 2-9) containing 100 mM lithium acetate, and incubated

for 30 min at room temperature with gentle agitation. DTT was added to a final concentration of 20 mM, and the incubation was continued for another 15 min. Cells were harvested by centrifugation at $2,000 \times g$, washed with a succession of 10 mL each of room-temperature water, ice-cold water, and ice-cold 1 M sorbitol. After washing, cells were resuspended in a minimal volume of ice-cold 1 M sorbitol after removal of the excess. 20 μ L of cells was mixed with 1 μ L of plasmid DNA and placed between the bosses of an ice-cold microelectroporation chamber (Bio-rad), submitted to an electrical pulse of 250 V (amplified to ~ 1.6 kV) at a capacitance of 2 μ F and a resistance of 4 k Ω using a Bio-rad MicroPulser. Cells were immediately resuspended in 100 μ L of ice-cold 1 M sorbitol and plated onto selective SM agar plates. Plates were incubated at 30°C for 3 to 5 days for colony formation.

2.4.4 Electroporation of *Y. lipolytica*

Y. lipolytica cells were made electrocompetent as recommended by Ausubel *et al.* (1989). Essentially, yeast cells were grown overnight in 10 mL of YPA and subcultured the following morning in 50 mL of fresh YEPD to a starting OD₆₀₀ of ~ 0.2 . After 4 to 5 h, or until the culture reached an OD₆₀₀ of ~ 1.0 , cells were harvested by centrifugation for 5 min at $2,000 \times g$, the supernatant was poured off and the pellet resuspended in 50 mL of a freshly prepared TE buffer, pH 7.5 (Table 2-9) containing 100 mM lithium acetate, and incubated for 30 min at room temperature or 30°C with gentle agitation. DTT was added to a final concentration of 20 mM, and the incubation was continued for another 15 min. Cells were harvested by centrifugation at $2,000 \times g$, washed with a succession of 10 mL each of room-temperature water, ice-cold water, and ice-cold 1 M sorbitol. After washing, cells were resuspended in a minimal volume of ice-cold 1 M sorbitol after removal of the excess. 20 μ L of cells was mixed with 1 μ L of plasmid DNA and placed between the bosses of an ice-cold microelectroporation chamber (Bio-rad), submitted to an electrical pulse of 250 V (amplified to ~ 1.6 kV) at a capacitance of 2 μ F and a resistance of 4 k Ω

using a Bio-rad MicroPulser. Cells were immediately resuspended in 100 μ L of ice-cold 1 M sorbitol and plated onto selective SM agar plates. Plates were incubated at 30°C for 3 to 5 days for colony formation.

2.5 Isolation of DNA from microorganisms

2.5.1 Isolation of plasmid DNA from bacteria

Single bacterial colonies were inoculated into 2.5 mL of LB containing ampicillin and incubated overnight at 37°C. Cells were harvested by microcentrifugation, and plasmid DNA was isolated using a QIAprep Spin Miniprep Kit according to the manufacturer's instructions (Qiagen). This method is based on the alkaline lysis of bacterial cells, followed by adsorption of DNA onto silica in the presence of high salt and elution of DNA in low salt buffer. Plasmid DNA was eluted in 20-50 μ L of the supplied elution buffer.

2.5.2 Isolation of chromosomal DNA from yeast

Yeast genomic DNA was prepared as recommended by Ausubel *et al.* (1989). Cells were grown overnight in 10 mL of YEPD, harvested by centrifugation for 3 min at 2,000 \times g, washed twice in 10 mL of water, resuspended in 400 μ L of breakage buffer (Table 2-9) and transferred to a 1.5 mL microcentrifuge tube. ~0.6 mL of glass beads were added and the mixture was vortexed for 3 to 5 min to lyse the cells. 250 μ L of phenol and 250 μ L of chloroform/isoamyl alcohol (24:1) were successively added to the cell lysate followed by a further vortex of 3 to 5 min to separate nucleic acids from proteins. The organic and aqueous phases were separated by centrifugation at 16,000 \times g for 10 min at room temperature. The aqueous phase was removed and added to 1 mL of absolute ethanol to precipitate the DNA. If necessary, a second extraction of the aqueous phase with an equal volume of phenol/chloroform/isoamyl alcohol (25:24:1) was performed to improve the purity of the DNA. DNA was precipitated by the addition of 2.5 volumes of absolute ethanol

and centrifugation at $16,000 \times g$ for 5 min at room temperature. The pellet was washed once with 1 ml 70% (v/v) ethanol, air dried and dissolved in 50 μ l of TE 8.0 containing 100 μ g RNase A/ml. DNA was incubated at 37°C for 1 to 2 h to allow for digestion of RNA.

2.6 Protein manipulation and analysis

2.6.1 Preparation of yeast whole cell lysates

Yeast whole cell lysates were prepared by denaturation in alkali solution with a reducing agent. Cells from an overnight 5 mL culture were harvested by centrifugation at $2,000 \times g$ for 5 min, transferred to a microcentrifuge tube, and resuspended in 240 μ L 1.85 M NaOH to which 7.4% (v/v) of 2-mercaptoethanol had been freshly added. The cell suspension was incubated on ice for 5 min and then mixed with an equal volume of 50% TCA by vortexing. The mixture was further incubated on ice for 5 min and subjected to microcentrifugation at $16,000 \times g$ for 10 min at 4°C. The pellet was washed once with water, resuspended first in 50 μ L of Magic A (1 M unbuffered Tris-HCl, 13% SDS) and then in an equal volume of Magic B (30% (v/v) glycerol, 200 mM DTT, 0.25% bromophenol blue). The mixture was incubated for 25 min at 70°C and then subjected to microcentrifugation at $16,000 \times g$ for 1 min. The supernatant was collected.

2.6.2 Precipitation of proteins

Proteins were precipitated from solution by adding TCA to a final concentration of 10% and deoxycholate to a final concentration of 0.01%. Incubation on ice varied from 30 min to overnight. Precipitates were collected by microcentrifugation at $16,000 \times g$ for 30 min at 4°C. The pellet was washed twice with 1 mL of ice-cold acetone, dried in a rotary vacuum dessicator and dissolved in 2 \times sample buffer (Table 2-9).

2.6.3 Determination of protein concentration

The protein concentration of a sample was determined by the method of Lowry (1953), as simplified by Peterson (1977). This assay is based on the reaction of cupric ions with peptide bonds under alkaline conditions, followed by reduction of Folin and Ciocalteu's reagent. These reactions produce a purple colour that can be measured by a spectrophotometer and the relative unknown protein concentration in a sample can be deduced by comparison to a standard curve. A standard curve was prepared from five 1:1 serial dilutions of a solution containing 100 µg/mL BSA. Samples were collected in duplicate, usually one of 5 µL and the second one of 10 µL. Standards and samples were made up in 1 mL of H₂O and protein was precipitated by addition of sodium deoxycholate and TCA (Section 2.6.2). Standards and samples were collected by centrifugation and the supernatant was aspirated. The standards and samples were resuspended in 400 µL of H₂O. A working solution of 1:1:1 (v/v/v) of copper-tartrate-carbonate (CTC) (10% sodium carbonate, 0.1% copper sulphate, 0.2% potassium tartrate), 10% SDS and 0.8 M NaOH is prepared and 400 µL is added to each standard and sample and incubated at room temperature for 10 min. To this solution is added 200 µL of 20% Folin-Ciocalteu's phenol reagent followed by another incubation of 30 min at room temperature. The absorbance was measured at 660 nm using a Beckman DU640 spectrophotometer. Absorbance values were plotted against the BSA concentrations to generate a standard curve. Absorbance of a protein sample was measured in the same way as for BSA standards, and the protein concentration was estimated by comparing the absorbance value with the standard curve.

The protein concentration of a sample was also determined by the method of Bradford (1976). A standard curve was prepared by adding 1 mL of Bio-Rad Protein Assay Dye to 100 µL aliquots of water containing 2, 4, 6, 8, 10, 12, 14, 16, 18 and 20 µg of BSA. Samples were incubated for 5 min at room temperature, and absorbance was measured at 595 nm using a Beckman DU640 spectrophotometer. Absorbance values were plotted against the BSA

concentrations to generate a standard curve. Absorbance of a protein sample was measured in the same way as for BSA standards, and the protein concentration was estimated by comparing the absorbance value with the standard curve.

2.6.4 Separation of proteins by electrophoresis

Proteins were separated by sodium dodecyl sulfate-polyacrylamide gel electrophoresis (SDS-PAGE) as described by Ausubel *et al.* (1989). Protein samples were mixed with an equal volume of 2 × sample buffer containing 10 mM DTT, denatured by boiling for 5 min, and separated by electrophoresis on discontinuous slab gels. Stacking gels contained 3% acrylamide (30:0.8 acrylamide:*N,N'*-methylene-bis-acrylamide), 60 mM Tris-HCl, pH 6.8, 0.1% SDS, 0.1% (v/v) TEMED, and 0.1% ammonium persulfate. Resolving gels contained 10% acrylamide (30:0.8 acrylamide:*N,N'*-methylene-bis-acrylamide), 370 mM Tris-HCl, pH 8.8, 0.1% SDS, 0.1% (v/v) TEMED, and 0.043% ammonium persulfate. Electrophoresis was conducted in 1 × SDS-PAGE running buffer (Table 2-4) at 50-200 V using a Bio-Rad Mini Protean III vertical gel system.

2.6.5 Detection of proteins by gel staining

Proteins in polyacrylamide gels were visualized by staining with 0.1% Coomassie Brilliant Blue R-250, 10% (v/v) acetic acid, 35% (v/v) methanol for 1 h with gentle agitation. Unbound dye was removed by multiple washes in 10% (v/v) acetic acid, 35% (v/v) methanol.

2.6.6 Detection of proteins by immunoblotting

Proteins separated by SDS-PAGE were transferred to nitrocellulose membrane (Bio-Rad) in 1 × transfer buffer (Table 2-4) at 100 V for 1 h at 4°C temperature using a Trans-Blot tank transfer system with plate electrodes (Bio-Rad). Proteins transferred to nitrocellulose were visualized by staining in Ponceau S (Table 2-4) for several min and destaining in water. The nitrocellulose was incubated in blocking solution (1% skim milk powder, 1 × TBST (Table 2-4))

with gentle agitation to prevent nonspecific binding of antibodies. Specific proteins on nitrocellulose were detected by incubation with primary antibody in blocking solution for 1 h at room temperature, or overnight at 4°C with gentle agitation. The nitrocellulose was then incubated with appropriate HRP-labeled secondary antibody in blocking solution for 1 h. After each antibody incubation, unbound antibodies were removed by washing the nitrocellulose three times with 1 × TBST for 10 min each. Antigen-antibody complexes were detected using an ECL Western Blotting Detection Kit according to the manufacturer's instructions (Amersham Biosciences) and exposing the nitrocellulose to X-Omat BT film (Kodak).

Used nitrocellulose could be reblotted using a Re-Blot Western Blot Recycling Kit according to the manufacturer's instructions (Chemicon). The nitrocellulose was incubated with 1 × Antibody Stripping Solution at room temperature for 15 to 30 min with gentle agitation, rinsed with 1 × TBST, and blotted as described above.

2.7 Polyclonal antibody production

Antibodies were raised in guinea pigs against protein fusions to maltose-binding protein (MBP) by Elena Savidov, Department of Cell Biology, University of Alberta. Production and purification of fusion proteins were performed using the pMAL Protein Fusion and Purification System according to manufacturer's instructions (NEB). This method is based on the induction of fusion protein synthesis by IPTG and affinity chromatography of the fusion proteins on amylose resin. DNA fragments were cloned into the vector pMAL-c2 (NEB) in-frame and downstream of the ORF encoding MBP. The plasmids were transformed into *DH5α*. Synthesis of fusion proteins was induced by adding IPTG to a final concentration of 1 mM to the growing cells when they had reached an OD₆₀₀ of 0.5. Cells were incubated in the presence of IPTG for 2 to 3 h at 37°C, harvested by centrifugation, and resuspended in fresh preparation of 1 mM DTT in column buffer (200 mM Tris-HCl, pH 7.4, 2 M NaCl, 10 mM EDTA, 1 × cOmplete protease inhibitors) at a

concentration of 10 mL per g of wet cells. Cells were lysed on ice by sonication with a Branson Sonifier 250 set to a duty of 30% and output control of 3. Lysis progressed by sonication for 10-15 sec pulses followed by 10-15 sec on ice to avoid heating the sample. The lysate was cleared of cell debris by centrifugation at $20,000 \times g$ and the resulting supernatant was diluted with two volumes of column buffer and before being passed through an amylose resin column. After washing with 10 bed volumes of column buffer MBP fusion proteins were eluted by addition of 10 mM maltose. Protein elution was tracked by measuring the OD_{280} .

The eluted MBP-fusion proteins were further purified by gel electrophoresis according to Harlow and Lane (1988). Proteins were separated on 10% SDS-PAGE gels and stained in 0.05% Coomassie Brilliant Blue R-250. Gel fragments containing the MBP-fusion proteins were excised, placed in dialysis tubing and incubated in elution buffer (0.2 M Tris-acetate, pH 7.4, 1% SDS, 10 mM DTT) at a concentration of 10 mL per g of wet gel. Proteins were eluted from the gel by electrophoresis at 50 V overnight at 4°C in 50 mM Tris-HCl, pH 7.4, 0.1% SDS. The eluate was placed in 2 – 3 new dialysis tubings and dialyzed against 4 L of 50 mM ammonium bicarbonate, first at room temperature and then at 4°C. The protein solution was then frozen at -80°C and dried by lyophilisation overnight. Lyophilised protein was resuspended in a minimal volume of water and protein concentration was determined.

Animals were immunized according to Harlow and Lane (1988). Proteins were adjusted to a concentration of 500 µg/mL and mixed with an equal volume of Freund's complete or incomplete adjuvant for primary and subsequent injections, respectively. Guinea pigs were injected with 1 mL, containing 200 µg of protein, and 0.4 mL, containing 80 µg of protein, respectively, at several subcutaneous sites every six weeks. Bleeds were taken 10 days after each injection and assessed for antigenic response to the MBP-fusion protein by immunoblotting. Serum was separated from red blood cells in clotted blood by centrifugation at $2,000 \times g$ for 15 min at room temperature.

2.7.1 Production of antisera directed against *S. cerevisiae* Pex30p and Pex29p.

A gene fragment amplified from *S. cerevisiae* genomic DNA by PCR, using primers 3246-ES-ScPEX30 and 0094-324RN, and encoding the C-terminal 241 residues of Pex30p with flanking XhoI and PstI restriction sites was directionally cloned into pMAL-c2 to produce pMAL-c2-PEX30. Similarly, a PCR amplified gene fragment, using primers 3244-FM190 and 3245-FM191, encoding the C-terminal 246 residues of Pex29p with flanking XbaI and HindIII restriction sites was directionally cloned into pMAL-c2 to produce pMAL-c2-PEX29. Antibodies to MBP-Pex30 and MBP-Pex29 fusion proteins were raised in guinea pigs.

2.8 Affinity purification of polyclonal antibodies

Polyclonal antibodies against Pex3p, Pex29p and Pex30p were affinity purified using a modified version of the method described by (Lillie and Brown, 1987). MBP-fusions of Pex3p, Pex29p and Pex30p were purified as described in section 2.7. Except, after separation on 10% SDS-PAGE gels the proteins were transferred to nitrocellulose, stained with Ponceau S and strips of nitrocellulose containing the separated MBP-fusion protein band were excised. The nitrocellulose strips were incubated in blocking solution (1% skim milk powder, 1 × TBST (Table 2-4)) with gentle agitation to prevent nonspecific binding of antibodies. These strips were then incubated overnight at room temperature with 200 µL of antibody serum specific to each fusion protein in a petri dish humidified by a damp paper towel and sealed with parafilm. The 'depleted' serum was removed by pipet and the strip was washed three times in 1 mL PBS for a total of 30 min. 'Affinity-purified' antibody was eluted by incubation of the strip with 200 µL glycine buffer (200 mM glycine, 1 mM-EGTA, pH 2.7) for 20 min. The affinity-purified antibody solution was removed by pipet and neutralized with addition of 2 µL of 5 N-NaOH (as judged by spotting 1 µL aliquots on pH paper). After neutralization, 200 µL of 2% BSA, 10% glycerol (v/v) in 2 × PBS was added to the affinity-purified solution and then stored at 4°C. The purity of the affinity-purified antibody was assessed

by immunoblotting whole cell lysates of wild-type, GFP-tagged, and deletion strains of the protein of interest. The affinity-purified antibody typically had a shelf-life of 3-6 months.

2.9 Subcellular fractionation of *S. cerevisiae* cells

Subcellular fractionation of *S. cerevisiae* cells was performed as described by Smith et al. (2002). Cells grown in YEPD or YPBO were harvested by centrifugation at $2000 \times g$ in a Beckman JA10 rotor at room temperature and washed twice with water. Cells were resuspended in 10 mM DTT, 100 mM Tris-HCl, pH 9.4, at a concentration of 10 mL per g of wet cells and incubated at 30°C for 35 min with gentle agitation to loosen the outer mannoprotein layer. Cells were collected by centrifugation at $2,000 \times g$ in a Beckman JS13.1 rotor for 7 min at room temperature and washed once with Zymolyase buffer (50 mM potassium phosphate, pH 7.5, 1.2 M sorbitol, 1 mM EDTA). Cells were resuspended in Zymolyase buffer containing 0.125 mg of Zymolyase 100T/mL at a concentration of 8 mL per g of wet cells and incubated at 30°C for 45 min to 1 h with gentle agitation to convert cells to spheroplasts. Spheroplasts were harvested by centrifugation at $2,000 \times g$ in a Beckman JS13.1 rotor for 8 min at room temperature and washed once with 1.2 M sorbitol, 2.5 mM MES, pH 6.0, 1 mM EDTA and harvested by centrifugation at $6,000 \times g$ at 4°C. They were then resuspended in buffer H (0.6 M sorbitol, 2.5 mM MES, pH 6.0, 1 mM EDTA, 1 × cOmplete protease inhibitor cocktail (Roche)) at a concentration of 2 mL per g of wet cells. Resuspended spheroplasts were transferred to a homogenization mortar and disrupted by 10-20 strokes of a Teflon pestle driven at 1,000 rpm by a stirrer motor (Model 4376-00, Cole-Parmer). Cell debris, unbroken cells and nuclei were pelleted by centrifugation at $1,000 \times g$ in a Beckman JS13.1 rotor for 8 min at 4°C. The postnuclear supernatant (PNS) was subjected to four additional centrifugations at $1,000 \times g$ in a Beckman JS13.1 rotor for 8 min at 4°C.

For cells grown in YEPD, 300 µL of PNS was mixed with 700 µL of 11% (w/v) Nycodenz in buffer H and loaded onto the top of a discontinuous Nycodenz gradient (6.6 mL of 17%, 16.5 mL

of 25%, 4.5 mL of 35% and 3 mL of 50% (w/v) Nycodenz in buffer H). Organelles were separated by ultracentrifugation at $100,000 \times g$ for 90 min at 4°C in a Beckman VTi50 rotor. 18 fractions of 2 mL each were collected from the bottom of the gradient.

For cells grown in YPBO the PNS was fractionated by centrifugation at $20,000 \times g$ in a Beckman JS13.1 rotor for 35 min at 4°C into pellet (20KgP) and supernatant (20KgS) fractions. The 20KgP was resuspended in 11% (w/v) Nycodenz in buffer H and loaded onto the top of a discontinuous Nycodenz gradient (6.6 mL of 17%, 16.5 mL of 25%, 4.5 mL of 35% and 3 mL of 50% (w/v) Nycodenz in buffer H). Organelles were separated by ultracentrifugation at $100,000 \times g$ for 90 min at 4°C in a Beckman VTi50 rotor. 18 fractions of 2 mL each were collected from the bottom of the gradient.

2.9.1 ER-mobility shift assay

As a variant of the preceding method, fractionation of cellular organelles after isopycnic centrifugation was also performed in the presence or absence of excess Mg^{2+} . Altering the concentration of divalent cations in the homogenization and gradient buffers alters the buoyant density of the ER relative to other organelles (Roberg et al., 1997). This likely occurs through disruption of the association of ribosomes with the ER-translocon. It is thought that divalent cations stabilize the interaction by forming salt bridges between the ribosome and translocon and that chelation of these cations results in a loss of association, and hence, lighter buoyant density. To induce ER-mobility in isopycnic density centrifugation, the homogenization and centrifugation steps were carried out under identical conditions varying only in the concentration of divalent cations in buffer H. For cells grown in YEPD three conditions were used, and buffer H made up in one of: 1 mM $MgCl_2$, 0.5 mM EDTA, or 5 mM EDTA. For cells grown in YPBO, only two conditions were used, and buffer H made up in either 0.5 mM EDTA or 5 mM EDTA.

2.10 Immunoprecipitation of protein complexes and identification by mass spectrometry

These experiments were performed by Dr. Arvind Jamakhandi and Dr. Ramsey Saleem, Seattle Biomedical Research Institute, Seattle, WA. To facilitate affinity-based purification, the respective protein of interest was C-terminally tagged with protein A (pA) at the genomic level and expressed as a fusion protein. Cells were grown to an OD₆₀₀ of 1.0-1.2 in YEPD medium, harvested by centrifugation, washed twice with cold 20 mM HEPES-KOH, pH 7.4, followed by a wash with cold 20 mM HEPES-KOH, pH 7.4, 1.2% polyvinylpyrrolidone, 1 mM DTT, 1:200 of protease inhibitor cocktail (PIC solution) (Sigma). Cells were subjected to centrifugation at 4,000 × g for 20 min, and the pellet was loaded into a plastic syringe and pushed through directly into liquid nitrogen to form "noodles". Noodles were then cryogenically ground into fine powder using a 25-mL stainless steel grinding jar and ball mill (Retsch PM100 Planetary Ball Mill, Haan, Germany). Each sample was subjected to four runs of grinding (3 min each at 450 rpm with 1 min immersion in liquid nitrogen between each run). The resulting yeast powder was stored at -80°C.

Yeast protein lysates were prepared by resuspending 4 g of yeast powder in 14 mL buffer containing 20 mM HEPES-KOH, pH 7.4, 110 mM potassium acetate, 1 mM DTT, 1 mM MgCl₂, 1 mM EDTA, 1:200 protease inhibitor cocktail, 0.006 % anti-foam B, 1 % digitonin (Calbiochem, Darmstadt, Germany). The resuspension was clarified by centrifugation at 4,000 × g for 5 min and then at 50,000 × g for 20 min. The supernatant was then passed through a 2.7 µm pore size glass microfiber, 25-mm diameter syringe filter (Whatman) and collected into a clean 15 mL falcon tube. 20 mg equivalent (140 µL volume) of IgG-conjugated magnetic beads prepared as per the manufacturer's instructions and stored in PBS, pH 7.4, at 4°C was added to the protein lysate and incubated with gentle agitation on a rocking platform for 40 min at 4°C. Magnetic beads were collected with a magnet, transferred to 1.5 mL microfuge tube and gently washed four times at room temperature (~25°C) with 500 µL of resuspension buffer containing 0.1 % digitonin. To

release protein complexes, the IgG-PrA interactions were disrupted by adding 50 μ L of 0.2 % SDS and incubation at room temperature for 15 min. The beads were separated by a magnet, and the eluate was collected in a fresh microfuge tube. The elution steps were repeated and the samples pooled (total volume = 100 μ L). 30 μ L of this sample were aliquoted for separation by SDS-PAGE (NuPAGE Bis-Tris Pre-Cast Gels, Invitrogen, Carlsbad, CA) followed by silver staining (Invitrogen) to visualize protein bands. The remaining sample was loaded onto a detergent removal spin column (Thermo Fisher Scientific) to remove SDS following the manufacturer's protocol. The detergent-free flow through was dried under vacuum and resuspended in 75 μ L of 100 mM Tris-HCl, pH 8.3, 1 mM EDTA, 6 M urea. The protein sample was reduced in 5 mM tris(2-carboxyethyl)phosphine at 37°C for 30 min and alkylated with 25 mM iodoacetamide at room temperature in the dark for 30 min. The alkylation reaction was quenched by adding DTT to a final concentration of 50 mM. The sample was diluted 4-fold to decrease the concentration of urea to 1.5 M. 1 mM CaCl_2 was added to the sample, which was then digested with 2 μ g of sequencing grade modified porcine trypsin (Promega, Madison, WI) overnight at 37°C. Digested samples were desalted using Vydac C18 Silica MicroSpin columns (The Nest Group, Southborough, MA) as per the manufacturer's instructions. Purified peptides were resuspended in 10 μ L of 0.1% trifluoroacetic acid (v/v) and 1% acetonitrile (v/v), and 6 μ L of the sample were analyzed by LTQ-MS/MS (Thermo Fisher). The resulting peptide fingerprints were identified by searching against a yeast peptide database using the Trans Proteomic Pipeline (Keller et al., 2005). Search result validation was done using Peptide Prophet (ver. 3.0) (Keller et al., 2002), and a probability of 1 was used to confidently identify a peptide. We report proteins for which at least two unique peptides were observed. Similar to earlier arguments, in all experiments, ribosomal proteins were excluded from the list of identification as common coeluting contaminants. (Krogan et al., 2006). For Pex29p-pA and Pex30p-pA samples, proteins were identified by both in-gel digestion

(Shevchenko et al., 2006) and the in-solution method. RtnIp-pA and YopIp-pA were analyzed by the in-solution method.

2.10.1 Isotopic determination of differentiation of interactions as random or targeted

The following experiments were performed by Dr. Ramsey Saleem, Seattle Biomedical Research Institute, Seattle, WA, and Dr. David Dilworth, Institute for Systems Biology, Seattle, WA. The respective protein of interest was C-terminally tagged with protein A (pA) at the genomic level and expressed as a fusion protein. Cells expressing the pA fusion protein were grown to an OD₆₀₀ of 1.0-1.2 in complete synthetic growth media, CSM, [20 g/L D-glucose (VWR, West Chester, PA, USA), 0.67 g/L Complete Supplement Mixture minus arginine, lysine, and histidine (Sunrise Science Products, San Diego, CA, USA), 1.7 g/L Difco yeast nitrogen base w/o amino acids and ammonium sulfate (BD, Franklin Lakes, NJ, USA), 5 g/L ammonium sulfate (Fisher, Pittsburgh, PA, USA), 30 mg/L L-histidine (Mallinckrodt Baker, Phillipsburg, NJ, USA), 45 mg/L L-Lysine (Fisher, Pittsburgh, PA, USA) and 50 mg/L L-arginine (Fisher, Pittsburgh, PA, USA)] to prepare the isotopically “light”-labeled lysates. Heavy preparations were obtained by growth of wild-type cells lacking the pA tag in SILAC-KR complete synthetic media, which is identical to standard CSM formulation above, except that L-Lysine-¹³C₆, ¹⁵N₂·HCl (Sigma-Aldrich, St. Louis, MO, USA) and L-Arginine-¹³C₆, ¹⁵N₄·HCl (Sigma-Aldrich, St. Louis, MO, USA) were included in place of their isotopically light variants. All samples were obtained from log phase, OD₆₀₀~1.0, cultures grown at 30 °C with shaking at 200 rpm. For each sample, ~1 × 10⁸ cells were harvested in 50 mL conical tubes by centrifugation at 7000 × g for 5 min, washed with 1 mL of sterile water in a 1.7 mL tube, centrifuged for 15 s at 10,000 × g and the cell pellet was flash frozen in liquid nitrogen and stored at -80 °C.

Yeast protein lysates and immunoisolations of protein complexes were carried out as described in section 2.10. Except that isotopically light and heavy cell pellets were mixed 1:1 (w/w) before disruption with the planetary ball mill. For shotgun MS/MS 50 µg of protein was brought to 100 µL with 100 mM ammonium bicarbonate, pH 9. The sample was reduced with tris(2-carboxyethyl)phosphine, alkylated with iodoacetamide and then digested with sequencing grade modified porcine trypsin (Promega, Madison, WI, USA). Digested samples were desalted using Vydac C18 Silica MicroSpin columns (The Nest Group, Southborough, MA, USA) by manufacturer's instructions. Purified peptides were diluted in load buffer (0.1% formic acid, vol/vol) before MS/MS analysis. Mass spectrometry was performed on Thermo Electron LTQ and LTQ-Orbitrap mass spectrometers equipped with an electrospray ionization source and an Agilent HPL100 liquid chromatography system. The gradient was run from 10 to 35% acetonitrile over 60 min at a constant flow rate of 0.350 µL/min. XCalibur Raw files were converted to mzXML format using ReAdW (ver. 4.2.0) using the readw profile and default parameters. Spectral searches were done for tryptic fragments using X!Tandem (Craig and Beavis, 2004) (ver. 2007.07.01.3) with the k-score plugin (MacLean et al., 2006). Searches were done against a non-redundant *S. cerevisiae* reference protein database (the union of the SGD, Ensembl, NCI, and GenBank databases, plus keratin and trypsin) containing 13,616 entries. Parent tolerance was ± 3 Da, the fragment mass tolerance was ± 0.4 Da, with no missed cleavages. A wide mass window was used to increase peptide identifications (Hsieh et al., 2010). Modifications included in the searches are as follows: static modification of cysteine 57.021464 Da (C[143.13]), and variable modifications of methionine 15.994915 Da M[147.19], glutamine -17.0306 Da Q[111.10], glutamic acid -18.01056 Da E[111.10], lysine 8.014199 Da, K[136.19], and arginine 10.008269 Da R[166.20].

Individual search results were processed using the Trans Proteomic Pipeline (Keller et al., 2005). Search result validation was done using Peptide Prophet (ver. 3.0) (Keller et al., 2002), and relative quantification of isotopically labeled peptides was reported by Xpress ratio (Han et al.,

2001). Tab-delimited Peptide Prophet text files were imported into the QTIPS application (Dilworth et al., 2010), which identifies informative peptides and calculates the frequency of heavy arginine or heavy lysine containing peptides in the population of informative peptides. The QTIPS application also determines the average Xpress incorporation values for informative peptides and presents histograms of their distributions. Protein-protein interaction networks were also visualized using BioFabrics (Institute for Systems Biology) (Longabaugh, 2012).

2.11 In vitro vesicle budding assay

The in vitro cell-free vesicle budding assay was performed according to the methods of Lam et al (2010) and Agrawal et al (2011). These assays are based on the similar assays developed for the characterization of COPII vesicles that mediate vesicular traffic from the ER to the Golgi (Barlowe et al., 1994). In the presence of cytosol, Pex19p and ATP, high-speed pelletable vesicles containing Pex3p, Pex15p, and Pex11p are released from ER donor membranes enclosed in permeabilized yeast cells.

2.11.1 Preparation of permeabilized yeast cells

Preparation of permeabilized yeast cells was performed according to the method of Groesch et al. (1992). Yeast strains are grown overnight in 1 L of YEPD to an OD_{600} of 4.0. The cells are collected by centrifugation at $2,000 \times g$ for 7 min at room temperature in a Beckman JA-10 rotor, resuspended in low glucose medium (YEPD but with 0.1% glucose final concentration), and incubated for 30 min at 25°C with vigorous shaking. The cells are harvested by centrifugation and resuspended in spheroplast medium (1 × yeast peptone, 1 g/L glucose, 1.4 M sorbitol, 50 mM potassium phosphate, pH 7.5, 50 mM 2-mercaptoethanol) supplemented with zymolase 100T at 1 mg/mL, to a final concentration of 8 mL/g of wet cells and incubated for 40 min at 37°C with gentle agitation. The spheroplasts are recovered by centrifugation and resuspended in recovery medium (1 × yeast peptone, 1 g/L glucose, 1 M sorbitol) and incubated at 37°C for 90 min to

allow partial regeneration of the cell wall. The regenerated spheroplasts are pelleted and used for generating permeabilized yeast cells and yeast cytosol.

Permeabilization is achieved by osmotic lysis in the presence of osmotic support. The pellet of regenerated spheroplasts is resuspended in ice cold spheroplast lysis buffer (100 mM potassium acetate, 200 mM sorbitol, 20 mM HEPES-KOH, pH 7.2, 2 mM MgCl_2) at a concentration of 5 mL/75 OD_{600} unit cell equivalents. The slurry is pipetted up and down with moderate force 5-10 times and incubated on ice for 20 min to osmotic equilibration. The permeabilized yeast cells are collected by centrifugation at $3,000 \times g$ for 5 min at 4°C and the supernatant is thoroughly removed.

2.11.2 Preparation of a concentrated yeast cytosol

Following the method of Groesch et al. (1992), concentrated wild-type yeast cytosol was prepared from regenerated spheroplasts (section 2.11.1) as follows: Regenerated spheroplasts were lysed in ice cold 20 mM HEPES-KOH, pH 7.4, at a concentration of 210 μL /75 OD_{600} unit cell equivalents. The slurry is pipetted 30 times with a 1 mL pipet to ensure efficient lysis. The cell debris is pelleted by centrifugation at $3,000 \times g$ for 5 min at 4°C and the supernatant is collected ($\sim 360 \mu\text{L}$). To the concentrated cytosol is added 50 μL of $10\times$ transport buffer (250 mM HEPES-KOH, pH 7.2, 1.15 M potassium acetate, 25 mM MgCl_2), cOmplete protease inhibitor cocktail (Roche) to $1\times$ concentration, and 50 μL of 2 M sorbitol.

2.11.3 In vitro ER-budding assay

Permeabilized yeast cells (PYCs) prepared from *pex19 Δ* , *pex19 Δ /pex29 Δ /pex30 Δ* , and *pex19/rtn1 Δ /rtn2 Δ /yop1 Δ* strains and were washed twice with TBPS (115 mM potassium acetate, 2.5 mM magnesium acetate, 0.25 M sorbitol, $1\times$ cOmplete protease inhibitor cocktail, 25 mM HEPES, pH 7.2) and then resuspended in TBPS at a concentration of 25 μL /5 OD_{600} unit cell equivalents. Pex3p was endogenously tagged with GFP in these strains to differentiate between

Pex3p from PYCs versus a potential contamination of Pex3p from cytosol. Reaction conditions were as follows: 25 μ L of PYCs, 25 μ L of wild-type cytosol, 25 μ L of a 4 \times ATP regenerating system (4 mM ATP, 0.4 mM GTP, 80 mM creatine phosphate, 0.8 mg/mL creatine phosphate kinase), and 25 μ L of 2 \times TBPS were mixed on ice. The reaction proceeded by incubation at room temperature for 90 min and chilling the samples on ice terminated the reaction. After the reaction was terminated, the PYCs were pelleted by centrifugation at 13,000 \times g for 5 min at 4°C. The supernatant of two identical reactions was pooled and spun at 200,000 \times g for 1 h at 4°C. The pellet, containing preperoxisomal vesicles, was resuspended in 2 \times sample buffer (4% SDS, 0.15 M tris-HCl pH 6.8, 4 mM EDTA, 20% glycerol, 2% 2-mercaptoethanol, 0.02% bromophenol blue) before being resolved by SDS-PAGE. The presence of Pex3-GFP was detected by immunoblotting with affinity purified Pex3p antibodies. Reactions carried out with PYCs alone, in the absence of exogenous ATP, and at 4°C were included as controls.

2.12 Microscopy

Images from the microscopy of biological phenomena are imperfect representations of that phenomena (Bolte and Cordelières, 2006). As such, care must be taken at every step of the process from the preparation of specimens to the handling of image files after processing. Microscopy methodology was followed according to the principles set out in the Handbook of Biological Confocal Microscopy (Pawley, 2006) and the methods of Bolte and Cordelières (2006).

2.12.1 Acquisition of a point spread function (PSF)

The calibration of the microscopes used in this study was routinely assayed by acquisition of a PSF. The shape and contrast of a PSF are useful indicators for ensuring the microscope approaches diffraction-limited imaging (Pawley, 2006). To acquire a PSF, PSF-Speck beads of 175 nm in diameter (Invitrogen) were added to “blanks” that mimicked the imaging conditions of the experiment (see below). PSF's were acquired under identical conditions of each microscopy

experiment performed and with identical acquisition settings, normalized for image brightness as required. To acquire an accurate PSF, the bead must be stable and remain fixed over the course of the acquisition. The resulting images of PSF beads were used to generate experimentally derived point spread functions using Huygens Professional software (Software Volume Imaging BV).

2.12.2 Confocal microscopy of peroxisome proliferation in yeast

Yeast expressing an endogenously encoded chimera of Pot1p-GFP were grown to an OD_{600} of ~ 1.0 in 25 mL of YEPD at 30°C. The cells were washed once with water before resuspension in 25 mL of YPBO and incubated at 30°C. 1 mL aliquots were taken after 0, 2, 4, 6, 8, and 24 h of incubation and prepared for imaging by 2 washes in 1 mL of water. Cells were resuspended in 100-200 μ L of water and 1.8 μ L was placed on a glass #1.5 coverslip for imaging. Five random field of views were chosen per strain, per time-point and images were captured with a Plan-Apochromat 63 \times /1.4 NA oil immersion DIC objective on an Axiovert 200 M inverted microscope equipped with a side-mounted LSM 510 META confocal scanner (Carl Zeiss). GFP was excited with a 488 nm laser, and its emission collected using a 505 nm long-pass filter. Images were captured at room temperature.

2.12.3 3D confocal microscopy of living yeast

Cells were grown in YEPD to an OD_{600} of 1.0 and either processed for image acquisition or incubated in YPBO (Table 2-8) for 8 h before processing for image acquisition. Slides were prepared according to (Adames et al., 2001) with modifications (Fagarasanu et al., 2009). Essentially, 200 μ L of hot 1% agarose in nonfluorescent medium (Table 2-9) was used to prepare a thin agarose pad on a slide with two 18-mm square wells (Cel-line Brand). 1 to 2 μ L of culture was placed onto the slide, covered with a cover slip and sealed with Valap (1:1:1 mixture of vaseline, lanolin and paraffin). Cells were incubated for 15-30 min at room temperature before image acquisition. Images were acquired as described (Hammond and Glick, 2000) using a modified LSM

510 META confocal microscope equipped with a 63×/1.3 NA Plan-Neofluor objective (Carl Zeiss). A piezoelectric actuator was used to drive continuous objective movement, allowing for the rapid collection of z-stacks. The sides of each pixel represented 0.057 μm of the sample. Stacks of 41 optical sections spaced 0.16 μm apart were captured. GFP was excited using a 488 nm laser, and its emission was collected using a 488 nm long-pass filter (Semrock).

For colocalization experiments, GFP was excited using a 488 nm laser and its emission was collected using a 514/25 nm band-pass filter (Semrock). mRFP was excited with a 543 nm laser and its emission collected with a 629/53 nm band-pass filter (Semrock). Images were captured at room temperature.

2.12.4 3D confocal microscopy of yeast strains encoding doxycycline regulated genes

Cells harbouring genes under the regulation of the *TetO₇* promoter were grown in YEPD to an OD₆₀₀ of 1.0. The cells were subcultured in fresh YEPD supplemented with doxycycline to a final concentration of 10 $\mu\text{g}/\text{mL}$ and incubated for 18 h at 30°C. Cells incubated in the presence of doxycycline were seeded at an increased density to obtain a comparable cell density to the untreated cell culture at the time of imaging, final OD₆₀₀ was between 1-2 and the dilution factor was empirically determined for each strain. Imaging conditions were identical to section 2.11.3, except for the de novo biogenesis assay with *rtn1 Δ /rtn2 Δ /yop1 Δ* and its isogenic wild-type strain. This experiment was performed by Dr. Arvind Jamakhandi, Seattle Biomedical Research Institute, Seattle, WA. In this experiment images were collected with a 100×/NA 1.4 objective on a Olympus IX-71 wide-field inverted fluorescence microscope with a 250 watt xenon LED transillumination light source, DeltaVision personalDV (Applied Precision). A GFP filter set was used to filter excitation and emission profiles. The images were deconvolved using the manufacturer's supplied deconvolution software (softWoRx).

2.12.5 3D confocal microscopy of temperature-sensitive yeast strains

For microscopy of the temperature sensitive *sec61* mutant strain, cells were processed as described in section 2.11.3. After image acquisition at room temperature, the temperature of the imaging environment was raised to 37°C by use of an environmental chamber (Okolabs). After 4 hours of incubation at 37°C additional image acquisition was performed.

2.12.6 2D confocal video microscopy of yeast

Cells were prepared as described in section 2.11.3. For image acquisition the confocal pinhole was opened as large as possible and images were acquired every 200 msec. To minimize photobleaching only a single optical section focused on the midplane of the cell was performed.

2.12.7 3D immunofluorescence widefield microscopy of yeast

Indirect immunofluorescence microscopy of yeast cells was performed according to Pringle et al (1991) with modifications. Cells were grown in YEPD to an OD₆₀₀ of 1.0. Fixation occurred for 45 min at room temperature in solution B (100 mM KH₂PO₄, 100 mM K₂HPO₄, 1.2 M sorbitol) containing 4% freshly prepared formaldehyde with regular mixing by inversion. Cells were then collected by centrifugation at 2,000 × g for 2 min, washed with 2 mL of solution B, and resuspended in solution B at a concentration of 1 ml per 100 µl of wet cells. The cell suspension was mixed with 40 µg of Zymolyase 100T/ml and 38 mM 2-mercaptoethanol and incubated for 15 to 60 min at 30°C with gentle rotation. Spheroplasts were blocked in 500 µL of 1% BSA in solution B for 1 h, incubated with primary antibody diluted in 1% BSA in solution B overnight, washed 5 times with 1% BSA in solution B, and then incubated with secondary antibody diluted in 1% BSA in solution B for 1 h. Spheroplasts were washed 5 times with 1% BSA in solution B and then cleared in solution B with successively increased concentrations of glycerol (10, 20, 30, 40, 50, 60, 70, 80, 90%) with 5 min incubations before resuspension in mounting medium (0.4% N-propyl gallate,

74.8% (w/v) glycerol in PBS, pH 7.4). 1.8 μ L of the suspension was added to coverslips, which were placed on top of slides, and the edges of the coverslips were sealed with nail polish.

Samples were imaged on a Deltavision OMX microscope with a 60 \times /1.4 NA objective (Applied Precision). The sides of a pixel were 0.08 μ m and 50 optical sections were spaced 0.2 μ m apart. Images were collected sequentially using the GFP and mRFP filter sets.

2.12.8 3D fluorescence microscopy of *Drosophila* S2 cell culture

Images of double-stranded RNA interference (RNAi)-treated S2 cells were acquired using a Plan-Apochromat 63 \times /1.4 NA oil DIC objective on an Axiovert 200 inverted microscope equipped with a LSM510 META confocal scanner (Carl Zeiss). GFP-SKL was excited with a 488 nm laser and its emission collected with a 505 nm long-pass filter or 515-535 nm band filter. Fusion proteins of *Drosophila* proteins tagged with mRFP were excited with a 543 nm laser and fluorescent emission collected with a 600 nm long-pass filter. Optical sections were spaced 200 nm apart.

2.12.9 3D immunofluorescence microscopy of *Drosophila* embryos

Preparation and staining of *Drosophila* embryos was carried out by Maninder Virk, Department of Cell Biology, University of Alberta. Embryos were fixed as described (Hughes and Krause, 1999) and stained with the following antibodies at 1:100 dilution and obtained from the Developmental Studies Hybridoma Bank, University of Iowa, Department of Biological Sciences, Iowa City, IA: mouse anti-CNS axons (BP102), mouse anti-Neuroglian (BP104), mouse anti-fasciclin 2 (1D4), mouse anti-repo (8D12), and mouse anti-Wrapper (10D3) (developed by Dr. Corey Goodman); mouse anti-Futsch (22C10) (developed by Dr. Seymour Benzer); mouse anti-Even-skipped (2B8) (developed by Dr. Kai Zinn); and mouse anti-Cut (2B10) (developed by Dr. Gerald M. Rubin). Rabbit anti-GFP (Invitrogen) and rat anti-myosin (Abcam) were used at 1:1000 dilution. Alexa488-, Alexa568-, Cy2-, and Cy5-conjugated secondary antibodies (Invitrogen, Jackson ImmunoResearch) were used at a 1:2000 dilution to recognize primary antibodies. To reduce the effects of spherical

aberrations, embryos were optically cleared in methyl salicylate after preparation for immunofluorescence (MacDonald and Rubel, 2008). Images were obtained using a UPlanFI 20×/0.5 NA air objective on an IX81 inverted epifluorescence microscope (Olympus) equipped with a CoolSNAP HQ digital camera (Roper Scientific) and an X-Cite 120 PC fluorescent illumination system (EXFO Life Sciences).

2.13 Deconvolution and image processing

Images were deconvolved using algorithms provided by Huygens Professional Software (Scientific Volume Imaging BV, The Netherlands). For deconvolution, 3D data sets were processed to remove noise and reassign blur by an iterative Classic Maximum Likelihood Estimation widefield algorithm and confocal algorithms, respectively, with experimentally derived point spread functions. Transmission images of yeast and *Drosophila* S2 cells were processed by applying a Gaussian filter in Huygens, and blue color was applied to the transmission images using Imaris software (Bitplane). Transmission images were processed to maximize the fluorescent signal while maintaining cell outlines. Imaris was then used to render the deconvolved 3D data set to the processed transmission image. Final figure assembly was performed in Adobe Photoshop, Adobe Illustrator or Adobe InDesign.

2.14 Quantification of colocalization

Pearson's correlation coefficient and Manders coefficient were calculated using the JACOP plugin (Bolte and Cordelières, 2006) for ImageJ (NIH).

Object based colocalization was performed using Imaris (Bitplane). Fluorescent signal from Pex30p-GFP or Pex29p-GFP was processed with the "Surface" command function and fluorescent signal from Mdh2p-mRFP or Pot1p-mRFP was processed with the "Spots" function. The ImarisXT plugin (Bitplane) was used to compute the distance between all spots and all surfaces and identify all "spots" within 0.28 μm of a "surface."

2.15 Quantification of peroxisome number, volume and intensity

Statistics on peroxisome number, volume and intensity were calculated using the Spot algorithm in Imaris (Bitplane).

2.16 *Drosophila* cell culture

Drosophila S2 cells were grown at 25°C in Schneider's *Drosophila* Medium (Invitrogen) supplemented with 10% heat-inactivated fetal bovine serum, 50 U penicillin/mL and 50 µg streptomycin sulfate/mL (Invitrogen). S2 cells constitutively expressing the fluorescent peroxisomal chimeric protein GFP-SKL (Kural et al., 2005) were kindly provided by Dr. Ronald Vale (University of California, San Francisco). Maintenance of the *Drosophila* S2 cultures was performed by Dr. Andrew Simmonds, Department of Cell Biology, University of Alberta.

2.17 RNAi Knockdown of *DmelPex* Homologs and Semi-quantitative PCR

Templates for dsRNAs targeting predicted *DmelPex* homologs were isolated from a template library (Foley and O'Farrell, 2004). A control template to make dsRNA that specifically targets Dredd was a gift from Dr. Edan Foley, University of Alberta. dsRNAs were synthesized using the T7 RiboMAX kit (Promega) using template-specific primers (Foley and O'Farrell, 2004).

The dsRNA treatment of cells was performed as follows: Day 1: Cells were split 1:2 with fresh SFX culture medium (Invitrogen). Day 2: 2×10^5 cells in 500 µl of SFX culture medium were added to each well of a 24-well dish (BD Biosciences). 20 µg of dsRNA to a gene of interest were added to one well, followed by gentle horizontal mixing. Plates were sealed with Parafilm M and incubated at 25°C for 96 h. Day 6: The cells in each well were split 1:2, and an additional 20 µg of dsRNA were added. The plates were resealed with Parafilm M and incubated at 25°C for 48 h. Day 8: 10% of the remaining volume of cells was transferred to LabTekII chambered coverslips (Nalge Nunc) for microscopic examination of peroxisomes.

Jing Li and Dr. Andrew Simmonds, Department of Cell Biology, University of Alberta performed the semi-quantitative PCR experiments. Total RNA was extracted from the remaining cells using RNeasy (Qiagen) and quantified with a NanoVue spectrophotometer (GE Healthcare). 200 ng of total RNA were used for reverse transcription using Superscriptase II (Invitrogen) and oligo-dT as the anchor primer. 2 µl of the resulting cDNA and gene-specific primers (Table 2- were then used in a 50-µl PCR reaction. For semi-quantitative PCR, specific *DmelPex* gene primers and control primers for an mRNA encoding a ribosomal protein (RP49) were used. The number of PCR cycles for each set of gene-specific primers was tested to ensure that the resulting reaction was within the linear range of amplification. Products were separated by electrophoresis on 1% agarose gels. Band intensity was measured using Image J and normalized to the control RP49 signal.

Table 2-14. Primers for RT-PCR confirmation of RNAi knockdown of *DmelPex* genes

gene	5'-primer	3'-primer	Size (bp)
CG6760	atgttcaaacgcacttttaaggtggtctatc	cgatctccttgccgctctgg	221
CG7081	ctatttgaacaaggacattgcccgc	gacggtcaggatgaaatggagcac	240
CG6859	ccatgctggttattgcttgagggt	caggtcgctaagggaagctgttcg	236
CG14815	gagcaaacccgccaacttca	gccagcaactgccagacctca	288
CG11919-RA	tgggtgttcgagtcaggaggt	ccagcagttggagcggatttga	284
CG11919-RB	tcgctttcaatccgctccaactg	cgaactcgctgcccttctctcc	317
CG6486	tctccctgtccagcgtaacctcca	gcctatccgttcaccttccacttc	289
CG8315	tgtcacaatcgctgttctcttcg	tcttcaccgtgtccacaactatgtcttt	312
CG3639	taaggaccaggatcaccaggcacg	caagacctccagcatctttaggaccac	233
CG4663	cttcggcgggtgggtacaacagatt	gatgaagggtccaggttcgataggc	320
CG4289	atccgaacaccgtcattagcattg	gaccgccttcttcttgacttgc	188
CG3947	ggacactctgaaggcatgctgaag	tgatgaggaaatcgacactggaa	127
CG5325	gccaaagctctccgtgaggacaag	agtgggatcgccgaagggaag	225
CG3696	gcgacgcactcaagtcacacaaatg	ccaaaggaaagcagtccttttccac	474
CG32226	cgtcttagcagcagcgaccatg	tgctgatgccataccggaagaacac	300
CG7486	atggccggatcaaacctgttg	cagctcctgccagcagaacc	312

2.18 Preparation of Antibodies to *DmelPexI* Protein and Immunoblotting

Antibodies to that recognize *DmelPexI* were raised against a fusion of maltose-binding protein and the N-terminal 200 amino acids of *DmelPexI* in guinea pig by Elena Savidov, Department of Cell Biology, University of Alberta. The antibodies were tested for specificity by immunoblotting of a S2 cell lysate using enhanced chemiluminescence (GE Healthcare). The protocol for raising the antibody is essentially as described before (Eitzen et al., 1997).

2.19 *Drosophila* Stocks

Drosophila stocks were maintained by Dr. Andrew Simmonds, University of Alberta. Oregon R (wild-type) and *DmelPexI*, (l(3)70Da, CG6760) strains (l(3)70Da^{s4868} and l(3)70Da^l) were obtained from the Bloomington *Drosophila* Stock Center at Indiana University. Stocks were maintained on standard Bloomington medium at 25°C, and embryos were collected at 25°C on apple juice-agar plates. To facilitate the identification of homozygous mutant embryos, lethal *DmelPexI* mutations were maintained over the w⁺; Sb¹/TM3, P{ActGFP}JMR2, Ser^l balancer. UASp-PexI was made by TOPO cloning of a PCR fragment corresponding to the open reading frame of *DmelPexI* into pENTR/D (Invitrogen). This was transferred using Clonase LR (Invitrogen) into the plasmid pPW (Terence Murphy), which was transformed into w¹¹¹⁸ embryos by P-element recombination.

2.20 Larval Survival, Growth and Mobility Assays

The following experiments were performed by Maninder Virk, and Dr. Andrew Simmonds, Department of Cell Biology, University of Alberta.

Parallel cultures of Oregon R and l(3)70Da^{s4868} adult flies were maintained for one week in a standard 2 L population cage at 25°C. Flies were allowed to lay eggs for 1 h on apple juice-agar plates, and cohorts of 100 randomly selected embryos of each genotype were placed on fresh apple juice-agar plates with yeast paste at the center of the plates. The lifespan of l(3)70Da^{s4868}

homozygous mutants was determined by observing larvae daily from hatching until death. Larvae were fed and watered regularly and kept in a 25°C incubator. The number of survivors was recorded daily. All homozygous mutants were dead by Day 6. However, wild-type and $l(3)70Da^{s4868}$ heterozygous larvae moulted normally at Day 6 and hatched into adult flies by Day 10. The survival assay was repeated 3 times with 100 larvae in each experimental group. To assay larval growth, cohorts of 20 larvae of each genotype that had hatched were selected randomly after 24 h. Staged larvae were placed on fresh apple juice-agar plates with yeast paste at the center of the plates, allowed to grow for an additional 72 h at 25°C, then visualized with a DF PLAPO 1.2× PF objective on a SZX12 microscope (Olympus) equipped with a PC1015 camera (Canon) and digitally photographed every 24 h after hatching. Larval cross-sectional area was measured using ImageJ software. Plates were monitored until Day 4. The growth assay was repeated 3 times with more than 20 larvae in each experimental group. To assay larval mobility, larvae of each genotype were placed at one end of an apple juice agar plate and allowed to crawl to yeast paste placed at other end of the plate. The distance crawled in 10 min was measured. Five-day old larvae of each genotype were digitally photographed with a SZX12 microscope as above. Images were assembled with ImageJ and Adobe Photoshop.

2.21 Microarray Analysis

RNA extraction was performed by Dr. Andrew Simmonds, University of Alberta and RNA labeling, hybridization, and microarray scanning was performed by Anna Hutton, University of Alberta.

Heterozygous $l(3)70Da^{s4868}/TM3, P\{ActGFP\}JMR2, Ser^l$ parents were allowed to lay embryos on apple juice-agar plates for 30 min at 25°C. The plates were then supplemented with yeast paste, and the embryos were allowed to develop for 48 h at 25°C and 70% humidity. Hatched larvae were then hand sorted under a SX61 fluorescence stereomicroscope (Olympus) to select homozygous $l(3)70Da^{s4868}$, i.e. those lacking GFP, larvae. Care was taken to select only larvae

judged clearly to be alive as evidenced by their movement. Corresponding wild-type siblings were isolated from $w^{1118}/TM3$, $P\{ActGFP\}MR2$, Ser^l parents. Total mRNA from 200 mg samples was isolated using Trizol (Invitrogen) and purified using RNeasy. The resulting RNA was tested for quality with an Agilent 2100 Bioanalyzer. 100 ng of the total RNA was labeled with the GeneChip 3' IVT Express Kit (Affymetrix). Poly-A RNA controls were added to the sample as per manufacturers instructions. The size of the biotin-modified antisense RNA (aRNA) with in vitro transcription labeling was evaluated using an Agilent 2100 Bioanalyzer RNA nano LabChip Kit (Affymetrix) and most aRNA was between 600-1200 nt. RNA was converted to labeled cRNA and hybridized to GeneChip Drosophila Genome 2.0 3'-UTR microarrays (Affymetrix). 10 ug of the fragmented biotin-modified aRNA was hybridized to the microarray and the arrays were hybridized for 16 hours at 45°C with the rotation of the oven set to 60 rpm in a GeneChip Hybridization Oven 640 (Affymetrix). 20x eukaryotic hybridization controls were added to the hybridization cocktail. Arrays were washed and stained using a GeneChip Fluidics Station 450 and a GeneChip Hybridization, Wash and Stain Kit (Affymetrix). Finally, the arrays were then read on a GeneChip Scanner 7G (Affymetrix). These experiments were run in triplicate. The resulting array data were normalized using the MAS5 algorithm and Expression Console software (Affymetrix). Genes showing a reproducible 3-fold increase or decrease in expression relative to their expression in wild-type siblings in 3 independent experiments were clustered based on their functional Gene Ontology annotations and known biochemical pathways using the DAVID package (Huang et al., 2009). Clustering of related genes according to their functional Gene Ontology annotations was done using the Cluego plugin (Bindea et al., 2009) for Cytoscape (www.cytoscape.org/).

2.22 Comparative Genomic Survey

Organisms whose genome sequences were surveyed in this study are listed in Table 2-15. We tailored this list to balance between maximizing sampling of taxonomic diversity within opisthokonts and delving more deeply into the fungal and metazoan groups, while maintaining computational tractability. Although we analyzed organisms having fully sequenced genomes wherever possible, we also sampled from organisms in several key lineages that have unpublished and unfinished genomes, including *Puccinia graminis*, *Batrachochytrium dendrobatidis*, *Spizellomyces punctatus*, *Allomyces macrogynus*, *Salpingoeca rosetta*, *Sphaeforma arctica*, *Capsaspora owczarzaki* and *Thecamonas trahens*. We recognize the limitations regarding statements of absence in comparative genomics and attempted when possible to only derive such conclusions from taxonomic groupings with more than one genome representative. Genome sequences were obtained from the Broad Institute, Joint Genome Institute, the National Center for Bioinformatics and Information (NCBI), and the Génolevures Sequencing Consortium.

Table 2-15. Organisms whose genomes were surveyed in this study.

Organism	Kingdom	Phylum	Subphylum/other	Reference
<i>Saccharomyces cerevisiae</i>	Fungi	Ascomycota	Saccharomycotina	(Goffeau et al., 1996; Cherry et al., 1998; Liti et al., 2009)
<i>Candida glabrata</i>	Fungi	Ascomycota	Saccharomycotina	(Dujon et al., 2004)
<i>Kluyveromyces lactis</i>	Fungi	Ascomycota	Saccharomycotina	(Dujon et al., 2004)
<i>Ashbya gossypii</i>	Fungi	Ascomycota	Saccharomycotina	(Dietrich et al., 2004)
<i>Debaryomyces hansenii</i>	Fungi	Ascomycota	Saccharomycotina	(Dujon et al., 2004)
<i>Pichia stipitis</i>	Fungi	Ascomycota	Saccharomycotina	(Jeffries et al., 2007)
<i>Candida albicans</i>	Fungi	Ascomycota	Saccharomycotina	(Jones et al., 2004b)
<i>Pichia pastoris</i>	Fungi	Ascomycota	Saccharomycotina	(de Schutter et al., 2009)
<i>Yarrowia lipolytica</i>	Fungi	Ascomycota	Saccharomycotina	(Dujon et al., 2004)
<i>Neurospora crassa</i>	Fungi	Ascomycota	Pezizomycotina	(Galagan et al., 2003)
<i>Gibberella zeae</i>	Fungi	Ascomycota	Pezizomycotina	Broad Institute ^a
<i>Botryotinia fuckeliana</i>	Fungi	Ascomycota	Pezizomycotina	Broad Institute ^b
<i>Coccidioides immitis</i>	Fungi	Ascomycota	Pezizomycotina	(Neafsey et al., 2010)
<i>Aspergillus nidulans</i>	Fungi	Ascomycota	Pezizomycotina	(Galagan et al., 2005)
<i>Pneumocystis carinii</i>	Fungi	Ascomycota	Taphrinomycotina	<i>Pneumocystis</i>

<i>Schizosaccharomyces japonicus</i>	Fungi	Ascomycota	Taphrinomycotina	Genome Project ^c Broad Institute ^d
<i>Schizosaccharomyces pombe</i>	Fungi	Ascomycota	Taphrinomycotina	Broad Institute ^d , (Wood et al., 2002)
<i>Laccaria bicolor</i>	Fungi	Basidiomycota	Agaricomycotina	(Martin et al., 2008)
<i>Coprinopsis cinerea</i>	Fungi	Basidiomycota	Agaricomycotina	(Stajich et al., 2010)
<i>Ustilago maydis</i>	Fungi	Basidiomycota	Ustilagomycotina	(Kämper et al., 2006)
<i>Puccinia graminis</i>	Fungi	Basidiomycota	Puccinomycotina	Broad Institute ^e
<i>Rhizopus oryzae</i>	Fungi	Zygomycota		(Ma et al., 2009)
<i>Encephalitozoon cuniculi</i>	Fungi	Microsporidia		(Katinka et al., 2001)
<i>Batrachochytrium dendrobatidis</i>	Fungi	Chytridiomycota		Broad Institute ^f
<i>Allomyces macrogynus</i>	Fungi	Chytridiomycota		Broad Institute ^g
<i>Spizellomyces punctatus</i>	Fungi	Chytridiomycota		Broad Institute ^g
<i>Sphaeroforma arctica</i>	Fungal/ Metazoan <i>insertae sedis</i>		Ichthyosporea	Broad Institute ^g
<i>Capsaspora owczarzaki</i>	Fungal/ Metazoan <i>insertae sedis</i>		Filasterea	Broad Institute ^g
<i>Monosiga brevicollis</i>	Fungal/ Metazoan <i>insertae sedis</i>		Choanoflagellida	(King et al., 2008)
<i>Salpingoeca rosetta</i>	Fungal/ Metazoan <i>insertae sedis</i>		Choanoflagellida	Broad Institute ^g
<i>Trichoplax adhaerens</i>	Metazoa	Placozoa		(Srivastava et al., 2008)
<i>Nematostella vectensis</i>	Metazoa	Cnidaria		(Putnam et al., 2007)
<i>Caenorhabditis elegans</i>	Metazoa	Nematoda		(C elegans Sequencing Consortium, 1998)

<i>Drosophila melanogaster</i>	Metazoa	Arthropoda		(Adams et al., 2000)
<i>Strongylocentrotus purpuratus</i>	Metazoa	Echinodermata		(Sea Urchin Genome Sequencing Consortium et al., 2006)
<i>Branchiostoma floridae</i>	Metazoa	Chordata	Cephalochordata	(Putnam et al., 2008)
<i>Fugu rubripes</i>	Metazoa	Chordata	Craniata	(Aparicio et al., 2002)
<i>Xenopus tropicalis</i>	Metazoa	Chordata	Craniata	Joint Genome Institute
<i>Gallus gallus</i>	Metazoa	Chordata	Craniata	(International Chicken Genome Sequencing Consortium, 2004)
<i>Mus musculus</i>	Metazoa	Chordata	Craniata	(Mouse Genome Sequencing Consortium et al., 2002)
<i>Homo sapiens</i>	Metazoa	Chordata	Craniata	(Lander et al., 2001; Venter et al., 2001)
<i>Thecamonas trahens</i>			Apusomonadidae	Broad Institute ^g
<i>Dictyostelium discoideum</i>			Dictyosteliida	(Eichinger et al., 2005)
<i>Dictyostelium purpureum</i>			Dictyosteliida	(Sucgang et al., 2011)

^aThe *Fusarium* Comparative Sequencing Project, Broad Institute of Harvard and MIT (broadinstitute.org)

^bThe *Botrytis cinerea* Genome Sequencing Project, Broad Institute of Harvard and MIT (broadinstitute.org)

^cThe *Pneumocystis* Genome Project, University of Cincinnati College of Medicine (pgp.cchmc.org)

^dThe *Schizosaccharomyces* Comparative Genome Project, Broad Institute of Harvard and MIT (broadinstitute.org)

^eThe *Batrachochytrium dendrobatidis* Genome Sequencing Project, Broad Institute of Harvard and MIT (broadinstitute.org)

^fThe Origins of Multicellularity Sequencing Project, Broad Institute of Harvard and MIT (broadinstitute.org)

^gThe *Xenopus tropicalis* Sequencing Project, The Joint Genome Institute (jgi.doe.gov)

2.22.1 Comparative genomic survey of Pex30p homologs

The identification of putative homologs of Pex30p followed a heuristic process of iterative searches using the basic local alignment search tool for proteins (BLASTP 2.2.22+) (Altschul et al., 1997) (Schäffer et al., 2001) and profile hidden Markov model (HMM) search algorithms, HMMER 2.3.3 (Eddy, 1998) and HMMER 3.0 (Eddy, 2009). Each survey was initiated by querying publicly hosted genomes at the NCBI using BLASTP with a cutoff expect (e-) value for positive candidate homologs set at 0.05. Those genomes not hosted by NCBI were queried locally using the BLASTP program. In order to reduce the chance for corruption in subsequent HMMs, and to verify

candidates, putative homolog sequences were used as BLASTp queries into the *S. cerevisiae* genome and considered validated if they returned the functionally characterized protein sequence as the best scoring retrieved sequence (Tatusov et al., 1997; Bork et al., 1998).

Validated sequences were aligned using MUSCLE 3.6 (Edgar, 2004) and used to build a HMM using a maximum likelihood architecture construction algorithm (Eddy, 2008; 1998). This model was then used to search the locally hosted genomes listed in Table 2-15 for putative homologs. Newly identified sequences below the 0.05 E-value cutoff were validated by reciprocal pHMMer and added to the HMM iteratively until all genomes had been searched and the list of candidate homologs was exhausted.

The identification of putative homologs of Pex30p in the Saccharomycotina followed a heuristic process of iterative searches using pHMMer (Eddy, 2009). Initially, simultaneous pHMMer searches using Pex30p, Pex29p, Pex28p, Pex31p and Pex32p of *Saccharomyces cerevisiae* and Pex23p and Pex24p of *Yarrowia lipolytica* were used to identify and classify putative homologs of each protein. Each survey was initiated by querying locally hosted genomes (Table 2-16) with a cutoff expect value for positive candidate homologs set at 0.05. Reciprocal pHMMer searches with these candidate homologs were considered validated if they returned the functionally characterized proteins as the best scoring retrieved sequence (Tatusov et al., 1997; Bork et al., 1998).

Table 2-16. Organisms in the Saccharomycotina whose genomes were surveyed for Pex30 family orthologs.

Organism	Taxonomy Info	Source ^a
<i>Saccharomyces cerevisiae</i>	<i>Saccharomycetaceae</i> ; <i>Saccharomyces</i>	SGD
<i>Saccharomyces paradoxus</i>	<i>Saccharomycetaceae</i> ; <i>Saccharomyces</i>	
<i>Saccharomyces mikatae</i>	<i>Saccharomycetaceae</i> ; <i>Saccharomyces</i>	
<i>Saccharomyces bayanus</i>	<i>Saccharomycetaceae</i> ; <i>Saccharomyces</i>	
<i>Candida glabrata</i>	<i>Saccharomycetaceae</i> ; <i>Nakaseomyces</i>	NCBI
<i>Saccharomyces castelii</i>	<i>Saccharomycetaceae</i> ; <i>Naumovozyma</i>	JGI
<i>Vanderwaltozyma polyspora</i>	<i>Saccharomycetaceae</i> ; <i>Vanderwaltozyma</i>	JGI

<i>Zygosaccharomyces rouxii</i>	Saccharomycetaceae; <i>Zygosaccharomyces</i>	JGI
<i>Kluyveromyces lactis</i>	Saccharomycetaceae; <i>Kluyveromyces</i>	NCBI
<i>Ashbya gossypii</i>	Saccharomycetaceae; <i>Eremothecium</i>	NCBI
<i>Saccharomyces kluyveri</i>	Saccharomycetaceae; <i>Lachancea</i>	JGI
<i>Kluyveromyces waltii</i>	Saccharomycetaceae; <i>Lachancea</i>	JGI
<i>Dekkera bruxellensis</i>	Saccharomycetaceae; <i>Dekkera</i>	JGI
<i>Pichia pastoris</i>	Saccharomycetaceae; <i>Komagataella</i>	NCBI
<i>Pachysolen tannophilus</i>	Saccharomycetaceae; <i>Pachysolen</i>	JGI
<i>Nadsonia fulvescens</i>	Saccharomycodaceae; <i>Nadsonia</i>	JGI
<i>Hanseniaspora valbyensis</i>	Saccharomycodaceae; <i>Hanseniaspora</i>	JGI
<i>Wickerhamomyces anomalus</i>	Phaffomycetaceae; <i>Wickerhamomyces</i>	JGI
<i>Babjeviella inositolivora</i>	Debaryomycetaceae; <i>Babjeviella</i>	JGI
<i>Lodderomyces elongisporus</i>	Debaryomycetaceae; <i>Lodderomyces</i>	Broad
<i>Spathaspora passalidarum</i>	Debaryomycetaceae; <i>Spathaspora</i>	JGI
<i>Pichia guilliermondii</i>	Debaryomycetaceae; <i>Meyerozyma</i>	JGI
<i>Pichia stipitis</i>	Debaryomycetaceae; <i>Scheffersomyces</i>	JGI
<i>Debaryomyces hansenii</i>	Debaryomycetaceae; <i>Debaryomyces</i>	NCBI
<i>Hyphopichia burtonii</i>	Metschnikowiaceae; <i>Hyphopichia</i>	JGI
<i>Clavispora lusitanae</i>	Metschnikowiaceae; <i>Clavispora</i>	JGI
<i>Metschnikowia bicuspidata</i>	Metschnikowiaceae; <i>Metschnikowia</i>	JGI
<i>Ascoidea rubescens</i>	Ascoideaceae; <i>Ascoidea</i>	JGI
<i>Candida arabinofementans</i>	mitosporic Saccharomycetales; <i>Candida</i>	JGI
<i>Candida albicans</i>	mitosporic Saccharomycetales; <i>Candida</i>	NCBI
<i>Candida caseinolytica</i>	mitosporic Saccharomycetales; <i>Candida</i>	JGI
<i>Candida parapsilosis</i>	mitosporic Saccharomycetales; <i>Candida</i>	JGI
<i>Candida tenuis</i>	mitosporic Saccharomycetales; <i>Candida</i>	JGI
<i>Candida tropicalis</i>	mitosporic Saccharomycetales; <i>Candida</i>	JGI
<i>Pichia membranifaciens</i>	Pichiaceae; <i>Pichia</i>	JGI
<i>Hansenula polymorpha</i>	Saccharomycetales incertae sedis; <i>Ogataea</i>	JGI
<i>Yarrowia lipolytica</i>	Dipodascaceae; <i>Yarrowia</i>	NCBI
<i>Lipomyces starkeyi</i>	Lipomycetaceae; <i>Lipomyces</i>	JGI

^aSGD: (yeastgenome.org)

NCBI: (ncbi.nlm.nih.gov)

JGI: (genome.jgi.doe.gov/programs/fungi/index.jsf)

2.22.2 Comparative genomic survey of organelle inheritance machinery

The identification of putative homologs of the organelle inheritance machinery followed a heuristic process of iterative searches using the basic local alignment search tool for proteins (BLASTP 2.2.22+) (Altschul et al., 1997) (Schäffer et al., 2001) and profile hidden Markov model (HMM) search algorithms, HMMER 2.3.3 (Eddy, 1998) and HMMER 3.0 (Eddy, 2009). Each survey was

initiated by querying publicly hosted genomes at the NCBI using BLASTP with a cutoff expect (e-) value for positive candidate homologs set at 0.05. Those genomes not hosted by NCBI were queried locally using the BLASTP program. In order to reduce the chance for corruption in subsequent HMMs, and to verify candidates, putative homolog sequences were used as BLASTp queries into the *S. cerevisiae* genome and considered validated if they returned the functionally characterized protein sequence as the best scoring retrieved sequence (Bork et al., 1998; Tatusov et al., 1997).

Validated sequences were aligned using MUSCLE 3.6 (Edgar, 2004) and used to build a HMM using a maximum likelihood architecture construction algorithm (Eddy, 1998; 2008). This model was then used to search the locally hosted genomes listed in Table 2-15 for putative homologs. Newly identified sequences below the 0.05 E-value cutoff were validated by reciprocal BLAST and added to the HMM iteratively until all genomes had been searched and the list of candidate homologs was exhausted. High scoring false-positives can result from gene paralogy, as in the case of the myosin superfamily, or the presence of highly conserved protein domains, as in the case of multiple armadillo repeats present in Vac8p (Wang et al., 1998). In the surveys for homologs of myosin V, Bim1p and Vac8p, it was necessary to perform an additional verification step using BLAST to query the human genome.

2.23 Alignment and Phylogenetic Analysis

PRANK (Löytynoja and Goldman, 2008) was used to align the validated homologs of Pex30p. MUSCLE 3.6 was used to align the validated homologs of Pex3p and myosin V. The alignments were then visually inspected and masked so as to retain only unambiguously homologous positions for analysis. For Pex30p, the analysis consisted of 49 sequences and 339 positions spanning the saccharomycotina with *Neurospora crassa*, *Magnaporthe grisea*, *Botryotinia fuckeliana*, and *Coprinopsis cinerea* as outgroups. For Pex3p, the analysis consisted of 39 sequences and 343 positions spanning

the opisthokonts with apusomonad and amoebae outgroups. Removal of these outgroups improves the branching order of the *Y. lipolytica* Pex3p paralogs (Figure 5-3). For myosin V, the analysis consisted of 69 sequences and 1488 positions.

Prot-test version 1.3 (Wiese et al., 2007) was used to estimate the optimal model of sequence evolution. Analyses were run incorporating corrections for the model of amino acid transition, as well as invariable and unequal rates among sites, as relevant. The optimal model for both Pex3 and myosin V was WAG +I +G.

Mr. Bayes version 3.2 (Ronquist and Huelsenbeck, 2003) was used to produce the optimal tree topology and posterior probability values. Analyses were run for 1,000,000 Markov chain Monte Carlo generations, and the burn-in values were obtained by ensuring that the two independent runs had converged with a split frequency of 0.1 and by removing all trees prior to a graphically determined plateau of $-lnl$ values. Additionally, maximum-likelihood (ML) bootstrap values were obtained using the programs PhyML version 2.44 (Guindon and Gascuel, 2003) and RAxML version 7.0.0 (Stamatakis, 2006) with values expressed as a percent based on 1000 pseudoreplicates.

For the phylogeny of Pex30p, PhyML version 2.44 was used to estimate the optimal tree topology and estimate the optimal model of sequence evolution. ML bootstrap values were obtained from both PhyML and RAxML based on 100 pseudoreplicates.

3 A reticulon-peroxin complex regulates peroxisome biogenesis from the ER

A version of this chapter has been submitted for publication.

Mast, F.D., A.P. Jamakhandi, R.A. Saleem, D.J. Dilworth, R.S. Rogers, R.A. Rachubinski and J.D. Aitchison. 2013. A reticulon-peroxin complex regulates peroxisome proliferation from the ER. *J Cell Biol.*

3.1 Peroxisome biogenesis in *S. cerevisiae*

Peroxisome biogenesis and proliferation occur through two separate pathways: de novo biogenesis, in which new peroxisomes derive from the ER, and the division of existing peroxisomes (Hettema and Motley, 2009). The interplay between these biogenesis pathways is envisaged to be tightly regulated spatially and temporally and to require the assembly of distinct protein complexes and the recruitment of distinct lipids at the interface between peroxisomes and the ER. Cells lacking peroxisomes due to a segregation defect required an average of four hours before de novo peroxisomes were detected (Hoepfner et al., 2005; Motley and Hettema, 2007). Compared to the ~90 minutes required for cell division (Johnston et al., 1977), these findings seem to indicate that de novo biogenesis of peroxisomes is an inefficient process in *S. cerevisiae*. However, the mechanisms regulating peroxisome biogenesis and proliferation remain poorly understood.

To begin to examine mechanisms regulating peroxisome proliferation, we first investigated the ways in which peroxisomes proliferate in yeast. Historically, peroxisome biogenesis and proliferation were studied in yeast grown in the presence of a non-fermentable carbon source such as oleic acid (Veenhuis et al., 1987). This is because peroxisomes are the sole site of β -oxidation in yeast, which makes use of this conditional requirement for peroxisome function a useful strategy in genetic screens designed to identify novel factors involved in peroxisome biogenesis (Erdmann et al., 1989; Smith et al., 2002; 2006). Peroxisomes are not essential for growth in the presence of a fermentable carbon source such as glucose (Smith et al., 2006). Furthermore, growth in the presence of a non-fermentable carbon source renders peroxisomes more amenable to ultrastructural analysis by electron microscopy and biochemical characterization by subcellular fractionation techniques (Erdmann and Blobel, 1995).

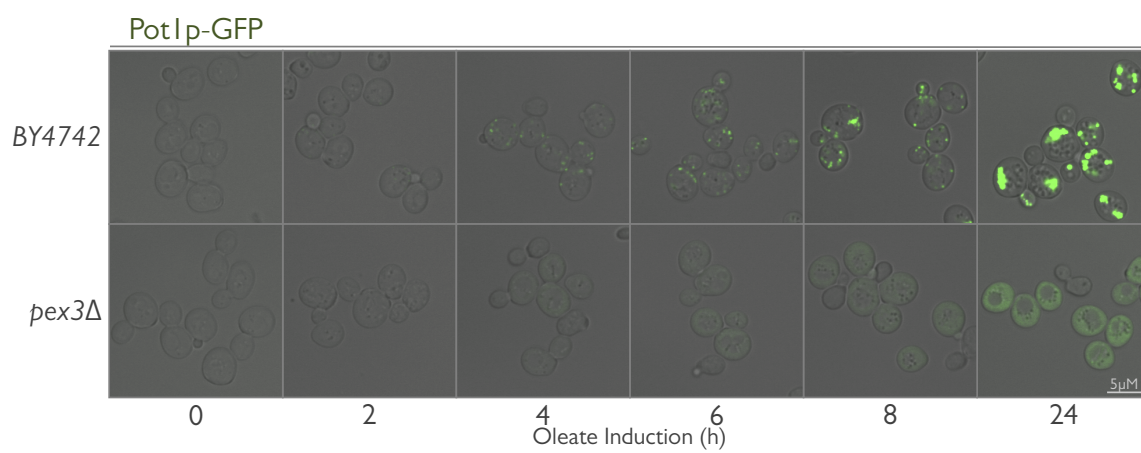
When grown in a medium containing a non-fermentable carbon source, yeast peroxisomes proliferate in size and number (Veenhuis et al., 1987). This can be demonstrated by imaging yeast cells expressing a chimera of 3-ketoacyl-CoA thiolase and green fluorescent protein, Pot1p-GFP,

after timed intervals of growth in an oleic acid containing medium using confocal microscopy (Figure 3-1) (Saleem et al., 2008). Within two hours of incubation peroxisomes are visible as fluorescent puncta distributed throughout the cytoplasm. Successively longer incubations of up to eight hours reveal more puncta of greater fluorescence intensity, but after this time peroxisomes appear to cluster in the center of the cell. The clustering of peroxisomes after prolonged periods of incubation in oleic acid containing medium has been confirmed by electron microscopy to be smaller individual peroxisomes tightly associated with each other and not one large peroxisome (Saleem et al., 2008).

Recent evidence suggests the primary phenotype of fatty acid-induced peroxisome proliferation is an increase in organelle size. Visualizing Pot1p-GFP by 3D confocal microscopy in wild-type cells incubated in an oleic acid containing medium showed the average number of peroxisomes per cell only increased from ~9 after 2 hours to ~11 after 8 hours (Tower et al., 2011). Over a similar timeframe, peroxisomes increased in density from 1.15 g/cm³ to 1.21 g/cm³ (Erdmann and Blobel, 1995). This increase in density is presumably accompanied by an increase in peroxisome size, as longer incubations in an oleic acid containing medium produce readily identifiable peroxisomes by electron microscopy, but this has never been formally tested.

To assess the degree of continuity between peroxisome populations from cells incubated in glucose containing medium to peroxisome populations from cells incubated in oleic acid containing medium, we performed a colocalization experiment between the PMP Pex3p, and the peroxisomal matrix protein, Pot1p, using 3D confocal microscopy (Figure 3-2A). Endogenous Pex3p was tagged at its C-terminus with GFP (Pex3p-GFP) and Pot1p was tagged at its C-terminus with monomeric red fluorescent protein (Pot1p-mRFP). Initially, only Pex3p-GFP puncta were visible and seen distributed throughout the cytoplasm of cells incubated in glucose containing medium. However, after two hours of incubation in oleic acid

Figure 3-1. Peroxisome biogenesis in *Saccharomyces cerevisiae*. Time course of peroxisome biogenesis over 24 h of incubation in oleate-containing YPBO medium. Peroxisomes are punctate structures appearing in wild-type *BY4742* cells after 2 h incubation. The fluorescent intensity of the Pot1p-GFP reporter increases over time, and peroxisomes cluster after prolonged exposure to oleic acid. In contrast, *pex3Δ* cells show a cytosolic accumulation of Pot1p-GFP over time. Bar, 5 μ m.

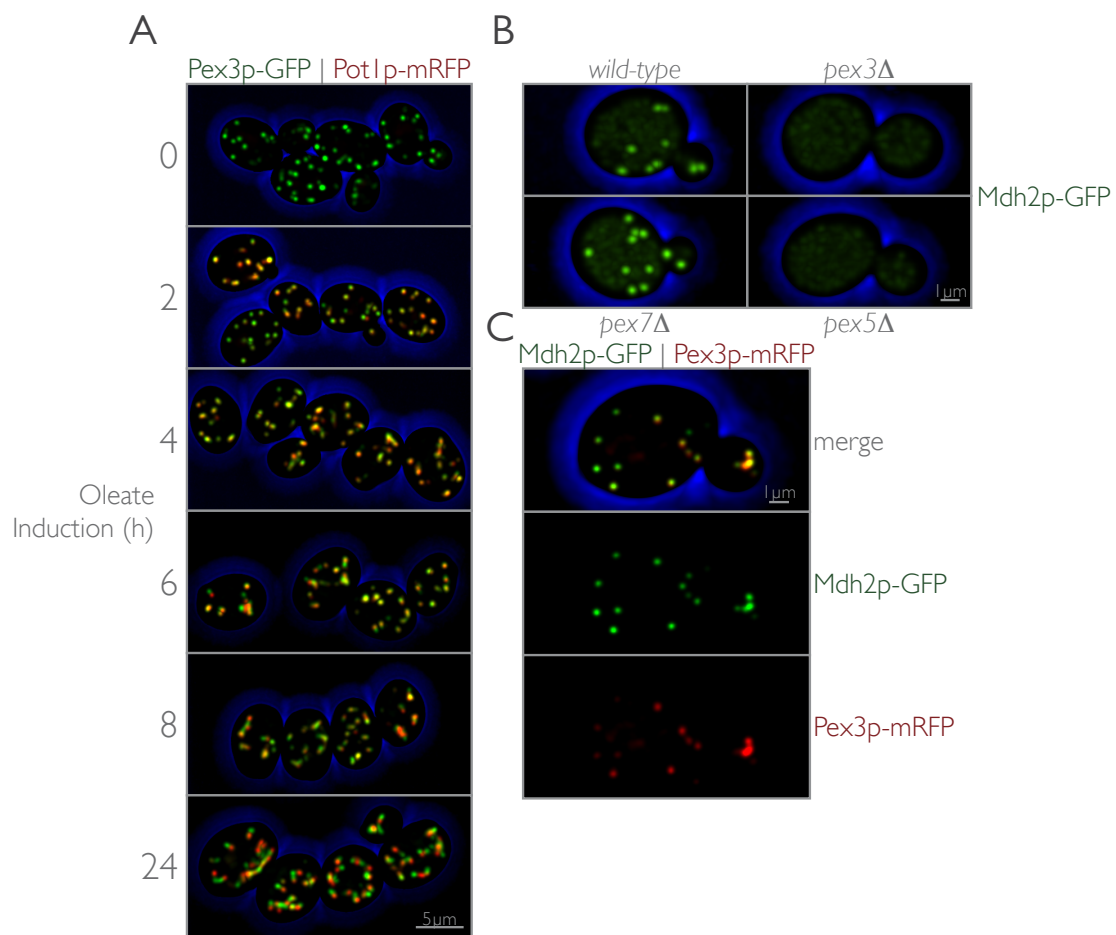


containing medium, Pot1p-mRFP fluorescent signal could be visualized overlapping the Pex3p-GFP signal. The intensity from the two fluorescent signals was not perfectly correlated, as each peroxisome varied in the levels of Pex3p-GFP and Pot1p-mRFP, but each peroxisome contained some level of red and some level of green fluorescent signal. Longer incubations did not dramatically alter this phenotype until the 8 hour timepoint, when a segregation of Pex3p-GFP and Pot1p-mRFP into distinguishable, partly overlapping but juxtaposed, fluorescent puncta became apparent (Figure 3-2A). The extent of this juxtaposition was enhanced at the 24 hour timepoint and may suggest remodeling events occurring in the peroxisome membrane after prolonged exposure to oleic acid.

These data demonstrate that all Pex3p-GFP labeled puncta become “mature” peroxisomes as defined by their import competency for Pot1p-GFP but leave unresolved the state of the Pex3p-GFP puncta in cells grown in the presence of glucose. Furthermore, this conversion to “maturity” must occur relatively early after incubation in oleic acid containing medium as demonstrated by the complete overlap of fluorescence between Pex3p-GFP and Pot1p-mRFP at the 2 hour timepoint.

Peroxisomes have been shown to import readily synthetic peroxisomal matrix proteins, like CFP-SKL or HcRed-SKL (Hoepfner et al., 2005; Motley and Hettema, 2007), when cells are grown in the presence of glucose, but this could represent an artifact of induction and not be representative of wild-type conditions. A search of the Yeast GFP Fusion Localization Database (yeastgfp.yeastgenome.org) revealed a potential endogenous peroxisomal matrix protein candidate for cells grown in the presence of glucose in malate dehydrogenase 2 (Mdh2p). Incidentally, Mdh2p was also identified as being a peroxisome constituent by quantitative mass spectrometric analysis of the peroxisome proteome (Marelli et al, 2004). Endogenously expressed Mdh2p-GFP localized to punctate structures characteristic of peroxisomes in cells grown in the presence of glucose in addition to a diffuse cytosolic pattern (Figure 3-2B). This localization requires peroxisomes to be present, as only the diffuse cytosolic signal was detected in a *pex3Δ*

Figure 3-2. Peroxisome morphology in cells grown in the presence of oleate or glucose. (A) Time course of peroxisome biogenesis in wild-type cells over 24 h of incubation in oleate-containing YPBO medium. Peroxisomes labeled by Pex3p-GFP appear as punctate structures at the 0 h timepoint. Pot1p-mRFP signal is detectable after 2 h incubation in oleate and colocalizes with the fluorescent signal from Pex3p-GFP. The fluorescence intensity of the Pot1p-mRFP reporter increases over time, and peroxisomes cluster after prolonged exposure to oleic acid. After 24 h of incubation, the Pex3p-GFP and Pot1p-mRFP signals appear juxtaposed and partially overlap. Bar, 5 μ m. **(B)** Mdh2p is a peroxisomal matrix protein in cells grown in the presence of glucose. Mdh2p-GFP localizes to punctate structures in wild-type and *pex7 Δ* , cells with some background cytosolic fluorescent signal also detected; however, it is exclusively cytosolic in *pex3 Δ* and *pex5 Δ* cells. Bar, 1 μ m. **(C)** Pex3p-mRFP in cells grown in the presence of glucose is exclusively peroxisomal. Mdh2p-GFP and Pex3p-mRFP colocalized to peroxisomes in glucose-grown cells. Bar, 1 μ m.



strain. Furthermore, import of Mdh2p-GFP into peroxisomes was dependent on the PTS1 import system as a *pex5Δ* strain also displayed only a diffuse cytosolic localization of Mdh2p-GFP, whereas a punctate localization was observed in a *pex7Δ* strain. Pex5p recognizes a tripeptide serine-lysine-leucine PTS1 motif at the C-terminus of proteins (Terlecky et al, 1995) but Mdh2p does not contain any recognizable PTS1. Furthermore, the appending of GFP to the C-terminus of Mdh2p would mask this targeting sequence and render a PTS1 containing protein incapable of being imported into peroxisomes. Regardless, Mdh2p-GFP is imported into peroxisomes and relies on Pex5p to achieve this import. It therefore interacts either with Pex5p in a non-PTS1 fashion or with a PTS1 containing protein and is then piggybacked into the peroxisome (Glover et al., 1994).

We next assessed the import competency of Pex3p-labeled puncta from cells grown in glucose-containing medium. Cells expressing Mdh2p-GFP and Pex3p-mRFP from their endogenous promoters were grown in glucose-containing medium and imaged by 3D confocal microscopy (Figure 3-2C). Colocalization between Mdh2p-GFP and Pex3p-mRFP was similar to what was observed at the 2 hour timepoint for Pex3p-GFP and Pot1p-mRFP (Figure 3-2A). Overlap in the fluorescence signal from each fluorophore in punctate structures characteristic of peroxisomes was detected, although a perfect correlation between fluorescent signals was again absent. Mdh2p is not the only soluble protein that localizes to peroxisomes in cells grown in the presence of glucose. Glycerol-6-phosphate dehydrogenase (Gpd1p) utilizes a PTS2 sequence that is regulated by reversible phosphorylation to gain access to peroxisomes via an interaction with the PTS2 receptor Pex7p, depending on metabolic conditions (Jung et al., 2010; Marelli et al., 2004). Similarly, pyrazinadase and nicotinamidase I (Pnc1p) also localizes to peroxisomes in a Pex7p-dependent manner (Anderson et al., 2003; Jung et al., 2010; Marelli, 2004).

Because of the relatively benign increase in peroxisome number and density under fatty-acid-inducing conditions, the use of fatty acid induction is likely not necessary for characterizing mechanisms of peroxisome biogenesis and proliferation. Thus far, my findings show that

peroxisomes from cells grown in the presence of glucose are “mature” peroxisomes (Figure 3-2C). Furthermore, Pex3p-GFP is a suitable marker of peroxisomes in wild-type cells, as all Pex3p-GFP puncta colocalized with the peroxisomal matrix protein, Mdh2p-GFP.

3.2 The regulation of peroxisome proliferation is independent of cell cycle regulation.

Considering that peroxisome numbers between cell generations remain relatively constant under fermentative and non-fermentative growth conditions, it is tempting to speculate that the fidelity of peroxisome inheritance mechanisms is sufficient enough to regulate peroxisome biogenesis and proliferation. Regulation would then entail a tight coupling between peroxisome division and inheritance in a way that ensured one half of the peroxisome population remained in the mother and one half was sent to the bud. Furthermore, peroxisome proliferation would have to be strictly coupled to the cell cycle in order to support the necessity of matching peroxisome growth with the requirement to divide the cell within the span of a cell cycle, thus ensuring equitable peroxisome retention and inheritance. This is not an inconsequential point, as sophisticated feedback mechanisms would be required to ensure peroxisomes would not become smaller or larger with each cell division. Additionally, in the case of a catastrophic loss of peroxisomes, such as in *inp2Δ* cells that retain all their peroxisomes in the mother cell (Fagarasanu et al., 2006a), the daughter cell would initially require rapid proliferation mechanisms to “catch-up” to the wild-type state and the mother cell would need to dramatically slow its peroxisome growth mechanisms because of all the extra peroxisomes it had retained. However, it is precisely in *inp2Δ* cells that de novo peroxisome biogenesis was demonstrated to be very slow and inefficient (Motley and Hettema, 2007).

Are there conditions where peroxisomes proliferate in number? Johnston and colleagues considered a similar question when they asked if cell growth, of which peroxisome biogenesis and

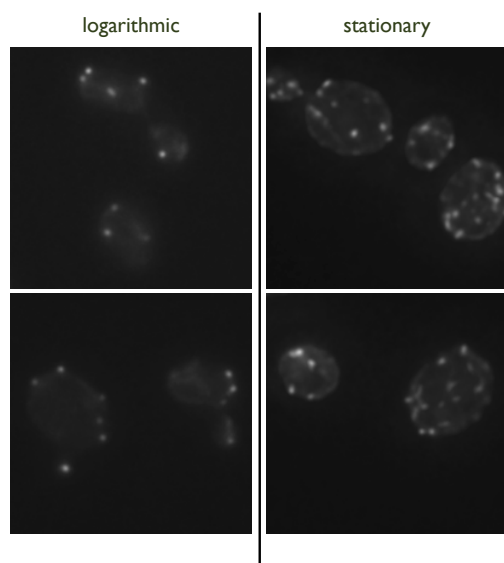
proliferation are a part, could be uncoupled from the cell cycle, i.e. DNA replication and cell division (Johnston et al., 1977). They demonstrated that arresting the cell cycle at different stages by using temperature-sensitive mutants of important cell cycle regulators did not inhibit cell growth, resulting in an uncoupling of the two processes. However, mutants that inhibited growth did inhibit the cell cycle, preventing cell division. The regulation of cell growth in yeast is primarily mediated by transduction of environmental cues through the protein kinase A (PKA) and target of rapamycin (TOR) pathways (Schneper et al., 2004).

Peroxisome number was assessed in conditions where cell growth is uncoupled from the cell cycle. The yeast cell cycle arrests in a stage termed G_0 as a culture moves from logarithmic growth into stationary phase (Herman, 2002). Under this condition of cell cycle arrest, the yeast cell is still metabolically active, growing and accumulating mass. The comparison between logarithmically growing cells and cells arrested in stationary phase provides a natural state for assessing the effect of uncoupling cell growth from the cell cycle on peroxisome proliferation. Cells expressing Pex3p-GFP were first maintained in an early logarithmic phase of growth before being allowed to arrest in stationary phase, and the number of Pex3p-GFP puncta per cell in each growth state was determined by 3D widefield microscopy (Figure 3-3A).

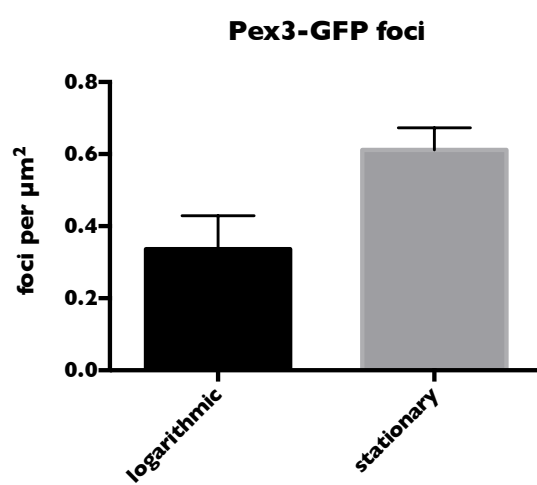
The number of peroxisomes was greater in stationary cells than cells growing logarithmically. Quantification showed that the number of Pex3p-GFP puncta, even when normalized for cell size, was 178% greater in stationary cells than cells growing logarithmically (Figure 3-3B). These data suggest that the regulation of peroxisome proliferation is not dependent on progression through the cell cycle but is rather correlated with the growth cycle of the cell. Therefore, peroxisome inheritance mechanisms and the regulation thereof are insufficient for explaining the regulation of peroxisome biogenesis and proliferation.

Figure 3-3. The number of Pex3p-GFP puncta per cell is growth-state-dependent. (A) Pex3p-GFP puncta are more numerous in stationary cells as compared to cells in a logarithmic stage of growth. (B) Quantification of the numerical density of peroxisomes as visualized by Pex3p-GFP from logarithmically grown cells and cells in stationary phase. Error bars represent the standard error of the mean from 3 individual experiments.

A



B



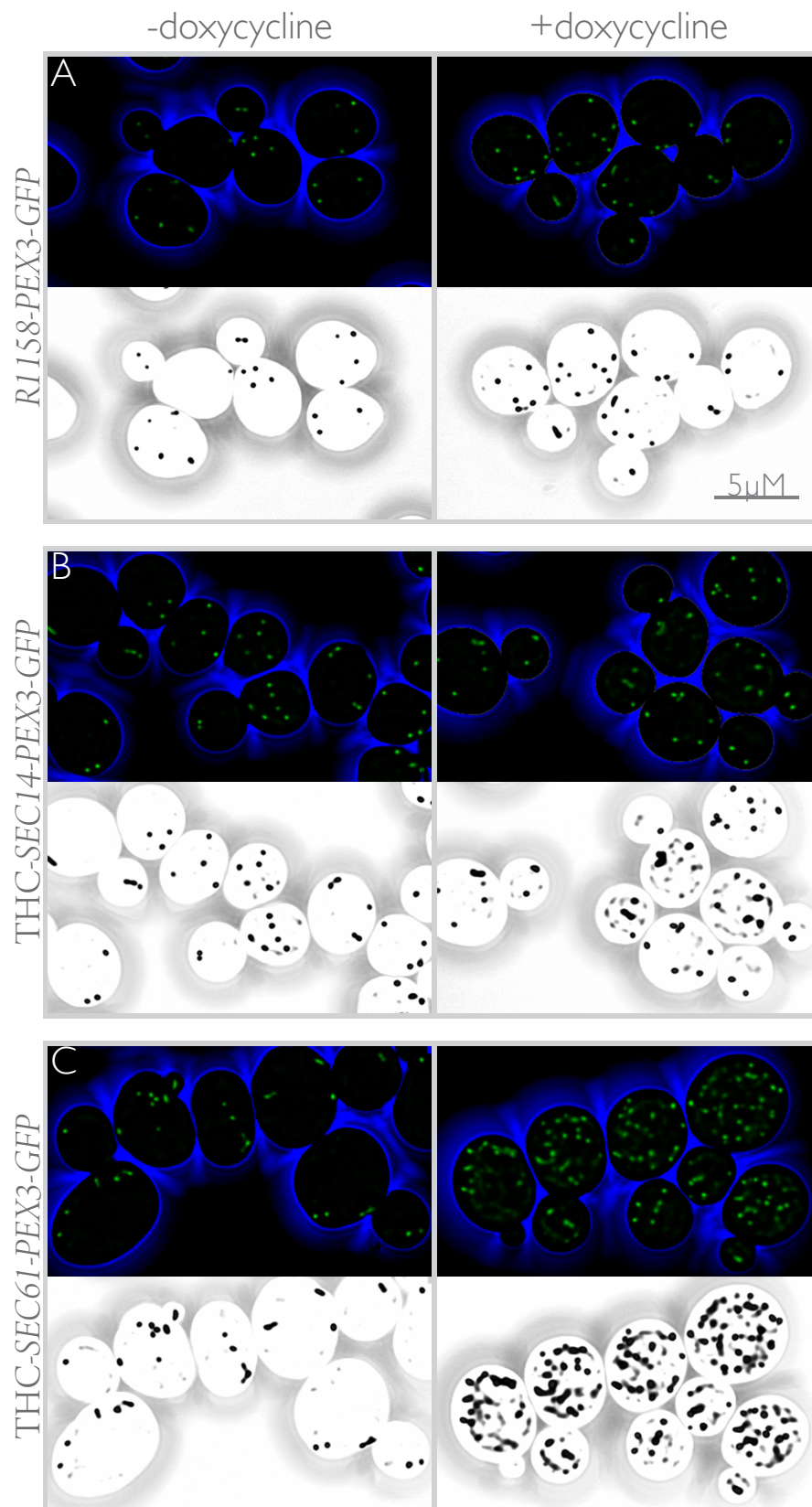
3.3 The ER is involved in regulating peroxisome proliferation in yeast

A screen of 19 essential *SEC* genes of either unknown function or previously implicated in ER to Golgi transport revealed an unexpected role for the ER in regulating peroxisome proliferation (Perry et al., 2009). In this screen the endogenous promoter of an essential gene was replaced by the regulatable TetO₇ promoter, which allowed for controlled repression of the essential gene by addition of doxycycline to the growth medium (Hughes et al., 2000; Mnaimneh et al., 2004). This system uses the tetracycline analogue, doxycycline, and a doxycycline repressible promoter, TetO₇, to tightly regulate gene expression (Garí et al., 1997) in a manner that does not interfere with yeast energy metabolism or global gene expression patterns (Wishart et al., 2005). Peroxisome morphology and assembly were monitored by visualizing Pot1p-GFP in cells grown in the presence or absence of doxycycline in oleic acid-containing medium (Perry et al., 2009). Surprisingly, loss of *SEC61* expression by addition of doxycycline resulted in an increased number of peroxisomes. Sec61p forms the central channel of the ER translocon (Rapoport, 2007). This effect was not specific to a loss of protein import into the ER per se, as repression of *SEC11*, the 18-kDa subunit of the signal peptidase complex (Böhni et al., 1988), or *SEC65*, a component of the signal recognition particle (Ng et al., 1996, Stirling et al., 1992), did not strongly affect peroxisome morphology or number (Perry et al., 2009).

The effect of repressing *SEC61* was further analyzed by monitoring the intracellular distribution of Pex3p-GFP. As expected, Pex3p-GFP localized to several discrete puncta typical of peroxisomes in the wild-type R1158 strain grown in the presence of glucose and irrespective of the presence or absence of doxycycline (Figure 3-4A) (Perry et al., 2009). Similarly, Pex3p-GFP also displayed normal peroxisome morphology in the *THC-SEC14-PEX3-GFP* strain irrespective of doxycycline presence or absence (Figure 3-4B). Sec14p is a phosphatidylinositol/phosphatidylcholine lipid transfer protein (Bankaitis et al., 1990) that is essential for secretory traffic to progress through the Golgi (Novick et al., 1981). Doxycycline

Figure 3-4. Pex3p-GFP labeled peroxisomes proliferate in cells repressed for *SEC61* expression.

(A) THC-*SEC* strains with genomically integrated *PEX3-GFP* were incubated for 18 h in YEPD (-doxycycline). Repression of *TetO₇* promoter-regulated genes was achieved by addition of doxycycline to a concentration of 10 µg/ml in YEPD (+doxycycline). Cells were fixed with formaldehyde, images were captured by confocal microscopy, and a maximum-intensity projection was created from a deconvolved 3D data set using Huygens software. Black-and-white images were generated using the “Blend” viewing mode in Imaris (Bitplane) to enhance the total fluorescence signal located within the cell compared to the maximum-intensity projection. Repression of *SEC61* but not *SEC14*, or addition of doxycycline to controls cells, resulted in peroxisome proliferation. Bar, 5 µm.



repression of *SEC61* resulted in an increased number of Pex3p-GFP puncta consistent with an enhanced peroxisome proliferation phenotype (Figure 3-4C). Therefore, the peroxisome proliferation phenotype appeared to originate at the level of the ER, as peroxisome proliferation was not affected by loss of an essential Golgi localized Sec-protein.

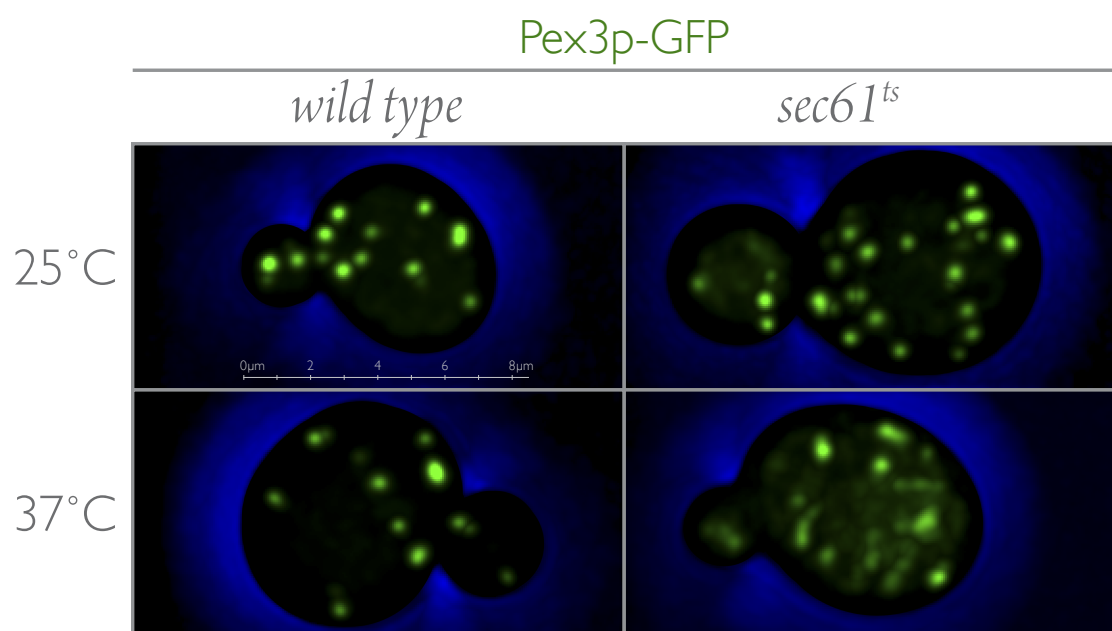
Because of the relatively long treatment time required for doxycycline-mediated repression – 18 hours – we next assessed whether the inactivation of Sec61p on a shorter time scale also resulted in an enhanced peroxisome proliferation phenotype. The localization of endogenously expressed Pex3p-GFP was assessed in a *sec61* temperature-sensitive strain and an isogenic wild-type strain (Stirling et al., 1992). Surprisingly, even at the permissive temperature, a peroxisome proliferation phenotype was detected in the *sec61* mutant strain, as Pex3p-GFP localized to more puncta per cell than in the wild-type strain as detected by 3D confocal microscopy (Figure 3-5). Cells were incubated at the non-permissive temperature for 4 hours before imaging again with 3D confocal microscopy. This time, Pex3p-GFP localized to numerous structures resembling elongated peroxisomes in the process of peroxisome division in the *sec61* mutant strain and again to normal peroxisomes in the wild-type strain.

These findings implicate the ER and the function of *SEC61* in the regulation of peroxisome biogenesis and proliferation.

3.4 Identification of peroxins involved in regulating peroxisome biogenesis and proliferation

Two classes of peroxins regulate peroxisome biogenesis and proliferation: one that promotes it, and one that restricts it (Fagarasanu et al., 2007). In *S. cerevisiae* the first class includes the paralogs Pex11/25/27 that promote peroxisome division by elongating and constricting the organelle (Erdmann and Blobel, 1995; Marshall et al., 1996; Rottensteiner et al., 2003; Smith et al., 2002; Tam et al., 2003). This family of proteins also functions in poorly understood processes required

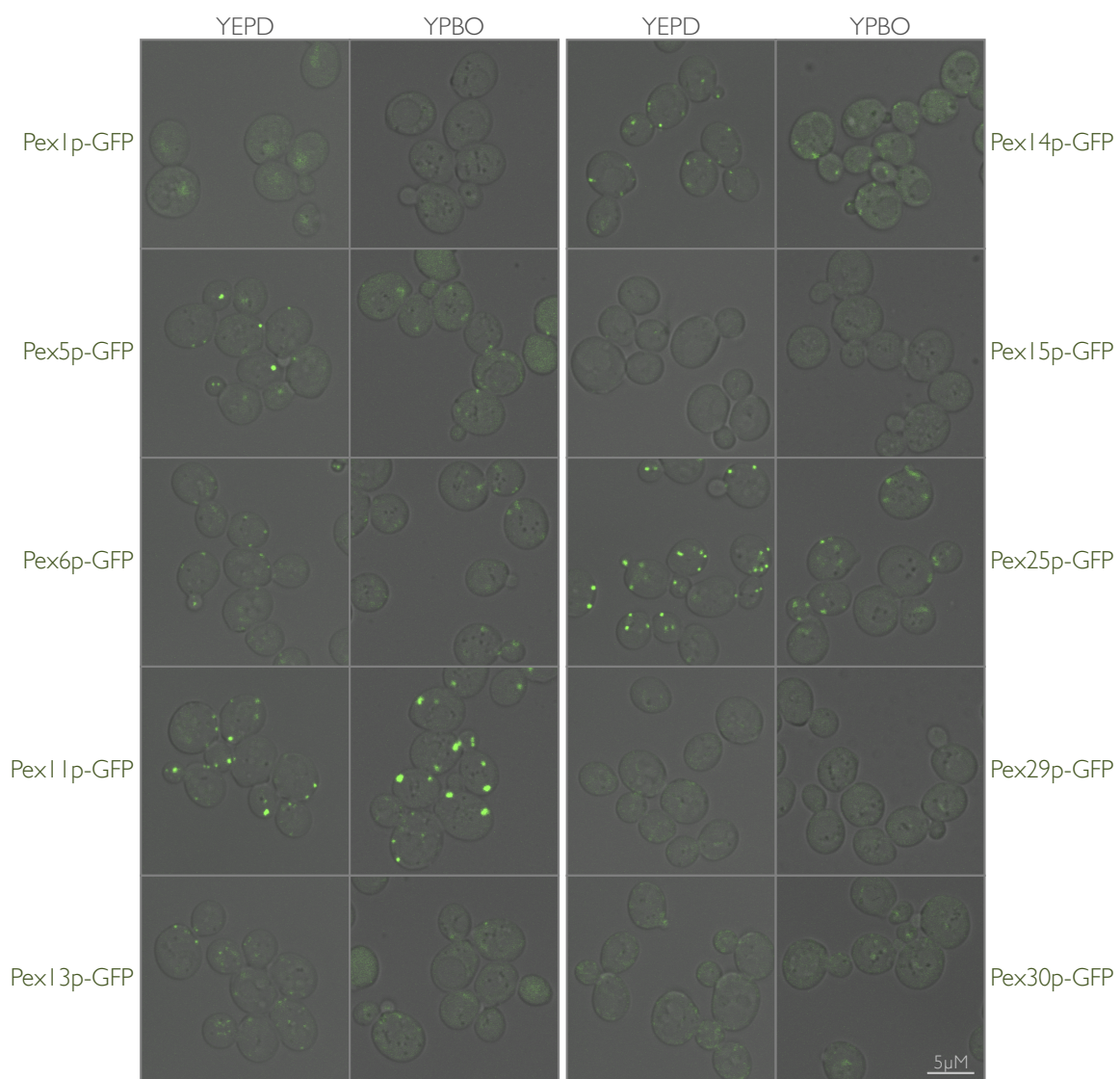
Figure 3-5. Peroxisomes proliferate in a temperature-sensitive mutant of *SEC61*. Wild-type and *sec61^{ts}* strains with genomically integrated *PEX3-GFP* were incubated in YEPD at a permissive temperature of 25°C and then shifted to a non-permissive temperature of 37°C. The *sec61^{ts}* strain shows a peroxisome proliferation phenotype at the permissive temperature, and peroxisomes appear elongated at the non-permissive temperature. Images were captured by confocal microscopy, and a maximum-intensity projection was created from a deconvolved 3D data set using Huygens software.



for de novo peroxisome biogenesis from the ER (Huber et al., 2012; Saraya et al., 2011; Tower et al., 2011). The second class includes Pex28/29/30/31/32, which share varying degrees of sequence similarity with one another (Kiel et al., 2006), but how these proteins regulate peroxisome numbers remains unknown (Vizeacoumar et al., 2003; 2004). Strains harboring single gene deletions of *PEX28*, *PEX31*, or *PEX32* have fewer and slightly enlarged peroxisomes whereas single deletions of *PEX29* or *PEX30* result in increased numbers of smaller peroxisomes. Epistasis experiments between deletion mutants of all five genes demonstrated that the phenotype of fewer enlarged peroxisomes is hypostatic to the phenotype of increased numbers of smaller peroxisomes (Vizeacoumar et al., 2004).

To determine whether these peroxins involved in regulating peroxisome biogenesis and proliferation localize to the ER we performed a morphological screen utilizing a collection of genomically integrated, C-terminally GFP-tagged peroxins (Huh et al., 2003). In addition to peroxins implicated in regulating peroxisome proliferation we also included the peroxins Pex1/5/6/13/14/15 to provide context, i.e. to assess comparatively whether the localizations noted for a particular peroxin were uniform or distinct from the others. We first assessed whether the peroxin-GFP fusion proteins could be visualized in wild-type cells using confocal microscopy. In general, the fluorescent signal from the tagged peroxins was weak and difficult to visualize. Some peroxins, such as Pex27/28/31/32, gave no detectable fluorescence and were not followed further. Additionally, we excluded both Pex3p-GFP and Pex19p-GFP from the list as they have both been previously demonstrated to have a structural role in peroxisome biogenesis and proliferation, i.e. we wanted to identify factors that regulated the functions of Pex3p and Pex19p. The remaining peroxin-GFP strains were grown in glucose-containing medium and imaged by confocal microscopy, and were followed by further incubation of cells for 4 hours in oleic acid-containing medium before imaging again (Figure 3-6).

Figure 3-6. Screening for candidate peroxins involved in regulating peroxisome biogenesis and proliferation. Wild-type strains individually genomically integrated with a *peroxin-GFP* were incubated in the presence of glucose and then incubated in the presence of oleic acid for 4 h. Images at each time point for the indicated strains were collected by confocal microscopy. Bar, 5 μm .



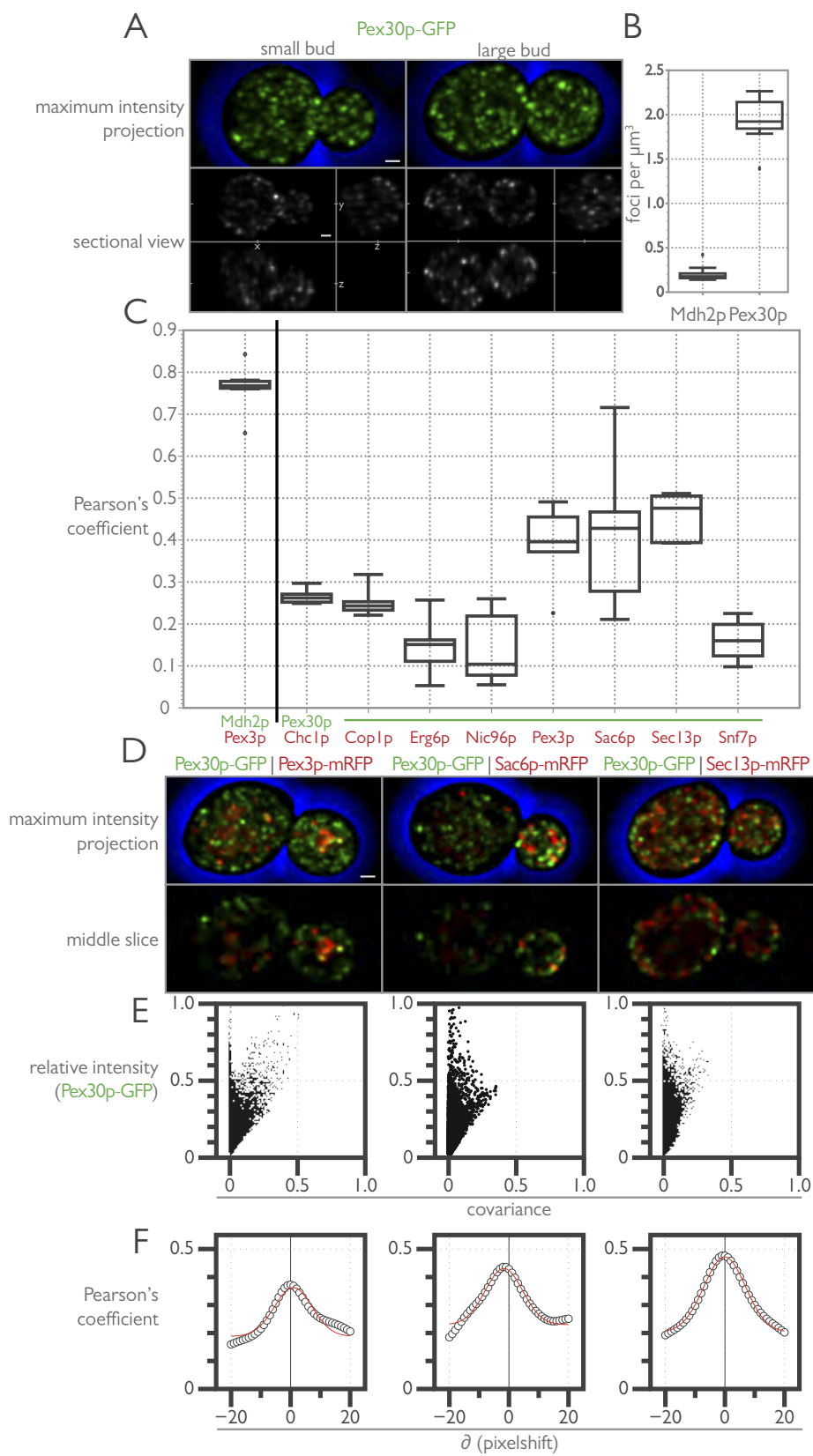
Three peroxins, Pex15p-GFP, Pex29p-GFP and Pex30p-GFP, exhibited distinct localization patterns separate from the other peroxins and, instead of being restricted to discrete puncta typical of peroxisomes, were localized to many small puncta and small tubular structures (Figure 3-6). The fluorescent signal from these three peroxins was significantly weaker than that of other peroxins, perhaps because of a more diffuse and less concentrated subcellular localization. Pex15p acts as a docking factor for the AAA-ATPases Pex1p and Pex6p (Birschmann et al., 2003). In this screen Pex1p-GFP gave a diffuse cytosolic signal that appeared to enrich in the nucleus, but this was not confirmed or followed further. Pex6p-GFP showed localization to puncta consistent with a peroxisomal localization. As Pex15p is a C-terminal membrane-anchored protein that is inserted into the ER by the Guided Entry of Tail-anchored proteins (GET) system before trafficking to peroxisomes (Lam et al., 2010; Schuldiner et al., 2008), appending a GFP to its C-terminus may disrupt its trafficking. Both Pex11p-GFP and Pex25p-GFP gave some of the brightest fluorescent signal and localized to puncta, consistent with a peroxisomal localization in this screen. However, the localization pattern of Pex11p-GFP suggested that peroxisome morphology may be affected in this strain, a phenotype that has been observed for Pex11p chimeras before (Koch et al., 2010).

In *Pichia pastoris*, Pex30p exhibits a dual localization between the ER and peroxisomes, and we therefore chose to investigate further Pex30p and its role in regulating peroxisome proliferation in *S. cerevisiae*.

3.5 The subcellular localization of Pex30p shares commonalities with both the ER and peroxisomes

To investigate the subcellular localization of Pex30p in further detail, we imaged Pex30p-GFP in wild-type yeast grown in the presence of glucose by 3D confocal microscopy (Figure 3-7A). For

Figure 3-7. An unbiased colocalization analysis shows Pex30p to colocalize with Pex3p and Sec13p. (A) Pex30p localizes to numerous puncta distributed throughout the cytoplasm. Wild-type cells with genomically integrated *PEX30-GFP* were incubated in YEPD and imaged by 3D confocal microscopy. A maximum intensity projection of the z-stacks and a sectional view showing cross-sections in the xy, xz and yz axes are shown for a small budded and large budded cell. Bar, 1 μ m. (B) Numerical density of peroxisomes and Pex30p-GFP puncta. The numerical density was calculated from the number of “spots” identified with Imaris (Bitplane) software per cell from Mdh2p-GFP and Pex30p-GFP labeled strains. Cell volume was determined by measuring the short and long axes of mother cells and buds and calculating the volume of an oblong spheroid for each cell. Interquartile box and whisker plots for Mdh2p and Pex30p show the results of 3 independent experiments measuring 20 cells per experiment. (C) Quantitative 3D colocalization microscopy with “punctate composite” proteins shows partial colocalization between Pex30p-GFP and Pex3p-mRFP, Sac6p-mRFP and Sec13p-mRFP. Diploid cells expressing the indicated fluorescent proteins were grown in YEPD and imaged by 3D confocal microscopy. Pearson’s coefficients were calculated for the deconvolved data sets using the JACOP plugin for Image J (NIH) and the data from a representative experiment of 5 images per strain are shown by interquartile box and whisker plots. (D) Maximum intensity projections and middle slice of the median image from (C) are displayed for the three punctate composite markers showing partial colocalization to Pex30p-GFP. Bar, 1 μ m. (E) Intensity correlation analysis (ICA) of the images shown in (D). The ICA plot displays the covariance of the Pex30p-GFP signal with a colocalization marker (Pex3p-mRFP, Sac6p-mRFP and Sec13p-mRFP) as a function of the relative intensity of Pex30p-GFP. ICA plots were calculated using the JACOP plugin for Image J (NIH). (F) Cross correlation function (CCF) analysis of the images shown in (D). The CCF is a plot of a series of Pearson’s coefficients calculated by shifting one image with respect to the other ± 20 pixels. The CCF for each image pair in (D) was calculated using the JACOP plugin for Image J (NIH).



3D confocal microscopy of living cells, we employ a fast acquisition protocol with continuous capture along the z-axis driven by a piezoelectric actuator (Hammond and Glick, 2000), which minimizes acquisition time and the introduction of small vibrations from the step-wise progression of a typical 3D acquisition. Use of a multi-immersion objective with correction collar allowed us to reduce the degrading effects of spherical aberration to image contrast by compensating for mismatches in the refractive indices of the imaging medium and living cells, as well as to correct for the necessary insertion of a coverslip into the light path (Pawley, 2006). To remove noise and reassign blur, deconvolution algorithms are applied to the post-acquisition dataset, which also correct for artifacts introduced by the digital discretization of the analog fluorescence signal. The resulting 3D reconstruction shows remarkable contrast for weak fluorescence signals, such as those collected by imaging Pex30p-GFP, with resolution on three axes approaching the diffraction limits of the confocal microscope (Figure 3-7A).

Pex30p-GFP localizes to numerous puncta distributed throughout the cell with both cortical and, what appear to be, perinuclear distribution patterns. This localization pattern was independent of cell size or progression through the cell cycle, although an enrichment of Pex30p-GFP signal was often seen in small- to mid-sized buds (Figure 3-7D). Quantification of the number of puncta per cell revealed an ~10-fold higher level of Pex30p-GFP puncta as compared to Mdh2p-GFP puncta (Figure 3-7B).

To determine the identity of the compartment(s) to which Pex30p-GFP localized, we performed quantitative colocalization experiments against a battery of proteins that give a “punctate-composite” localization by light microscopy. These proteins were previously used in a global analysis of protein localization in yeast (Huh et al., 2003). A wild-type haploid strain expressing Pex30p-GFP was mated to haploid strains expressing chimeras of each of the punctate-composite proteins and mRFP. The resulting diploid cells were then imaged by 3D confocal microscopy, and an estimate of the strength of association between the two fluorophores was

made by comparing Pearson's correlation coefficients calculated from the different 3D image datasets (Manders et al., 1992) (Figure 3-7C). As a positive control, Pearson's correlation coefficients were calculated for images acquired of Pex3p-mRFP and Mdh2p-GFP.

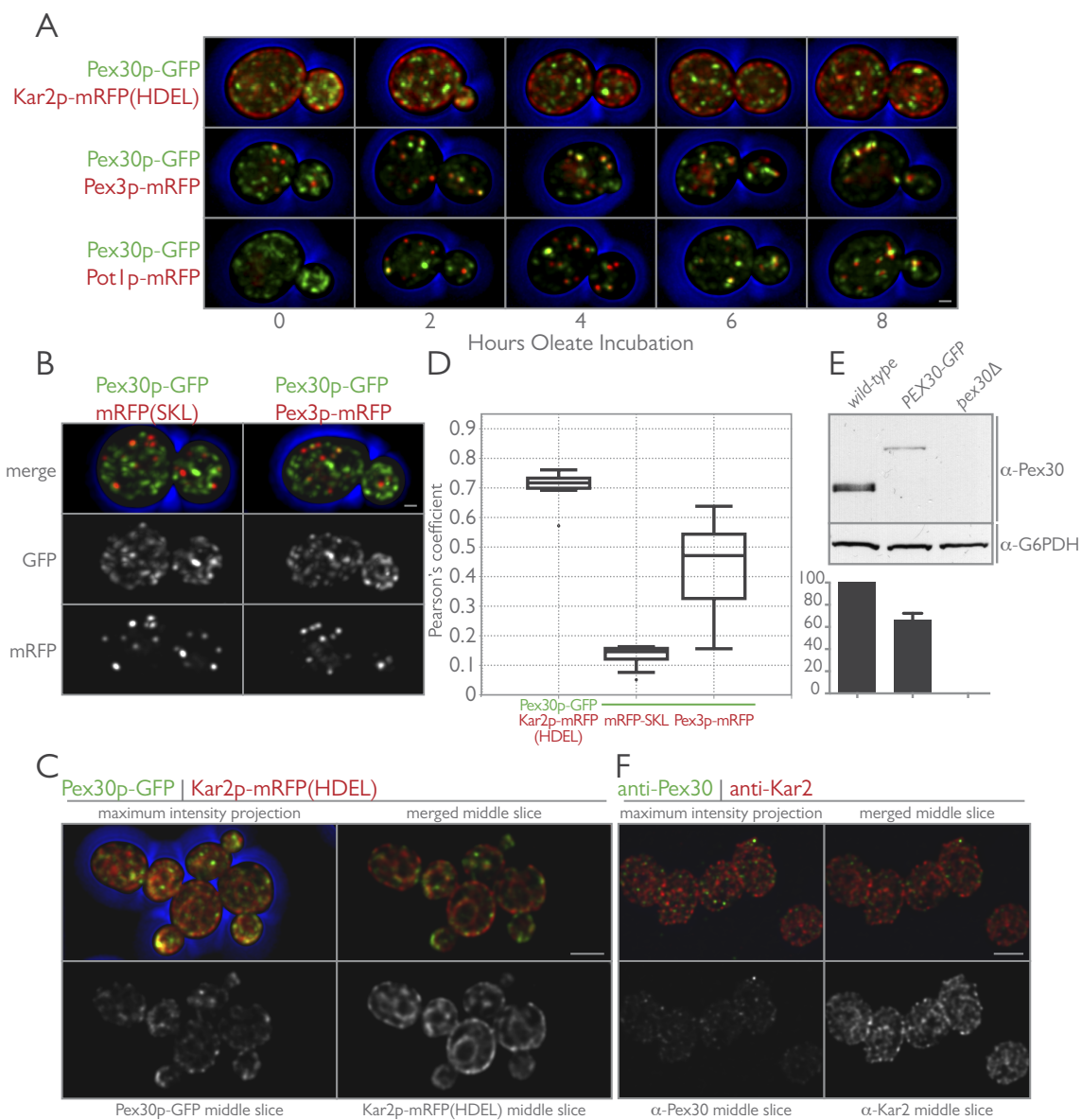
The graphical representation of the data revealed stronger correlations between Pex30p-GFP and Pex3p-mRFP, Sac6p-mRFP and Sec13p-mRFP as compared to correlations between Pex30p-GFP and Chc1p-mRFP, Cop1p-mRFP, Erg6p-mRFP, Nic96p-mRFP and Snf7p-mRFP. Sac6p is yeast fimbrin, an actin bundling and plus-end binding protein (Adams et al., 1991), whereas Sec13p is a structural component of CopII vesicles and the nuclear pore complex (Field et al., 2011). Pearson's correlation coefficients between the ranges of 0.3 and 0.6 could result from random, spurious and coincident associations or could be the result of a partial colocalization between subsets of the two populations of proteins (Bolte and Cordelières, 2006). To distinguish between these possibilities we performed additional analyses according to the methods of Li and colleagues (Li et al., 2004) and van Steensel and colleagues (van Steensel et al., 1996), as shown for representative images of Pex30p-GFP with Pex3p-mRFP, Sac6p-mRFP or Sec13p-mRFP (Figure 3-7D-F). Intensity correlation analysis showed high intensity fluorescence from Pex30p-GFP covaried with Pex3p-mRFP and to a lesser extent with Sec13p-mRFP, but not with Sac6p-mRFP, with which low intensity covariance dominated (Figure 3-7E). Furthermore, computation of a cross correlation function for each image dataset picked up coincident colocalization between Pex30p-GFP and Sac6p-mRFP, which had an unequal right tail skew likely due to the propensity of both proteins to show enriched signal in the yeast bud (Figure 3-7D and F). We therefore conclude that the partial colocalization between Pex30p-GFP and Pex3p-mRFP is the result of specific and discrete associations between a subset of each protein population. Partial colocalization between Pex30p-GFP and Sec13p-mRFP likely results from a broad coincident colocalization of the two proteins residing in the same subcellular compartment, the ER.

3.6 Pex30p associates with peroxisomes when yeast are grown in the presence of oleic acid

Earlier studies indicated that Pex30p localizes to peroxisomes in cells grown in medium containing oleic acid (Vizeacoumar et al., 2004). We therefore imaged yeast cells endogenously coexpressing Pex30p-GFP and one of Kar2p-mRFP(HDEL), Pex3p-mRFP or Pot1p-mRFP, after timed intervals of growth in an oleic acid containing-medium using 3D confocal microscopy (Figure 3-8A). Kar2p is the yeast homolog of binding protein, BiP, an ER lumenal chaperone protein (Rose et al., 1989). Pex30p-GFP displayed strong colocalization with Kar2p-mRFP(HDEL) when imaged in cells grown in the presence of glucose; however, Pex30p-GFP appeared to redistribute to peroxisomes with excessively longer incubations in oleic acid-containing medium. Pex30p-GFP showed increased colocalization with both Pex3p-mRFP and Pot1p-mRFP as a function of time during incubation in oleic acid-containing medium.

We asked whether Pex30p's transit to peroxisomes was delayed or aberrantly affected by appendage of GFP to its C-terminus. While generally considered inert with respect to protein function, a GFP tag, such as in the case of Pex11p-GFP, can potentially alter function (Koch et al., 2010). Polyclonal antibodies were raised against the C-terminus of GFP and affinity-purified. Analysis of whole cell lysates revealed reduced levels of Pex30p-GFP, as compared to untagged Pex30p, with quantification showing a 40% reduction in protein levels (Figure 3-8E). However, despite this effect, Pex30p still localized to numerous puncta distributed throughout the cytosol that colocalized with Kar2p as revealed by immunofluorescence microscopy of wild-type cells grown in the presence of glucose. Cells expressing Pex30p-GFP grew like wild-type cells and exhibited normal peroxisome morphology.

Figure 3-8. Pex30p dynamically localizes to the ER or peroxisomes depending on the carbon source utilized. (A) Pex30p associates with peroxisomes when cells are grown in the presence of oleic acid. Endogenously expressed Pex30p-GFP was localized in vivo with Kar2pmRFP(HDEL) (top), Pex3p-mRFP (middle) or Pot1p-mRFP (bottom) in wild-type cells under conditions of peroxisome induction. Cells were precultured in glucose-containing YPD medium and imaged at the indicated time points following a shift to oleic acid-containing YPBO medium. With increasing incubation times in oleic acid-containing medium, Pex30p-GFP colocalization with the ER marker, Kar2p-mRFP(HDEL), and the peroxisomal markers, Pex3p-mRFP and Pot1p-mRFP, is lost and gained, respectively. Bar, 1 μ m. (B) Pex30p does not colocalize with peroxisomal matrix proteins when cells are grown in the presence of glucose. Pex30p-GFP was localized in vivo with mRFP-SKL (left) or Pex3p-mRFP (right) in wild-type cells. Maximum intensity projections of the merged and individual fluorescent channels are displayed. Bar, 1 μ m. (C) Pex30p localizes to the ER in glucose-grown cells. Endogenously expressed Pex30p-GFP and Kar2p-mRFP(HDEL) were imaged in wild-type cells grown in the presence of glucose. Shown are a maximum intensity projection of all optical sections and single z-sections through the midplane of cells. Bar, 5 μ m. (D) Cells expressing the indicated fluorescent proteins were grown in YEPD and imaged by 3D confocal microscopy. Pearson's coefficients were calculated for the deconvolved data sets using the JACOP plugin for Image J (NIH), and the data from a representative experiment of 5 images per strain are shown by interquartile box and whisker plots. (E) Endogenously tagging Pex30p-GFP affects its expression levels. Whole cell lysates from *wild-type*, *PEX30-GFP* and *pex30 Δ* strains were separated by SDS-PAGE, transferred to nitrocellulose and probed with affinity-purified antibodies to Pex30p, and antibodies to G6PDH. Graphical results of Pex30p protein levels normalized to wild-type show the means and standard error of the mean from three independent experiments. (F) Endogenous untagged Pex30p shows a localization pattern similar to Pex30p-GFP. Unlabeled wild-type cells were grown in glucose and processed for immunofluorescence microscopy using affinity-purified antibodies to Pex30p and antibodies to Kar2p. Shown are a maximum intensity projection of all optical sections and single z-sections through the midplane of cells. Bar, 5 μ m

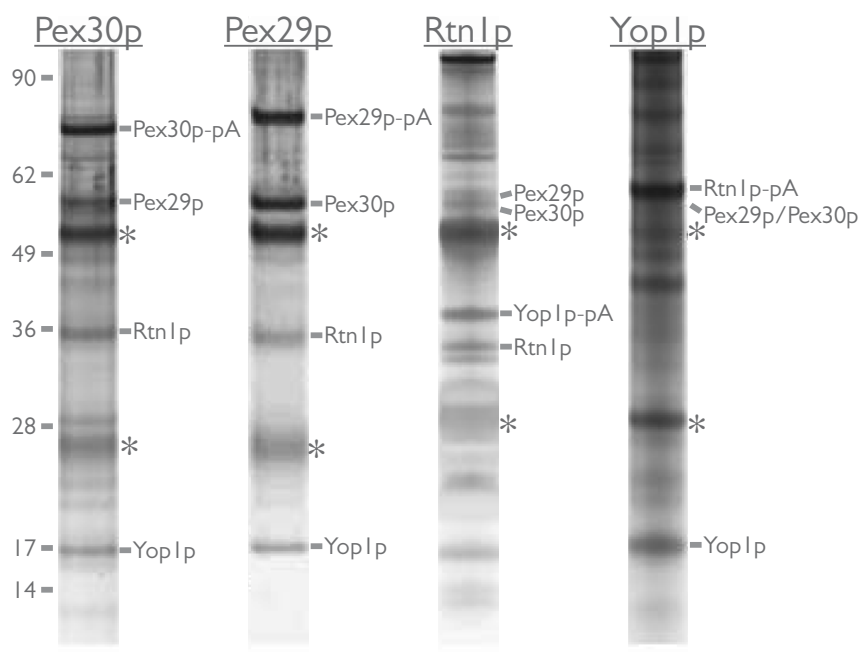


3.7 Identification of a reticulon-peroxin complex

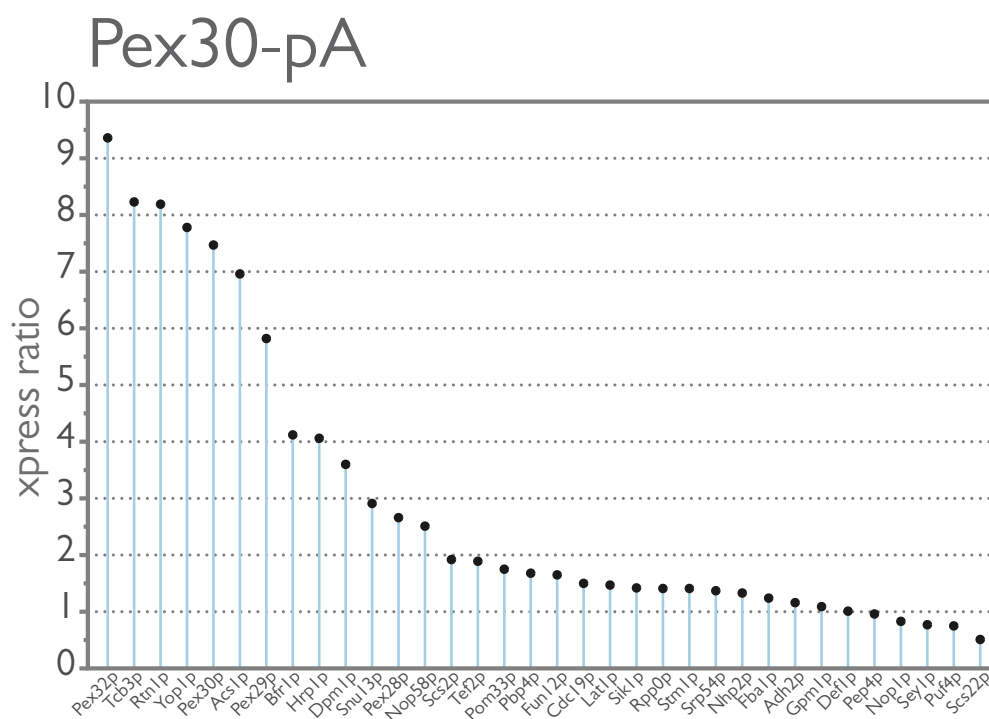
To gain a better understanding of Pex30p function we next sought to identify interacting partners of Pex30p by immunoaffinity isolation followed by identification by mass spectrometry. Pex30p was tagged at its C-terminus with Protein A, Pex30p-pA, and immunoisolation of Pex30p-pA containing complexes was performed with whole cell extracts prepared from cells grown in the presence of glucose. Unlike previous efforts to immunopurify PMPs, which employed enrichment of peroxisomes by ultracentrifugation prior to immunoisolation of protein complexes (Agne et al., 2003; Marelli et al., 2004), we used whole cell lysates with the intention of probing for all potential Pex30p-containing protein complexes that would be depleted from enriched peroxisomal fractions. Cells were flash frozen in liquid nitrogen and lysed under cryogenic conditions using a planetary ball mill to maintain native protein complexes. The resulting grindate was used for rapid immunoisolation on IgG-coated magnetic beads (Cristea et al., 2005; Oeffinger et al., 2007). This approach reduces the number of steps prior to protein complex purification, thereby leading to a more confident identification of protein complexes (Tackett et al., 2005a). Experimental conditions were iteratively optimized to provide appropriate solubilization of integral membrane protein complexes while maintaining protein interactions (Aitchison et al., 1995; Rout et al., 1997). Prominent bands representing putative Pex30p-pA interacting proteins were excised and identified by mass spectrometry.

The major proteins that copurify with Pex30p-pA were identified as Pex29p, Rtn1p and Yop1p (Figure 3-9A). Identification of Pex29p as a Pex30p-pA interacting protein was not unexpected, as it showed a similar subcellular localization in our peroxin-GFP screen (Figure 3-6) and *pex29Δ* and *pex30Δ* strains share similar peroxisome proliferation phenotypes (Vizeacoumar et al., 2003; 2004). Similarly to Pex30p-pA, isolation of Pex29p-pA yielded Pex30p, Rtn1p and

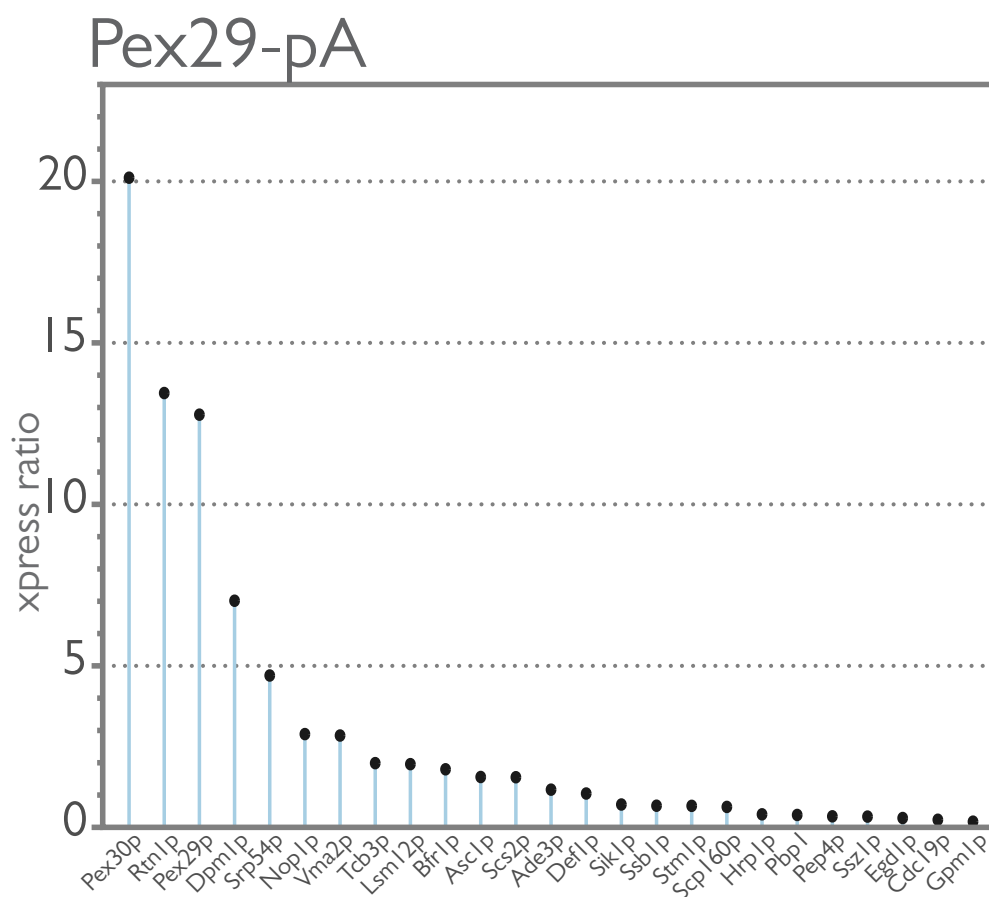
Figure 3-9. Pex29p and Pex30p copurify with the ER resident proteins, Rtn1p and Yop1p. (A) Endogenously expressed Pex29p and Pex30p C-terminally tagged with Protein A were immunopurified from wild-type yeast whole cell lysates under conditions that promote the capture of integral membrane proteins. Shown are silver-stained SDS-PAGE gels exhibiting the typical patterns of proteins observed to copurify with these Protein A-tagged baits. Proteins in eluates were identified by two complementary methods, i.e. in-gel digestion of prominent bands excised from silver-stained gels and global shotgun analysis of eluate fractions. The identity of bands excised from Pex29p-PrA and Pex30p-PrA gels are indicated. In both immunopurifications, the resident ER proteins, Rtn1p and Yop1p, were found to copurify with Pex29p-PrA and Pex30p-PrA under these conditions. In support of this interaction, both Pex29p and Pex30p were identified by shotgun mass spectrometry in reciprocal immunisolations using Rtn1p-PrA and Yop1p-PrA as bait. (B-C) Expression ratio (Xpress ratio = light isotope / heavy isotope) for proteins identified by the I-DIRT experiments and shotgun mass spectrometry. An Xpress ratio of > 2 was used as a set point to define specific Pex30p-pA (B) and Pex29p-pA (C) interacting proteins. (D) Network level view of the protein-protein interactions identified in this study. Horizontal lines represent protein nodes (as labeled in the figure), and vertical lines represent the protein-protein interactions. Graphical representation of the data was generated using BioFabric (Institute for Systems Biology, Seattle, WA). (E) Same as (D) but including all protein-protein interactions reported in the literature for the proteins found in (D). The String database (string-db.org) was used to identify these additional protein-protein interactions.

A

B

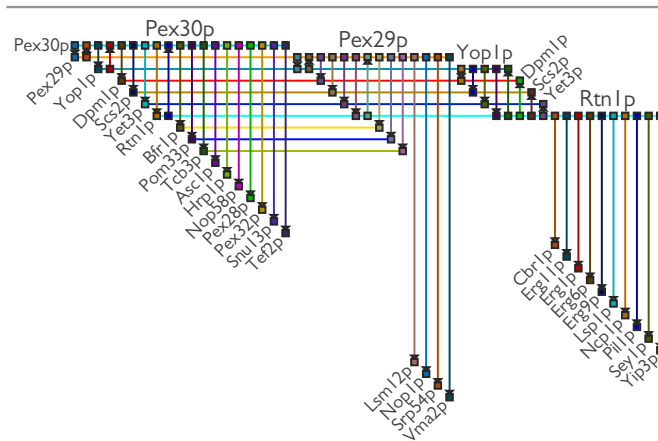


C



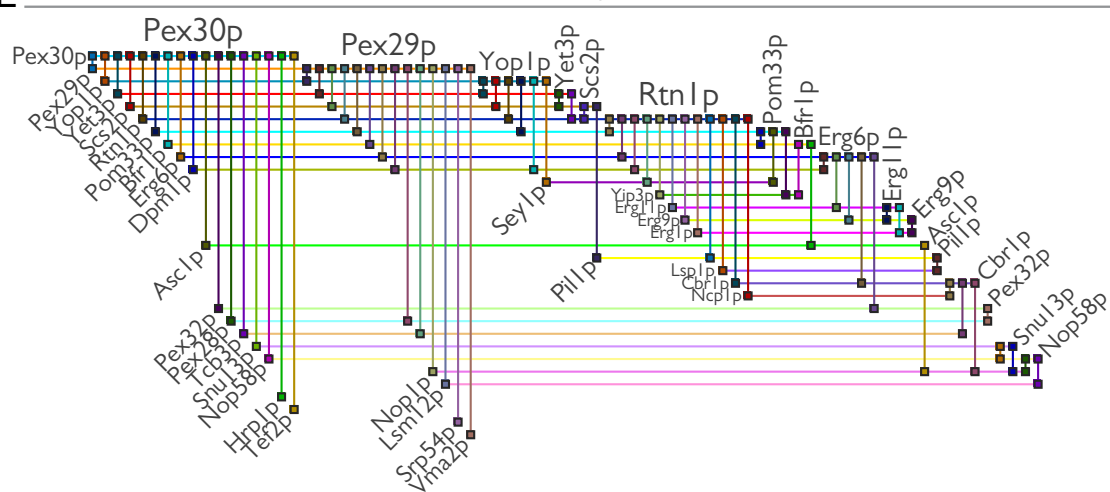
D

Interaction network for IP's



E

Interaction network for IP's + all published interactions



Yop1p as major copurifying proteins. Rtn1p and Yop1p are members of the reticulon-like A subfamily of integral membrane proteins involved in establishing and maintaining the cortical ER membrane in yeast (de Craene et al., 2006; Voeltz et al., 2006). These proteins are proposed to form a wedge-like structure within the ER membrane, inducing membrane curvature and facilitating ER tubular structure formation (Hu et al., 2008). Furthermore, the meshwork of the cortical ER is maintained by physical interaction between Rtn1p and Sey1p (Hu et al., 2009), the yeast ortholog of the dynamin-like GTPase, Atlastin (Orso et al., 2009). While both Rtn1p and Yop1p are reported to interact with the GTPase Sey1p, we did not find Sey1p associated with either Pex29p or Pex30p. This suggests the presence of different Rtn1p and Yop1p subcomplexes in yeast cells, or that this interaction is not maintained in our immunopurification conditions. From this initial characterization it remains undetermined if Pex30p and Pex29p exist in a single complex or multiple distinct complexes.

To confirm the interactions between Pex30p, Pex29p, Rtn1p and Yop1p, we performed reciprocal immunoprecipitations, this time using Rtn1p-pA and Yop1p-pA as baits (Figure 3-9A). For these immunopurified eluates, proteins were identified by mass spectrometry using in-solution digests rather than gel excision of prominent bands. As expected, both Pex30p and Pex29p were detected in Rtn1p-pA and Yop1p-pA immunoprecipitations, strongly suggesting that these four proteins are bona fide interacting proteins that exist in a complex that we term the “reticulon-peroxin complex”. Several other potential interacting proteins, summarized in Table 3-1, were identified in these experiments. Of note, all four immunoprecipitations identified Scs2p, Dpm1p and Yet3p as interacting partners. Scs2p is the yeast homolog of VAP and a component of the ER-plasma membrane tethering complex involved in the regulation of the phosphoinositol-4-phosphate phosphatase, Sac1p (Manford et al., 2012; Stefan et al., 2013). Dpm1p is a dolichol-phosphate mannosyltransferase and an integral membrane protein of the ER, but it also interacts with and has an important role in regulating Sac1p (Faulhammer et al., 2005; 2007). Interestingly,

we detected Pom33p, an integral membrane protein recently shown to interact with Rtn1p and dynamically associate with the yeast nuclear pore complex (NPC) (Chadrin et al., 2010) in both Pex29p-pA and Pex30p-pA eluates. Unexpectedly, we did not identify Pom33p in Rtn1p-pA or Yop1p-pA eluates. However, we did identify Sey1p and several additional proteins involved in lipid metabolism in the Rtn1p-pA eluate (Table 3-1).

Table 3-1. Proteins identified by mass spectrometry of Pex30p-pA, Pex29p-pA, Rtn1p-pA and Yop1p-pA immunoisolations

Protein	IMP ^a	Localization ^b	Mol Wt (kD) ^c	GO annotation ^d
Proteins identified with Pex30p-pA, Pex29p-pA, Rtn1p-pA and Yop1p-pA				
Rtn1p	Yes	ER	32.9	ER membrane structure
Yop1p	Yes	ER	20.2	ER membrane structure
Pex29p	Yes	ER/P	63.5	regulates peroxisome abundance
Pex30p	Yes	ER/P	59.4	regulates peroxisome abundance
Scs2p	Yes	ER	26.9	regulates phospholipid metabolism
Dpm1p	Yes	ER	30.3	dolichol mannose phosphate synthase
Yet3p	Yes	ER	22.9	invertase secretion decreased
Proteins identified only with Pex30p-pA and Pex29p-pA				
Pom33p	Yes	ER	32.2	nuclear pore complex dynamics
Proteins identified only with Rtn1p-pA				
Erg6p	No	ER	43.4	ergosterol biosynthesis
Erg1p	Yes	ER	55.1	ergosterol biosynthesis
Erg9p	No	ER	43.4	ergosterol biosynthesis
Erg11p	Yes	ER	60.7	ergosterol biosynthesis
Cbr1p	Yes	ER/M	31.4	microsomal cytochrome b reductase
Ncp1p	No	ER	76.7	ergosterol biosynthesis
Yip3p	Yes	ER	19.4	ER to Golgi transport
Lsp1p	No	E	38	Primary component of eisosomes
Pil1p	No	E	38.3	Primary component of eisosomes
Sey1p	Yes	PC	89.4	GTPase with a role in ER morphology

^a IMP: integral membrane protein prediction based on hydropathy index as catalogued in the Saccharomyces Genome Database (yeastgenome.org).

^b Localization: subcellular localization of protein as catalogued in the Saccharomyces Genome Database - curated from (Huh et al., 2003).

ER: endoplasmic reticulum; P: peroxisome; M: Mitochondrion; E: eisosome; PC: punctate composite.

^c Mol wt: Molecular weight as catalogued in the Saccharomyces Genome Database.

^d Go annotation: Truncated gene ontology from the Saccharomyces Genome Database

To assess the stability of the reticulon-peroxin complex and to identify additional interacting proteins of Pex30p and Pex29p, we performed isotopic differentiation of interactions as random or targeted (I-DIRT) experiments (Tackett et al., 2005b) with Pex30p-pA and Pex29p-pA

followed by shotgun mass spectrometry. This method differentiates between specific and non-specific interacting proteins by immunoisolation of affinity-tagged protein complexes from cells grown in the presence of isotopically “light” medium, which is subsequently mixed in a 1:1 ratio with cell lysates grown in the presence of isotopically “heavy” medium before protein identification by mass spectrometry (Tackett et al., 2005b). In vivo stably interacting proteins will be isotopically light, whereas spurious interactions that result from lysis and mixing during immunoisolation will have a ratio of light to heavy approximating 1:1.

Rtn1p, Yop1p and Pex29p were among the top hits for Pex30p-pA, confirming the association of these proteins in a complex (Figure 3-9B). Additionally, Pex32p and Pex28p, two proteins previously identified as Pex30p interactors by two-hybrid experiments (Vizeacoumar et al., 2004), were also stably associated with Pex30p-pA, validating our proteomics approach. Interestingly, these experiments identified a stable association between Pex30p-pA and Tcb3p, another component of the ER-plasma membrane tether (Manford et al., 2012). Scs2p was also identified as a stable interactor, but at a lower ratio of light-to-heavy isotope. In addition to these phosphatidylinositol-4-phosphate (PI4P) regulators, Dpm1p also made the cutoff. Pex30p was the top hit for Pex29p-pA experiments with a ratio of light-to-heavy of just over 20, the highest ratio in these experiments (Figure 3-9C). Pex29p-pA also stably associates with Rtn1p, but surprisingly Yop1p was not identified as a stable interactor of Pex29p in these experiments despite the identification of “light” Yop1p peptides. The strong connectivity of Pex30p and Pex29p was easily visualized in a network map of the protein-protein interaction data (Figure 3-9D). This view also reinforced the association of Dpm1p, Scs2p and Yet3p as additional peripheral components of the reticulon-peroxin complex. To help gain a broader perspective, we created a second network that included all previously reported protein-protein interactions among the proteins identified in our proteomics experiments. Known and curated protein-protein interactions were taken from the STRING database (string-db.org). This view maintained the strong interactivity between the

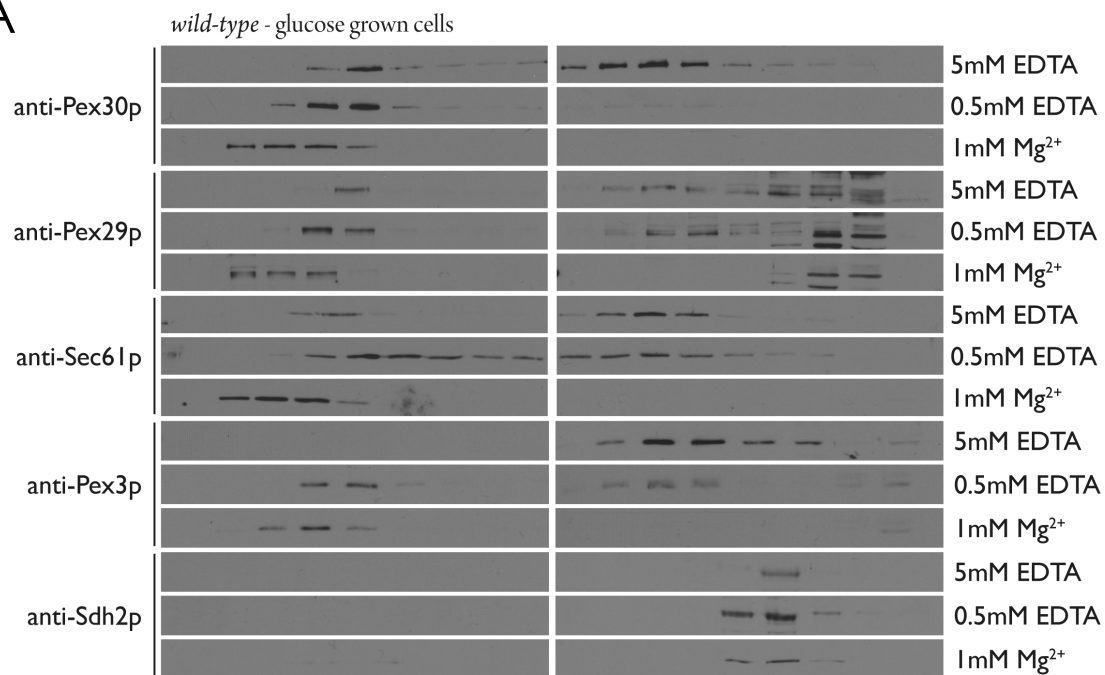
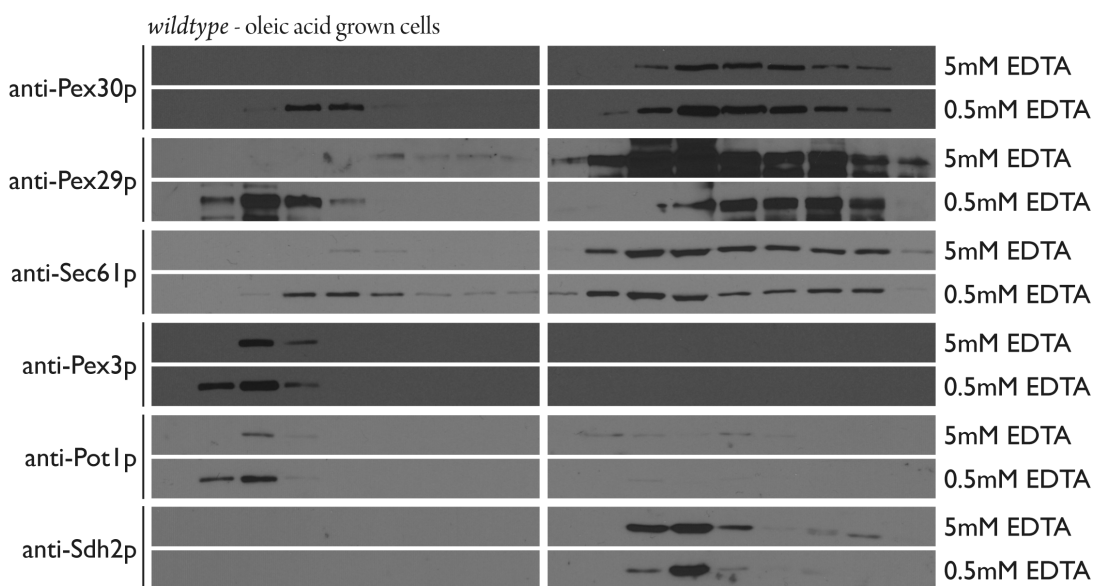
Pex30p and Pex29p interaction networks and increased the association between the Rtn1p and Yop1p interaction networks.

3.8 Pex30p and Pex29p are ER resident proteins even when cells are grown in the presence of oleic acid

Because most of the proteins interacting with Pex30p and Pex29p were ER-resident proteins we readdressed and further explored the subcellular localization of these proteins using an ER mobility shift assay (Figure 3-10). This assay employs biochemical fractionation of lysed cells by isopycnic density gradient centrifugation in the presence or absence of magnesium (Roberg et al., 1997). In the presence of excess Mg^{2+} , the ER has increased buoyant density that is most likely due to the strengthened association of ribosomes with the Sec61p complex. Immunoblot analysis of the separated fractions using antibodies to detect Pex30p, Pex29p, Pex3p, Sec61p, and Sdh2p revealed cofractionation of Pex30p and Pex29p with the ER marker Sec61p under all conditions from cells grown in the presence of glucose (Figure 3-10A). Interestingly, Pex3p also cofractionated with Sec61p, moving from fractions of light density to fractions of heavy density with the increase of Mg^{2+} concentration. The mitochondria, as represented by the matrix protein Sdh2p, was not affected by changes in Mg^{2+} and remained in fractions of light density in these experiments. These data suggest that peroxisomes, as labeled by Pex3p, associate with the ER in glucose-grown cells, but in regions distinct from mitochondria. ER-mitochondria contact sites are well documented in *S. cerevisiae* (Kornmann et al., 2009) but did not appear to affect the density of mitochondria in our experiments.

Pex30p and Pex29p also cofractionated with Sec61p under all conditions from cells grown in the presence of oleic acid (Figure 3-10B). However, this time Pex3p was found exclusively in fractions of heavy density and cofractionated with the peroxisomal matrix protein Pot1p, as has been demonstrated previously (Perry et al., 2009). As seen for the fractionation of cells grown in

Figure 3-10. Pex30p and Pex29p cofractionate with Sec61p in an ER-shift assay. (A) Wild-type yeast lysates from cells grown in the presence of glucose were prepared in buffer containing either 5 mM EDTA (no Mg^{2+}), 0.5 mM EDTA or 1 mM Mg^{2+} and postnuclear supernatants were subjected to isopycnic centrifugation through discontinuous nycodenz density gradients. Eighteen fractions of increasing density were collected, 1.25% of the fraction volume was separated by SDS-PAGE, and the indicated proteins were detected by immunoblotting. Cofractionation of Pex30p and Pex29p with the ER marker, Sec61p, is observed, and a concomitant shift results from increasing the buoyant density of ER by the presence of Mg^{2+} . Pex3p also cofractionates with Sec61p, but Sdh2p remains in the lighter fractions. (B) Similar to (A) but this time cells were grown in the presence of oleic acid before preparation of lysates. Lysates were prepared in buffer containing either 5 mM EDTA or 0.5 mM EDTA. Cofractionation of Pex30p and Pex29p with the ER marker, Sec61p, is observed but this time Pex3p is found exclusively in fractions of heavy density and cofractionates with Pot1p.

A**B**

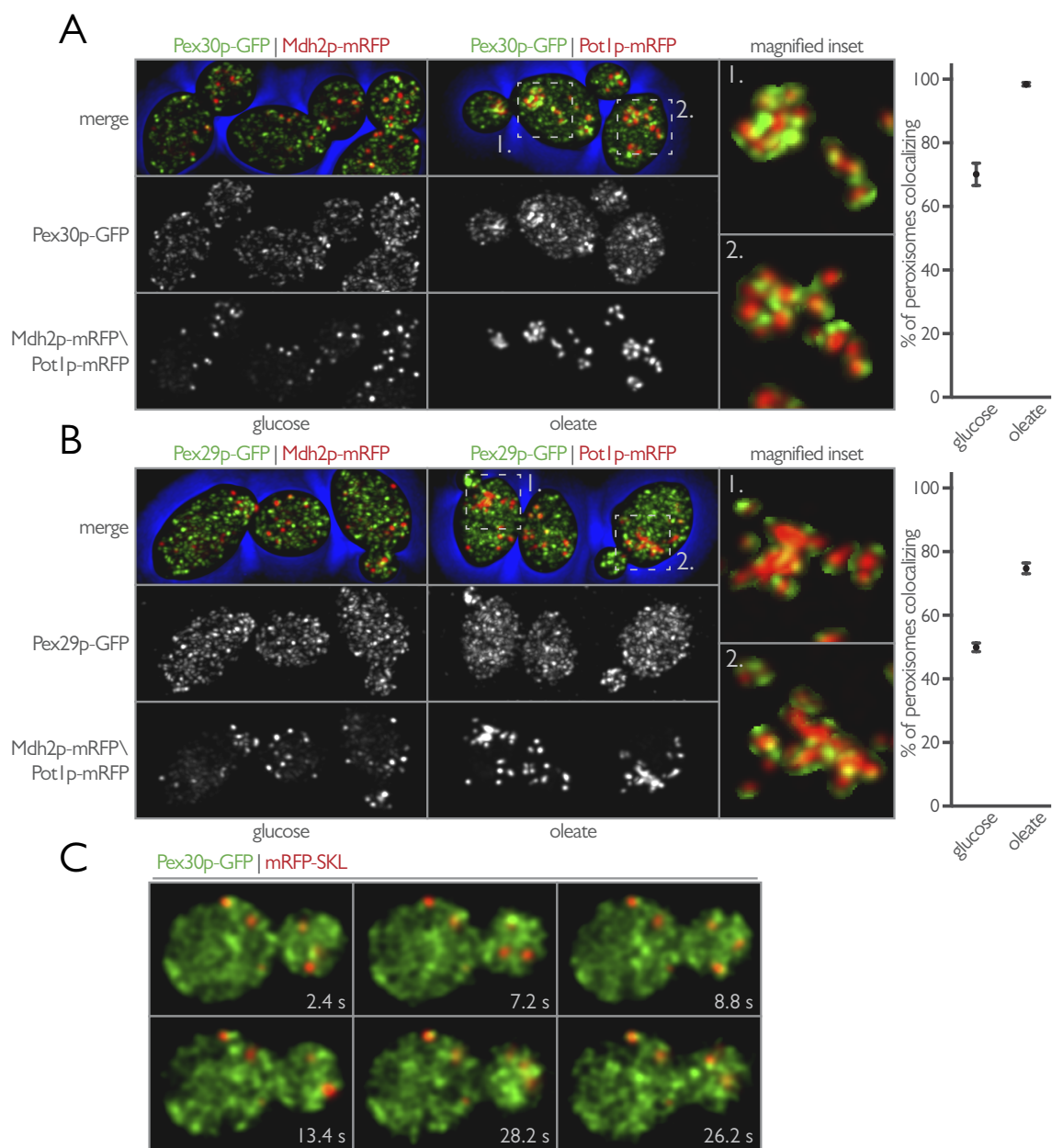
the presence of glucose, Sdh2p remained in fractions of light density under all experimental conditions. These data confirm Pex30p and Pex29p as ER resident proteins and not as residents of mature peroxisomes.

We re-evaluated the association of Pex30p and Pex29p to peroxisomes using quantitative 3D colocalization confocal microscopy. Cells endogenously expressing Pex30p-GFP or Pex29p-mRFP were mated to cells endogenously expressing Mdh2p-mRFP or Pot1p-mRFP. The resulting diploid cells expressing Mdh2p-mRFP and either Pex30p-GFP or Pex29p-GFP were grown in the presence of glucose, whereas diploid cells expressing Pot1p-mRFP and either Pex30p-GFP or Pex29p-GFP were grown in the presence of oleic acid.

Pex30p-GFP associated with peroxisomes more strongly than Pex29p-GFP. Quantification showed that 70% of peroxisomes were in contact with Pex30p-GFP puncta using an object based colocalization algorithm (Figure 3-11A). This number increased to nearly 100% when cells were grown in the presence of oleic acid. Under these conditions, Pex30p-GFP could be seen to associate with peroxisomes and to enrich at sites between peroxisomes that had clustered after growth in the presence of oleic acid. But Pex30p-GFP did not overlap with signal from Pot1p-mRFP, consistent with our ER shift experiments demonstrating Pex30p to be an ER protein. The association between Pex29p-GFP and peroxisomes also increased when cells were grown in the presence of oleic acid so that 75% of peroxisomes were in contact with Pex29p-GFP puncta (Figure 3-11B). However, Pex29p-GFP did not redistribute and associate with peroxisomes to the same extent as Pex30p, and the overall morphology appeared similar to Pex29p-GFP in cells grown in the presence of glucose. Despite this lack of redistribution, Pex29p-GFP could also be found associated with peroxisomes and enriched at sites between clustered peroxisomes from cells grown in the presence of oleic acid.

To investigate the association of Pex30p-GFP with peroxisomes in further detail, we performed 2D video microscopy on cells expressing Pex30p-GFP and the peroxisomal matrix

Figure 3-11. Pex30p, and to a lesser extent Pex29p, associate with peroxisomes under peroxisome proliferating conditions as part of a peroxisome-associated ER membrane. (A) Endogenously expressed Pex30p-GFP was localized in vivo with Mdh2p-mRFP (left) and Pot1p-mRFP (right) in wild-type diploid cells grown in the presence of glucose or oleate, respectively. Shown is the maximum intensity projection of all optical sections both merged and shown individually. Magnified inserts of the merged image from Pex30p-GFP and Pot1p-mRFP show the association of Pex30p-GFP with peroxisomes. Graphical results show the percentage of peroxisomes in contact with Pex30p-GFP as calculated using an object-based colocalization algorithm using Imaris (Bitplane). (B) Similar to (A) but with Pex29p-GFP instead of Pex30p-GFP. (C) Pex30p dynamically associates with peroxisomes. 2D video microscopy of wild-type cells expressing Pex30p-GFP and mRFP-SKL. Images of the midplane of cells were captured every 200 msec, and selected frames from the video are displayed with the indicated time stamp acting as a guide. Pex30p-GFP can be seen to associate dynamically with static peroxisomes in the mother cell and also with mobile peroxisomes in the bud.



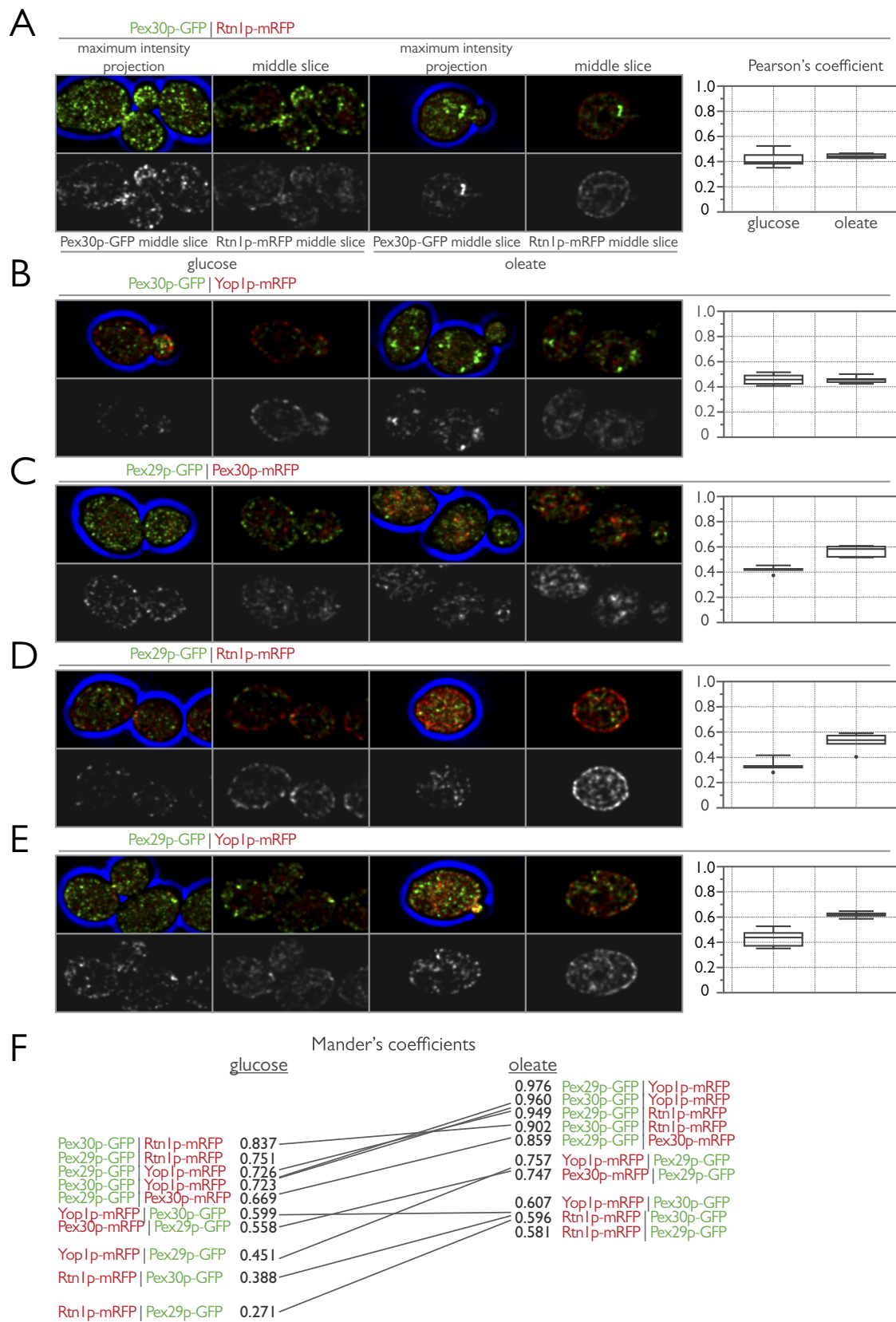
marker mRFP-SKL (Figure 3-11C). This was necessary to minimize photobleaching and the loss of fluorescence signal. We acquired video frames at a rate of 200 msec per frame to provide high temporal resolution in our movies.

Under these conditions, Pex30p-GFP could be seen to interact dynamically with peroxisomes. These associations were frequent enough that individual peroxisomes were visited several times over the course of our image capture. The dynamic movement of Pex30p-GFP throughout the cytoplasm is consistent with previous reports showing the yeast ER to be a highly dynamic structure (Prinz et al., 2000). The association of Pex30p with peroxisomes was also independent of peroxisome placement in the cell, and the dynamic interactions were visualized for static, anchored peroxisomes in the mother cell as well as for moving peroxisomes in the bud (Figure 3-11C).

3.9 In vivo redistribution of members of the reticulon-peroxin complex

We next studied the interactions between members of the reticulon-peroxin complex by quantitative colocalization 3D confocal microscopy. We fused GFP to the C-terminus of Pex29p or Pex30p and mRFP to the C-terminus of Rtn1p or Yop1p and tested for colocalization of Pex29pGFP with Pex30p-mRFP, Rtn1p-mRFP, or Yop1p-mRFP, as well as colocalization of Pex30p-GFP with Rtn1p-mRFP or Yop1p-mRFP in diploid cells grown in the presence of glucose or grown in the presence of oleic acid (Figure 3-12). For each protein pair, partial colocalization, as assessed by comparison of Pearson's coefficients, was observed. In contrast to Pex30p-GFP, which showed stable colocalization with Rtn1p-mRFP and Yop1p-mRFP under both growth conditions, Pex29p-GFP associated more strongly with all of its interacting partners when cells were grown in the presence of oleic acid. These findings are consistent with our immunoprecipitation experiments where Pex29p-GFP association with Yop1p wasn't stable in immunisolations from cells grown in the presence of glucose (Figure 3-9C). A slopegraph of the Manders coefficients

Figure 3-12. Colocalization analysis between members of the reticulon-peroxin complex. (A) Endogenously expressed Pex30p-GFP was localized in vivo with Rtn1p-mRFP in cells grown in the presence of glucose (left), or oleic acid (right) in wild-type diploid cells. Shown are a maximum intensity projection of all optical sections and single z-sections through the midplane of cells. Pearson's coefficients were calculated for the deconvolved data sets using the JACOP plugin for Image J (NIH) and the data from a representative experiment of 5 images per strain are shown by interquartile box and whisker plots. (B) Similar to (A) but with Pex30p-GFP and Yop1p-mRFP. (C) Pex29p-GFP and Pex30p-mRFP. (D) Pex29p-GFP and Rtn1p-mRFP. (E) Pex29p-GFP and Yop1p-mRFP. (F) A slopegraph of the median Manders coefficient from the images in (A-E). Manders coefficients were calculated for the deconvolved data sets using the JACOP plugin for Image J (NIH).



calculated for each imaging pair reinforced this view (Figure 3-12). The general trend was for stronger association between members of the reticulon-peroxin complex when cells were grown in the presence of oleic acid.

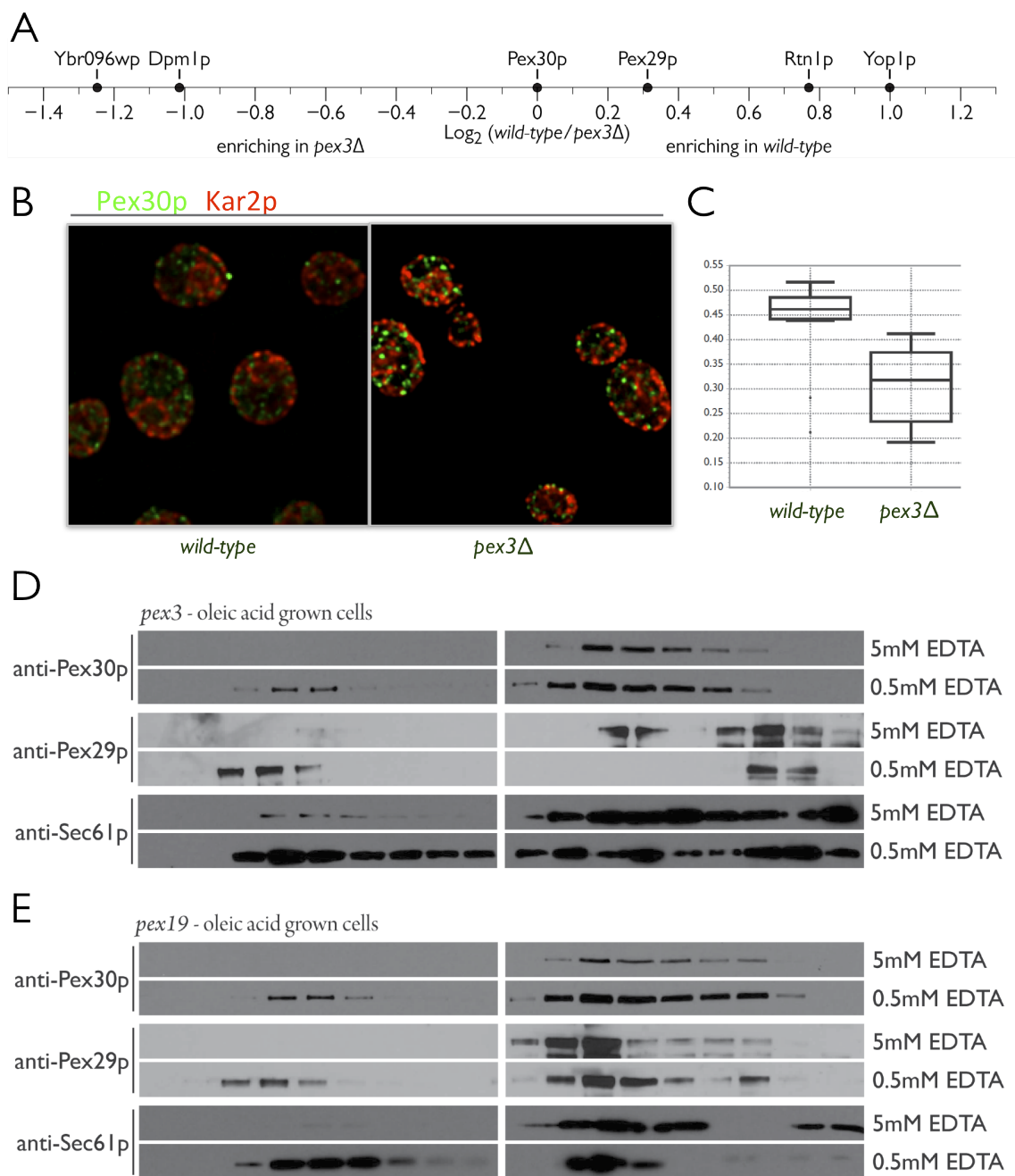
We next investigated the effect of the loss of peroxisomes on the stability of the reticulon-peroxin complex. To test this, a comparison of relative enrichment of the reticulon-peroxin complex members in immunoprecipitation of Pex29p-pA from wild-type cells and cells deleted for *PEX3* was performed. We chose Pex29p-pA because it was more dynamic protein than other complex members (Figure 3-12C-F). Both Rtn1p and Yop1p strongly enriched with Pex29p-pA under wild-type conditions when peroxisomes are present (Figure 3-13). Yop1p enrichment was 2-fold greater than when peroxisomes were absent. Interestingly, the association of Pex29p with Dpm1p was enriched 2-fold when peroxisomes were absent reinforcing the view that layers of regulation exist over the association of proteins within the complex.

We next assessed the effect of the loss of peroxisomes on Pex30p subcellular localization with immunofluorescence microscopy (Figure 3-13B). Quantification of Pearson's coefficients calculated from images collected from wild-type and *pex3Δ* strains showed a loss of stability for Pex30p localization within the ER (Figure 3-13C). However, ER-shift assays performed using lysates from *pex3Δ* cells or *pex19Δ* cells demonstrated that both Pex30p and Pex29p remained in the ER (Figure 3-13DE).

3.10 Peroxisome biogenesis is altered in cells lacking *RTN1*, *RTN2* and *YOP1*

To further investigate a potential role for Rtn1p and Yop1p in peroxisome biogenesis and function, we asked whether growth of cells on oleic acid medium requires *RTN1*, *YOP1* and/or *RTN2*, which was included based on its established role in ER structure and because transcriptional upregulation of the *RTN2* locus occurs upon loss of *RTN1* (Voeltz et al., 2006). Because growth on oleic acid is dependent on functional peroxisomes, this is a common assay used to evaluate peroxisome

Figure 3-13. The stability of the peroxin-reticulon complex is dependent on the presence of peroxisomes. (A) Endogenously expressed Pex29p-pA was immunopurified from wild-type and *pex3Δ* yeast whole cell lysates under conditions that promote the capture of integral membrane proteins. Shown is the comparative enrichment of members of the reticulon-peroxin complex plotted on a Log₂ scale. (B) Loss of peroxisomes alters the localization of Pex30p within the ER. Unlabeled wild-type and *pex3Δ* cells were grown in glucose and processed for immunofluorescence microscopy using affinity purified antibodies to Pex30p and antibodies to Kar2p. Shown are a maximum intensity projection of all optical sections. Pearson's coefficients were calculated for the deconvolved data sets using the JACOP plugin for Image J (NIH) and the data from a representative experiment of 10 images per strain are shown by interquartile box and whisker plots. (C) *pex3Δ* yeast lysates from cells grown in the presence of oleic acid were prepared in buffer containing either 5 mM EDTA or 0.5 mM EDTA. Cofractionation of Pex30p and Pex29p with the ER marker, Sec61p, is observed. (D) Similar to (C) but with *pex19Δ* yeast lysates.



biogenesis and function. As discussed earlier, yeast cells carrying single or double deletion(s) of *PEX29* and *PEX30* exhibit an increased number of peroxisomes per cell and a decreased average peroxisome volume when grown in oleic acid-containing medium; however, neither deletion affects the viability of yeast cells during growth in glucose- or oleic acid-containing medium (Vizeacoumar et al., 2003; 2004). Similarly, no detectable growth defect was observed on oleic acid-containing medium for cells deleted for *RTN1*, *YOP1* and *RTN2* (Figure 3-14).

We next asked if Rtn1p, Yop1p and Rtn2p directly or through the establishment of tubular ER structures contribute to the de novo biogenesis of peroxisomes. Specifically, we measured the kinetics of de novo peroxisome biogenesis in wild-type and mutant strains. To monitor de novo peroxisome biogenesis, we made strains in which the expression of *PEX19*, a gene essential for peroxisome biogenesis, was tightly regulated. This system is similar to a previously described system used to investigate de novo peroxisome biogenesis (Hoepfner et al., 2005), but instead of regulating gene expression by a galactose inducible promoter, we used the regulatable TetO₇ promoter (Hughes et al., 2000; Mnaimneh et al., 2004).

To visualize peroxisome biogenesis, we introduced an endogenously expressed Gpd1p-GFP into both wild-type and triple null, *rtn1Δ/rtn2Δ/yop1Δ*, strains in which *PEX19* expression is under the control of the TetO₇ promoter. The rationale behind using the peroxisomal matrix protein, Gpd1p, was to facilitate visualization of mature peroxisomes capable of importing matrix proteins, thereby providing a measurement of functional peroxisomes. With this system, we could assess the temporal dynamics of peroxisome biogenesis in individual cells. After prolonged culturing in the presence of doxycycline, repression of *PEX19* expression led to the absence of detectable peroxisomes (Figure 3-15A). Upon removal of doxycycline, *PEX19* expression resumed and led to the time-dependent reappearance of detectable peroxisomes. Temporal analysis of the percentage of cells in which peroxisomes were detectable following the release of *PEX19* repression showed that peroxisome reappearance occurred more quickly in *rtn1Δ/rtn2Δ/yop1Δ* cells relative to wild-

Figure 3-14. Triple deletion of *RTN1*, *RTN2* and *YOP1* does not abrogate the ability of cells to grow on medium containing oleic acid as the sole carbon source. Cells dividing logarithmically in glucose-containing medium were washed to remove glucose, serially diluted in water and spotted onto YPBO-agar plates. Shown are colonies formed after incubation at 30°C for 3 days are shown. *pex3Δ* cells serve as a negative control for this assay because they lack peroxisomes and exhibit reduced growth on this medium. Wild-type cells serve as the positive control. Cells of two independently isolated *rtn1Δ/rtn2Δ/yop1Δ* strains were tested, and neither strain exhibited a growth defect when presented with oleic acid as the sole carbon source.

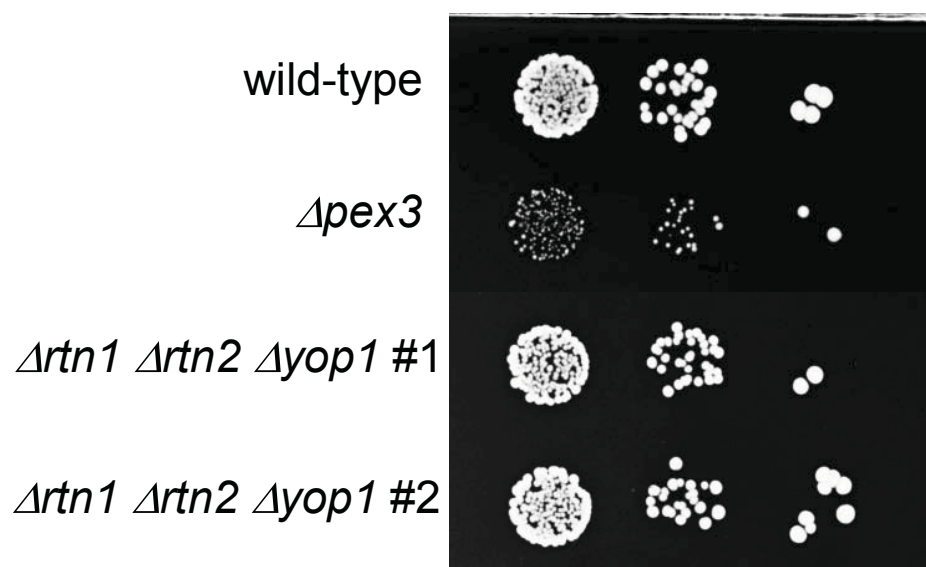
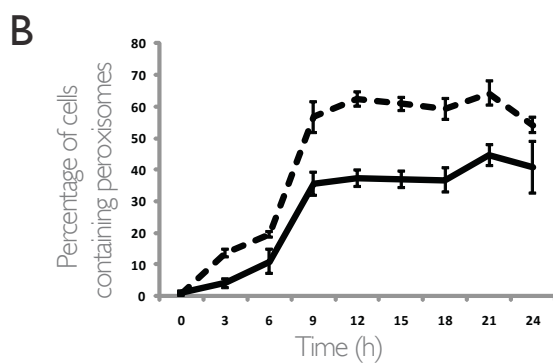
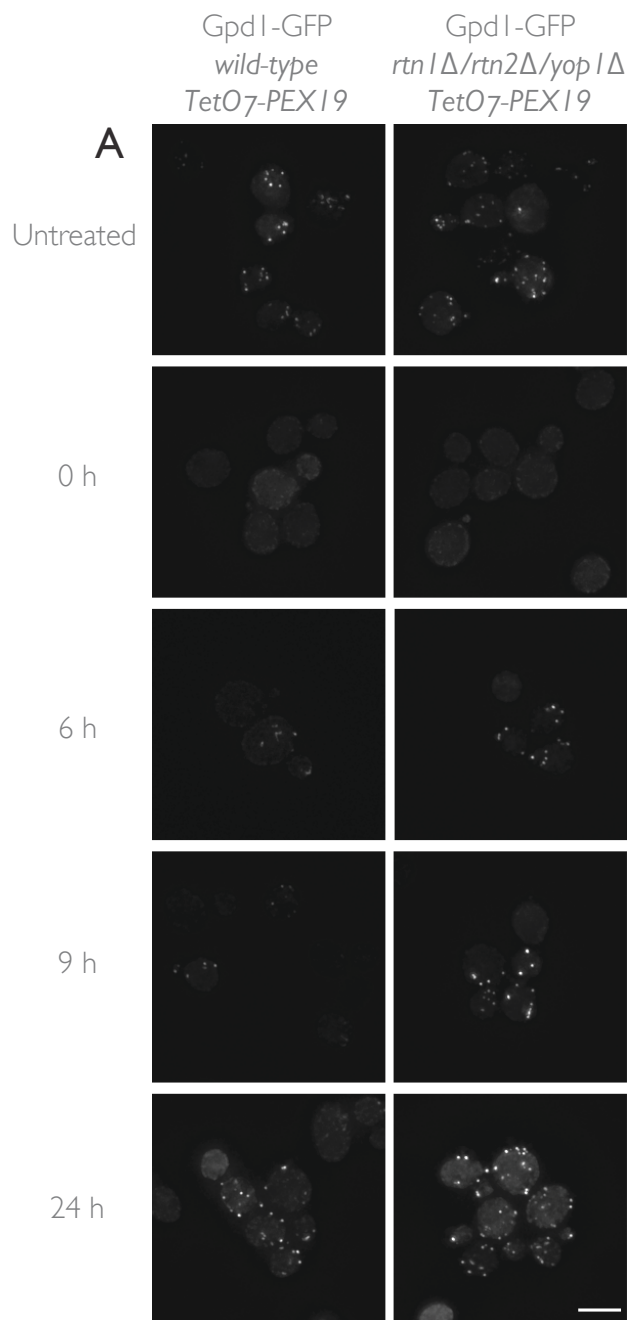


Figure 3-15. Deletion of *RTN1*, *RTN2* and *YOPI* increases peroxisome formation and the prevalence of cells containing peroxisomes. The genomically encoded copy of *PEX19* was placed under the control of a tetracycline repressible TetO7 promoter to allow regulatable peroxisome production in wild-type and *rtn1Δ/rtn2Δ/yop1Δ* triple null cells expressing Gpd1p-GFP as a peroxisomal marker. (A) Gpd1p-GFP localization is presented as maximum intensity projections of z-stack sections through wild-type (left) and *rtn1Δ/rtn2Δ/yop1Δ* (right) cells. In both strains, peroxisomes are present when cells are grown in the absence of doxycycline (Untreated) and absent in the most cells after overnight culturing in medium containing doxycycline (0 h). Release of *PEX19* repression by removal of doxycycline from medium results in a partially penetrant, time-dependent reappearance of peroxisomes in cells of both the wild-type and triple null strains. Scale bar, 5 μm. (B) Quantification of the percentage of cells in which peroxisome could be observed at the indicated time points after removal of doxycycline for the wild-type (solid line) and *rtn1Δ/rtn2Δ/yop1Δ* (dashed line) strains. Relative to the wild-type control, triple null cells exhibited a more rapid reappearance of peroxisomes and also an overall increase in the total percentage of cells containing peroxisomes throughout the timecourse. At least 200 cells were counted for each time point. Error bars represent the standard deviation between two independent biological replicates.



type cells (Figure 3-15B). Furthermore, despite observing a plateau in the percentage of cells with detectable peroxisomes for both strains, peroxisome reemergence was more penetrant in the *rtn1Δ/rtn2Δ/yop1Δ* strain, as this triple null mutant reached a higher plateau. We interpret these data to suggest that the dynamics of peroxisome formation are accelerated in the mutant cells compared to wild-type cells and demonstrate a role for the ER resident proteins Rtn1p and Yop1p in peroxisome biogenesis.

3.11 Egress of preperoxisomal vesicles is enhanced in deletion mutants of the reticulon-peroxin complex


Our preceding experiments suggested to us a role for the reticulon-peroxin complex in regulating preperoxisomal vesicle egression from the ER. To function as regulators of peroxisome-destined vesicular flow from the ER is consistent with the observed ER localization of the reticulon-peroxin complex and its dynamic association with peroxisomes. To test this hypothesis we reconstituted peroxisome biogenesis in vitro. A preperoxisomal vesicle budding assay has been previously shown to require the presence of Pex3p in the ER and Pex19p in the cytosol (Lam et al., 2010). ATP hydrolysis is required for successful budding to occur and in addition to Pex3p, additional peroxins, such as Pex15p and Pex11p, have been shown to be present in the vesicles (Agrawal et al., 2011; Lam et al., 2010).

Vesicle egression was enhanced in cells deleted for *PEX29* and *PEX30* and also for cells deleted for *RTN1*, *RTN2*, and *YOP1* as compared to the control (Figure 3-16A). As reported previously, the reaction was dependent on the presence of ATP and could be slowed by incubation at 4°C.

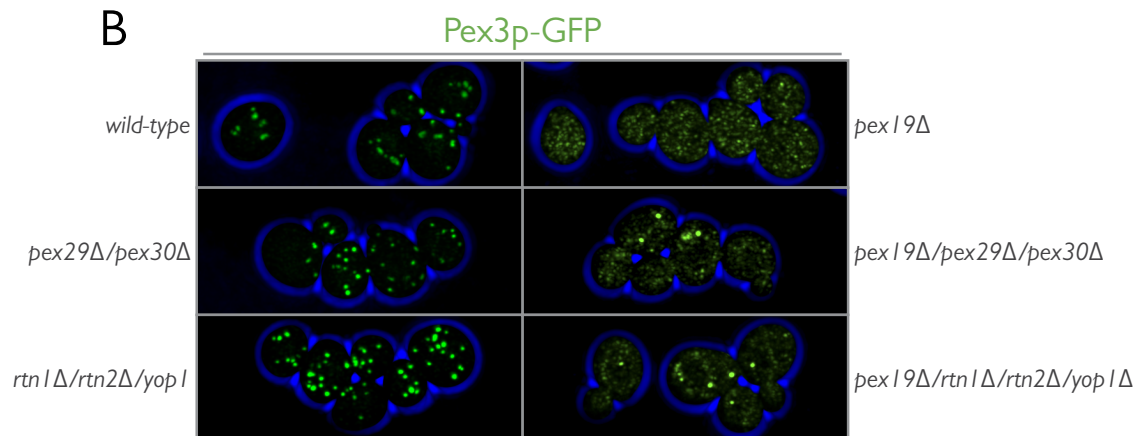
We imaged the strains used to prepare donor membranes for the in vitro reactions. Surprisingly, Pex3p-GFP localized to discrete puncta in *pex19Δ/pex29Δ/pex30Δ*, and

Figure 3-16. Egression of preperoxisomal vesicles is enhanced in reticulon-peroxin deletion strains as shown by a cell-free in vitro budding assay. Permeabilized yeast cells (PYCs) prepared from *pex19Δ*, *pex19Δ/pex29Δ/pex30Δ* and *pex19Δ/rtn1Δ/rtn2Δ/yop1Δ* cells expressing Pex3p-GFP were incubated with wild-type cytosol for 90 min at room temperature in the presence of an ATP-regenerating system (lanes 5, 7 and 8, respectively). Controls included incubating the PYCs alone (lanes 1,2 and 3), with cytosol but no ATP (lane 4, *pex19Δ* PYCs only), or with cytosol and ATP, but at 4°C (lane 6, *pex19Δ* PYCs only). At the end of the budding reaction, samples were centrifuged at $13,000 \times g$ for 2 min to pellet the PYCs. The supernatant was collected and the subjected to centrifugation at $200,000 \times g$ for 1 h. The pellet was resuspended in sample buffer and separated by SDS-PAGE. Immunoblotting for the presence of Pex3p-GFP was performed with affinity purified antibodies to Pex3p. (B) Cells from wild-type, *pex29Δ/pex30Δ*, *rtn1Δ/rtn2Δ/yop1Δ* *pex19Δ*, *pex19Δ/pex29Δ/pex30Δ* and *pex19Δ/rtn1Δ/rtn2Δ/yop1Δ* strains endogenously expressing Pex3p-GFP were grown in the presence of glucose and imaged by 3D confocal microscopy. Shown is a maximum intensity projection of all optical sections.

A

<i>pex1</i> Δ PYCs	+	-	-	+	+	+	-	-
<i>pex1</i> Δ/ <i>pex29</i> Δ/ <i>pex30</i> Δ PYCs	-	+	-	-	-	-	+	-
<i>pex1</i> Δ/ <i>rtn1</i> Δ/ <i>rtn2</i> Δ/ <i>yop1</i> PYCs	-	-	+	-	-	-	-	+
wild-type cytosol	-	-	-	+	+	+	+	+
ATP	-	-	-	-	+	+	+	+
4°C	-	-	-	-	-	+	-	-
anti-Pex3								

B



pex19Δ/rtn1Δ/rtn2Δ/yop1Δ cells suggesting that the loss of these proteins removed an inhibition to sort into packageable vesicles (Figure 3-16B).

3.12 Discussion

Pex30p and Pex29p are integral membrane proteins that have been shown to regulate peroxisome proliferation in the yeast *S. cerevisiae*. In this study, we show that these proteins are ER resident proteins that form a complex with the ER resident proteins Rtn1p and Yop1p. Both Rtn1p and Yop1p play roles in ER membrane curvature and establishing the peripheral ER, a site where de novo peroxisome biogenesis is proposed to occur (Tam et al., 2005). The absence of Rtn1p, Rtn2p and Yop1p results in disruption of the peripheral ER (Voeltz et al., 2006), and we demonstrate here that the absence of these proteins also leads to the dysregulation of de novo peroxisome biogenesis.

3.12.1 The ER in peroxisome biogenesis

The suggestion that peroxisomes are derived from the ER was based initially on electron microscopy that revealed close apposition of peroxisomes and specialized domains of the ER in guinea pig kidney cells (Novikoff et al., 1972). However, protein trafficking between the ER and peroxisomes was not evident in these studies, and most peroxisomal proteins examined, including membrane proteins, were shown to be synthesized on free cytosolic polysomes and to be imported directly from the cytosol into the peroxisome (Goldman and Blobel, 1978)(Goldman and Blobel, 1978; Robbi and Lazarow, 1982). Nonetheless, biochemical fractionation of ribosomes engaged in translation, and characterization of the associated mRNA and nascent proteins, demonstrated that the site of synthesis of at least one peroxisomal rat membrane protein, PMP50, was on ER-bound polysomes, lending credence to the idea that ER is the site of membranes destined to mature into peroxisomes (Bodnar and Rachubinski, 1991). Since these early studies, an increasing number of PMPs have been shown to traffic through the ER during their biogenesis

(Nuttall et al., 2011; Titorenko and Rachubinski, 2009). Indeed, 16 PMPs in *S. cerevisiae* have been shown to traffic through the ER prior to their incorporation into peroxisomes (van der Zand et al., 2010). Most of the proteins examined require the functional Sec61p complex for integration into the ER, while Get3p is especially required for the efficient trafficking of the tail-anchored protein, Pex15p (Schuldiner et al., 2008). Moreover, various studies have since shown that the integral membrane protein, Pex3p, routes through the ER. Release of Pex3p from the ER is required for subsequent peroxisome formation (Hoepfner et al., 2005; Tam et al., 2005). These studies have led to a model where Pex3p-containing nascent peroxisomes are formed from the ER in a Pex19p-dependent manner (Hettema et al., 2000; Hoepfner et al., 2005; Lam et al., 2010). A role for the ER in de novo peroxisome biogenesis explains the long established observation that peroxisomes can form in the apparent absence of preexisting peroxisomes, albeit very inefficiently in *S. cerevisiae* (Motley and Hettema, 2007). This is observed in yeasts where mutations lead to a lack of peroxisomes, yet functional peroxisomes reform by the introduction of the appropriate wild-type *PEX* gene (Matsuzono et al., 1999). Similarly, heterokaryons formed from peroxisome-deficient fibroblasts isolated from Zellweger patients of different complementation groups rapidly form new peroxisomes (Brul et al., 1988). Thus, the axiom “omnis membrana e membrana” (every membrane from a membrane), as stated by Günter Blobel, is not violated by the peroxisome (Blobel, 1980).

3.12.2 Regulation of peroxisome proliferation: the role of the ER

The molecular mechanisms of ER-mediated peroxisome biogenesis remain to be defined; however, comprehensive analyses including morphological, proteomic and genetic techniques, as shown here, combined with the recent development of an in vitro biochemical assay to produce peroxisome-like vesicles from microsomal fractions (Figure 3-16)(Agrawal et al., 2011; Lam et al., 2011) promise to reveal the molecular requirements of this fundamental process. To date,

components the DSLI complex are the only ER resident proteins that are linked to peroxisome biogenesis per se, as opposed to ER translocon proteins required for protein import into the ER (Perry et al., 2009). However, COP components have been detected in fractions of purified peroxisomes (Marelli, 2004) and are thought to play a role in rat liver peroxisome biogenesis (Passreiter et al., 1998). Inhibition of CopI expression also affects peroxisome numbers in *S. cerevisiae* (Perry et al., 2009). In the yeast *Hansenula polymorpha*, Pex25p and RhoIp were recently shown to be required for the biogenesis of peroxisomes when peroxisome biogenesis is controlled by the synthesis of Pex3p, presumably from the ER (Saraya et al., 2011). Pex25p and RhoIp are thus thought to play a role early in biogenesis. In *S. cerevisiae*, RhoIp is recruited to peroxisomes under conditions that induce the organelle (oleic acid) and, with Pex25p, regulates actin dynamics on peroxisomes (Marelli, 2004). Recent evidence also suggests a role for these proteins in peroxisome biogenesis in *S. cerevisiae* (Huber et al., 2012; Tower et al., 2011). Mutants in *PEX25* contain a heterogeneous population of small peroxisomes. While earlier studies in *S. cerevisiae* did not determine a specific temporal role for Pex25p and RhoIp in biogenesis, the phenotype was interpreted to suggest a role for Pex25p and RhoIp late in the biogenesis program. However, in addition to the interaction between Pex25p and RhoIp, these earlier studies also revealed an interaction between RhoIp and Pex30p (Marelli, 2004). Taken together, it appears that, like Pex29p and Pex30p, Pex25p and RhoIp may be involved in biogenesis at the ER. While deletion of *PEX25* causes fewer and larger peroxisomes and *pex29Δ* and *pex30Δ* mutants exhibit increased numbers of smaller peroxisomes (Vizeacoumar et al., 2003; 2004), it seems clear that defects in regulating peroxisome biogenesis from the ER can manifest in the accumulation of smaller or larger peroxisomes. These discoveries establish the ER as a master regulator of peroxisome proliferation.

Negatively regulating peroxisome biogenesis at the ER seems to be at least one of the functions of the reticulon-peroxin complex. Cells lacking these proteins, and the second reticulon

Rtn2p, produce peroxisomes more quickly upon reintroduction of Pex19p in the genetic system we used here (Figure 3-15). Deletion mutants also led to enhanced egress of Pex3p containing vesicles (Figure 3-16). Why would cells need to regulate biogenesis at the ER? As noted above, several PMPs transit through the ER and, as with other proteins transiting through the ER, assembly must be controlled (Braakman and Bulleid, 2011). One simple mechanism to achieve this control, and to prevent the premature assembly of peroxisomal membrane complexes, is to segregate PMPs within the ER. Distinct membrane protein-containing vesicles might then bud from the ER, and subsequent fusion would lead to the formation of import-competent organelles. Similar models have previously been suggested based on biochemical fractionation of distinct peroxisomal populations from the yeast *Yarrowia lipolytica* (Titorenko et al., 2000). Here, we monitored peroxisome formation using only a limited set of peroxisomal marker proteins, namely Pex3p, Mdh2p, Pot1p and Gpd1p. Thus, while it is clear that peroxisomes in *rtn1Δ/rtn2Δ/yop1Δ* cells can import Gpd1p with improved kinetics over wild-type, it is not clear whether the peroxisome population is homogeneous. It would be expected that inappropriate preperoxisomal vesicle release from the ER could lead to an aberrant vesicle population.

3.13 A conserved mechanism for reticulon proteins in ER-derived organelle biogenesis?

A role for Rtn1p and Yop1p in organelle biogenesis is not unique to peroxisomes. Rtn1p also interacts with Yli023p, which has been renamed as Pom33p. Similar to the results shown here for peroxisomes, it appears that Pom33p is required for NPC assembly and transiently interacts with Rtn1p during NPC biogenesis (Chadrin et al., 2010). As in peroxisome biogenesis, Rtn1p does not form part of the NPC but rather transiently interacts with Pom33p to form normal NPCs. Similarly, Pex29p and Pex30p appear to interact transiently with Rtn1p and Yop1p, and the latter two proteins do not assemble into mature peroxisomes. We also found Pom33p in immunisolations

containing Pex29p, Pex30p, Rtn1p and Yop1p. Whether Pom33p plays a role in peroxisome biogenesis in this context is not known. The roles Rtn1p and Yop1p play in NPC and peroxisome biogenesis are likely related to their capacity to induce and maintain membrane curvature (Dawson et al., 2009), and such bending mechanisms may represent a common mechanism for the biogenesis of additional ER-derived organelles.

De novo peroxisome biogenesis has long been debated in the field. Our findings, taken together with the likelihood of a conserved function of Rtn1p and Yop1p as mediators of membrane curvature in organelle formation/biogenesis, have led us to propose a model in which the emergence of preperoxisomal vesicles from the peripheral ER is controlled by members of the reticulon-peroxin complex, and that this control demands a functionally and spatially defined ER. These results are the first demonstration of a direct role for ER resident proteins in the de novo synthesis of peroxisomes, which establishes a foothold for the further dissection of the molecular events of this process at the ER.

4 The evolution of the Pex23p/Pex30p family of peroxins

4.1 Overview

The discovery of a reticulon-peroxin complex involved in the regulation of peroxisome proliferation by regulating the flow of vesicular traffic from the ER to the peroxisome raises some interesting questions. Is this mechanism and the reticulon-peroxin complex members conserved? If so, to what extent are they conserved?

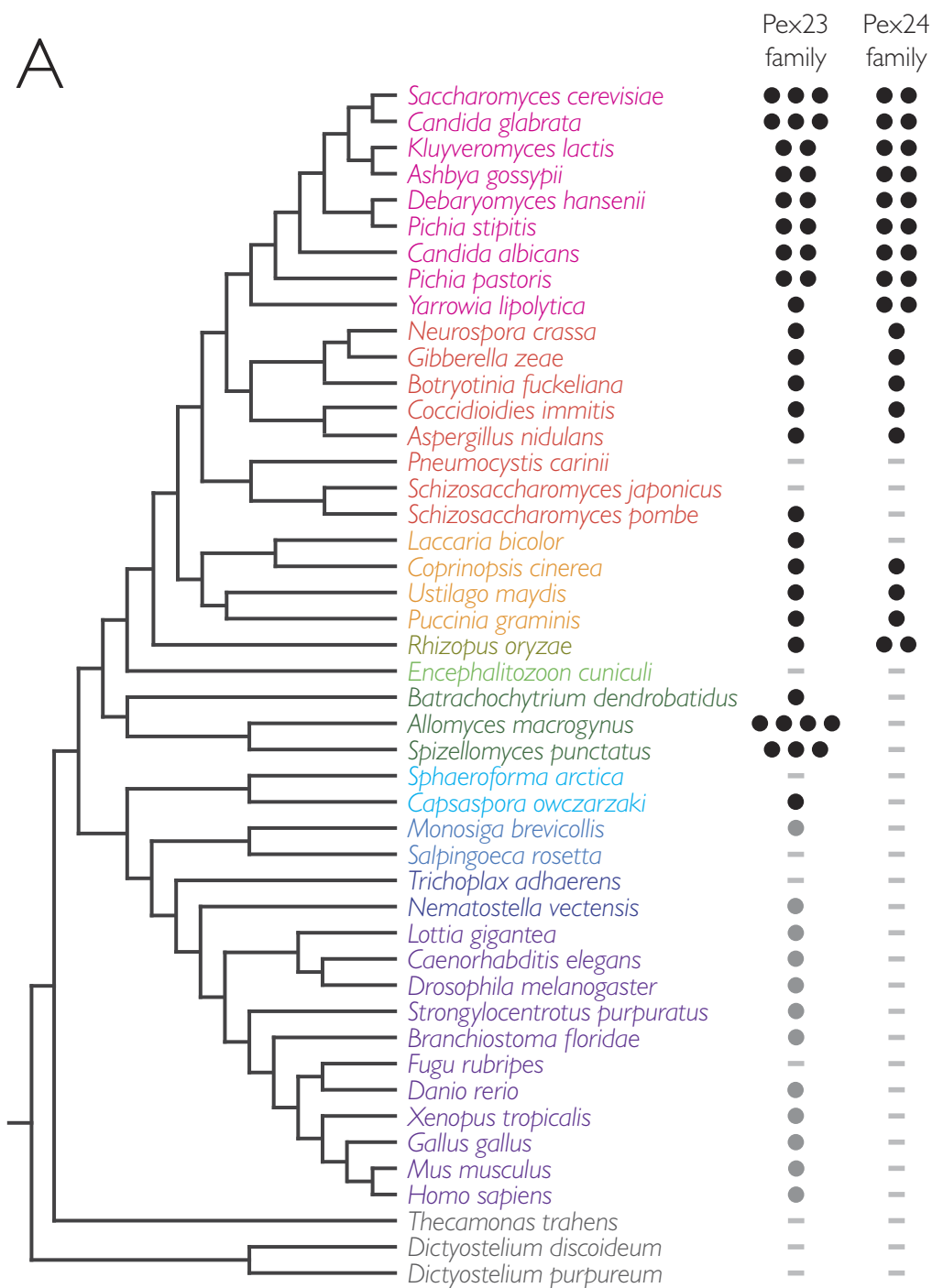
A previous comparative genomic and phylogenetic analysis of the reticulon family identified orthologs in fungi, metazoans and members of the archaeplastida, as well as in *Leishmania* sp., *Mastigamoeba balamuthi* and *Dictyostelium discoideum* (Oertle et al., 2003). The reticulon family has undergone extensive genetic rearrangements and multiple emergences of novel domain regions leading the authors to propose a complex intron-rich ancestor and highly variable pattern of gene evolution in each of the different eukaryotic lineages.

Initial comparative genomic analysis of peroxins concluded that Pex30p and Pex29p are fungal innovations (Kiel et al., 2006; Schluter, 2006). Pex30p is the ortholog of *Y. lipolytica* Pex23p and the Pex23p/Pex30p family includes Pex23p/Pex30p, Pex31p and Pex32p. Pex29p is a homolog of *Y. lipolytica* Pex24p and the Pex24p family includes Pex24p/Pex28p, and Pex29p. We therefore decided to readdress the evolution of these fungal proteins given the availability of many newly sequenced eukaryotic genomes and also the adoption of more powerful homology searching algorithms (Eddy, 2009).

4.2 A comparative genomic analysis of the Pex23p/Pex30p family in Opisthokonts

To explore the conservation of the Pex23 family of proteins we surveyed 41 complete, or nearly complete, databases from publicly available genome sequencing projects to identify putative proteins homologous to Pex23 and its family members (Figure 4-1). This list of organisms spans the available genomic diversity of the fungal and metazoan lineages and samples major branch

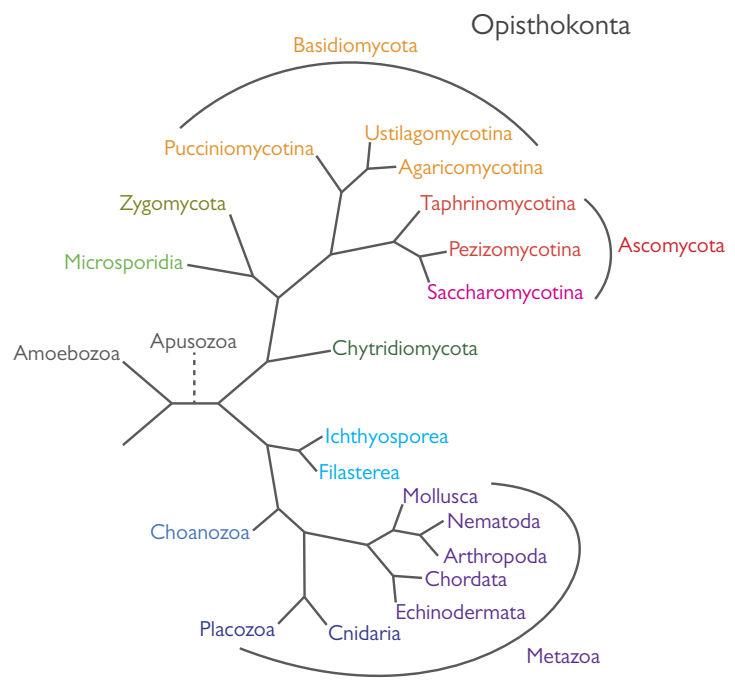
Figure 4-1. Comparative genomic survey of the Pex23p/Pex30p family in opisthokonts. Results from the comparative genomic survey. Each column, labeled at the top, represents Pex23p or Pex24p. Individual species from the survey are color coded as (B) and grouped according to established taxonomic classification. A circle indicates the presence of a protein as verified by BLAST and hidden Markov model searches. Black denotes a greater than 50% max similarity score in BLAST searches with the *B. dendrobatidis* Pex23p homolog, whereas grey denotes a max similarity score of less than 50%. Multiple circles under a protein column indicate multiple putative orthologs for that protein in the indicated species. (B) A tree illustrating the relative evolutionary relationships of lineages with genome sequences available in the fungi and metazoans with additional taxa including Choanozoa and Filasterea from the base of the Opisthokonta supergroup (<http://www.ncbi.nlm.nih.gov/taxonomy/>; James et al. 2006). The dotted line to Apusozoa denotes the uncertainty of their evolutionary position. (C) An example HMM and reciprocal BLAST score for the Pex23p ortholog in *B. dendrobatidis*. *B. dendrobatidis* Pex23p is also the ortholog of the Pex24p family as demonstrated by HMM and reciprocal BLAST scores for Pex24p. (D) Reciprocal BLAST scores between *B. dendrobatidis* Pex23p and human TecPR1.



Pex23 family members: Pex23/Pex30, Pex31, Pex32

Pex24 family members: Pex24/Pex28, Pex29

B



C

<i>Batrachochytrium dendrobatidis</i>	Pex23 HMM Top Hit BDET_07010 - 0.0015	Pex24 HMM Top Hit BDET_07010 - 3.8e ⁻⁰⁵
BDET_07010 Reciprocal BLAST:	<i>Yarrowia lipolytica</i> XP_503356 (Pex23p) - 1e ⁻¹⁵ XP_502718 (Pex24p) - 1e ⁻⁰⁴ XP_505627 (Pex29p) - 0.001	<i>Saccharomyces cerevisiae</i> NP_013428 (Pex30p) - 1e ⁻¹⁷ NP_011518 (Pex31p) - 7e ⁻¹³ NP_010767 (Pex29p) - 7e ⁻¹⁰ NP_009727 (Pex32p) - 8e ⁻⁰⁷ NP_012020 (Pex28p) - 8e ⁻⁰⁷

D

	Query Protein	Top Hit
<i>Batrachochytrium dendrobatidis</i> - BDET_07010		<i>Homo sapiens</i> - NP_056210 - 9e ⁻⁰⁷
<i>Homo sapiens</i> - NP_056210		<i>Batrachochytrium dendrobatidis</i> - BDET_07010 - 7e ⁻⁰⁵

points in the opisthokont supergroup (Figure 4-1B). The summary of this comparative analysis can be found in Figure 4-1A.

Initial BLAST queries with *S. cerevisiae* readily identified the functionally characterized homolog in *Pichia pastoris* and *Yarrowia lipolytica*, as has been described previously (Brown et al., 2000; Vizeacoumar et al., 2004; Yan et al., 2008). These three homologs were chosen as a starting point for building a more sensitive search strategy based on hidden markov models (HMM) (Eddy, 2009), and were sufficient for identifying Pex23p homologs in the Saccharomycotina. Iteratively adding verified homologs to the HMM allowed for the identification of Pex23p homologs down to the base of Opisthokonts and into the metazoan branch of the supergroup as well. Notable absences in the taphrinomycetes *Schizosaccharomyces japonicas* and *Pneumocystis carinii* are consistent with reports of the taxa being highly divergent from sister ascomycete lineages (Liu et al., 2009). However, in addition to these taxa, an absence in *Sphaeroforma arctica*, *Salpingoeca rosetta*, and *Fugu rubripes* is consistent with a noted absence of Pex3p (Chapter 5 of this thesis), and may reflect the loss of peroxisomes in these organisms.

The addition of putative Pex23p homologs from chytridiomycetes to the HMM resulted in the appearance of Pex24p family members in searches designed to validate the new HMM. Furthermore, and in particular, the putative Pex23p homolog identified in *Batrachochytrium dendrobatidis* returned all Pex23p and Pex24p family members in reciprocal BLAST searches into both *Yarrowia lipolytica* and *S. cerevisiae* (Figure 4-1C). We therefore decided to also carry out independent comparative analyses of the Pex24 family (Figure 4-1A). Interestingly, these searches identified an uncharacterized homolog of Pex24 in *Y. lipolytica*, which returned Pex29p in *S. cerevisiae* as its best hit.

While a HMM based on Pex23p homologs identified putative metazoan Pex23 proteins, a HMM based solely on Pex24p homologs did not. Inspection of the alignments generated in these searches revealed that the primary region of sequence similarity between fungal Pex23 proteins

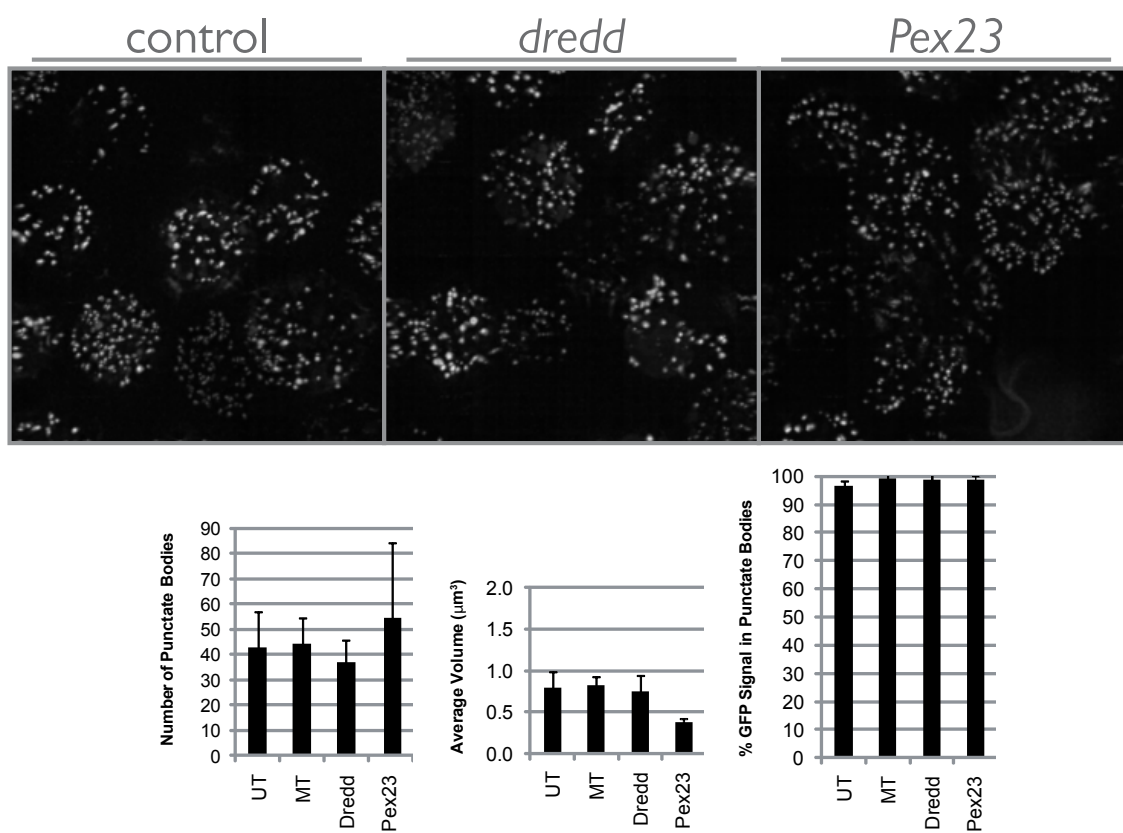
and the putative metazoan Pex23 proteins was the presence of a dysferlin motif, which is lacking in Pex24p family members. The dysferlin motif is named after the dysferlin protein where it was first discovered (Lek et al., 2012). However, our searches consistently picked up proteins distinct from the dysferlins and a similar comparative analysis of dysferlin genes failed to pick up the putative metazoan Pex23 proteins or yeast Pex23 proteins, despite also recognizing the presence of dysferlin domains in yeast Pex23 family members (Lek et al., 2010).

To differentiate between those proteins identified only by similarity to the dysferlin motif and those proteins with more extensive sequence similarity, we sorted putative homologs with reciprocal BLAST searches using the putative *B. dendrobatidis* Pex23, as query as shown for *Homo sapiens* (Figure 4-1D). Homologs with max identity scores greater than 50% were labeled with a black dot and those with scores less than 50% were labeled with a grey dot (Figure 4-1A). This analysis revealed the presence of a single putative Pex23p homolog sharing conserved protein topology with the fungal Pex23 proteins in *Capsaspora owczarzaki*. We also searched in outgroup apusozoa and amoebozoa species but did not detect any Pex23 homologs.

4.3 *Drosophila* Pex23 is involved in peroxisome biogenesis

To test the validity of the putative Pex23p homologs in metazoan lineages we performed dsRNA interference (RNAi) knockdown (Foley and O'Farrell, 2004) of the putative *Drosophila* Pex23 in S2 cells expressing a fluorescent peroxisomal matrix protein, GFP-SKL (Kural et al., 2005). RNAi knockdown of *Drosophila* Pex23 resulted in increased numbers of smaller peroxisomes, a phenotype similar to loss of Pex23 proteins in yeast (Figure 4-2). We therefore conclude that Pex23 homologs are present across the diversity of eukaryotes and are notably present in metazoans. Furthermore, our comparative analysis demonstrates for the first time a shared ancestry between the Pex23 and Pex24 families, which had been hinted at previously (Kiel et al., 2006).

Figure 4-2. *Drosophila* Pex23 (*DmelPex23*) is involved in peroxisome biogenesis. S2 cells constitutively expressing the fluorescent peroxisomal reporter protein GFP-SKL (Kural *et al.*, 2005) were treated with dsRNA to the putative *DmelPex23* gene, mock-treated, or treated with dsRNA targeting *Dredd*, which has no known role in peroxisome biogenesis or peroxisome function. GFP-SKL in S2 cells targets to punctae characteristic of peroxisomes. Mock-treated cells and cells treated with dsRNA targeting *Dredd* exhibited punctae like control cells. Cells treated with dsRNAs to *DmelPex23* exhibited increased heterogeneous peroxisomal numbers and decreased volume as assessed by quantification of the 3D data sets with the Imaris (Bitplane) spot algorithm. Bar, 5 μ m.



4.4 A phylogeny of the Pex23p family in Saccharomycotina

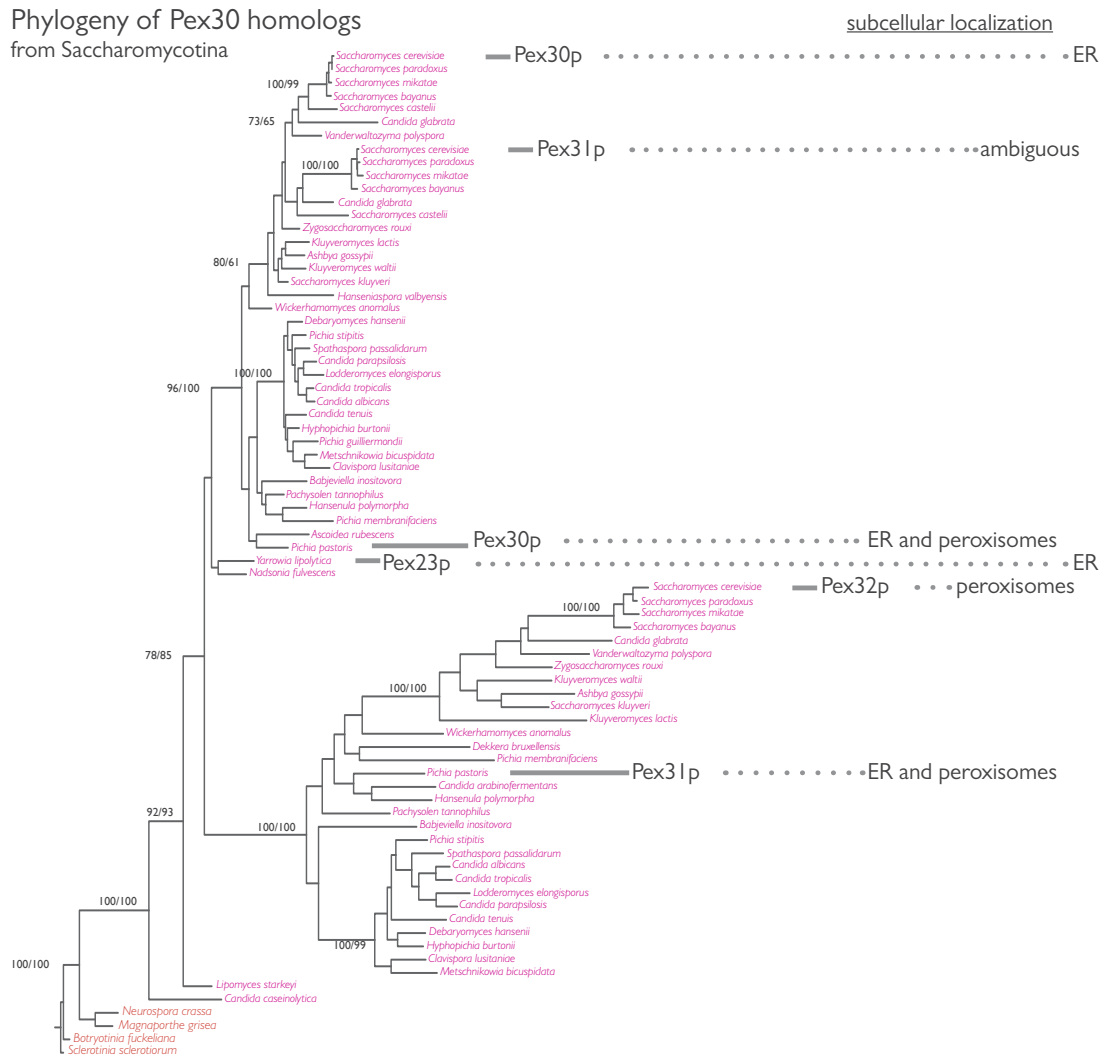
We next evaluated the relationship between the Pex23 proteins in the Saccharomycotina. To gain a broader taxonomic sampling, we performed additional comparative genomic analyses in an expanded list of organisms from this group (Figure 4-3B). Most of the Saccharomycotina genomes searched had two or three putative homologs, whereas *Yarrowia lipolytica* had one. We determined the phylogenetic relationships between these putative homologs and included homologs from *Neurospora crassa*, *Magnaporthe grisea*, *Botryotinia fuckeliana*, and *Sclerotinia sclerotiorum* as outgroups (Figure 4-3A). The data demonstrate that all Saccharomycotina Pex23 homologs originated from a common ancestor at the base of the Saccharomycotina and are divided into two major clades. Pex30p from *S. cerevisiae* and Pex23p from *Y. lipolytica* were present in one clade, along with Pex30p from *P. pastoris*. The second clade included Pex32p from *S. cerevisiae* and Pex31p from *P. pastoris*. The *P. pastoris* Pex31p is therefore more closely related to Pex32p from *S. cerevisiae* and would benefit from reclassification. Interestingly, the data suggest the split between the major Pex30p and Pex32p branches happened before the emergence of *Y. lipolytica* and therefore than ancestor of *Y. lipolytica* likely had a Pex32p homolog that was subsequently lost. The emergence of Pex31p likely occurred with the whole genome duplication event in the ancestor of *S. cerevisiae* and its closely related yeasts.

4.5 Pex23p localizes to the ER

We imaged the Pex30p paralogs in *S. cerevisiae* to determine if they too, localized to the ER (Figure 4-4). Cells expressing Pex30p-GFP, Pex31p-GFP or Pex32p-GFP were imaged in strains expressing Pot1p-mRFP or Rtn1p-mRFP and followed over a timecourse of incubation in oleic acid containing medium. As was expected, Pex30p-GFP partially colocalized with Rtn1p-mRFP throughout the timecourse (Figure 4-4B) and associated with Pot1p-mRFP containing peroxisomes when cells were grown in the presence of oleic acid (Figure 4-4A). Pex31p-GFP displayed an

Figure 4-3. Comparative genomic survey and phylogenetic analysis of the Pex23p/Pex30p family in the Saccharomycotina. (A) Phylogeny of the Pex23p/Pex30p proteins found in the Saccharomycotina. In this phylogenetic analysis, the optimum tree topology as determined by maximum likelihood is shown rooted on the Pezizomycotina outgroup taxa. PhyML and RaxML bootstrap values from 100 pseudoreplicates are displayed for important branch nodes. (B) Results from the comparative genomic survey. Individual species from the Saccharomycotina are grouped according to established taxonomic classification (<http://www.ncbi.nlm.nih.gov/taxonomy/>). A circle indicates the presence of a protein as verified by profile hidden Markov model searches.

A Phylogeny of Pex30 homologs from Saccharomycotina



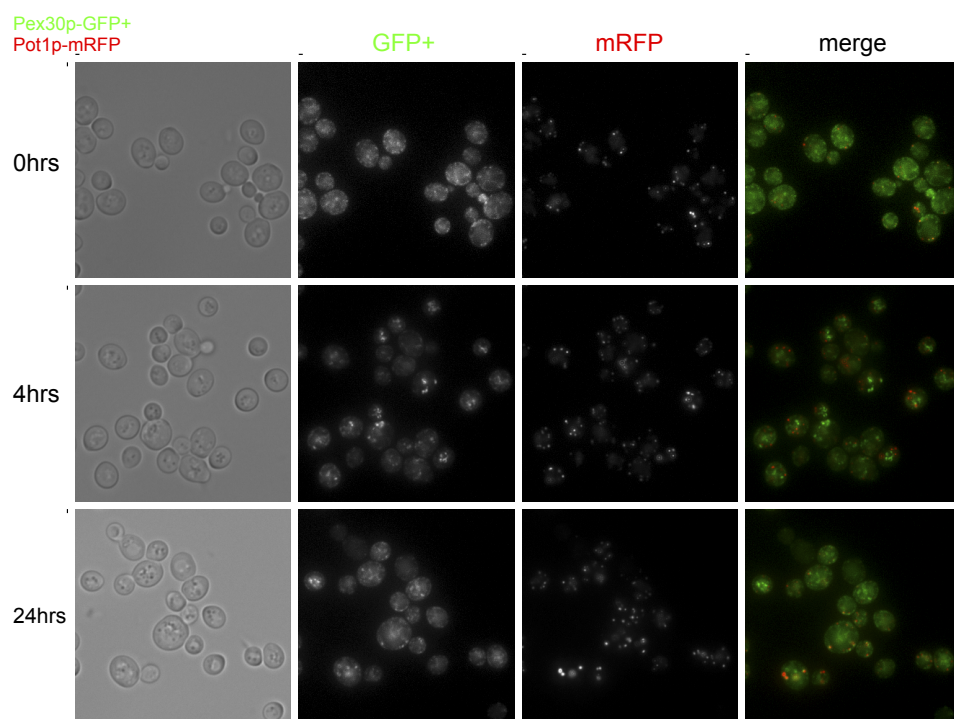
B

Pex23 family

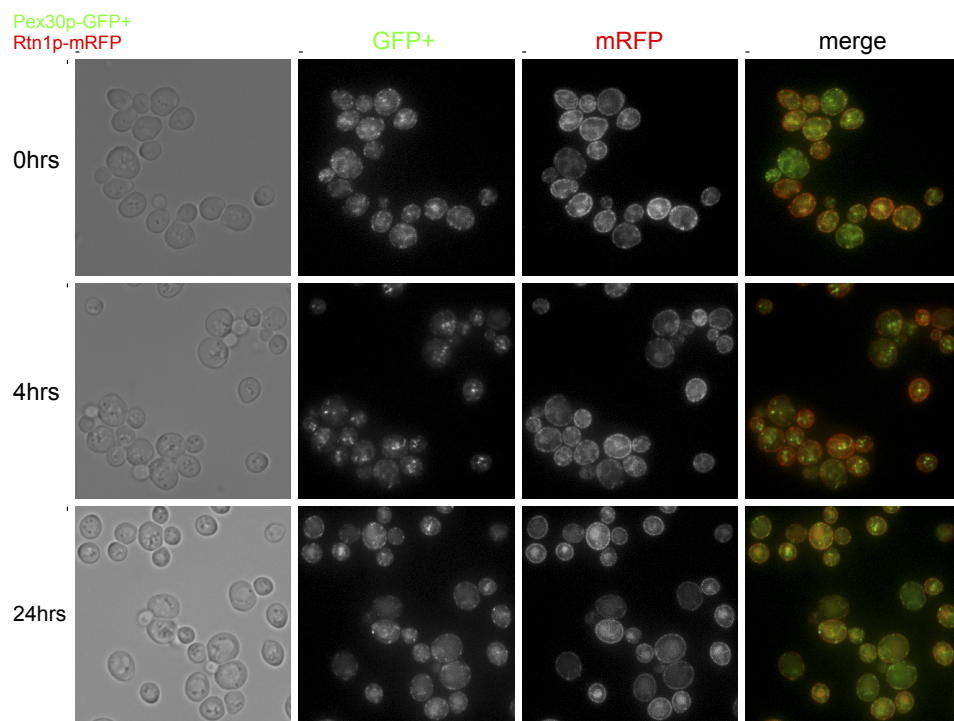
Saccharomycetaceae	<i>Saccharomyces cerevisiae</i>	●●●●
	<i>Saccharomyces paradoxus</i>	●●●●
	<i>Saccharomyces mikatae</i>	●●●●
	<i>Saccharomyces bayanus</i>	●●●●
	<i>Candida glabrata</i>	●●●●
	<i>Saccharomyces castelii</i>	●●
	<i>Vanderwaltozyma polyspora</i>	●●●●
	<i>Zygosaccharomyces rouxi</i>	●●
	<i>Kluyveromyces lactis</i>	●●
	<i>Ashbya gossypii</i>	●●
	<i>Kluyveromyces waltii</i>	●●
	<i>Saccharomyces kluyveri</i>	●●
	<i>Dekkera bruxellensis</i>	●●
	<i>Pichia pastoris</i>	●●
	<i>Pachysolen tannophilus</i>	●●
Saccharomycodaceae	<i>Hanseniaspora valbyensis</i>	●
	<i>Nadsonia fulvescens</i>	●
Phaffomycetaceae	<i>Wickerhamomyces anomalus</i>	●●
Debaryomycetaceae	<i>Babjeviella inositovora</i>	●●
	<i>Lodderomyces elongisporus</i>	●●
	<i>Spathaspora passalidarum</i>	●●
	<i>Pichia guilliermondii</i>	●
	<i>Pichia stipitis</i>	●●
	<i>Debaryomyces hansenii</i>	●●
Metschnikowiaceae	<i>Hyphopichia burtonii</i>	●●
	<i>Clavispora lusitaniae</i>	●●
	<i>Metschnikowia bicuspidata</i>	●●
Ascoideaceae	<i>Ascoidea rubescens</i>	●
mitosporic Saccharomycetales	<i>Candida arabinoferrmentans</i>	●●
	<i>Candida albicans</i>	●●
	<i>Candida tropicalis</i>	●●
	<i>Candida parapsilosis</i>	●●
	<i>Candida caseinolytica</i>	●
	<i>Candida tenuis</i>	●●
Pichiaceae	<i>Pichia membranifaciens</i>	●●
Saccharomycetales incertae sedis	<i>Hansenula polymorpha</i>	●●
	<i>Dipodascaceae</i>	●
Lipomycetaceae	<i>Lipomyces starkeyi</i>	●

Figure 4-4. Subcellular localization of Pex30 paralogs in *S. cerevisiae*. The localization of Pex30p-GFP, Pex31p-GFP and Pex32p-GFP was tracked over a 24 h incubation in oleate containing, YPBO medium. Each paralog of Pex30p was colocalized with the peroxisomal reporter Pot1p-mRFP (ACE) or the ER localized Rtn1p-mRFP (BDF) by widefield microscopy. Shown are the transmission, single and merged fluorescent channels from a typical field of view.

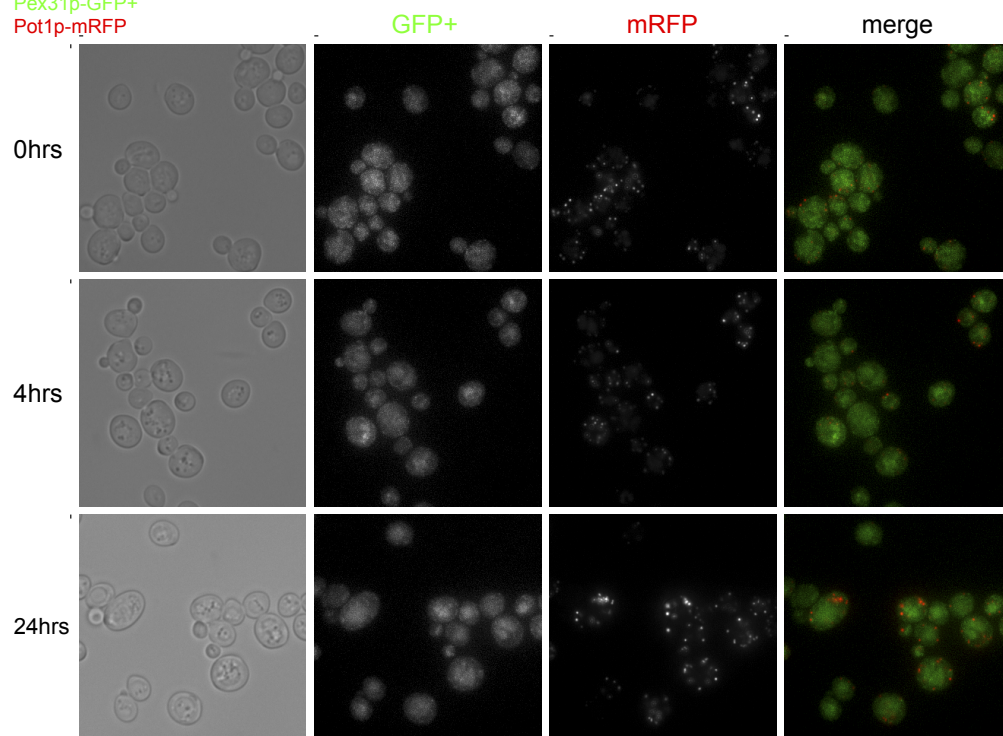
A



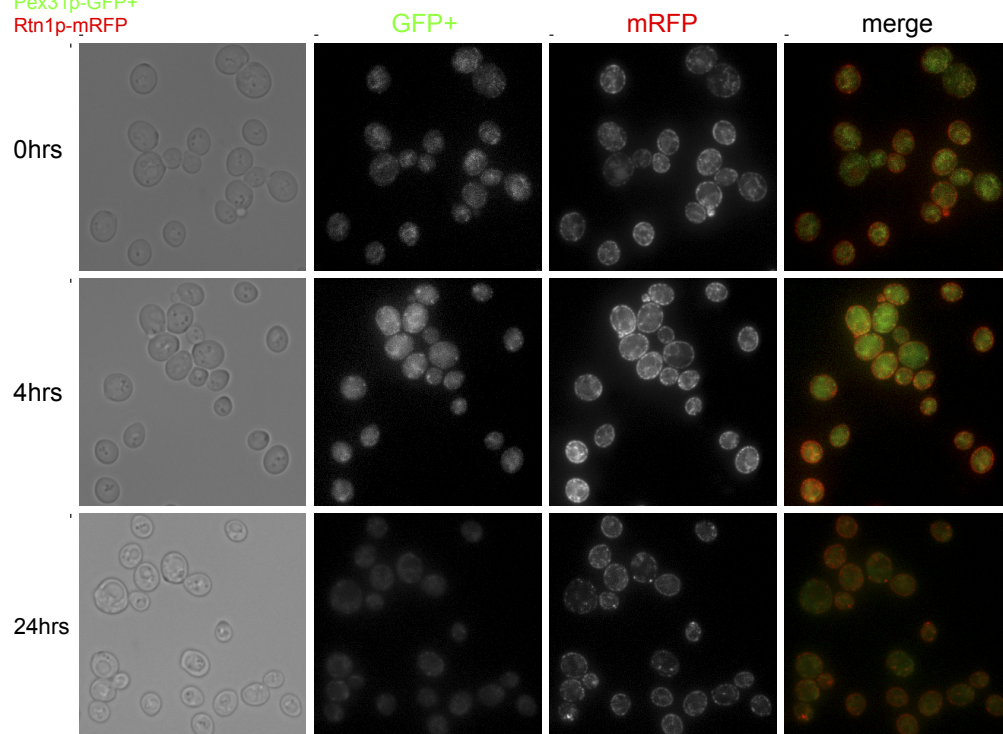
B



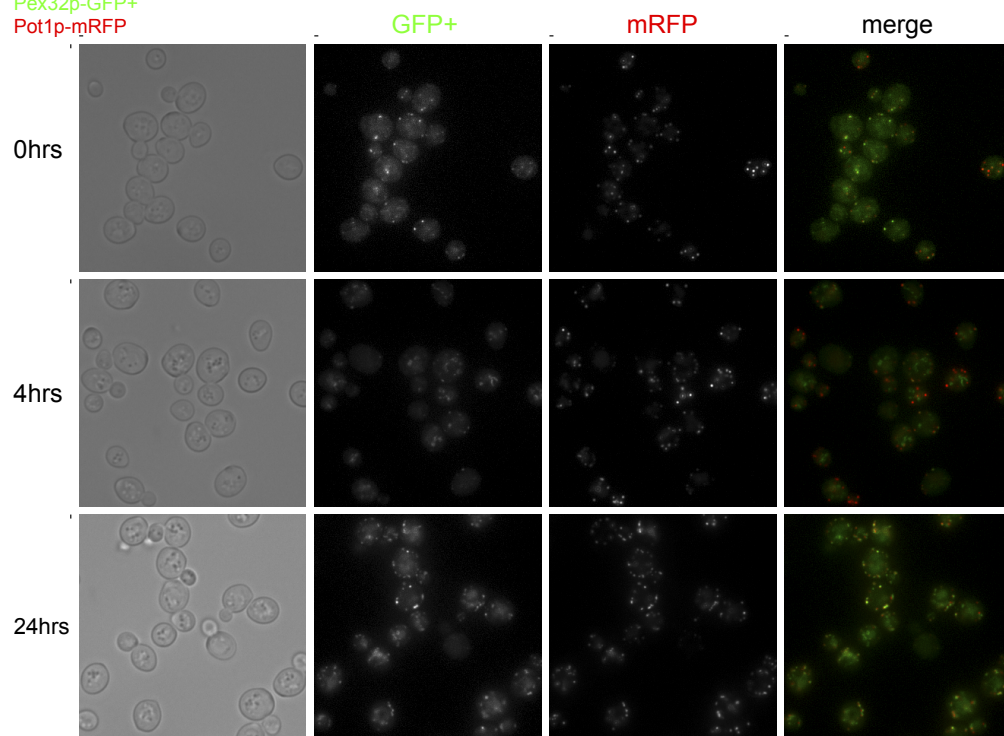
C

Pex31p-GFP+
Pot1p-mRFP

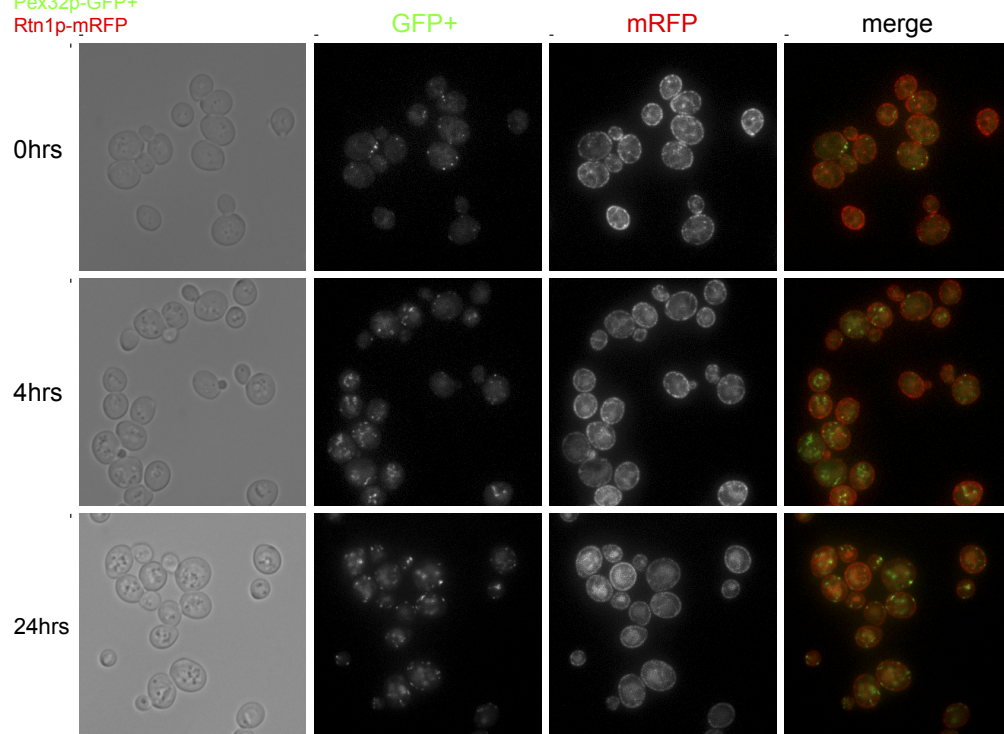
D

Pex31p-GFP+
Rtn1p-mRFP

E

Pex32p-GFP+
Pot1p-mRFP

F

Pex32p-GFP+
Rtn1p-mRFP

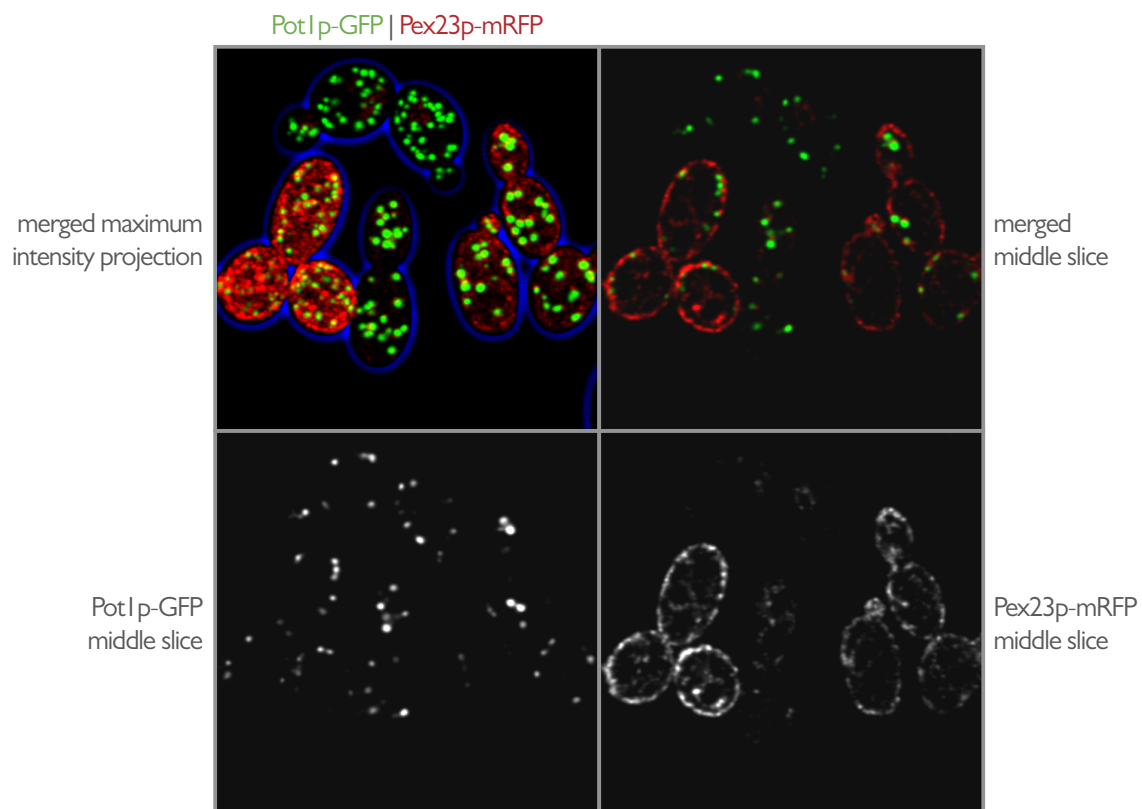
ambiguous localization in these experiments and could sometimes be seen to partially colocalized with both Pot1p-mRFP and Rtn1p-mRFP (Figure 4-4CD). In contrast to this, Pex32p-GFP colocalized exclusively with Pot1p-mRFP under all conditions and is therefore likely a peroxisomal protein (Figure 4-4EF).

Because of the peroxisomal localization of Pex32p-GFP we asked if the localization of Pex30p-GFP to the ER was unique or common to Pex30p orthologs. To answer this question we imaged Pex23p-mRFP in *Y. lipolytica*. Pex23-mRFP was expressed exogenously in *Y. lipolytica* cells endogenously expressing Pot1p-GFP. Pex23p-mRFP appeared to localize to the ER in these strains and cortical and perinuclear localization patterns could be detected (Figure 4-5). We therefore concluded that the ancestral subcellular localization of Pex30p was likely the ER and that the gene duplication giving rise to Pex32p also resulted in it targeting to peroxisomes. However, this awaits further experimental verification.

4.6 A sensitive search algorithm identifies a putative Pex23 homolog outside of the Opisthokonta

We next asked if Pex23p homologs could be found outside of the Opisthokonta. Our comparative genomic analysis had failed to identify homologs in the outgroup apusozoa and amoebozoan taxa and so we decided to use a more sensitive version of our HMM algorithm that functions akin to PSI-BLAST searches. We used as initial query, the single *B. dendrobatidis* Pex23p homolog and built an initial HMM from top hits of a pHMMer search into the NR database. This HMM identified a single hit outside of the Opisthokonts in *Tetrahymena thermophila*, a paramecium member of the SAR clade. Therefore, there may be additional homologs of Pex23p outside of the Opisthokont clade that await further study.

Figure 4-5. The *Y.lipolytica* Pex23p also localizes to the ER. The localization of exogenously expressed Pex23p-mRFP was assessed in wild-type E34 cells endogenously expressing Pot1p-GFP. Shown are a maximum intensity projection of all optical sections and single z-sections through the midplane of cells



5 Emergent complexity in myosin V-based organelle inheritance

A version of this chapter has been published.

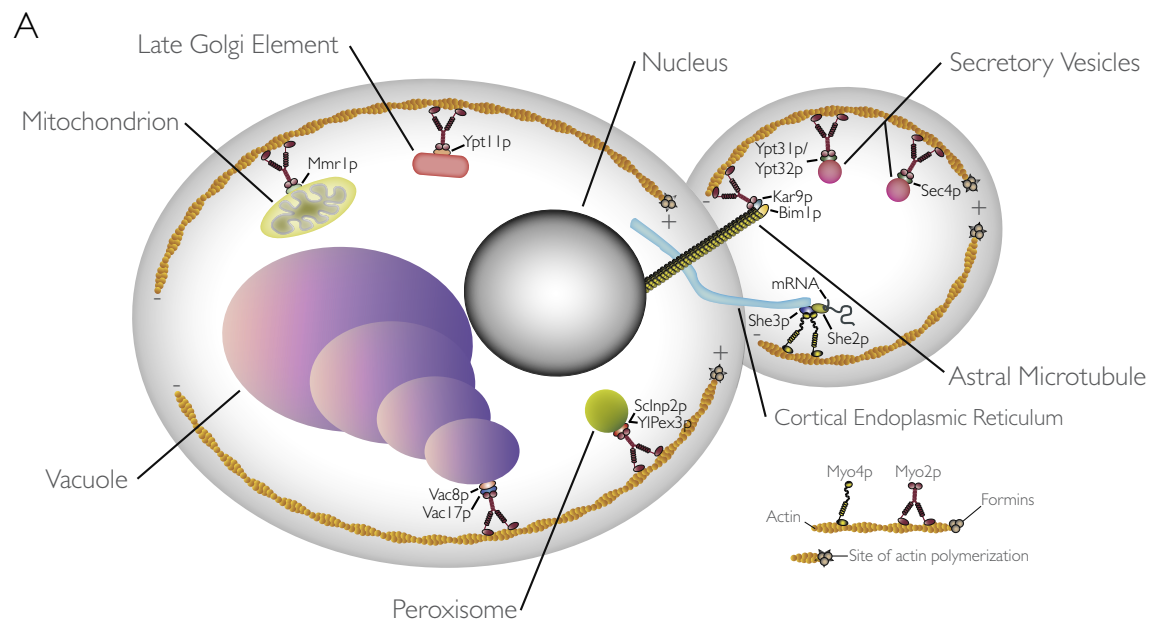
Mast, F.D., R.A. Rachubinski and J.B.Dacks. 2013. Emergent complexity in myosin V-based organelle inheritance. *Mol Biol Evo.* 29:975–984. doi:10.1093/molbev/msr264.

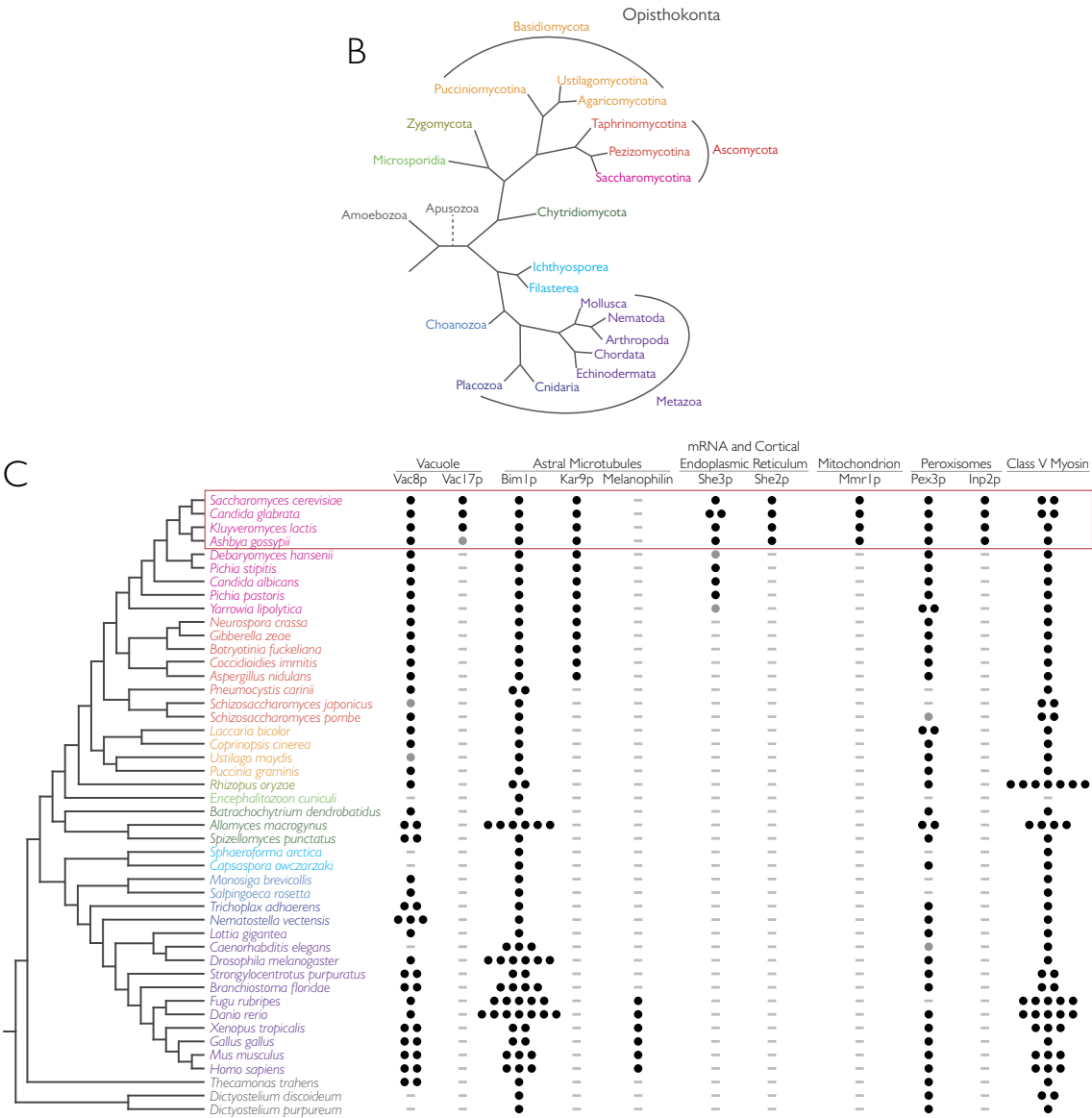
5.1 Overview

Budding yeasts, and in particular *Saccharomyces cerevisiae*, have emerged as powerful model organisms for the study of inheritance mechanisms because their distinctive growth via budding allows for ready observation and manipulation of the asymmetrical partitioning of cellular components (Fagarasanu and Rachubinski, 2007). During cell division, signaling from the Ras and Rho family GTPases, Rsr1p and Cdc42p, recruit actin-polymerizing formins to nucleate cables of polarized actin with their plus or 'barbed' ends oriented toward the incipient bud site and their negative or 'pointed' ends extending deep into the mother cell (Park and Bi, 2007; Pruyne et al., 2004). This alignment of actin along the mother-bud axis allows for the transport of secretory components that, even while they mature, are trafficked to and deposited at the growing bud tip (Santiago-Tirado et al., 2011). The transport of secretory vesicles relies on the molecular motor myosin V to power their vectorial transfer to the bud (Govindan et al., 1995). In turn, secretory vesicles require the coupled Rab GTPases Ypt31p/Ypt32p and Sec4p to bind to the globular tail of the myosin V motor (Lipatova et al., 2008; Santiago-Tirado et al., 2011). The polarized actin cables act to shuttle not only a constant supply of secretory vesicles to the growing bud site but other cargoes as well (Fagarasanu and Rachubinski, 2007). As the bud grows, the transport of most organelles, including peroxisomes, mitochondria, the vacuole, cortical endoplasmic reticulum and late Golgi elements, as well as astral microtubules and some mRNAs, are similarly transported by myosin V and organelle-specific receptors and adaptors (Fagarasanu et al., 2010) (Figure 5-1A). The recruitment of myosin V by each of its diverse cargoes requires the presence of a diverse array of cargo-specific adaptor protein complexes (Akhmanova and Hammer, 2010).

We wanted to determine the generality of the current model of organelle inheritance that has emerged from studies in *S. cerevisiae* to see if broad insights could be derived from these studies. It is now evident that 'yeasts to man' represents only a fraction of overall eukaryotic diversity (Walker et al., 2011). Nonetheless, the bulk of eukaryotic genome sequence information is

Figure 5-1. Comparative genomic survey of the machinery for organelle inheritance in opisthokonts. (A) A model for myosin V-based organelle inheritance and transport in budding yeast. The vectorial transfer of cell components (see the figure) is dependent on a polarized actin cytoskeleton created by bud-neck- and bud-tip-localized formins that is travelled on by class V myosin motor complexes. In *Saccharomyces cerevisiae* each cargo interacts independently with a myosin V motor, either Myo2p or Myo4p, via distinct cargo-specific proteins or protein complexes. They are: Ypt11p for late Golgi elements; Ypt31p, Ypt32p and Sec4p for secretory vesicles; Vac8p and Vac17p for vacuoles; Bim1p and Kar9p for astral microtubules; She2p and She3p for cortical endoplasmic reticulum and mRNA; Mmr1p for mitochondria; and Inp2p for peroxisomes. In *Yarrowia lipolytica* peroxisomes are trafficked through direct interaction between Pex3p and myosin V. (B) A tree illustrating the relative evolutionary relationships of lineages with genome sequences available in the fungi and metazoans with additional taxa including Choanozoa and Filasterea from the base of the Opisthokonta supergroup (<http://www.ncbi.nlm.nih.gov/taxonomy/> (James et al. 2006)). (C) Results from the comparative genomic survey. Each column, labeled at the top, represents a protein family that has a characterized role in organelle inheritance in *S. cerevisiae* or *Y. lipolytica* (peroxisomes only). Individual species from the survey are color-coded and grouped according to established taxonomic classification. A black circle indicates the presence of a protein as verified by BLAST and Hidden Markov Model searches, whereas a gray circle indicates the presence of a protein as verified by reciprocal BLAST using more closely related family members for which functional data are lacking. Multiple circles under a protein column indicate multiple putative orthologs for that protein in the indicated species. The red box highlights all organisms that have a complete set of organelle inheritance proteins.





focused within this ‘opisthokont’ supergroup, which, although it is in some ways limiting, makes our understanding of the interrelationships between the major opisthokont lineages relatively robust (Figure 5-1B). In addition, most functional studies characterizing organelle inheritance have been conducted in model organisms that are overwhelmingly found in this supergroup (Weisman, 2006). We have therefore performed a comparative genomic and molecular phylogenetic analysis of the machinery responsible for organelle inheritance.

5.2 A comparative genomic survey of the organelle inheritance machinery in budding yeast

To understand the extent of conservation of the organelle inheritance machinery functioning in budding yeast, we surveyed 41 complete, or nearly complete, databases from publicly available genome sequencing projects to identify putative proteins homologous to the machinery involved in vectorial transport and inheritance in *S. cerevisiae* (Figure 5-1 and Table 2-15 in the Materials and Methods). This list of organisms spans the diversity of the fungal and metazoan lineages and samples major branch points in the opisthokont supergroup (Figure 5-1B).

The repertoire of factors that enable organelle inheritance in *S. cerevisiae* appears to be restricted to a group of budding yeasts closely related to *S. cerevisiae* (Figure 5-1C). Of the 41 genomes sampled, only four contained a complete set of the proteins functionally characterized as having a role in organelle inheritance in *S. cerevisiae*. These four organisms have previously been shown to represent a subgroup within the *Saccharomycetaceae* family and are here referred to as the “SACK” (*S. cerevisiae*, *Ashbya gossypii*, *Candida glabrata*, *Kluyveromyces lactis*) clade (James et al., 2006).

Nevertheless, an interesting pattern of conservation has emerged from our studies whereby several cargoes of myosin V couple a conserved protein found throughout the opisthokonts, with a novel protein restricted in distribution to a small taxonomic range for their transport (Figure 5-

1C). Conserved proteins include Vac8p, Bim1p and Pex3p, while a group composed of Vac17p, Kar9p, Inp2p, She3p, She2p and Mmr1p show a restricted distribution and are found only in the Ascomycota. This division appears to be delineated along functional lines, with the conserved group being composed of proteins possessing a core role essential for the identity and maintenance of their respective organelle and the restricted group being composed of adaptor proteins responsible for regulating the association of myosin V with a particular organelle or cargo (Weisman 2006; Fagarasanu et al. 2010).

An example of a pairing between a conserved biogenic protein and an evolutionarily novel adaptor is seen in the inheritance machinery for vacuoles. Vacuoles are linked to myosin V via a complex composed of Vac8p and Vac17p for their delivery to the bud (Tang et al., 2003; Wang et al., 1998). While Vac17p could be found only in organisms of the SACK clade, Vac8p homologs could be identified in every organism searched, excluding *Encephalitozoon cuniculi* and *Capsaspora owczarzaki* (Figure 5-1C). Interestingly, Vac8p has been functionally characterized only in fungal species (Fleckenstein et al., 1998; Pan and Goldfarb, 1998; Wang et al., 1998; Weisman, 2006). One explanation for high-scoring sequence alignments for Vac8p from metazoan species could be that multiple armadillo repeat domains are present in Vac8p. Indeed, the presence of armadillo repeats in other well known protein families, such as the importin- α (Herold et al., 1998) and the β -catenin (Huber et al., 1997) superfamilies, resulted in their inclusion in long lists of high-scoring hits in our comparative genomic analysis. Notwithstanding this, Vac8p and its putative orthologs consistently recognized a pair of uncharacterized, armadillo-repeat proteins in human with several orders of magnitude improvement in E-value scores over those for β -catenin and importin- α homologs. For example, using the putative Vac8p from *Y. lipolytica* as query for a BLAST search in *Homo sapiens* returned armadillo repeat-containing protein 3 with an e-value of $2e-15$, whereas an importin- α ortholog returned an e-value of $2e-12$, and β -catenin, $4e-09$. We defined a Vac8p

homolog as a protein sequence that would return both the *S. cerevisiae* homolog and its putative human counterpart. Therefore, although functional verification is required, our analysis may have identified putative Vac8p homologs in metazoans.

Delivery of the plus ends of astral microtubules to the daughter cell for alignment of the mitotic spindle also relies on the interaction of a paired complex made up of Kar9p and Bim1p (Beach et al., 2000; Yin et al., 2000). Bim1p is the yeast homolog of end binding 1 (EB1) protein and is responsible for the stability and polymerization of the plus ends of microtubules (Schwartz et al., 1997). In our study, Bim1p was the most widely distributed and retained protein across organisms, being found in all organisms surveyed, including *E. cuniculi*, a parasite from the basal Microsporidian lineage with a reduced and compact genome (Katinka et al., 2001). Curiously, Kar9p was also the most conserved adaptor protein surveyed and was found in members of both the Saccharomycotina and Pezizomycotina (Figure 5-1C). It is interesting to note that this list of Kar9p-containing organisms overlaps with those fungi that employ a form of closed mitosis and for which proper alignment of the mitotic spindle is essential for accurate nuclear and genomic segregation (De Souza and Osmani, 2007; Stajich et al., 2009).

Functional information regarding the role of myosin V-based inheritance factors in the transport of mitochondria and the cortical endoplasmic reticulum currently lags behind that of other organelles. Factors implicated as adaptors for these organelles include Mmr1p for mitochondria (Itoh et al., 2004) and a complex composed of She3p and She2p for the cortical endoplasmic reticulum (Estrada et al., 2003). The She3p/She2p complex has been better characterized as an adaptor for the myosin V-based transport of mRNA complexes (Böhl et al., 2000; Heuck et al., 2010; Münchow et al., 1999). We found each of these proteins to be of limited distribution and restricted to the Saccharomycotina, with She2p and Mmr1p being found only in the SACK clade of the *Saccharomycetaceae* (Figure 5-1C).

The final set of proteins examined were those responsible for peroxisome inheritance. It has been shown that myosin V-based transport of peroxisomes in *S. cerevisiae* requires an adaptor protein, Inp2p (Fagarasanu et al., 2006b; 2009). Similar to the pattern of conservation noted for Vac17p, She2p and Mmr1p, Inp2p was restricted to the SACK clade (Figure 5-1C). We previously showed in the basal budding yeast *Yarrowia lipolytica*, which lacks Inp2p, that peroxisome inheritance requires the peroxisome factors Pex3p and Pex3Bp, involved in both de novo peroxisome formation from the ER, import of PMPs and delivery of peroxisomes to the daughter cell during division (Chang et al., 2009). Our comparative genomic analysis confirmed previous observations that Pex3p is a highly conserved protein (Schluter, 2006), here extending the depth of sampling within the opisthokonts and confirming its presence in apusomonads (Figure 5-1C). However, Pex3p orthologs also exhibit lower sequence similarity than their conserved counterparts, as judged by E-values, and appear to be missing from several lineages, including members of the taphrinomycetes, choanoflagellates and the pufferfish, *Fugu rubripes* (Figure 5-1C). In those cases in which no obvious homologous candidate for Pex3p presented itself, we tried reciprocal searches using putative homologs identified in more closely related species. This approach was necessary to identify the candidate Pex3p ortholog in *C. elegans*, which failed to retrieve *S. cerevisiae* Pex3p with statistical significance but did retrieve human Pex3p. Furthermore, the lack of a Pex3p ortholog in *F. rubripes* was also shown to be genome/species-specific, as we did find Pex3p orthologs in *Danio rerio*, another fish species (Figure 5-1C; 5-2).

5.3 Pex3 proteins in the Saccharomycotina share common ancestry with the myosin V adaptor Pex3Bp

While Pex3p retains a peroxisome biogenic role in *Y. lipolytica*, Pex3Bp appears to have a preferred role in peroxisome inheritance (Chang et al., 2009). To assess the relevance of Pex3p in the *S. cerevisiae* model of organelle inheritance, we determined the relationship of the two Y.

Figure 5-2. Phylogeny of Pex3 proteins found in opisthokonts. (A) In this phylogenetic analysis as well as in Figure 5-3, and Figure 5-4, the best Bayesian topology is shown with the root selected between the base of fungi and metazoans according to established opisthokont phylogeny. Node support values are given in the order of Bayesian posterior probabilities, PHYML bootstrap percentages and RaxML bootstrap percentages and are coded in the legend according to statistical strength. Highlighted is the resolved branching order of the *Y. lipolytica* paralogs.

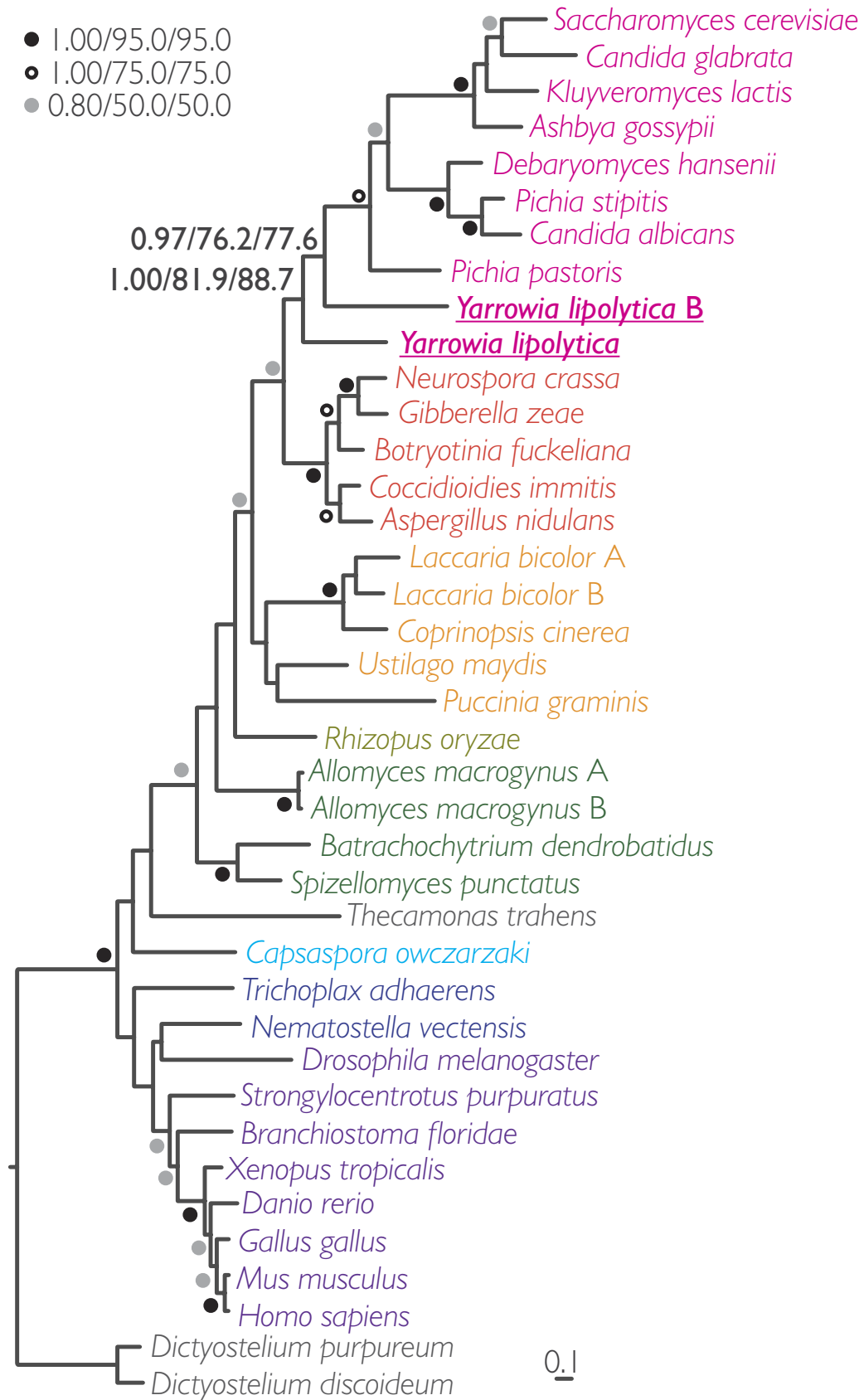
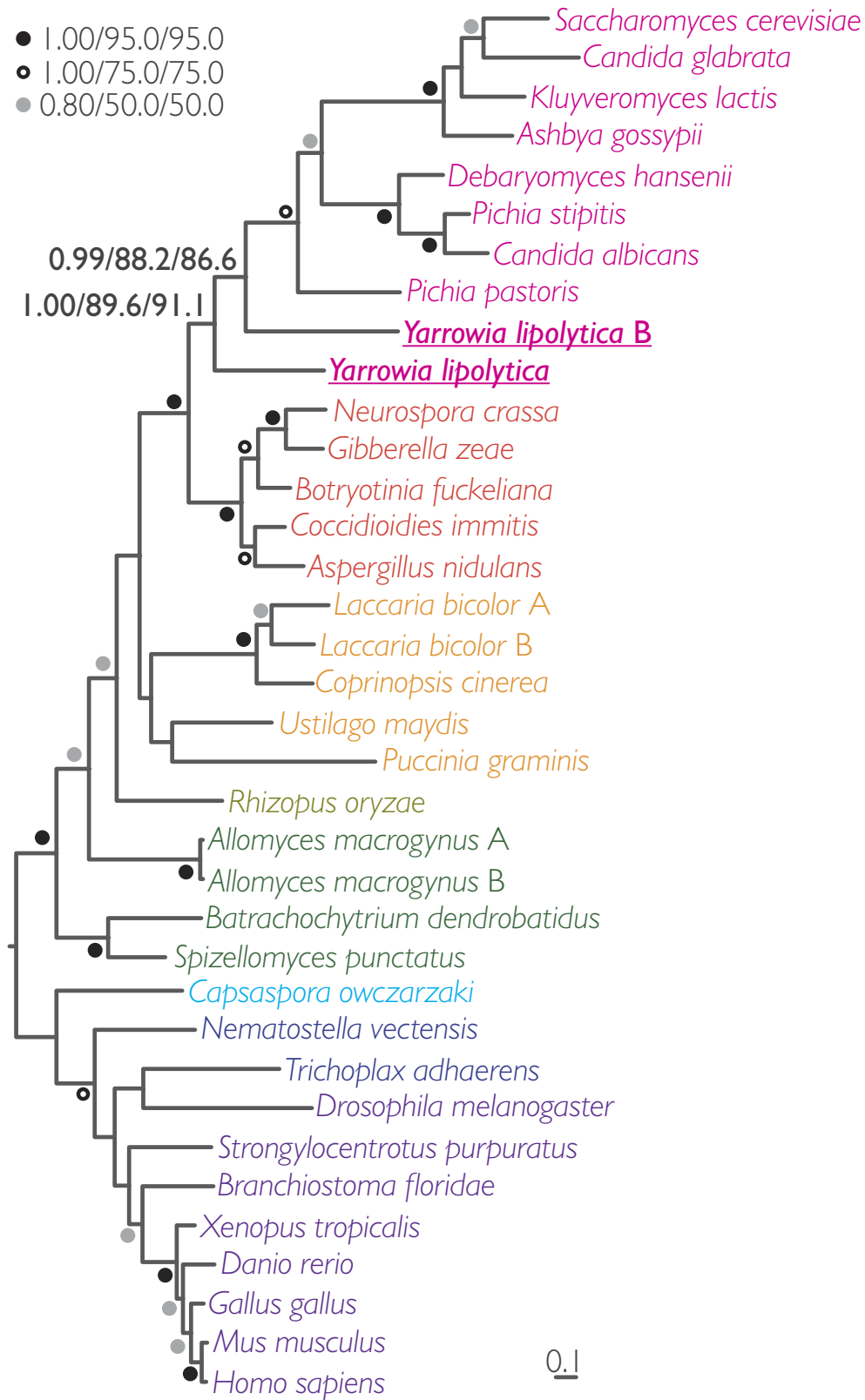


Figure 5-3. Phylogeny of Pex3 proteins found in opisthokonts. (A) This phylogenetic analysis identical to Figure 5-2, but with outgroup removed. Topology and node values as in Figure 5-2. Highlighted is the resolved branching order of the *Y. lipolytica* paralogs.

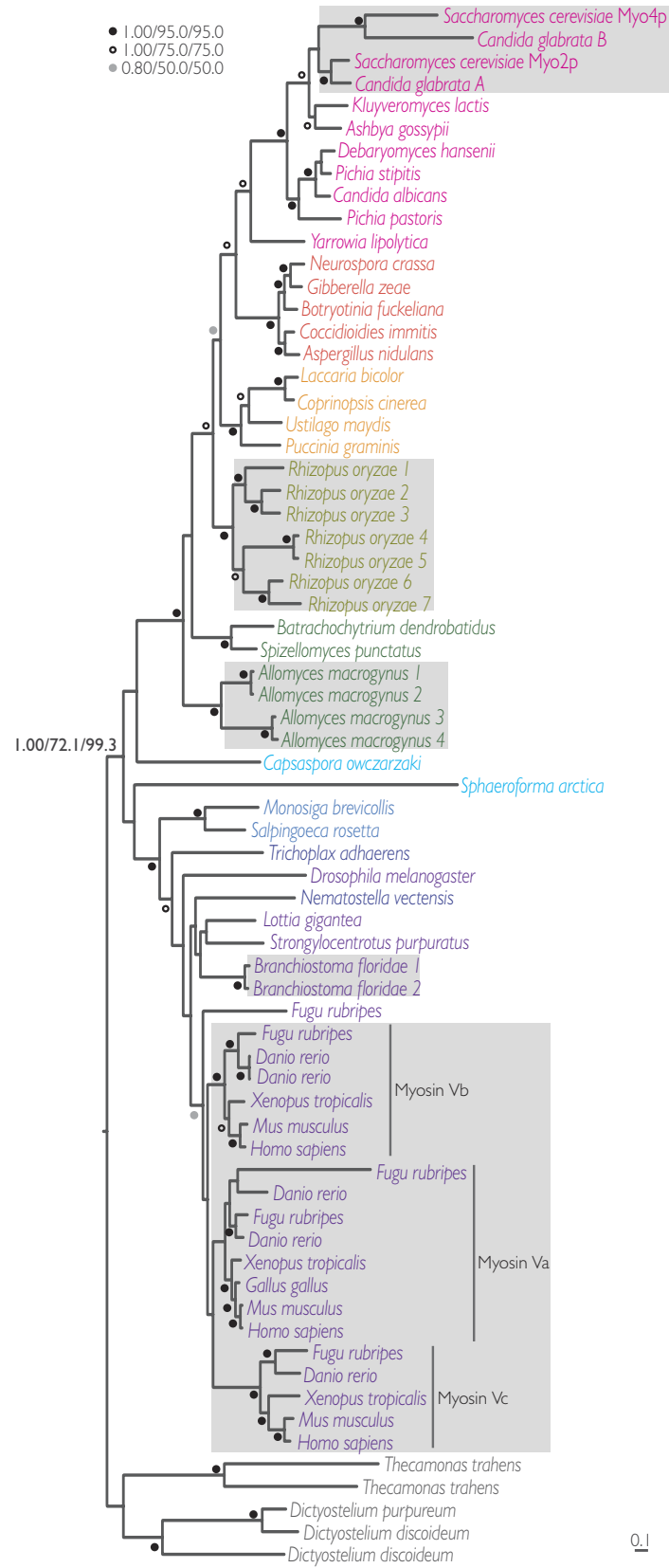


lipolytica Pex3p paralogs, Pex3p and Pex3Bp, to the single versions of Pex3p in the *Saccharomycetaceae*, as well as to Pex3p homologs in the remaining opisthokonts. Pex3p and Pex3Bp in *Y. lipolytica* were paraphyletic with Pex3p orthologs in the *Saccharomycetaceae*, suggesting a common shared ancestor between the Pex3p orthologs from the *Saccharomycetaceae* and Pex3Bp, as opposed to an organism-specific duplication in *Y. lipolytica* followed by a co-option of both proteins for myosin V-based transport (Figure 5-2; 5-3). Our findings support a role for Pex3p in myosin V-based vectorial transfer that predates the appearance of Inp2p and justifies that functional data in *Y. lipolytica* can be extrapolated to Pex3 proteins in the *Saccharomycetaceae*. The involvement in organelle inheritance of a conserved protein that predates the appearance of an adaptor is supported by independent observations that Vac8p has a role in vacuole inheritance in *Candida albicans* and *Pichia pastoris* despite the apparent lack of a Vac17p ortholog in these organisms (Barelle et al., 2006) (Figure 5-1C).

5.4 Evolution and conservation of class V myosins in opisthokonts

We next assessed the distribution of class V myosins in the opisthokonts. We found class V myosins in most of the lineages sampled (Figure 5-1C). This conservation was not unexpected, as class V myosins were previously shown to arise from one of three ancestral myosin motor families most likely present in the LECA (Richards and Cavalier-Smith, 2005). However, the presence of multiple putative myosin V homologs in chordates on the metazoan side, and in the Taphrinomycetes, Saccharomycetes and the basal Zygomycete and Chytridiomycete lineages on the fungal side, raised the possibility of deep paralogy and gene loss of myosin V proteins, which would bring into question the validity of functional comparisons between different opisthokont model systems. Our phylogenetic analysis of myosin V supports the conclusion that expansions within this protein family are lineage-specific in opisthokonts (Figure 5-4). For example, the duplication event that led to the myosin V split in *S. cerevisiae* to produce

Figure 5-4. Phylogeny of class V myosins found in opisthokonts. (A) Topology and node values as in Figure 2. Lineage-specific expansions of the myosin V family are enclosed in gray boxes.



Myo2p and Myo4p was probably due to a whole genome duplication event in *S. cerevisiae*'s recent past (Scannell et al., 2006). Therefore, our data are consistent with a single myosin V giving rise to all current myosin Vs in the opisthokonts.

With the monophyly of myosin V established, we next looked at the conservation of adaptor binding sites on the surface of the myosin V tail (Fagarasanu et al., 2010; Heuck et al., 2010; Pashkova et al., 2006). Interestingly, the degree of conservation of the adaptors correlated with conservation of their binding sites on the myosin V tail. The binding regions for vacuoles and mitochondria are less conserved than the binding regions for secretory vesicles and peroxisomes (Figure 5-5). In particular, an asparagine at position 1307, a critical residue in the binding region for mitochondria and vacuoles (Pashkova et al., 2006), is not conserved and is present as a histidine in *Y. lipolytica* and other compared organisms (Figure 5-5). Additionally, those organisms with conserved binding regions for vacuoles and mitochondria contain an insertion of eight amino acids that is not found in those organisms that lack the conserved binding regions.

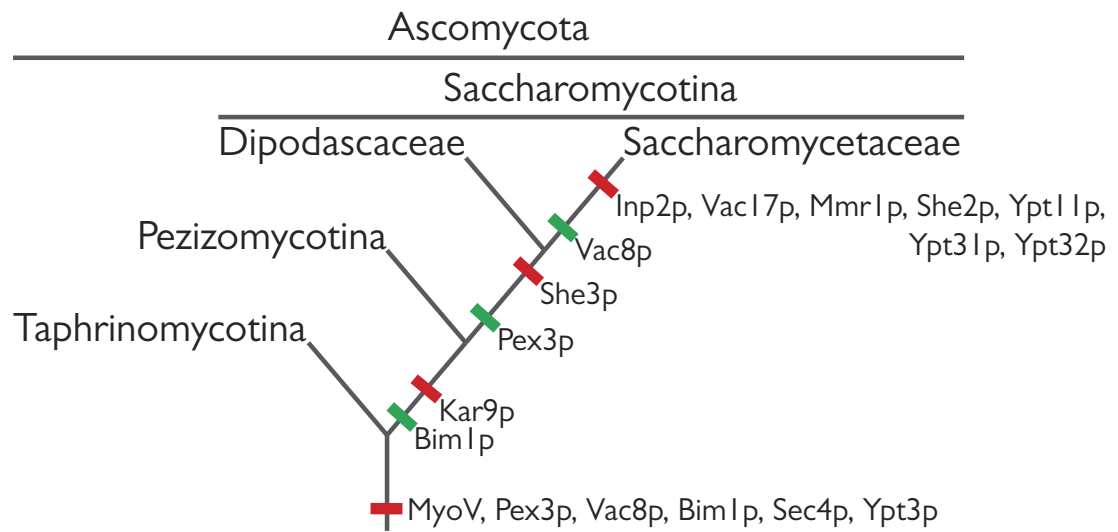
5.5 Recent emergence and lineage-specific novelty is a common feature of myosin V adaptors.

Our model of a conserved factor pairing with a novel adaptor for myosin V transport and specificity has been derived thus far from observations in members of the Saccharomycotina and Pezizomycotina. In these fungi, the emergence of factors for organelle transport and inheritance in *S. cerevisiae* follows a pattern of co-option of conserved factors followed by the appearance of adaptors for myosin V (Figure 5-6). If this model holds true for the opisthokonts in general, one would predict the presence of lineage-specific adaptors paired with conserved biogenic factors in metazoans. To test this hypothesis, we turned to another functionally characterized adaptor molecule in mammals, melanophilin, which targets myosin V to melanosomes (Provance et al., 2002). If the emergence of adaptor proteins is a general feature of myosin V adaptors, then we

Figure 5-5. Conservation, or the lack thereof, of receptor binding sites on class V myosins (A) A surface representation of the globular tail domain of myosin V is depicted with functionally characterized binding sites for vacuoles and mitochondria pseudocolored red and the binding sites for secretory vesicles and peroxisomes pseudocolored in shades of green (adapted from Pashkova et al, 2006; Fagarasanu et al, 2010). (B) Sequence alignment of myosin V homologs from Ascomycota. Amino acid sequences corresponding to the binding sites for organelle receptors in myosin V were aligned using the program MUSCLE. Identical residues (colored black and labeled with a colon) and similar residues (colored dark gray and labeled with a period) are indicated in the figure. Residues with poor conservation are light gray. Similarity rules: G = A = S; A = V; V = I = L = M; I = L = M = F = Y = W; K = R = H; D = E = Q = N; and S = T = Q = N. Dashes represent gaps. Organelle binding sites on the surface of the Myo2p globular tail domain of *Saccharomyces cerevisiae* (shown at left) are colored red in the alignments. The asparagine at residue 1307 that is not conserved but critical for mitochondrial and vacuolar trafficking by Myo2p in *S. cerevisiae* is marked with an arrow. Residues marked with an asterisk are surface residues that have been published as experimentally tested for the ability to bind to organelle receptors.

.....* * * * *
Candida glabrata (XP_446637) NLNVANHLVIRISVDFETGILIEKLNLTLLYECEBLKSLNCRNSTRQTSMSKLQLQLSISSVEELRVVQCYCFALNLTQTHALLAQK-ASSDEKMPYIVYVKRVQSWA
Saccharomyces cerevisiae (NP_009373) NVMLFNDLITKCPALNMYGEVONRIEIVSWFEPR-IEDVRNLTQIQAVKLTQLKISINLEFIDFLDWFYALPAQIQTAQLLYKPKANGKAGPGLNLTNLYNLAIV
Candida glabrata (XP_446603) DALCFNDLMRRNPLSWKRGQLQYNNVTRIEEWCKSHGVPDGTQCLHLQITSLKQLVKRYISIEDILIRGICVSLPAQLKQLITQOYVA-DYESPQBEILNVVADIV
Saccharomyces cerevisiae (NP_014971) DALCFNMLMRNPLSWKRGQLQYNNVTRIEEWCKHGLDGTGECQLHLQITAKLQVKRYITVEDILIRGICVSLPAQLKQLISQOYVA-DYESPQBEILNVVADIV
Kluyveromyces fragilis (XP_451171) DALCFNDLILRNPLSWKRGQLQYNNVTRIEEWCKSHHSEVSVCLHLQITAKLQKRRIVADIDICWNLCLPQIKLQKITQOYVA-DYEEPIAPLQVVAEKV
Asbya gossypii (NP_984450) DALCFNDMLMRNPLSWKRGQLQYNNVTRIEEWCKVHHIPGSGDCEHLMQASKLQKLNKANNDINIEWICVSLPAQIKQLISQOYVA-DYVEPQBEILSVFADRV
Candida albicans (XP_7222191) DALCFNDLMRRNPLSWKRGQLQYNNVTRIEEWCKHBIQEGSGYNLHLQAKLQKRNKTPDDIIEITCYALPQIKQLISQOYVA-DYETPIAPNVQAVADK
Debaryomyces hansenii (XP_458708) DALCFNDMLMRNPLSWKRGQLQYNNVTRIEEWCKHBIQEGSAYNHLQAKLQKRNKTPDDIIEITCYALPQIKQLISQOYVA-DYETPIAPNVQAVADK
Pichia stipitis (XP_001387193) DALCFNDLMRRNPLSWKRGQLQYNNVTRIEEWCKSHDIEGSYNLHLQAKLQKRNKTPDDIIEITCYALPQIKQLISQOYVA-DYETPIAPNVQAVADK
Pichia pastoris (XP_002490823) DALCFNDLMRRNPLSWKRGQLQYNNVTRIEEWCKSHDIEGKDSLTHLMHVAHAKLQKRNKTPVDIIEFTICVLPQIKQLISQOYVA-DYETPLAPGVSAVERV
Yarrowia lipolytica (XP_503362) GVTAFNDLMRRNPLSWKRGQLQYNNITRIEAWCKSHDIAVGVRKLEHLMQASKLQKLSLTEDIIEYDICWILPSQIHRHLQGYLSA-DYEAPISSEIMNTISEKV
Aspergillus nidulans (XP_682131) GVTAFNDLMRRNPLSWKRGQLQYNNITRIEAWCKSHMPEGTQLEHLMQATKLQKKNATIDIEITQICWNLSPQIKQLNQLQYVA-DYEQPENGINEIMKAVSRV
Coccidioides immitis (XP_001242465) GVTAFNDLMRRNPLSWKRGQLQYNNITRIEAWCKSHMPEGTQLEHLMQATKLQKKNATIDIEITQICWNLSPQIKQLNQLQYVA-DYEQPENGINEIMKAVSRV
Botrytis fuckeliana (XP_001555378) GVTAFNDLMRRNPLSWKRGQLQYNNITRIEAWCKSHMPEGTQLEHLMQATKLQKKNATIDIEITQICWNLSPQIKQLNQLQYVA-DYEQPENGINEIMKAVSRV
Gibberella zeae (XP_387645) GVTAFNDLMRRNPLSWKRGQLQYNNITRIEAWCKSHMPEGTQLEHLMQATKLQKKNATIDIEITQICWNLSPQIKQLNQLQYVA-DYEQPENGINEIMKAVSRV
Neurospora crassa (XP_001555378) GVTAFNDLMRRNPLSWKRGQLQYNNITRIEAWCKSHMPEGTQLEHLM-.....-V-S-.....

Figure 5-6. Evolutionary history for the emergence of the organelle inheritance machinery in ascomycete fungi. A red bar indicates the proposed appearance and co-option of the protein for organelle transport and inheritance, while a green bar indicates co-option at the earliest node supported by functional studies.



would expect a limited distribution for melanophilin. Comparative genomic analysis confirmed that melanophilin was found only in chordates, and we therefore can conclude that the adoption of novel myosin V adaptor molecules is a mechanism that spans the breadth of the opisthokonts (Figure 5-1C).

5.6 Discussion

Our molecular evolutionary analysis has revealed limitations in the general applicability of the model of organelle inheritance resulting from investigations in *S. cerevisiae*; however, it has also uncovered a pattern whereby conserved factors involved in organelle replication and inheritance are paired with adaptor proteins to form complexes essential for cargo interaction with a myosin V motor. This pattern appears to be conserved from yeasts to human and holds true for vacuoles (Vac8p/Vac17p) and astral microtubules (Bim1p/Kar9p/melanophilin), for which functional data have elucidated this arrangement in both yeasts and mammals (Weisman, 2006). Here, our phylogenetic analysis suggests this pattern also holds true for peroxisomes, as both Pex3p and Pex3Bp were shown to be paraphyletic with Pex3 proteins in the *Saccharomycetaceae*. This suggests that selective pressures exist to ensure the involvement of a key protein required for organelle identity in the transport of that organelle. We propose that this involvement is necessary for maintaining organelle specificity in myosin V-based transport. In the case of mitochondria, cortical endoplasmic reticulum and mRNA complexes, our model predicts an unappreciated role for a conserved factor in myosin V transport and specificity. Recently, She3p and She2p have been shown to interact with poly-A binding protein, which is an evolutionarily conserved protein that is critical for mRNA translation and could aid in providing specificity for mRNA transport (Chung and Takizawa, 2010). We therefore predict that the mitochondrial myosin V receptor, Mmr1p, also works in concert with an as yet unknown conserved and essential mitochondrial protein(s) that is also involved in the biogenesis and maintenance of the organelle. Similarly, the role of She3p and

She2p in the inheritance of cortical endoplasmic reticulum is also predicted to be mediated through, and by interaction with, a protein(s) involved in maintaining the cortical endoplasmic reticulum.

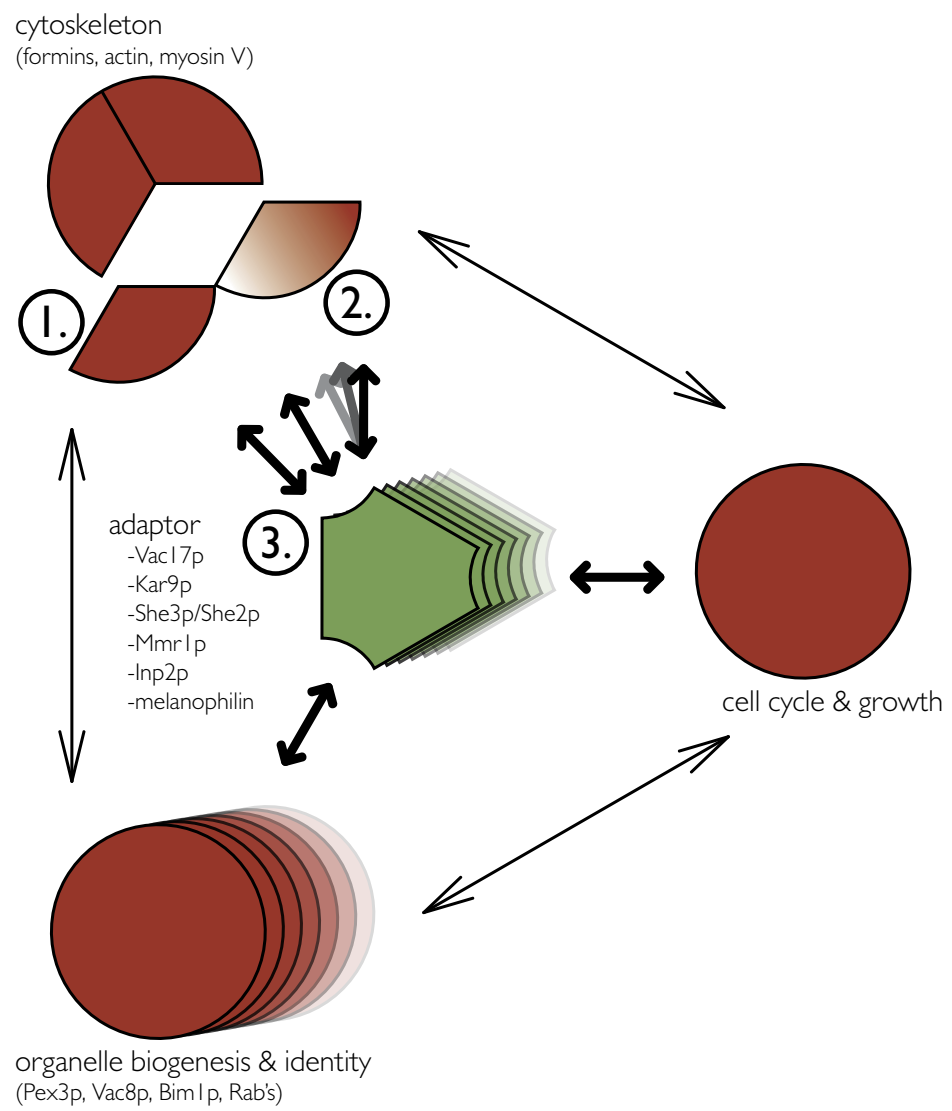
This pattern of pairing a biogenic factor with an adaptor protein for specific organelle transport is mirrored by the evolution of Rab proteins (Dacks et al., 2008; Pereira-Leal, 2008). In both yeasts and mammals, Rab proteins have been functionally characterized as imparting identity to various components of the secretory and endocytic pathways. The conserved Rab pair Ypt31p/Ypt32p in *S. cerevisiae* has been shown to function as a molecular adaptor for Myo2p in the transport of secretory vesicles (Lipatova et al., 2008). It is interesting to note that the pattern of gene duplication and asymmetric gene loss seen in the fungal Ypt3 protein family (Pereira-Leal, 2008) is reminiscent of our findings in the case for Pex3 proteins in the Saccharomycotina (Figures 5-1C and 5-2). Similarly, Sec4p, another conserved Rab, also functions as a Myo2p adaptor just before secretory vesicles are delivered to the exocyst complex for fusion with the plasma membrane of the bud (Santiago-Tirado et al., 2011). Interestingly, Ypt11p, a novel Rab specific to the *Saccharomycetaceae*, was shown to function in the transport of late Golgi elements (Arai et al., 2008; Rossanese et al., 2001). Ypt11p also associates with Ret2p, the delta subunit of coatamer, suggesting that Rabs can be viewed as either conserved identity factors or adaptors depending on the circumstance.

One way of conceptualizing cellular function is to view cellular systems as modular. A module, as defined by Hartwell and colleagues, is composed of molecules of different type whose coordinated actions evoke a discrete response (Hartwell et al., 1999). The machinery involved in organelle inheritance brings together three disparate modules of cellular machinery, each crucial for cell survival and under its own selective constraints: organelle biogenesis and identity, the cytoskeleton, and the cell cycle (Figure 5-7). These modules are presumably ancient, emerging before the appearance of the LECA (Dacks and Field, 2007; Richards and Cavalier-Smith, 2005;

Schluter et al., 2006; Wickstead et al., 2010), and because of their essential functions would exhibit resistance to perturbation. In the case of myosin V-based organelle transport and inheritance, where one cargo competes with other cargoes for access to a single motor, the question arises as to how novelty and adaptability are generated in such a complex and constrained system. In our model, the task of fulfilling the requirements of organelle inheritance is achieved via three distinct evolutionary processes (Figure 5-7).

One way of introducing novelty and adaptability to a system of constrained modules is to divide labor through paralogy, an established evolutionary mechanism (Dacks et al., 2009). Our results demonstrate that myosin V underwent at least five independent and lineage-specific gene duplications in the opisthokonts (Figure 5-4). In the case of *S. cerevisiae*, the emergence of Myo2p and Myo4p from a whole genome duplication event (Byrne and Wolfe, 2005; Scannell et al., 2006) resulted in a division of labor between the two myosins. This division of labor is unequal, with Myo2p transporting secretory vesicles, late Golgi elements, the vacuole, astral microtubules, mitochondria and peroxisomes, and Myo4p transporting only cortical endoplasmic reticulum and mRNA complexes (Fagarasanu et al., 2010). Interestingly, the She3p binding site on Myo4p was recently shown to overlap the binding site for secretory vesicles and peroxisomes on Myo2p (Heuck et al., 2010). Therefore, competition for the same binding site may account for retention of both myosin V motors in *S. cerevisiae* through a division of the cargoes for which each motor is responsible. Paralogy may also address the issue of organelle specificity. It is becoming apparent that a cascade of Rab-based vesicle maturation in the secretory pathway of *S. cerevisiae* is correlated with myosin V-based transport to the bud (Santiago-Tirado et al., 2011). Ypt11p, Ypt31p/Ypt32p and Sec4p each localize and provide identity to late Golgi elements, the *trans*-Golgi network, and secretory vesicles, respectively. All these Rabs also bind directly to Myo2p and assist in the transport of secretory components to the bud. Furthermore, paralogy can also deal with factor specificity, as can be seen in the case of Pex3p and Pex3Bp in *Y. lipolytica*, for which

Figure 5-7. A model for the evolution of myosin V-based organelle inheritance. Adaptation through paralogy (1.) and sequence divergence of binding regions on the myosin tail (2.) provide two well-characterized mechanisms for enhancing the interaction between the robust cellular modules of the cytoskeleton, organelle biogenesis and identity, and cell cycle and growth (represented by red circles). Unexpectedly, a third phenomenon, the innovation of novel cargo adaptors (3.), functionally and sometimes physically links the three conserved modules, allowing for lineage-specific adaptability in the process of organelle inheritance. The strength of interaction between these modules is reflected by the thickness of the bidirectional arrows between them, which is greatly increased by the presence of an evolutionarily novel adaptor (green shape). Depth of the different cargoes and adaptors whose transport is facilitated by myosin V and regulated by the cell cycle is depicted, as is the idea that each of the robust modules will be composed of multiple individual factors, which is seen for the cytoskeleton.



selective pressures on the necessity of having peroxisomes is greater than in other yeasts due to the lipid-rich environment in which *Y. lipolytica* is naturally found. Pex3 proteins across the diversity of eukaryotes are multifunctional proteins essential for peroxisome formation and are involved in *de novo* peroxisome formation from the endoplasmic reticulum, membrane protein targeting and organelle anchoring and retention (Ma et al., 2011).

A second mechanism in our evolutionary model is the exploration of sequence space to introduce additional binding sites for cargo on the surface of the myosin V tail. Functional characterization has revealed two distinct cargo-binding sites on the surface of the globular tail domain of Myo2p in *S. cerevisiae* (Pashkova et al., 2006). Here, we demonstrated a correlation between the conservation of those residues critical for mitochondria and vacuole binding with the emergence of vacuole- and mitochondrion-specific adaptor proteins for myosin V-based transport (Figure 5-1C and Figure 5-5). Thus, using a greater proportion of the surface of the globular tail domain may ease the constraints of specificity. However, the ability of myosin V motor complexes to carry more than one cargo at a time has yet to be demonstrated experimentally.

Our findings also suggest a third and unexpected way of providing novelty and adaptability to a system: co-option of established machinery for the novel function of organelle delivery, combined with the emergence of novel factors (Figures 5-6 and 5-7). Within the framework of the model, interaction among the relatively robust modules of cell cycle, organelle biogenesis and identity, and cytoskeleton is proposed to be facilitated by evolutionarily novel adaptors. Rather than attempt to modify robust and essential modules, it is envisaged to be advantageous for an organism to use an evolutionarily novel and recently emerged adaptor protein to bridge these robust modules and facilitate new phenotypes through these interactions (Hartwell et al., 1999). Support for this scenario comes from the observation that the different cargoes appear to use the same mechanism of attaching to myosin V despite their not having similar origins.

Overall, our model for the evolution of organelle inheritance takes into consideration the plasticity evident in the many ways cargo specificity and traffic are achieved (Akhmanova and Hammer, 2010; Fagarasanu et al., 2010). Moreover, this model may well be applicable to the specificity of cellular trafficking in general. In the secretory endomembrane system, the twin aspects of specificity of vesicle formation and specificity of vesicle fusion have been shown to be highly conserved across all eukaryotes (Dacks et al., 2009; Bock et al., 2001; Brighthouse et al., 2010). The missing link between the derivation of membranous carriers and their delivery is vesicle transport and the selection of particular cargoes by specific motors. Whereas myosin V-based transport has become essential for organelle inheritance in yeast, its role in cell polarity, maturation and recycling in the secretory and endomembrane systems is more prominent in mammalian cells (Akhmanova and Hammer, 2010; Weisman, 2006). Similar to myosin V-based transport in yeast, transport of cargo in mammalian cells also requires the pairing of conserved biogenic proteins, such as Rabs and EBI, with novel adaptors, such as melanophilin (Provance et al., 2002; Weisman, 2006). Therefore, our model of multiple specificity factors competing for the myosin V tail may be more broadly applicable to other types of myosin V-based transport.

From these observations of organelle inheritance in yeast, a larger hypothesis can be proposed (Figure 5-7). Under conditions whereby novel functions arise from interactions between several ancient, and therefore robust, cellular modules, there will be a bias for the incorporation and accretion of evolutionarily novel adaptor proteins, which we term “widgets”, that lack the exposure to negative selection pressure that is present in the components of the more ancient cellular modules. The interactions formed between modules with these widgets could arise through constructive neutral evolution (Lukes et al., 2011; Stoltzfus, 1999) or could be positively selected for because they provide a spontaneous increase in fitness to the cell.

In conclusion, the various lineages of opisthokonts have each evolved solutions to bring conserved and robust cellular modules into communication through a combination of paralogy,

mutation and emergence of novel adaptors. The lack of a conserved mechanism for myosin V-based transport might be explained by the diversity of cell division and cell asymmetry exhibited by opisthokonts. At the same time, the existence of effective and multi-approach solutions for myosin V-based transport, that fail to constrain evolution and adaptation, could well have facilitated the emergence of the body plan and tissue differentiation diversity observed in the opisthokonts. These diverse strategies illustrate that the evolution of organelle inheritance may well be framed in terms of 'survival of the fittest' and not necessarily 'survival of the most elegant'.

6 A *Drosophila* model for the Zellweger spectrum of peroxisome biogenesis disorders

A version of this chapter has been published.

Mast, F. D., Li, J., Virk, M. K., Hughes, S. C., Simmonds, A. J., & Rachubinski, R. A. 2011. A *Drosophila* model for the Zellweger spectrum of peroxisome biogenesis disorders. *Dis Mod Mech.* 4:659-672. doi:10.1242/dmm.007419.

6.1 Overview

Although single-cell systems like yeast and mammalian cell culture have been invaluable for identifying the proteins and basic processes involved in peroxisome biogenesis, they cannot act *de facto* as models for the study of the role of peroxisomes in the development of multicellular organisms or in the molecular mechanisms leading to the PBDs. *Drosophila* has been shown to be both a valid and valuable model system for the study of normal and abnormal development of more complex multicellular organisms, including humans. Over seventy-five percent of known human disease genes have a recognizable match in the genome of *Drosophila* (Reiter et al., 2001), and *Drosophila* now serves as a model for more than 20 diseases, including Huntington's, Parkinson's, Alzheimer's, fragile X mental retardation, and spinocerebellar ataxia I (Bilen and Bonini, 2005; Cauchi and van den Heuvel, 2006; Raymond and Tarpey, 2006; Sánchez-Martínez et al., 2006). Surprisingly, there have been few studies of the functional roles for peroxisomes in *Drosophila* and until this study, none focused on the effects of peroxisome function on early development. The longest known role of peroxisomes in flies is in the formation of eye pigments. The *rosy* (*ry*) gene encodes the enzyme xanthine dehydrogenase (Bridges and Brehme, 1944; Glassman and Mitchell, 1959). Xanthine dehydrogenase is targeted to peroxisomes in malpighian tubule cells and fat cells (Beard and Holtzman, 1987). Recent studies have also suggested a role for peroxins in the process of spermatogenesis in adult males (Chen et al., 2010). However, no study has focused specifically on the functional roles of peroxisome biogenesis genes of *Drosophila melanogaster* (*DmelPex*) or on the defects in early fly development arising from mutation of a *DmelPex* gene and the similarity between those defects and the developmental defects observed in PBD patients mutant for the corresponding human *PEX* gene.

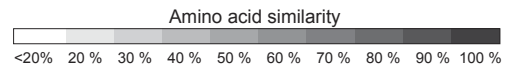
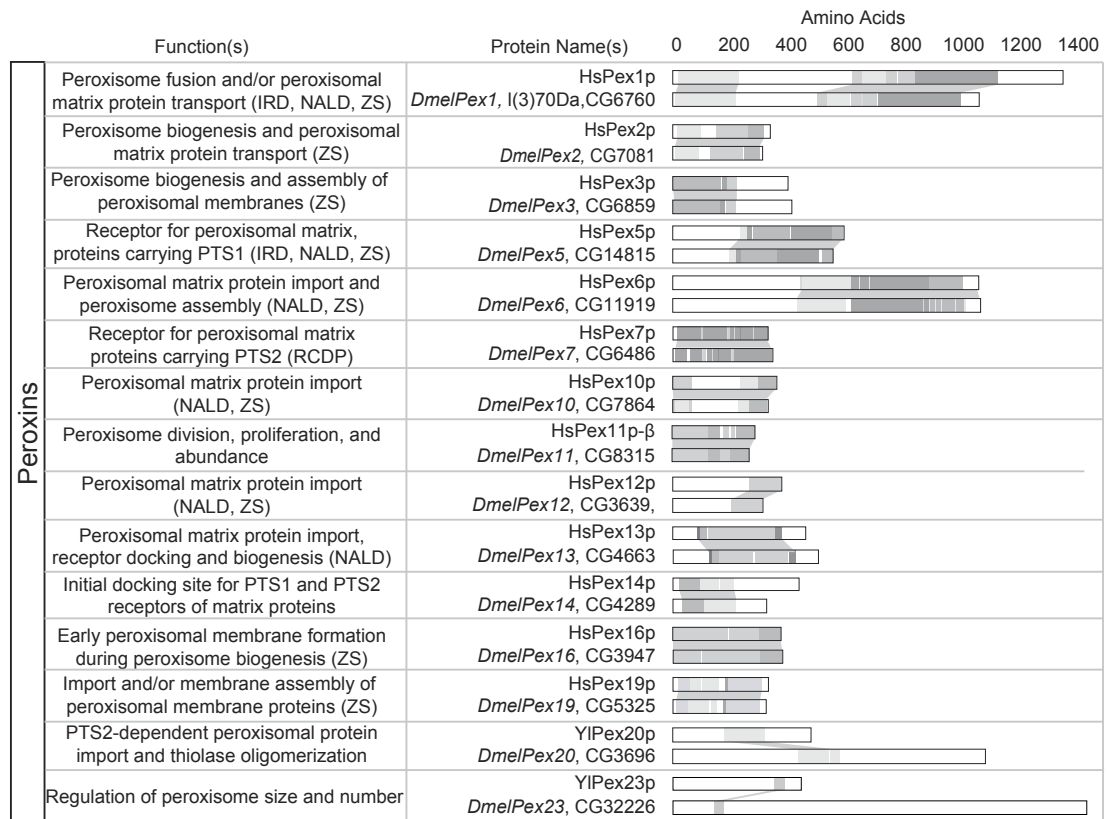
6.2 RNAi analysis in S2 cells confirms that the majority of the known genes required for peroxisome assembly are conserved in *Drosophila*

Fifteen putative *Pex* genes are predicted in the *Drosophila* genome. Thirteen genes are showed sequence similarity to known human *PEX* genes, while two genes showed sequence similarity to the *PEX20* and *PEX23* genes of the yeast *Yarrowia lipolytica* (Figure 6-1). These *DmelPex* genes correlate with genes predicted by others as *Drosophila* homologs for *PEX* genes found in other species (Adams et al., 2000; Chen et al., 2010). Twelve of these genes are homologous to known human *PEX* genes for which mutations causing PBDs have been characterized.

Mutations in *PEX* genes typically result in the mislocalization of peroxisomal matrix proteins to the cytosol and this mislocalization of matrix proteins is used along with other biochemical lab diagnostics in characterizing a PBD (Shimozawa, 2011; Shimozawa et al., 1998; Steinberg et al., 2006). We performed systematic RNAi knockdown of each gene in S2 cells constitutively expressing a chimeric reporter protein, GFP-SKL. The SKL tripeptide is the evolutionarily conserved C-terminal peroxisome targeting signal I (PTS1) consisting of serine-lysine-leucine (SKL) that targets specifically to peroxisomes to produce a characteristic punctate pattern in fluorescence microscopy (Kural et al., 2005; Petriv et al., 2002). GFP-SKL expressing S2 cells were treated with dsRNAs targeting 14 individual putative *DmelPex*s for knockdown: *DmelPex1* (CG6760), *DmelPex2* (CG7081), *DmelPex3* (CG6859), *DmelPex5* (CG14815), *DmelPex6* (CG11919), *DmelPex7* (CG6486), *DmelPex11* (CG8315), *DmelPex12* (CG3639), *DmelPex13* (CG4663), *DmelPex14* (CG4289), *DmelPex16* (CG3947), *DmelPex19* (CG5325), *DmelPex20* (CG3696) and *DmelPex23* (CG32226) (Figure 6-1). As a control for specificity of the RNAi knockdown, we performed a mock RNAi treatment (no dsRNA), as well as a RNAi knockdown of *Dredd*, which has no known role in peroxisome biogenesis or function.

Untreated GFP-SKL S2 cells exhibited a punctate pattern of fluorescence characteristic of peroxisomes (Figure 6-2) (Kural et al., 2005). Similarly, in mock-treated and *Dredd* RNAi-treated

Figure 6-1. Peroxins and their putative homologs in *Drosophila*. The putative *Drosophila* homologs of known peroxins we identified *in silico* are presented. The main function in peroxisome biogenesis of each known peroxin is given. The PBD in which a *PEX* gene has been implicated is indicated in brackets. Pairwise alignment is made between the human or yeast peroxin (upper) and the putative *Drosophila* homolog (lower) using the SIM alignment algorithm (<http://ca.expasy.org/tools/sim-prot.html>) and visualized using Jalnview (<http://pbil.univ-lyon1.fr/software/jalnview.html>). The extent of amino acid similarity between regions of two aligned proteins is given by the Heat map at bottom. Hs, *Homo sapiens*; Yl, *Yarrowia lipolytica*

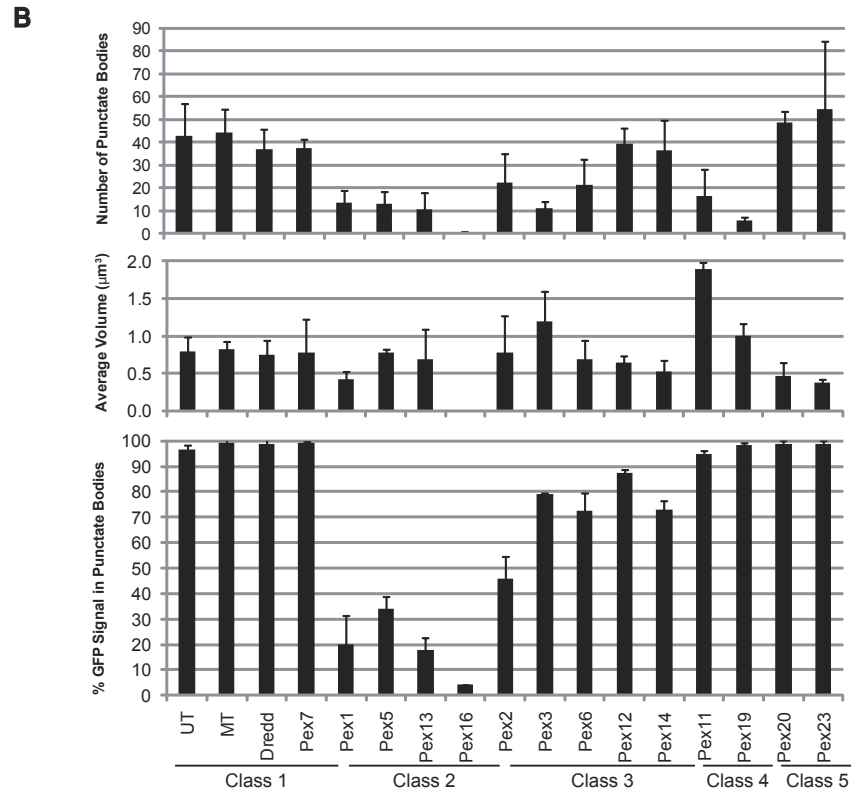
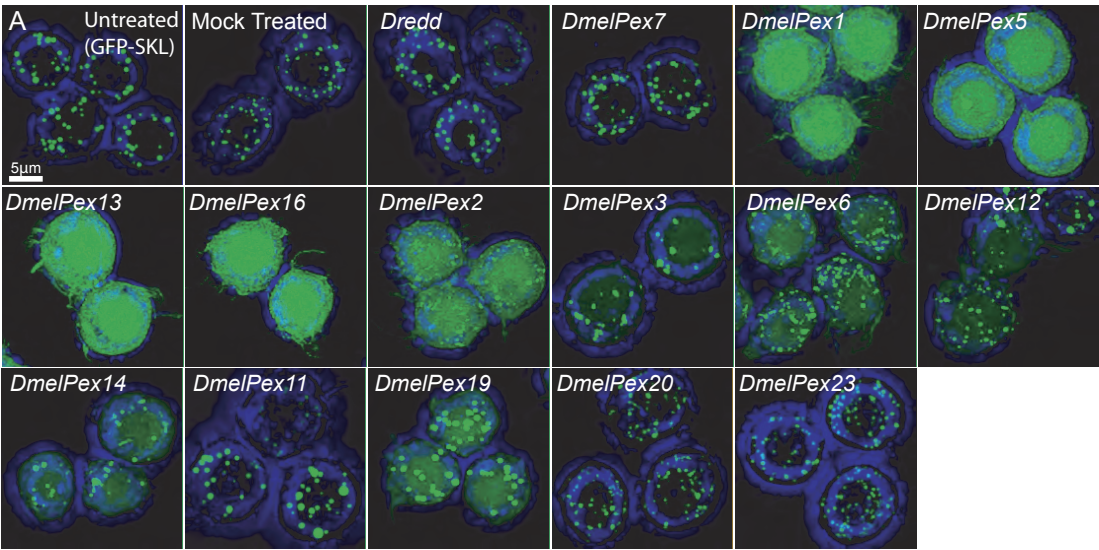


cells, the GFP-SKL signal also appeared in punctate structures consistent with peroxisome localization. The peroxisomes in control and untreated cells were spherical, of essentially uniform size, and randomly distributed throughout the cell.

In S2 cells, RNAi knockdown of many of the putative *DmelPex* genes we identified (Figure 6-2C) resulted in GFP-SKL fluorescence patterns that were significantly different from the punctate fluorescence pattern observed in untreated or control-treated cells (Figure 6-2A). We grouped these patterns into five classes (Figure 6-2B). Class 1 cells exhibit a pattern of GFP-SKL fluorescence essentially indistinguishable from that of untreated cells. Mock-treated and *Dredd* RNAi-treated cells were categorized as Class 1, as were cells treated with dsRNA targeting *DmelPex7*. This was not unexpected, as Pex7p has been shown to function in the targeting to peroxisomes of proteins containing a N-terminally localized PTS2 but not of proteins containing a C-terminally localized PTS1 (Lazarow, 2006), like the chimeric reporter GFP-SKL being expressed in these S2 cells. In Class 2 cells, most of the GFP signal was excluded from punctate bodies. Putative *DmelPex* genes in Class 2 include *DmelPex1*, *DmelPex5*, *DmelPex13* and *DmelPex16*. Class 3 cells show an appreciable amount of cytosolic GFP signal but contain fluorescent punctate bodies in numbers approaching those of untreated cells and were observed in RNAi knockdown of *DmelPex2*, *DmelPex3*, *DmelPex6*, *DmelPex12* and *DmelPex14*. Class 4 cells have a reduced number of fluorescent punctate bodies of increased size as compared to untreated cells but show no appreciable accumulation of GFP signal in the cytosol. RNAi knockdown of the *DmelPex11* and *DmelPex19* genes produced a Class 4 pattern. In Class 5 cells, the average volume of punctate bodies was less and the average number of punctate bodies per cell was greater than that of untreated cells, and the entire GFP signal was essentially localized to punctate bodies. Cells treated with dsRNA to *DmelPex20* or *DmelPex23* were categorized as Class 5.

The specificity of transcript knockdown by RNAi was verified for the case of *DmelPex1* by semi-quantitative RT-PCR (Figure 6-3A) and by immunoblotting of whole S2 cell lysates with

Figure 6-2. Peroxisomes are absent or exhibit altered morphology in S2 cells treated with dsRNA to putative *DmelPex* genes. (A) S2 cells constitutively expressing the fluorescent peroxisomal reporter protein GFP-SKL (Kural *et al.*, 2005) were treated with dsRNA to the indicated putative *DmelPex* genes, mock-treated, or treated with dsRNA targeting *Dredd*, which has no known role in peroxisome biogenesis or peroxisome function. GFP-SKL in S2 cells targets to punctae characteristic of peroxisomes. Mock-treated cells and cells treated with dsRNA targeting *Dredd* exhibited punctae like control cells. Cells treated with dsRNAs to different *DmelPexs* exhibit mislocalization of the GFP-SKL peroxisomal reporter to the cytosol and/or altered peroxisomal size and number. Cells treated with dsRNA to *DmelPex7* or *DmelPex20* exhibit punctate peroxisomes essentially like those of wild-type cells, as *PEX7* and *PEX20* affect the targeting only of peroxisomal proteins containing a PTS2 and not of those containing PTS1, such as GFP-SKL. Scale bar, 5 μ m. (B) Quantitative description of peroxisome morphologies in S2 cells treated with dsRNA to putative Pex genes. Images were scored for numbers of punctate bodies, the average volume of these punctate bodies and the intensity of fluorescent signal from these punctate bodies.



antibody to DmelPexI protein (Figure 6-3B). The levels of *DmelPexI* mRNA were reduced in GFP-SKL S2 cells by treatment with *DmelPexI* dsRNA but not by treatment with *Dredd* dsRNA or by mock-treatment (Figure 6-3A). DmelPexI protein was reduced in lysates of S2 cells treated with *DmelPexI* dsRNA but not in lysates of mock-treated S2 cells or S2 cells treated with *DmelPex7* dsRNA (Figure 6-3B). The results of our RNAi analysis in S2 cells demonstrate that loss of function in the majority (13 of 14) of putative *DmelPex* genes identified *in silico* produces abnormal peroxisome assembly phenotypes in *Drosophila* S2 cells.

6.3 Mutation of *DmelPexI* leads to tissue-specific defects in developing embryos

PEX1 genes in organisms from yeast to human encode members of the family of AAA-ATPases and are essential for peroxisome assembly. Mutation of human *PEX1* results in ZS and is the most common cause of the PBDs, accounting for 70% or more of all patients (Reuber et al., 1997; Steinberg et al., 2006). Because of the prevalence of the *PEX1* mutation in the PBDs, studies of *DmelPexI* mutations were a natural starting point for evaluation of a *Drosophila* model for the systemic effects of the PBDs, and more specifically, the ZS of PBDs.

To study the functional consequences of compromised peroxisome biogenesis in the early development of *Drosophila*, we performed an in-depth phenotypic characterization of how loss-of-function mutations in the *DmelPexI* gene affect basic tissue patterning, survival and the functional response of the organism in terms of altered gene expression.

Both P-element and X-ray-induced mutations in *DmelPexI*, *l(3)70Da^{s4868}* and *l(3)70Da^l*, were characterized in terms of defects during early development. These alleles are lethal when homozygous, in trans, or when heterozygous to a large deletion, *Df(3L)fz-GS/a*, that removes the chromosomal region 70D2-70E5 that includes the *DmelPexI* locus. However, we noted that the genomic region encoding the 3'-UTR of the *DmelPexI*, *l(3)70Da* mRNA overlaps the genomic

Figure 6-3. Detection of *DmelPexI* transcripts by RT-PCR and *DmelPexI* protein by immunoblotting. (A) The specific bands corresponding to the expression levels of *DmelPexI* and the gene *Rpl32* encoding an ubiquitously expressed ribosomal protein and used as a loading control are indicated by arrows. Heterozygous *l(3)70Da* animals are indicated with the symbol, /+. The mRNA isolated from *l(3)70Da*^{S4648} homozygotes produced no *DmelPexI*-specific band, while *l(3)70Da*^l homozygous animals showed a severe reduction in this band compared to the *Rpl32* loading control. Similarly, the level of *DmelPexI* transcript was reduced in the dsRNA-treated S2 cells compared to untreated, mock-treated or S2 cells treated with a dsRNA that targets the *Dredd* gene, which is involved in the immune response. For each set of primers, specific amounts of the wild-type RT-reaction were analyzed to confirm that 2.5 µl of experimental sample yielded a product within the linear range of amplification by the subsequent PCR. (B) *DmelPexI* protein is reduced specifically in cells treated with dsRNA to the *DmelPexI* transcript. Lysates of untreated S2 cells, mock-treated S2 cells, S2 cells treated with dsRNA to *DmelPexI* mRNA and S2 cells treated with dsRNA to *DmelPex7* mRNA were separated by SDS-PAGE and subjected to immunoblotting with anti-*DmelPexI* protein antibodies. Reduced levels of *DmelPexI* protein are observed only in the lane containing lysate of S2 cells treated with dsRNA to *DmelPexI* mRNA. A protein detected nonspecifically by the antibodies to *DmelPexI* protein serves as a control for protein loading. Numbers at left represent the migrations of molecular weight standards in kDa. (C) RT-PCR confirmation of RNAi knockdown of predicted *DmelPex* genes. The specific primer pairs that recognize a predicted *DmelPex* gene are listed in Table 2-14. KD, S2 cells expressing GFP-SKL treated with dsRNA. Ctrl, mock-treated S2 cells expressing GFP-SKL.

region encoding the 5'-UTR of the adjacent gene, *breathless* (*btl*) (Adams et al., 2000; Klämbt et al., 1992). The primary phenotype associated with mutation of *btl* is defective tracheal development. No tracheal defects were observed in homozygous *l(3)70Da^{s4868}* or *l(3)70Da^l* mutants. However, to avoid the possibility of confounding phenotypes, we used only the alleles *l(3)70Da^{s4868}* and *l(3)70Da^l*, which harbor smaller mutations affecting only the 5'-region of the *DmelPexI* gene, for subsequent developmental characterizations. Finally, ubiquitous expression of a UASp-*DmelPexI* transgene via Tub-GAL4 in the early embryo allowed homozygous *l(3)70Da^{s4868}* and *l(3)70Da^l* mutants to survive past the second larval instar, confirming that the early larval lethality observed in these mutants was caused by loss of *DmelPexI*.

RT-PCR and immunoblotting confirmed specific reduction in the *DmelPexI* transcript and protein expression in homozygous mutant *l(3)70Da^{s4868}* and *l(3)70Da^l* larvae 2 days after hatching (Figure 6-3A). Heterozygous *DmelPexI^{s4868}* flies grew (Figure 6-4) and survived (Figure 6-5) like wild-type flies, and within 2 hours of hatching both wild-type and heterozygous *DmelPexI* larvae exhibited the same coordinated locomotory activity in their movement toward a food source. (Figure 6-6). This is in contrast to animals homozygous for the *l(3)70Da^{s4868}* allele, which grew much more slowly than wild-type or heterozygous flies (Figure 6-4) and died at the L1 or L2 stage (Figure 6-5). These homozygous mutant larvae were consistently much smaller than wild-type or heterozygous larvae, exhibited little or no coordinated locomotion when placed on agar plates, failed to show effective feeding and exhibited developmental delay (Figure 6-6). There is some phenotypic pleiotropy associated with the *l(3)70Da^{s4868}* and *l(3)70Da^l* alleles, and in extreme cases, homozygous mutants were unable to fully crawl out of their eggshells and died within a few hours of hatching. Overall, our results demonstrate that *DmelPexI*, like *PEXI* for humans, is essential for normal embryonic development.

Figure 6-4. *DmelPexI^{s4868}* homozygous larvae exhibit defects in growth. Each data point represents the average size in mm² of 20 randomly selected *DmelPexI^{s4868}* homozygous (green), *DmelPexI^{s4868}* heterozygous (red) and wild-type (blue) larvae. On Day 4, the mean area representing growth of *DmelPexI^{s4868}* homozygous larvae is significantly reduced, as compared to wild-type and heterozygous larvae ($P < 0.0001$). Wild-type and heterozygous larvae did not show any statistically significant difference in growth. Error bars indicate standard deviation.

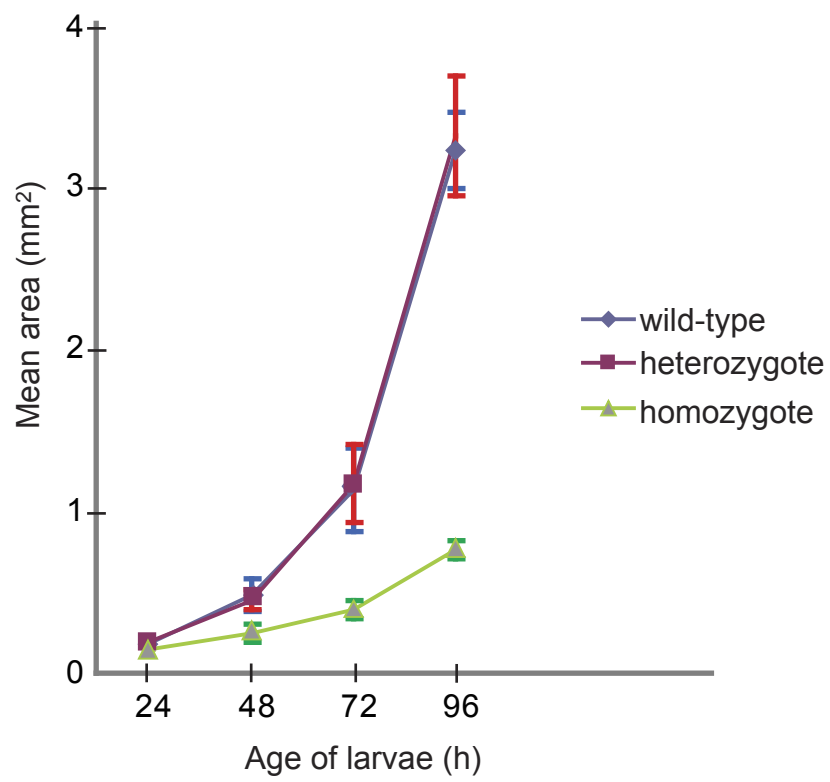


Figure 6-5. *DmelPexI*^{s4868} homozygous flies have reduced lifespan. Survival curve of *DmelPexI*^{s4868} homozygous (green), *DmelPexI*^{s4868} heterozygous (red) and wild-type (blue) flies. All *DmelPexI*^{s4868} homozygous flies died by Day 6 at pupariation. Wild-type and heterozygous larvae pupated on Day 6. Error bars indicate standard deviation.

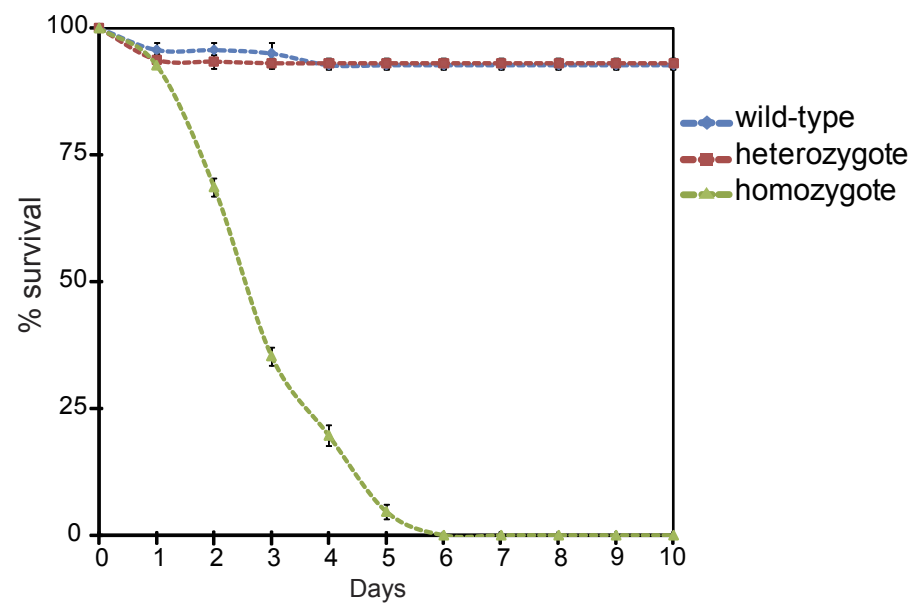
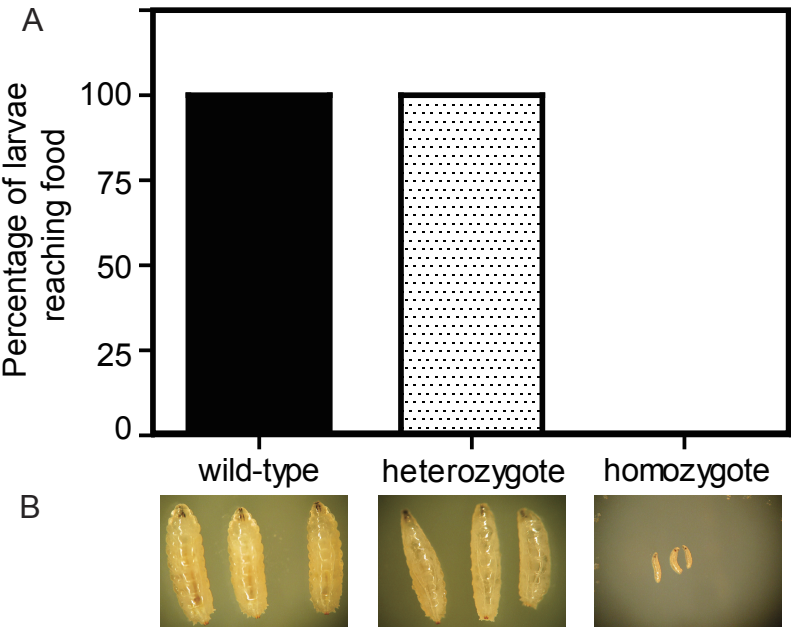


Figure 6-6. *DmelPexI*^{s4868} homozygous larvae are smaller in size and fail to show coordinated movement toward food. Images of 5-day old wild-type, *DmelPexI*^{s4868} heterozygous and *DmelPexI*^{s4868} homozygous larvae are shown. Homozygous larvae are much smaller than heterozygous or wild-type larvae. A histogram reporting the percentage of larvae that reach food in a fixed period of 20 min is presented. All wild-type and heterozygous larvae, but no homozygous larvae, were able to reach the food source in the prescribed time



6.4 Developing *DmelPexI* homozygous mutant embryos do not show obvious muscle defects

The locomotory defects observed in *DmelPexI*^{s4868} homozygous larvae (Figure 6-6) could be attributed to aberrations in either neuronal or muscle development (or both). We therefore assayed the developing musculature in *DmelPexI*^{s4868} mutant larvae to determine whether the absence of *DmelPexI* affects muscle development in terms of gross morphology. Staining with an antibody to myosin (MAC147) showed an essentially wild-type pattern of musculature in the homozygous mutant embryos, as both wild-type and homozygous mutant late (stage 15) embryos exhibited an evenly repeated pattern of longitudinal and oblique muscles (Figure 6-7).

6.5 *DmelPexI* homozygous mutants exhibit malformed central and peripheral nervous systems

Patients affected with a PBD present symptoms arising from significant defects in the CNS and peripheral nervous system (PNS), including mental retardation, seizures, muscular hypotonia and absence of deep tendon reflexes (Steinberg et al., 2006). We therefore examined the overall organization of the CNS and PNS in embryos homozygous for the *DmelPexI*^{s4868} mutant allele. Stage 15 embryos were stained with antibodies that decorate specifically the CNS and PNS and observed by immunofluorescence microscopy (Figure 6-8). Monoclonal antibody BP102 stains axons of the CNS (anti-CNS axons) and is an excellent marker for the pattern of commissures and connectives in the CNS of embryos. Wild-type embryos decorated with BP102 show a ventral nerve cord (VNC) with well-organized and well-formed anterior and posterior commissures and longitudinal connectives. In contrast, *DmelPexI*^{s4868} homozygous embryos showed malformation of the VNC, with a lack of some commissures, breaks in the longitudinal connectives and the presence of underdeveloped commissures, resulting overall in a widening of the distance between the longitudinal connectives of the VNC (Figure 6-8).

Figure 6-7. *DmelPexI*^{s4868} homozygous embryos exhibit an essentially wild-type musculature. Wild-type and *DmelPexI*^{s4868} homozygous mutant embryos (stage 15) were analyzed by immunofluorescence microscopy using monoclonal antibody MAC147 to myosin, which recognizes all muscle. Anterior is at right in all images. In lateral views, dorsal is up. Scale bar, 100 μm .

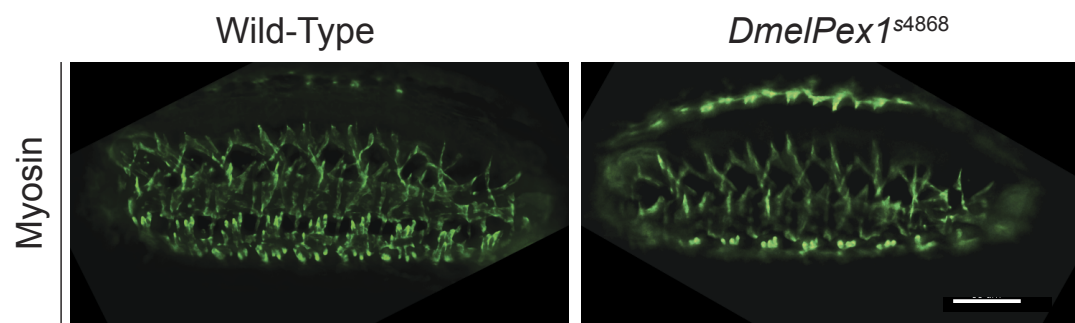
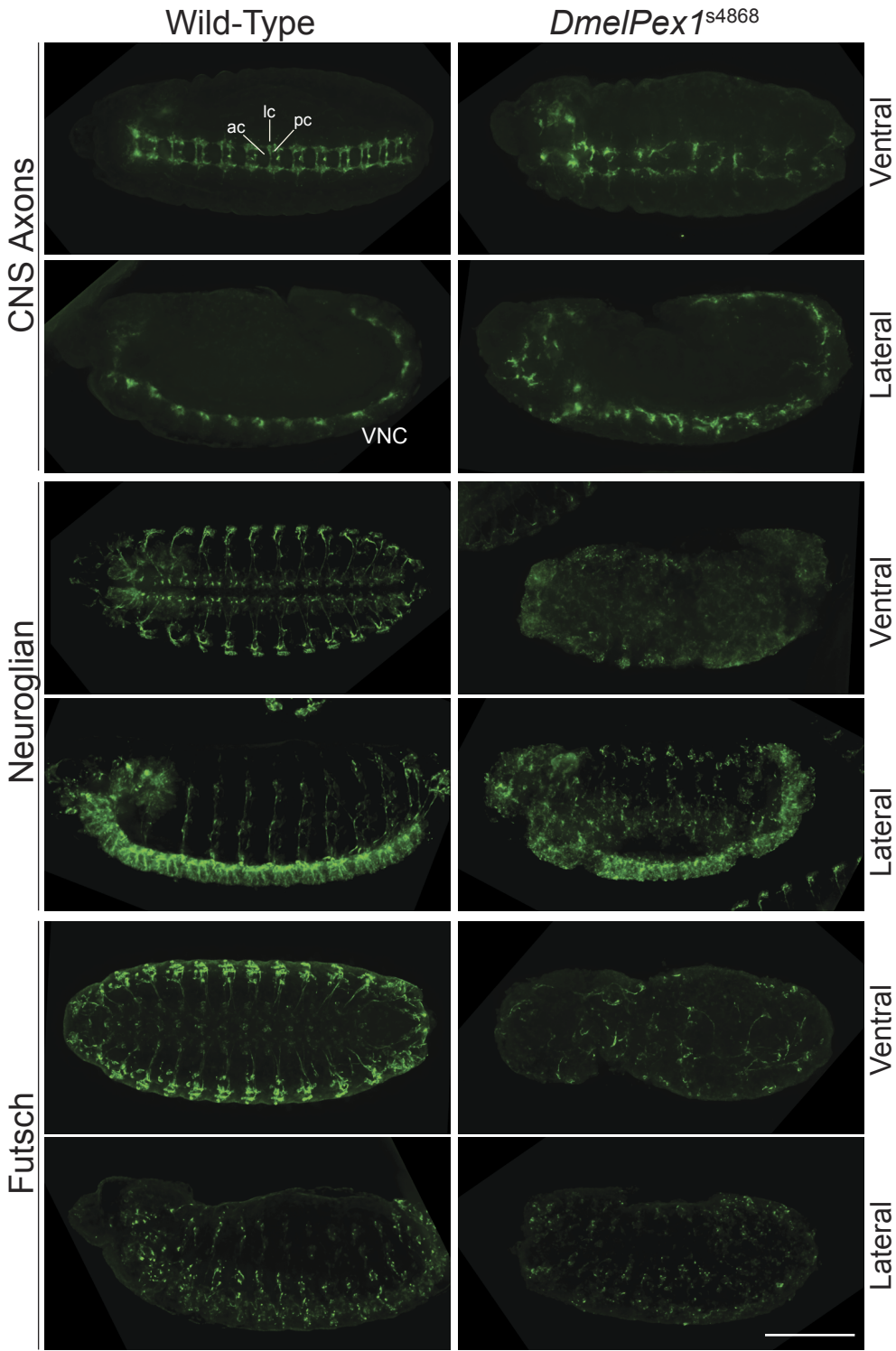


Figure 6-8. The overall pattern of CNS and PNS development is abnormal in *DmelPexI*^{s4868} homozygous embryos. Wild-type and *DmelPexI*^{s4868} homozygous embryos (stage 15) were analyzed by immunofluorescence microscopy using monoclonal antibodies BP102 (anti-CNS axons), BP104 (anti-Nrg recognizing CNS and PNS neurons) and 22C10 (anti-Futsch recognizing neuron and axon subsets of the CNS and PNS). Anterior is at right in all images. In lateral views, dorsal is up for BP102 and 22C10 and down for BP104. ac, anterior commissure; lc, longitudinal connective; pc, posterior commissure; VNC, ventral nerve cord. Scale bar, 100 μ m



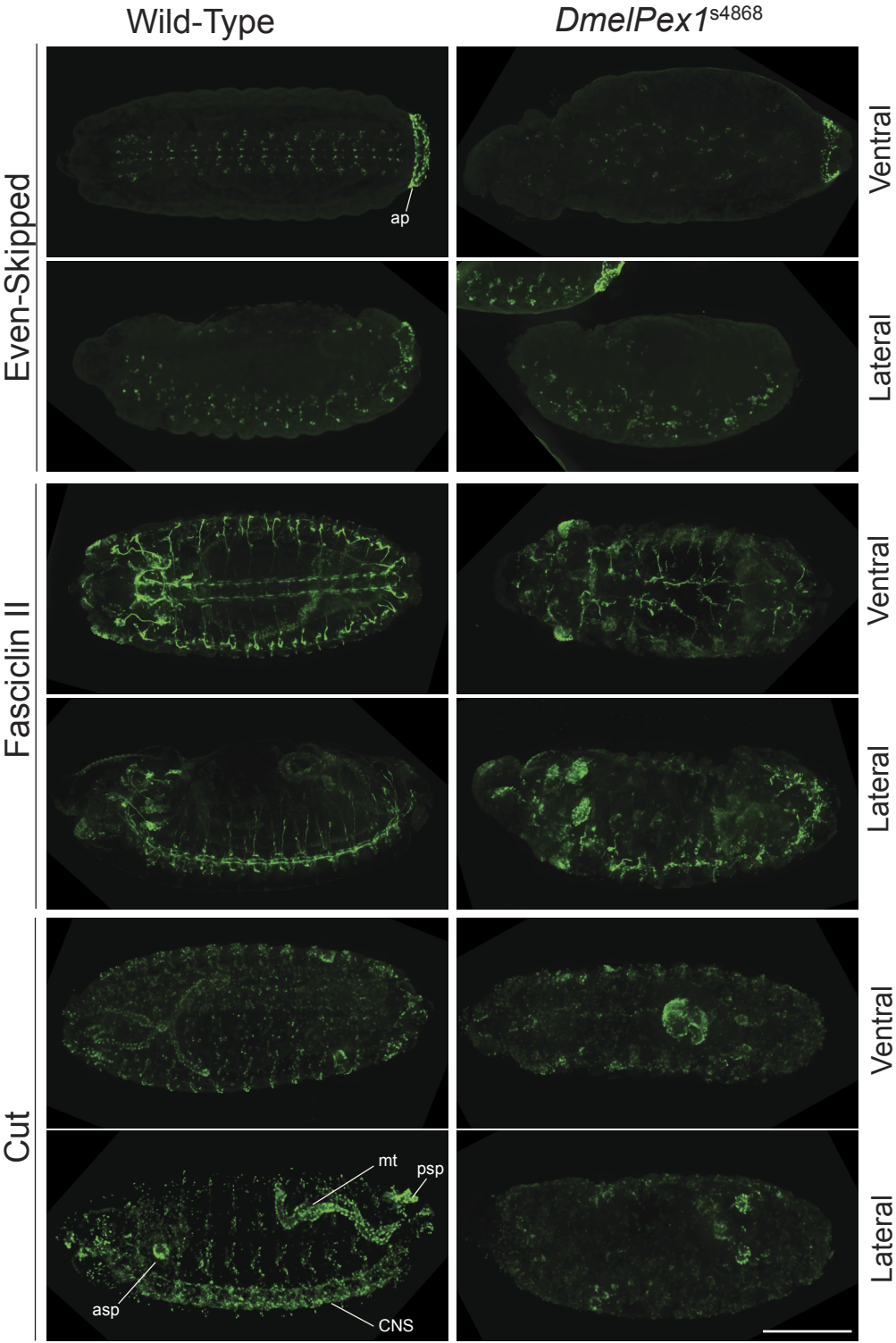
Monoclonal antibody BP104 (anti-Neuroglian, Nrg) stains all neurons of the CNS and PNS and a small number of non-neuronal support cells in the PNS. We observed profound differences in staining between wild-type and homozygous mutant embryos when using anti-Nrg antibody (Figure 6-8). In contrast to the CNS and PNS of wild-type embryos, *DmelPexI*^{s4868} homozygous embryos exhibited a marked loss and hypoplasia of neurons in the PNS, evidence of neuronal degeneration, disorganization of the neuronal pattern in the CNS and PNS, and severely malformed developing eye discs.

Staining with monoclonal antibody 22C10 (anti-Futsch) also showed dramatic differences in the CNS and PNS of wild-type and homozygous mutant embryos (Figure 6-8). Wild-type embryos again exhibited a well organized PNS and distinct neuron/neurite subsets within the VNC, while homozygous mutant embryos exhibited severe disruption, disorganization and loss of both PNS neurons and VNC neuron/neurite subsets.

6.6 Loss of *DmelPexI* causes disorganization in specific subsets of CNS and PNS neurons

We used monoclonal antibodies to Even-skipped (Eve, 2B8) and Fasciclin 2 (Fas2, 1D4) to probe more deeply the organization of the CNS and PNS in wild-type and *DmelPexI*^{s4868} homozygous mutant embryos (Figure 6-9). Antibody to Eve stains the nuclei of a small subset of neurons in the CNS, while anti-Fas2 antibody recognizes the surface of a subset of neurons and axons in the VNC, including some motor neuron axons that innervate striated muscle cells in the periphery of the embryo. Eve expression in the CNS of a wild-type embryo is well organized and well defined when compared to that of the homozygous mutant embryo. However, the pattern of Eve expression in the anal plate is well organized in both wild-type and mutant embryos. Staining of homozygous embryos with anti-Fas2 antibody showed severe abnormalities in the VNC, extensive hypoplasia of

Figure 6-9. CNS and PNS neurons are disorganized in *DmelPexI*^{s4868} homozygous embryos. Wild-type and *DmelPexI*^{s4868} homozygous embryos (stage 15) were analyzed by immunofluorescence microscopy using monoclonal antibodies 2B8 (anti-Eve recognizing the nuclei of a subset of CNS neurons), 1D4 (anti-Fas2 recognizing motor neurons and their axons in the VNC), and 2B10 (anti-Cut recognizing the nuclei of cells of external sensory organ precursors). Anterior is at right in all images. In lateral views, dorsal is down for anti-Eve and up for Fas 2 and anti-Cut. ap, anal plate; asp, anterior spiracle; CNS, central nervous system; mt, malpighian tubules; psp, posterior spiracle; VNC, ventral nerve cord. Scale bar, 100 μ m.



developing eye discs and, in the region of the brain, axon mislocalization and a reduction in the number of motor neurons and in their organization (Figure 6-9).

Anti-Cut antibody is known to demark a subset of cells in the PNS, specifically the nuclei of cells of external sensory organ precursors, including the malpighian tubules, which are the *Drosophila* counterpart of the mammalian kidney. *DmelPexI*^{s4868} homozygous embryos exhibited massive abnormalities in the structure of developing malpighian tubules and in the anterior and posterior spiracles, together with a severe loss of neurons in the CNS (Figure 6-9).

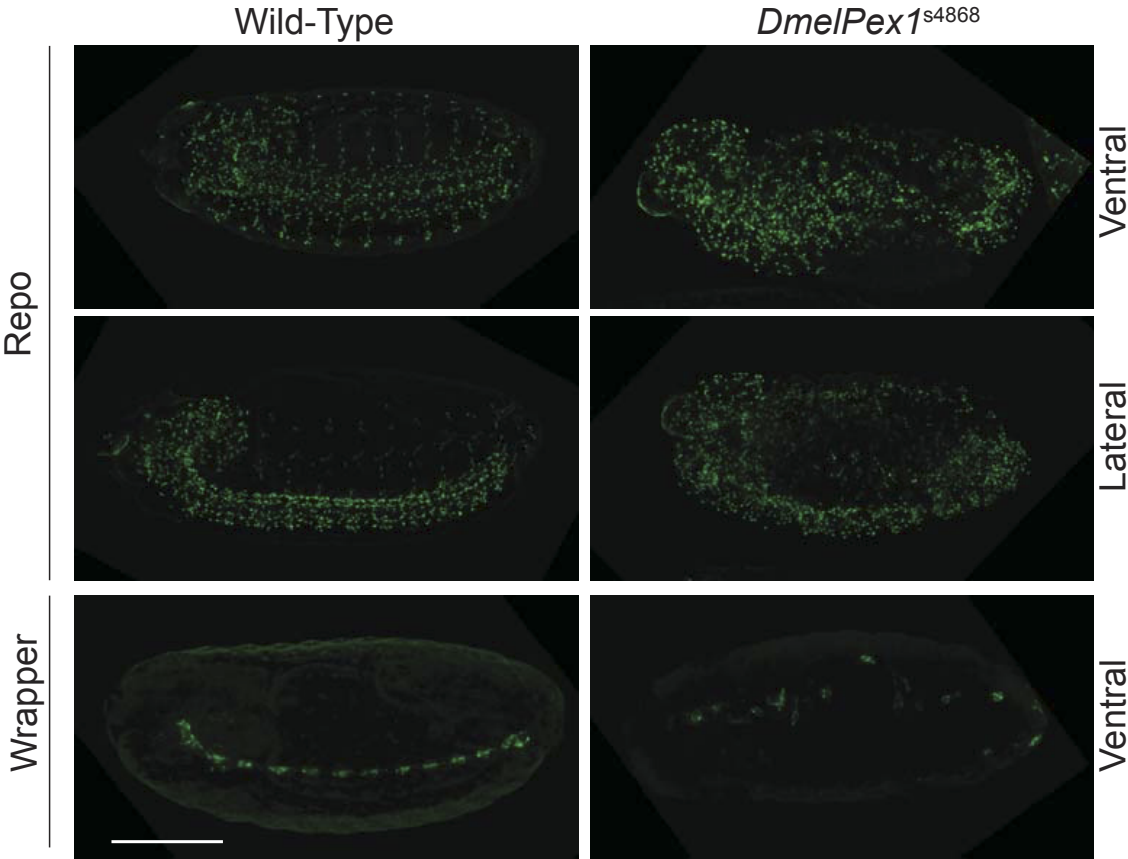
6.7 *DmelPexI* homozygous mutant embryos also show disorganized glia

Demyelination of axons occurs in the CNS of PBD patients (Steinberg et al., 2006). While *Drosophila* lacks myelin, glial cells perform a similar function in flies (Freeman and Doherty, 2006). We used monoclonal antibodies to Reversed Polarity (Repo, 8D12) and Wrapper (10D3) to label the glial cells of embryos (Figure 6-10). Repo is an ubiquitous glial marker found in the nuclei of all glial subtypes and many PNS glia-support cells, but it is not expressed in the midline glia that ensheath commissural axons. We used anti-Wrapper antibody to recognize midline glia. A dramatic disorganization of glia was observed in *DmelPexI*^{s4868} homozygous embryos compared to wild-type embryos. Taken altogether, our data demonstrate an essential role for the *DmelPexI* gene in the development of the fly nervous system.

6.8 Tissue defects correlate with genome-wide changes in gene expression in *DmelPexI* mutant embryos

Because so little is known regarding how mutations in the different *PEX* genes lead to the underlying pathology of the PBDs, we reasoned that an unbiased systems level approach would be a good starting point for elucidating new pathways and mechanisms. One strategy of potential use is a comprehensive expression analysis of transcription using microarrays. Loss of peroxisome

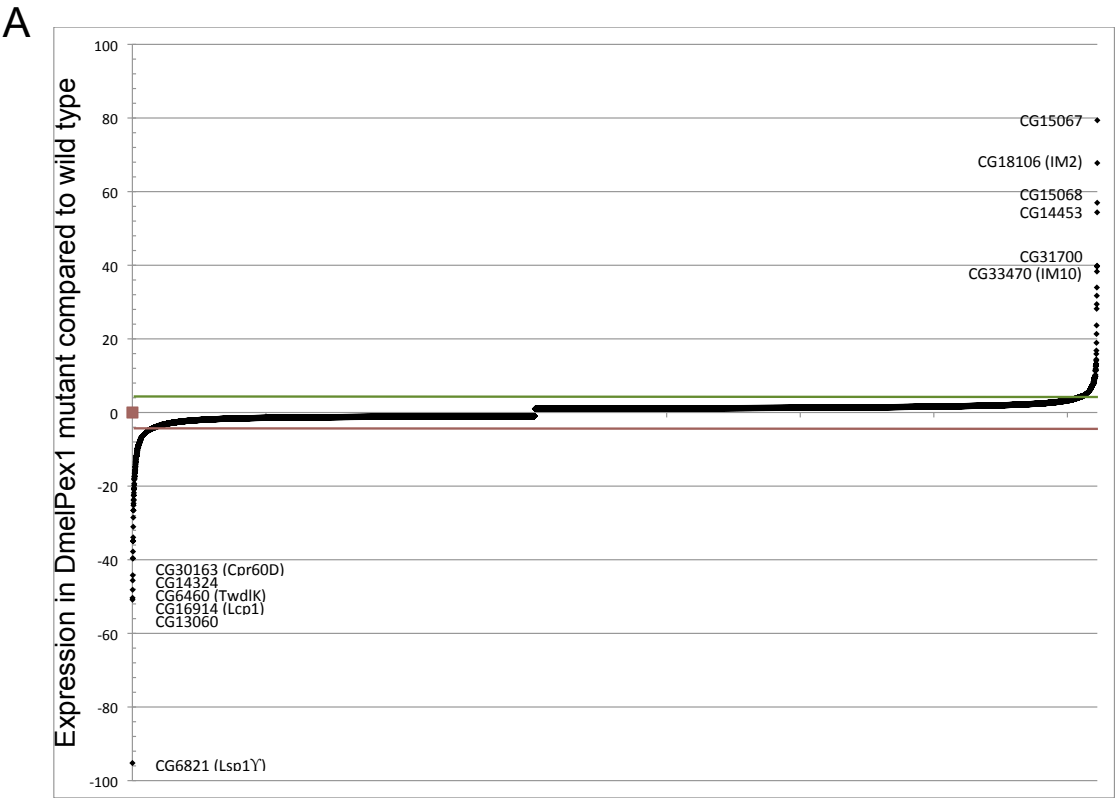
Figure 6-10. Glial cells are disorganized in *DmelPexI*^{s4868} homozygous embryos. Wild-type and *DmelPexI*^{s4868} homozygous embryos (stage 15) were analyzed by immunofluorescence microscopy using monoclonal antibodies 8D12 (anti-Repo recognizing all glial cells except midline glia) and 10D3 (anti-Wrapper recognizing midline glia). Anterior is at right in all images. In lateral views, dorsal is up. Scale bar, 100 μ m.



function is expected to result in the dysregulation of metabolic pathways that could potentially lead to pan-genomic changes in gene expression at each of the cellular, tissue and organismal levels.

We performed a comparative genome-wide RNA expression analysis of transcription between wild-type and *DmelPexI*^{s4868} homozygous embryos. (Figure 6-11). Microarray analysis showed that the expression of 551 distinct protein coding genes showed a consistently greater than 3-fold difference in expression in 48 h-old larvae homozygous for the *DmelPexI* (*l(3)70Da*^{s4868}) mutation compared to wild-type larvae (Figure 6-11B). Of these genes, 396 were upregulated (Tables 6-1) and 145 were downregulated (Table 6-2) in their expression *vis-à-vis* the wild-type condition. Notably, genes that were upregulated could be clustered by their predicted Gene Ontology (GO) annotations into several groups whose protein functions correlate strongly with the observed phenotypes of the *DmelPexI* homozygous mutant (Figure 6-11CD). These functions include neural development and activity; behavior; respiration; nucleotide biosynthesis; peptidase function, adenylate cyclase, and GTPase activities; and cell death. Additional pathways whose gene expression was upregulated include those involved with innate immunity, metabolism of purines and mitotic regulation (Figure 6-11C, Table 6-1). Genes whose expression was strongly downregulated in the *DmelPexI* homozygous mutant included, as expected, *DmelPexI* itself, as well as genes coding for transcription factors involved in gametogenesis and proteins involved in taste sensation, proteolysis, and vesicular transport (Figure 6-11D, Table 6-2). To test for a potential bias of association based on GO annotation, we also clustered randomly generated lists of genes, which typically generated fewer and sparser networks around annotations distinct from those generated by our microarray data. However, 'nucleus organization' was a common annotation that appeared in both the randomly generated lists and our list, which may indicate that this annotation is an over-represented GO term.

Figure 6-11. Systems level view of changes in gene expression in *DmelPexI*^{s4868} homozygous embryos. (A) Relative positive and negative changes in gene expression from an Affymetrix GeneChip arrays done in triplicate using wild-type and *DmelPexI*^{s4868} homozygous embryos. (B) Heat maps for genes with more than a 3-fold change in expression levels in *DmelPexI*^{s4868} homozygous embryos. Bright red indicates a greater than 10-fold decrease in expression levels whereas bright green indicates a greater than 10-fold increase in expression levels for genes annotated in Flybase. (<http://www.flybase.org>). The three-color columns each represent the results from an individual experiment. (See Table 6-1 and 6-2 for the list of genes for each row in the heat map grouped by GO term.) Genes whose expression levels were increased greater than 3-fold (C) or decreased more than 3-fold (D) in *DmelPexI*^{s4868} homozygous embryos as compared to wild-type are grouped according to gene ontology using the ClueGO plugin (<http://www.ici.upmc.fr/cluego/cluegoDownload.shtml>) for Cytoscape (<http://www.cytoscape.org>).



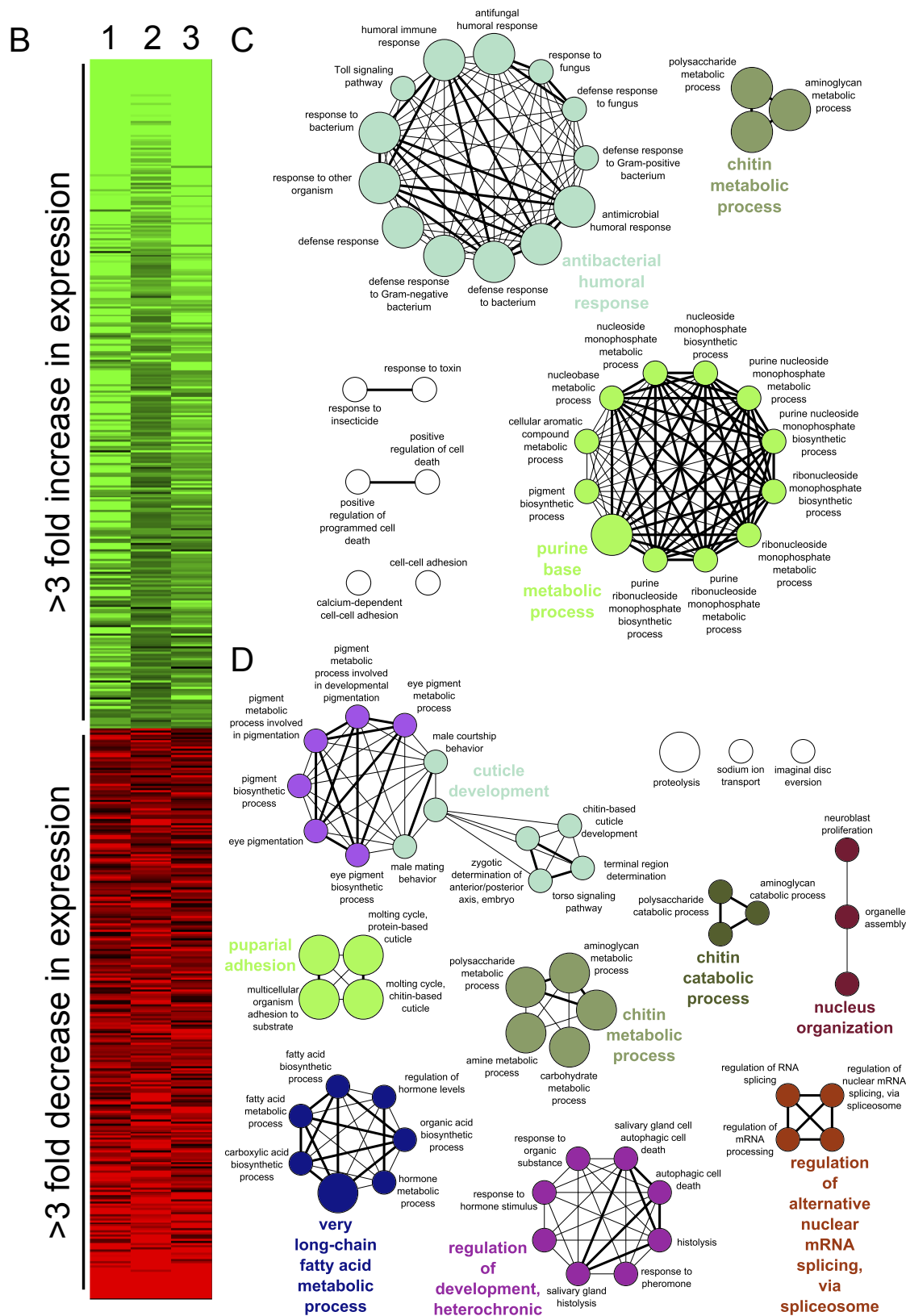


Table 6-1. Genes upregulated more than 3-fold in *DmelPex I* homozygous mutant larvae

Clustered Gene Ontology (GO) terms	Genes
GO:0007186~G-protein coupled receptor protein signaling pathway GO:0007166~cell surface receptor linked signal transduction GO:0007606~sensory perception of chemical stimulus GO:0050890~cognition GO:0007600~sensory perception GO:0004984~olfactory receptor activity GO:0007608~sensory perception of smell GO:0008527~taste receptor activity GO:0050909~sensory perception of taste GO:0005549~odorant binding GO:0050877~neurological system process GO:0005886~plasma membrane GO:0031224~intrinsic to membrane GO:0016021~integral to membrane	<i>odorant receptor 82a</i> , <i>trehalose-sensitivity</i> , <i>odorant receptor 24a</i> , <i>odorant receptor 67b</i> , <i>odorant receptor 1a</i> , <i>gustatory receptor 93d</i> , <i>odorant receptor 92a</i> , <i>odorant receptor 33b</i> , <i>gustatory receptor 39b</i> , <i>gustatory receptor 98a</i> , <i>odorant receptor 35a</i> , <i>gustatory receptor 33a</i> , <i>rhodopsin 7</i> , <i>gustatory receptor 22c</i> , <i>odorant receptor 85d</i> , <i>gustatory receptor 39a</i> , <i>odorant receptor 65b</i> , <i>odorant receptor 2a</i> , <i>gustatory receptor 59e</i> , <i>period</i> , <i>amnesiac</i> , <i>oskar</i> , <i>serendipity alpha</i> , <i>CG8422</i> , <i>stardust</i> , <i>female sterile (1) M3</i> , <i>dopamine receptor 2</i> , <i>protein Shroom</i> , <i>CG32397</i> , <i>octopamine receptor 2</i> , <i>Ras-related protein Rab-26</i> , <i>CG8681</i> , <i>occludin-related Y</i> , <i>neurotransmitter transporter-like</i> , <i>methuselah-like 7</i> , <i>CG42313</i> , <i>CNG channel-like</i> , <i>secretory pathway calcium ATPase</i> , <i>CG9270</i> , <i>mitochondrial import receptor subunit TOM40 homolog 2</i> , <i>tetraspanin 66A</i> , <i>stargazin-like protein</i> , <i>CG17637</i> , <i>ripped pocket</i> , <i>CG5348</i> , <i>CG13646</i> , <i>CG17929</i> , <i>CG33234</i> , <i>CG7994</i> , <i>CG42260</i> , <i>pipe</i> , <i>rhomboid-6</i> , <i>CG18363</i> , <i>Down syndrome cell adhesion molecule-like protein CG42256</i>
GO:0070011~peptidase activity, acting on L-amino acid peptides GO:0006508~proteolysis GO:0004175~endopeptidase activity GO:0008233~peptidase activity GO:0008236~serine-type peptidase activity GO:0017171~serine hydrolase activity GO:0004252~serine-type endopeptidase activity	<i>CG2045</i> , <i>CG12374</i> , <i>CG31661</i> , <i>CG32755</i> , <i>sina homolog</i> , <i>CG4439</i> , <i>CG31205</i> , <i>serine protease 12</i> , <i>CG11626</i> , <i>CG16735</i> , <i>CG10104</i> , <i>CG17988</i> , <i>CG31220</i> , <i>CG6508</i> , <i>CG34130</i> , <i>CG7573</i> , <i>CG34171</i> , <i>CG33159</i> , <i>CG5909</i> , <i>CG32383</i> , <i>CG17301</i> , <i>CG6592</i> , <i>CG11864</i> , <i>rhomboid-6</i> , <i>CG31840</i> , <i>CG7573</i>
GO:0019798~procollagen-proline dioxygenase activity GO:0004656~procollagen-proline 4-dioxygenase activity GO:0031545~peptidyl-proline 4-dioxygenase activity GO:0031543~peptidyl-proline dioxygenase activity GO:0031418~L-ascorbic acid binding GO:0016702~oxidoreductase activity, acting on single donors with incorporation of molecular oxygen, incorporation of two atoms of oxygen GO:0016701~oxidoreductase activity, acting on single donors with incorporation of molecular oxygen GO:0016706~oxidoreductase activity, acting on paired donors, with incorporation or reduction of molecular oxygen, 2-oxoglutarate as one donor, and incorporation of one atom each of oxygen into both donors	<i>prolyl-4-hydroxylase-alpha NE3</i> , <i>CG31524</i> , <i>CG31013</i> , <i>CG18233</i> , <i>CG18231</i> , <i>guanylyl cyclase at 88E</i> , <i>CG6969</i> , <i>CG33093</i> , <i>CG32655</i> , <i>scully</i> , <i>CG5718</i> , <i>CG7024</i> , <i>CG4716</i> , <i>diphenol oxidase A3</i> , <i>secretory pathway calcium ATPase</i> , <i>CG31661</i> , <i>CG12374</i> , <i>CG32755</i> , <i>rhomboid-6</i> , <i>CG4439</i> , <i>CG31205</i> , <i>serine protease 12</i> , <i>CG11626</i> , <i>CG16735</i> , <i>CG10104</i> , <i>CG17988</i> , <i>CG31220</i> , <i>CG6508</i> , <i>CG34130</i> , <i>CG34171</i> , <i>CG33159</i> , <i>CG5909</i> , <i>CG32383</i> , <i>CG6592</i> , <i>CG2045</i>

Clustered Gene Ontology (GO) terms	Genes
GO:0031406~carboxylic acid binding GO:0019842~vitamin binding GO:0005506~iron ion binding GO:0055114~oxidation reduction GO:0005783~endoplasmic reticulum	
GO:0007190~activation of adenylate cyclase activity GO:0031281~positive regulation of cyclase activity GO:0045762~positive regulation of adenylate cyclase activity GO:0051349~positive regulation of lyase activity GO:0031279~regulation of cyclase activity GO:0045761~regulation of adenylate cyclase activity GO:0030799~regulation of cyclic nucleotide metabolic process GO:0030802~regulation of cyclic nucleotide biosynthetic process GO:0030808~regulation of nucleotide biosynthetic process GO:0030814~regulation of cAMP metabolic process GO:0030817~regulation of cAMP biosynthetic process GO:0019932~second-messenger-mediated signaling GO:0051339~regulation of lyase activity GO:0006140~regulation of nucleotide metabolic process GO:0043085~positive regulation of catalytic activity GO:0019933~cAMP-mediated signaling GO:0019935~cyclic-nucleotide-mediated signaling GO:0051336~regulation of hydrolase activity GO:0044093~positive regulation of molecular function GO:0051345~positive regulation of hydrolase activity	<i>octopamine receptor 2, dopamine receptor 2, amnesiac, secretory pathway calcium ATPase, CG18389, intraflagellar transport protein 57 homolog, CG32506, CG32580</i>
GO:0006732~coenzyme metabolic process GO:0046356~acetyl-CoA catabolic process GO:0006099~tricarboxylic acid cycle GO:0009109~coenzyme catabolic process GO:0051187~cofactor catabolic process GO:0009060~aerobic respiration GO:0006084~acetyl-CoA metabolic process GO:0051186~cofactor metabolic process GO:0006091~generation of precursor metabolites and energy GO:0045333~cellular respiration GO:0015980~energy derivation by oxidation of organic compounds	<i>CG3875, CG5718, citrate synthase, CG4706, scully, CG5075, CG7024, CG14909</i>
GO:0005085~guanyl-nucleotide exchange factor activity GO:0051056~regulation of small GTPase mediated signal transduction	<i>CG34393, CG31158, CG42378, CG32506, CG32580, GTPase-activating protein RacGAP84C</i>

Clustered Gene Ontology (GO) terms	Genes
GO:0046578~regulation of Ras protein signal transduction GO:0030695~GTPase regulator activity GO:0005083~small GTPase regulator activity GO:0060589~nucleoside-triphosphatase regulator activity GO:0005099~Ras GTPase activator activity GO:0005096~GTPase activator activity GO:0008047~enzyme activator activity	
GO:0022836~gated channel activity GO:0005216~ion channel activity GO:0022834~ligand-gated channel activity GO:0015276~ligand-gated ion channel activity GO:0022838~substrate specific channel activity GO:0022803~passive transmembrane transporter activity GO:0015267~channel activity GO:0046873~metal ion transmembrane transporter activity GO:0005261~cation channel activity GO:0006811~ion transport	<i>CNG channel-like, CG8681, ripped pocket, CG4587, mitochondrial import receptor subunit TOM40 homolog 2, CG42260, pickpocket 25, secretory pathway calcium ATPase, CG5075, CGI4909</i>
GO:0008017~microtubule binding GO:0015631~tubulin binding GO:0008092~cytoskeletal protein binding	<i>male fertility factor kl3, male fertility factor kl5, nuclear distribution protein nudE homolog, CG32371, serendipity alpha, protein Shroom, alpha actinin 3</i>
GO:0007616~long-term memory GO:0007613~memory GO:0007611~learning or memory GO:0007610~behavior	<i>period, oskar, amnesiac, accessory gland-specific peptide 98AB, odorant receptor 1a, accessory gland peptide Acp33A, pickpocket 25, insulin-like peptide 4</i>
GO:0005179~hormone activity GO:0033057~reproductive behavior in a multicellular organism GO:0007617~mating behavior GO:0051705~behavioral interaction between organisms GO:0007618~mating GO:0010033~response to organic substance GO:0019098~reproductive behavior GO:0060179~male mating behavior GO:0008049~male courtship behavior GO:0007619~courtship behavior GO:0007610~behavior GO:0048609~reproductive process in a multicellular organism GO:0032504~multicellular organism reproduction GO:0003006~reproductive developmental process GO:0048610~reproductive cellular process GO:0007276~gamete generation	<i>accessory gland-specific peptide 98AB, accessory gland peptide Acp33A, CG8422, partner of burs, insulin-like peptide 4, amnesiac, period, pickpocket 25, CGI8389, broad, odorant receptor 1a, oskar, GTPase-activating protein RacGAP84C, dynein heavy chain 64C, female sterile (1) M3, pipe, TBP-associated factor 30kD subunit alpha-2, neurotransmitter transporter-like, rhino</i>

Clustered Gene Ontology (GO) terms	Genes
GO:0019953~sexual reproduction GO:0048477~oogenesis GO:0007292~female gamete generation	
GO:0005615~extracellular space GO:0009617~response to bacterium GO:0042742~defense response to bacterium GO:0006955~immune response GO:0006952~defense response GO:0045087~innate immune response GO:0019730~antimicrobial humoral response GO:0006955~immune response GO:0006959~humoral immune response	<i>Turandot X, Dipteracin B, CG13076, CG34227, partner of burs, Cecropin C, CG32383, amnesiac, TNF-receptor-associated factor 4</i>
GO:0035071~salivary gland cell autophagic cell death GO:0035070~salivary gland histolysis GO:0048102~autophagic cell death GO:0016271~tissue death GO:0007559~histolysis GO:0012501~programmed cell death GO:0022612~gland morphogenesis GO:0007435~salivary gland morphogenesis GO:0008219~cell death GO:0016265~death GO:0043068~positive regulation of programmed cell death GO:0010942~positive regulation of cell death GO:0035272~exocrine system development GO:0007431~salivary gland development GO:0043067~regulation of programmed cell death GO:0010941~regulation of cell death GO:0048732~gland development GO:0006915~apoptosis GO:0042981~regulation of apoptosis GO:0002165~instar larval or pupal development GO:0048707~instar larval or pupal morphogenesis GO:0009886~post-embryonic morphogenesis GO:0009791~post-embryonic development GO:0007552~metamorphosis	<i>CG7588, CG18389, TNF-receptor-associated factor 4, broad, CG8364, intraflagellar transport protein 57 homolog, PDGF- and VEGF-related factor 3, scully</i>
GO:0009190~cyclic nucleotide biosynthetic process GO:0009187~cyclic nucleotide metabolic process GO:0009165~nucleotide biosynthetic process GO:0034654~nucleobase, nucleoside, nucleotide and nucleic acid biosynthetic process GO:0034404~nucleobase, nucleoside and nucleotide biosynthetic process GO:0007242~intracellular signaling cascade GO:0006164~purine nucleotide biosynthetic process GO:0009144~purine nucleoside triphosphate	<i>CG5983, guanylyl cyclase at 88E, amnesiac, CG5075, secretory pathway calcium ATPase, CG14909, octopamine receptor 2, dopamine receptor 2, CG34393, Ras-related protein Rab-26, GTPase-activating protein RacGAP84C, ripped pocket, pickpocket 25</i>

Clustered Gene Ontology (GO) terms	Genes
<p>metabolic process GO:0009205~purine ribonucleoside triphosphate metabolic process GO:0009199~ribonucleoside triphosphate metabolic process GO:0006163~purine nucleotide metabolic process GO:0009141~nucleoside triphosphate metabolic process GO:0009124~nucleoside monophosphate biosynthetic process GO:0009123~nucleoside monophosphate metabolic process GO:0009150~purine ribonucleotide metabolic process GO:0009259~ribonucleotide metabolic process GO:0006754~ATP biosynthetic process GO:0046034~ATP metabolic process GO:0044271~nitrogen compound biosynthetic process GO:0009145~purine nucleoside triphosphate biosynthetic process GO:0009206~purine ribonucleoside triphosphate biosynthetic process GO:0009142~nucleoside triphosphate biosynthetic process GO:0009201~ribonucleoside triphosphate biosynthetic process GO:0009152~purine ribonucleotide biosynthetic process GO:0009260~ribonucleotide biosynthetic process GO:0006812~cation transport GO:0022890~inorganic cation transmembrane transporter activity</p>	
<p>GO:0015630~microtubule cytoskeleton GO:0030286~dynein complex GO:0005856~cytoskeleton GO:0003777~microtubule motor activity GO:0003774~motor activity GO:0007018~microtubule-based movement GO:0005874~microtubule GO:0044430~cytoskeletal part GO:0005875~microtubule associated complex GO:0007017~microtubule-based process GO:0042624~ATPase activity, uncoupled GO:0042623~ATPase activity, coupled GO:0016887~ATPase activity GO:0043232~intracellular non-membrane-bounded organelle GO:0043228~non-membrane-bounded organelle</p>	<p><i>CG17150</i>, <i>protein Shroom</i>, <i>CG7051</i>, <i>CG15684</i>, <i>male fertility factor kl3</i>, <i>male fertility factor kl5</i>, <i>nuclear distribution protein nudE homolog</i>, <i>CG17364</i>, <i>CG31907</i>, <i>intraflagellar transport protein 57 homolog</i>, <i>dynein heavy chain 64C</i>, <i>CG32371</i>, <i>uncharacterized protein CG42248</i>, <i>short spindle 2</i>, <i>oskar</i>, <i>CG9270</i>, <i>CG33087</i>, <i>CG5075</i>, <i>secretory pathway calcium ATPase</i>, <i>ribosomal protein L10Aa</i>, <i>CG7045</i>, <i>CG18389</i>, <i>troponin C isoform 4</i>, <i>pipe</i>, <i>male-specific-transcript-35Ba</i>, <i>rhino</i>, <i>CG12640</i>, <i>guanylyl cyclase at 88E</i>, <i>CG15543</i>, <i>Ras-related protein Rab-26</i>, <i>CG5718</i></p>

Clustered Gene Ontology (GO) terms	Genes
<p>GO:0032553~ribonucleotide binding GO:0032555~purine ribonucleotide binding GO:0017076~purine nucleotide binding GO:0030554~adenyl nucleotide binding GO:0005524~ATP binding GO:0032559~adenyl ribonucleotide binding GO:0001883~purine nucleoside binding GO:0001882~nucleoside binding GO:0000166~nucleotide binding</p>	
<p>GO:0022884~macromolecule transmembrane transporter activity GO:0015450~P-P-bond-hydrolysis-driven protein transmembrane transporter activity GO:0006626~protein targeting to mitochondrion GO:0070585~protein localization in mitochondrion GO:0008320~protein transmembrane transporter activity GO:0015399~primary active transmembrane transporter activity GO:0015405~P-P-bond-hydrolysis-driven transmembrane transporter activity GO:0006839~mitochondrial transport GO:0017038~protein import GO:0008565~protein transporter activity GO:0033365~protein localization in organelle GO:0044455~mitochondrial membrane part GO:0006605~protein targeting GO:0006886~intracellular protein transport GO:0034613~cellular protein localization GO:0070727~cellular macromolecule localization GO:0008104~protein localization GO:0015031~protein transport GO:0045184~establishment of protein localization GO:0031966~mitochondrial membrane GO:0031967~organelle envelope GO:0031975~envelope GO:0005740~mitochondrial envelope GO:0005739~mitochondrion GO:0031090~organelle membrane GO:0046907~intracellular transport GO:0005743~mitochondrial inner membrane GO:0019866~organelle inner membrane GO:0044429~mitochondrial part</p>	<p><i>mitochondrial import receptor subunit TOM40 homolog 2, mitochondrial import inner membrane translocase subunit Tim13, CG14690, CG5075, secretory pathway calcium ATPase, CG9270, CG5718, dynein heavy chain 64C, oskar, Ras-related protein Rab-26, TNF-receptor-associated factor 4, CG18363, CG3748, nuclear distribution protein nudE homolog, citrate synthase, CG4706, CG31679, neurotransmitter transporter-like, scully, dopamine receptor 2, pipe</i></p>
<p>GO:0043565~sequence-specific DNA binding GO:0003700~transcription factor activity GO:0030528~transcription regulator activity GO:0045449~regulation of transcription</p>	<p><i>CG8591, CG15696, CG9571, CG4328, H6-like-homeobox, brain-specific homeobox, CG33980, CG6892, hormone receptor-like in 38, CG18389, 48 related 1, broad, period, CG14907, CG14906,</i></p>

Clustered Gene Ontology (GO) terms	Genes
GO:0006355~regulation of transcription, DNA-dependent GO:0051252~regulation of RNA metabolic process GO:0003677~DNA binding	<i>CG1343, CG2932, TBP-associated factor 30kD subunit alpha-2, oskar, CG7045, CG31700, male-specific-transcript-35Ba</i>
GO:0006911~phagocytosis, engulfment GO:0006909~phagocytosis GO:0016044~membrane organization GO:0010324~membrane invagination GO:0006897~endocytosis GO:0016192~vesicle-mediated transport	<i>ribosomal protein L10Aa, CG4328, CG34127, CG18389, hormone receptor-like in 38, TNF-receptor-associated factor 4, neurotransmitter transporter-like, mitochondrial import inner membrane translocase subunit Tim13</i>
GO:0015399~primary active transmembrane transporter activity GO:0015405~P-P-bond-hydrolysis-driven transmembrane transporter activity GO:0042623~ATPase activity, coupled GO:0042626~ATPase activity, coupled to transmembrane movement of substances GO:0043492~ATPase activity, coupled to movement of substances GO:0016820~hydrolase activity, acting on acid anhydrides, catalyzing transmembrane movement of substances	<i>CG5075, secretory pathway calcium ATPase, CG9270, mitochondrial import receptor subunit TOM40 homolog 2, mitochondrial import inner membrane translocase subunit Tim13, CG14690, CG17150, CG7051, male fertility factor kl3, male fertility factor kl5, dynein heavy chain 64C</i>
GO:0046872~metal ion binding GO:0043169~cation binding GO:0046914~transition metal ion binding GO:0043167~ion binding GO:0008270~zinc ion binding	<i>guanylyl cyclase at 88E, CG31840, CG31679, mitochondrial import inner membrane translocase subunit Tim13, troponin C isoform 4, alpha actinin 3, broad, GTPase-activating protein RacGAP84C, CG8591, ripped pocket, sina homolog, CG4439, CG10102, CG31524, diphenol oxidase A3, CG33490, CG11041, CG4328, CG6969, CG13287, CG31013, CG17770, CG18233, hormone receptor-like in 38, TNF-receptor-associated factor 4, CG10899, CG33087, CG1343, CG2932, CG11864, CG12374, CG11966, prolyl-4-hydroxylase-alpha NE3, CG30378, CG33093, CG18231, senseless-2, CG5334</i>
GO:0032990~cell part morphogenesis GO:0000902~cell morphogenesis GO:0048858~cell projection morphogenesis GO:0032989~cellular component morphogenesis GO:0030030~cell projection organization GO:0048812~neuron projection morphogenesis GO:0031175~neuron projection development GO:0048667~cell morphogenesis involved in neuron differentiation GO:0000904~cell morphogenesis involved in differentiation GO:0030182~neuron differentiation GO:0048666~neuron development	<i>CG4328, neurotransmitter transporter-like, CG14870, capricious, intraflagellar transport protein 57 homolog, dynein heavy chain 64C, protein Shroom, stardust, broad</i>

Clustered Gene Ontology (GO) terms	Genes
GO:0007052~mitotic spindle organization GO:0051301~cell division GO:0000226~microtubule cytoskeleton organization GO:0007051~spindle organization GO:0007010~cytoskeleton organization GO:0000278~mitotic cell cycle GO:0022402~cell cycle process GO:0000279~M phase GO:0022403~cell cycle phase GO:0007049~cell cycle	<i>short spindle 2, nuclear distribution protein nudE homolog, dynein heavy chain 64C, serendipity alpha, oskar, alpha actinin 3, TBP-associated factor 30kD subunit alpha-2</i>
Other	<i>casein kinase II beta2 subunit, Cecropin pseudogene 1, chibby, chorion protein c at 7F, CG10124, CG10134, CG10486, CG10680, CG10734, CG10919, CG10934, CG11125, CG11231, CG11322, CG11369, CG11373, CG11588, CG11598, CG11630, CG11983, CG12158, CG12250, CG12420, CG12611, CG12851, CG12862, CG12983, CG13054, CG13125, CG1314, CG13186, CG13251, CG13299, CG13457, CG13541, CG13589, CG13653, CG13749, CG13771, CG13804, CG13842, CG13871, CG13884, CG13891, CG13955, CG13998, CG14070, CG14115, CG14190, CG14246, CG14245, CG14280, CG14309, CG14330, CG14339, CG14341, CG14448, CG14459, CG14502, CG14538, CG14579, CG14691, CG14823, CG14837, CG15035, CG1504, CG15233, CG15337, CG15425, CG15470, CG15580, CG15594, CG15634, CG15699, CG15734, CG15767, CG15800, CG15824, CG15876, CG15878, CG16723, CG16848, CG16853, CG17122, CG17319, CG17376, CG17380, CG18130, CG18301, CG18371, CG18469, CG18539, CG18628, CG2457, CG2871, CG2955, CG30001, CG30284, CG30321, CG30350, CG30419, CG30432, CG31088, CG31190, CG31204, CG31286, CG31606, CG31752, CG31771, CG31790, CG31862, CG31870, CG32118, CG32141, CG32141, CG32192, CG32193, CG32203, CG32233, CG32235, CG32319, CG32440, CG32602, CG32614, CG32631, CG32652, CG32741, CG32846, CG32984, CG33287, CG33482, CG33484, CG33507, CG33758, CG33988, CG33993, CG34021, CG34028, CG34030, CG34139, CG34144, CG34161, CG34169, CG34252, CG34256, CG34259, CG34300, CG34338, CG34353, CG34353, CG34430, CG3640, CG3687, CG3706, CG40164, CG40195, CG40282, CG40336, CG40924, CG40924, CG41012, CG41452, CG4198, CG42283, CG42324, CG42352, CG42355, CG4270, CG4329, CG4829, CG4970, CG14929, CG5111, CG5122, CG5458, CG5568, CG5614, CG5762, CG5866, CG6138, CG6280,</i>

Clustered Gene Ontology (GO) terms	Genes
	<i>CG6435, CG6599, CG6761, CG6902, CG7164, CG7325, CG7442, CG7557, CG7773, CG7975, CG8006, CG8838, CG9173, CG9316, CG9392, CG9525, CG9592, CG9863, CR15821, CR40450, CR41056, CR41056, female-specific independent of transformer, fish-lips, J domain-containing protein, munin, Wnt, UPF0279 protein CG14505, ventrally expressed gene D protein</i>

Table 6-2. Genes downregulated more than 3-fold in *DmelPexI* homozygous mutant larvae

Clustered Gene Ontology (GO) terms	Genes
GO:0007186~G-protein coupled receptor protein signaling pathway GO:0016021~integral to membrane GO:0031224~intrinsic to membrane GO:0007166~cell surface receptor linked signal transduction GO:0005886~plasma membrane GO:0007606~sensory perception of chemical stimulus GO:0007600~sensory perception GO:0008527~taste receptor activity GO:0050909~sensory perception of taste GO:0050890~cognition GO:0050877~neurological system process GO:0005549~odorant binding	<i>CG32547, octopamine receptor in mushroom bodies, gustatory receptor 59f, odorant receptor 85a, odorant receptor 67c, gustatory receptor 47b, gustatory receptor 58b, methuselah-like 12, octopamine receptor beta-2R, CG30379, CG11262, CG17137, CG4323, derailed 2, goliath, CG32305, CG1887, CG8743, tailless, insulin-like peptide 3, dystrophin; snoRNA:122, odorant-binding protein 22a, couch potato</i>
GO:0045449~regulation of transcription GO:0006355~regulation of transcription DNA-dependent GO:0030528~transcription regulator activity GO:0043565~sequence-specific DNA binding GO:0051252~regulation of RNA metabolic process GO:0003700~transcription factor activity GO:0006350~transcription GO:0003677~DNA binding	<i>timeless, CR34648, tailless, CG13188, goliath, tonalli, buttonless, homeobox protein unc-4, Pox meso, gooseberry-neuro, octopamine receptor beta-2R, CG9642, maternal gene required for meiosis, no hitter, CG12936</i>
GO:0005887~integral to plasma membrane GO:0031226~intrinsic to plasma membrane GO:0044459~plasma membrane part	<i>CG30379, derailed 2, octopamine receptor in mushroom bodies, CG1887, dystrophin; snoRNA:122</i>
GO:0005216~ion channel activity GO:0022838~substrate specific channel activity GO:0022803~passive transmembrane transporter activity GO:0015267~channel activity GO:0005261~cation channel activity GO:0046873~metal ion transmembrane transporter	<i>CG33061, CG11775, CG17137, CG8743, CG11262</i>

Clustered Gene Ontology (GO) terms	Genes
activity GO:0006811~ion transport	
GO:0008234~cysteine-type peptidase activity GO:0006508~proteolysis GO:0070011~peptidase activity acting on L-amino acid peptides GO:0008233~peptidase activity GO:0004175~endopeptidase activity	<i>CG1075</i> , <i>ubiquitin carboxyl-terminal hydrolase</i> , <i>CG32377</i> , <i>CG14227</i> , <i>CG4793</i> , <i>CG4017</i> , <i>echinus</i> , <i>CG9868</i>
GO:0034654~nucleobase, nucleoside, nucleotide and nucleic acid biosynthetic process GO:0034404~nucleobase, nucleoside and nucleotide biosynthetic process GO:0044271~nitrogen compound biosynthetic process	<i>CG32305</i> , <i>CG3809</i> , <i>guanylyl cyclase at 76C</i>
GO:0006508~proteolysis GO:0044257~cellular protein catabolic process GO:0051603~proteolysis involved in cellular protein catabolic process GO:0030163~protein catabolic process GO:0044265~cellular macromolecule catabolic process GO:0009057~macromolecule catabolic process	<i>CG1075</i> , <i>CG14227</i> , <i>ubiquitin carboxyl-terminal hydrolase</i> , <i>CG4793</i> , <i>CG4017</i> , <i>echinus</i> , <i>CG32377</i> , <i>CG9868</i>
GO:0016044~membrane organization GO:0010324~membrane invagination GO:0006897~endocytosis GO:0016192~vesicle-mediated transport	<i>sprint</i> , <i>CG31094</i> , <i>peroxidasin</i> , <i>misfire</i>
GO:0048232~male gamete generation GO:0007283~spermatogenesis GO:0007276~gamete generation GO:0019953~sexual reproduction GO:0048609~reproductive process in a multicellular organism GO:0032504~multicellular organism reproduction GO:0048610~reproductive cellular process GO:0003006~reproductive developmental process GO:0007292~female gamete generation	<i>spermatocyte arrest</i> , <i>no hitter</i> , <i>misfire</i> , <i>sprint</i> , <i>octopamine receptor in mushroom bodies</i> , <i>maternal gene required for meiosis</i>
GO:0007126~meiosis GO:0051327~M phase of meiotic cell cycle GO:0051321~meiotic cell cycle GO:0000279~M phase GO:0022403~cell cycle phase GO:0022402~cell cycle process GO:0007049~cell cycle	<i>spermatocyte arrest</i> , <i>hold'em</i> , <i>maternal gene required for meiosis</i>
GO:0008270~zinc ion binding GO:0046914~transition metal ion binding GO:0046872~metal ion binding GO:0043169~cation binding	<i>tailless</i> , <i>goliath</i> , <i>CG11966</i> , <i>dystrophin</i> ; <i>snoRNA:122</i> , <i>tonalli</i> , <i>maternal gene required for meiosis</i> , <i>CG17329</i> , <i>CG4017</i> , <i>CG12362</i> , <i>probable cytochrome P450 313a1</i> , <i>peroxidasin</i> , <i>CG31094</i> , <i>androcarn</i>

Clustered Gene Ontology (GO) terms	Genes
GO:0043167~ion binding	
GO:0005856~cytoskeleton GO:0043232~intracellular non-membrane-bounded organelle GO:0043228~non-membrane-bounded organelle	<i>dystrophin</i> ; <i>snoRNA:122</i> , <i>CG33957</i> , <i>CG3339</i> , <i>spermatocyte arrest</i>
GO:0000166~nucleotide binding GO:0005524~ATP binding GO:0032559~adenyl ribonucleotide binding GO:0032555~purine ribonucleotide binding GO:0032553~ribonucleotide binding GO:0030554~adenyl nucleotide binding GO:0017076~purine nucleotide binding GO:0001883~purine nucleoside binding GO:0001882~nucleoside binding	<i>derailed 2</i> , <i>CG32305</i> , <i>CG11356</i> , <i>guanylyl cyclase at 76C</i> , <i>CG3339</i> , <i>RNA-binding protein Musashi homolog Rbp6</i> , <i>heat shock protein cognate 1</i> , <i>couch potato</i>
Other	<i>CG12309</i> , <i>CG12525</i> , <i>CG13074</i> , <i>CG1308</i> , <i>CG13310</i> , <i>CG13681</i> , <i>CG13693</i> , <i>CG13721</i> , <i>CG14017</i> , <i>CG14035</i> , <i>CG1409</i> , <i>CG1428</i> , <i>CG14301</i> , <i>CG14446</i> , <i>CG14684</i> , <i>CG14689</i> , <i>CG14946</i> , <i>CG14974</i> , <i>CG15005</i> , <i>CG15711</i> , <i>CG15728</i> , <i>CG16733</i> , <i>CG1791</i> , <i>CG18157</i> , <i>CG2861</i> , <i>CG30062</i> , <i>CG30103</i> , <i>CG30395</i> , <i>CG30469</i> , <i>CG31461</i> , <i>CG31493</i> , <i>CG31647</i> , <i>CG31709</i> , <i>CG31921</i> , <i>CG32160</i> , <i>CG32212</i> , <i>CG32248</i> , <i>CG32487</i> , <i>CG32694</i> , <i>CG32821</i> , <i>CG32985</i> , <i>CG33060</i> , <i>CG33156</i> , <i>CG33252</i> , <i>CG33464</i> , <i>CG33530</i> , <i>CG34184</i> , <i>CG34429</i> , <i>CG3927</i> , <i>CG3975</i> , <i>CG40121</i> , <i>CG40164</i> , <i>CG40211</i> , <i>CG4161</i> , <i>CG42329</i> , <i>CG42377</i> , <i>CG4468</i> , <i>CG4582</i> , <i>CG5017</i> , <i>CG5062</i> , <i>CG5644</i> , <i>CG5867</i> , <i>CG6429</i> , <i>CG6559</i> , CG6760*[(3)70Da , DmelPex1), <i>CG6788</i> ; <i>CG32496</i> , <i>CG6793</i> , <i>CG7208</i> , <i>CG8179</i> ; <i>CG34318</i> , <i>CG8813</i> , <i>nimrod C2</i> , <i>nuclear export factor 4</i> , <i>odorant receptor 98a pseudogene</i> , <i>tonalli</i> , <i>TweedleZ</i> , <i>WD repeat-containing protein on Y chromosome</i>

6.9 Discussion

6.9.1 Peroxisome assembly in *Drosophila* is mechanistically similar to human peroxisome assembly

To make robust conclusions regarding the suitability of *Drosophila* as a model for PBDs, compared to other models, it was necessary to determine if the overall gene pathways required for peroxisome biogenesis in *Drosophila* are largely conserved with those in humans. Our systematic

RNAi knockdown of 14 *Drosophila* genes that are homologous to mammalian and/or yeast PEX genes in S2 cells confirmed that at least 13 are bona fide *DmelPex*s. Homologs of these genes have been shown to be required for peroxisome assembly in organisms from yeast to human (Platta and Erdmann, 2007; Schrader and Fahimi, 2008). Importantly, mutation in 12 of these genes cause PBDs and make up 12 of the 13 known complementation groups in the PBDs. The 13th complementation group belongs to mutations in *Pex26*, a gene that we and others were unable to find in *Drosophila* (Schluter, 2006). *Pex26*p is the docking site for the AAA ATPases *Pex1*p and *Pex6*p in humans, which are necessary for the recycling of the matrix protein receptor *Pex5*p (Matsumoto et al., 2003). However, this receptor is not conserved across eukaryotes and other unrelated receptors have been characterized in yeast (Birschmann et al., 2003; Elgersma et al., 1997) and plants (Goto et al., 2011). Despite being unrelated, all three of these proteins function similarly. Therefore, *Drosophila* most likely possesses a receptor for *Pex1*p and *Pex6*p that remains to be discovered.

Cells from PBD patients typically demonstrate increased cytosolic localization of peroxisomal matrix proteins. RNAi of *DmelPex2*, *DmelPex6*, *DmelPex13*, *DmelPex16* and *DmelPex19* dsRNA produced clear reductions in the amounts of the corresponding mRNAs in treated S2 cells (Figure 6-3C), while RNAi of the other *DmelPex*s produced a less robust, yet still demonstrable, reduction in the corresponding mRNAs. Despite this variation in the reduction of mRNA levels, knockdown of *DmelPex1*, *DmelPex2*, *DmelPex3*, *DmelPex6*, *DmelPex12*, *DmelPex13*, *DmelPex14* and *DmelPex16* reduced or eliminated the punctate structures characteristic of peroxisomes and mislocalized a GFP-SKL reporter to the cytosol.

Although the knockdown of *DmelPex5* by RNAi was somewhat variable, cells consistently showed an exclusively cytosolic signal for the GFP-SKL reporter. *DmelPex5* thus likely encodes the PTS1 receptor in *Drosophila*. Conversely, *Pex7*p functions as the receptor for proteins targeted to peroxisomes by PTS2, independently of the PTS1(SKL) targeting sequence. This makes the

knockdown of *DmelPex7* somewhat difficult to interpret, as we would not expect a change in the characteristic punctate pattern produced by GFP-SKL. Likewise, the presence of a putative *PEX20* homolog in *Drosophila* would suggest that there are parallels in the peroxisomal protein import pathways of insects and fungi. Several species of yeast have been shown to rely on the interaction between Pex7p and a Pex20-like protein for PTS2 protein import, while mammalian cells import PTS2 proteins via an interaction between Pex7p and a larger splice variant of Pex5p known as Pex5L (Girzalsky et al., 2010).

Pex19 protein has been shown to be required for peroxisomal membrane formation and has been suggested to function as the receptor for PMPs and/or as a chaperone acting to stabilize membrane proteins at the peroxisomal membrane. Absence of Pex19p in most organisms leads to an inability of cells to assemble peroxisomes and an absence of identifiable peroxisomal membrane structures (Hettema et al., 2000). Interestingly, although we could show a clear and reproducible reduction in the mRNA of the putative *Drosophila* homolog of *PEX19* in RNAi-treated S2 cells (Figure 6-3C), this nevertheless did not prevent the assembly of peroxisomes but instead led to a reduction in the number and increase in the size of punctate structures containing GFP-SKL and partial mislocalization of GFP-SKL to the cytosol. These differences in peroxisomal phenotype between the cells of other organisms lacking Pex19 protein and S2 cells subjected to RNAi for *DmelPex19* mRNA could arise for a variety of reasons: 1) *DmelPex19* may not be the true *Drosophila* homolog of *PEX19* in other organisms. However, the degree of sequence similarity between human Pex19 and DmelPex19 (Figure 6-1) makes this unlikely. 2) DmelPex19 protein may have functions in peroxisome biogenesis different from those of Pex19 protein in other organisms. Because of the predicted multivariate nature of functions attributed to Pex19, further study DmelPex19 might be able to provide a better understanding of Pex19 function. 3) *Drosophila* may have another protein whose function in peroxisome biogenesis and peroxisomal membrane formation is redundant to that of DmelPex19 protein. The de novo synthesis of peroxisomes from

the ER has been shown to rely on additional proteins, such as Dsl1p, Sec39p and Sec20p in *S. cerevisiae* (Perry et al., 2009) and essential secretory proteins may play a more prominent role in this process in *Drosophila*. Other proteins, such as the p24 family of proteins (Marelli et al., 2004; Otzen et al., 2006) may also affect this trafficking pathway. The *Drosophila* system remains an excellent model organism for the discovery of new secretory mechanisms (Bard et al., 2006). 4) RNAi reduction of *DmelPex19* was insufficient to give a loss-of-function phenotype. A similar phenotype has been described for the yeast *Y. lipolytica* in which deletion of the *PEX19* gene results in the accumulation of peroxisomal structures that are similar in morphology to wild-type peroxisomes but are defective in matrix protein import (Lambkin and Rachubinski, 2001). Together, these observations suggest that Pex19p may participate in several aspects of peroxisome biogenesis and be tailored for one or more aspects in individual organisms (Ma et al., 2011).

PEX11 is conserved among eukaryotes and controls peroxisome division and proliferation. A loss of Pex11 protein produces cells with decreased numbers of enlarged peroxisomes (Erdmann and Blobel, 1995). *DmelPex11* probably functions similarly to *PEX11* genes in other organisms because RNAi to *PEX11* transcript resulted in S2 cells containing few and enlarged peroxisomes but unaffected in their ability to import GFP-SKL into peroxisomes.

DmelPex23 exhibits limited similarity to *Y. lipolytica* Pex23p. Nevertheless, the peroxisome phenotype of RNAi-treated S2 cells (Figure 6-2) is consistent with a role for *DmelPex23* in peroxisome biogenesis. Interestingly, the region of highest similarity between *DmelPex23* and *Y. lipolytica* Pex23p is in the unique dysferlin motif that is common to all members of the Pex23 protein family. Dysferlin motifs are thought to aid proteins in binding to certain phosphoinositides like phosphoinositide-4-phosphate. This feature is proposed to aid the Pex23 family of proteins in their function of controlling peroxisome number and size in different yeast species (Brown et al., 2000; Vizeacoumar et al., 2004; Yan et al., 2008). S2 cells treated by RNAi against the transcript of *DmelPex23* had increased numbers of small peroxisomes as compared to control S2 cells and no

mislocalization of GFP-SKL to the cytosol. Therefore, notwithstanding the evolutionary distance between flies and yeasts, *Drosophila* has apparently retained some *PEX* genes heretofore only reported in yeasts and maintained their involvement in peroxisome biogenesis.

6.9.2 *DmelPex1* Mutants Mirror the Early Developmental Defects Associated with Human PBDs

A recent study of flies harboring mutant *DmelPex2* and *DmelPex10* peroxins has demonstrated a requirement for peroxisomes in normal spermatogenesis and the control of very-long chain fatty acid levels in adult *Drosophila* (Chen et al., 2010). However, it is difficult to ascertain if gametogenesis is affected in PDB patients as mutation of the 13 *PEX* genes involved in the PBDs cause early developmental defects and usually death within one year (Shimozawa et al., 2005; Steinberg et al., 2006). Since inherited mutations of *PEX1* are the most common cause of ZS (Reuber et al., 1997; Steinberg et al., 2006), we wanted to examine the effect of *DmelPex1* mutations on early development. The organismal phenotype associated with loss of *DmelPex1* protein is strikingly similar to the ZS phenotypic spectrum. *DmelPex1* mutant larvae were smaller in size than their wild-type counterparts, failed to show coordinated movement or effective feeding habits, and exhibited severe malformations of the nervous system, with loss and/or mislocalization of axons and neurons in both the CNS and PNS during embryonic development. There are additional parallels between the abnormalities exhibited by ZS patients and flies mutant in the *DmelPex1* gene. ZS patients have severely demyelinated axons in both the CNS and PNS (Powers et al., 1985; Steinberg et al., 2006). While *Drosophila* axons are not myelinated, *DmelPex1* mutant flies have extensively disorganized glial cells, which provide support and insulation to the axons of the CNS and PNS of flies in a manner akin to myelination in mammals (Freeman and Doherty, 2006). *DmelPex1* mutants also exhibit malformed malpighian tubules, whose functions are similar

to those of mammalian kidneys. ZS patients also show structural abnormalities in the kidney (Steinberg et al., 2006).

The use of a simple genetic model like *Drosophila* allows the examination of the cellular and organismal response to loss of *DmelPex1* in terms of gene expression. Thus, for the first time, we were able to evaluate the results of the loss of *Pex1* at a systems level using transcriptomics profiling. In mutant animals, the primary systemic molecular response to loss of peroxisome function can be linked to changes in 551 of 13,767, or approximately 4%, protein coding genes. Furthermore, the majority of these genes can be functionally grouped into relatively few genetic pathways. However, the diversity of genetic pathways altered by loss of peroxisome function underscores the widespread and varied responses seen in both clinical and biochemical presentation of PBDs. Our transcriptomics data reveal large scale alterations in the expression of genes involved in chitin metabolism and puparial adhesion. This might implicate peroxisomes in the metabolic pathways of complex polysaccharides such as chitin or may reflect changes in the secretory pathway through dysregulation and loss of peroxisome function. It has recently been demonstrated in the yeast *Pichia pastoris* that non-conventional secretion of acyl-CoA binding protein requires proper peroxisome metabolism (Manjithaya, 2010). These findings underscore our present lack of knowledge regarding peroxisome biology, which is essential for better understanding disease progression in the PBDs. The increase in expression of genes involved in innate immunity and humoral responses might be due to a response to increased levels of unused peroxisomal metabolites. Plasma levels of the plasmalogen precursors di- and trihydroxycholestanoic acid are increased in PBD patients, as is a C₂₉-dicarboxylic acid that is not typically found in serum of normal individuals (Ferdinandusse et al., 2009). The accumulation of these compounds and long chain fatty acids esterified to cholesterol (Kovacs et al., 2004; 2009) are thought to contribute to the pleiotropic defects exhibited by PBD patients (Steinberg et al., 2006). However, changes in expression of innate immunity genes might underlie a currently

unexplored role for peroxisomes in immune responses. Recently, mammalian peroxisomes were shown to function as signaling platforms for antiviral innate immunity (Dixit et al., 2010). The upregulation of genes involved in the immune response in *DmelPex1* mutants suggests that peroxisomes may also function in modulating the immune response of *Drosophila*.

Our profiling of changes in gene expression in response to loss of peroxisome function provides a tractable method to monitor disease progression. It may also prove to be a suitable tool for screening novel therapeutic drug candidates and monitoring disease regression in response to novel therapies of the PBDs. Current attempts at finding small molecules and diet regimens that might alleviate symptoms of PBDs require extensive and time-consuming biochemical verification (Dranchak et al., 2010; Zhang et al., 2010). This process could be aided by transcriptomic profiling as a way to identify treatments that return gene expression profiles back to normal levels.

Based on the multiple classes of defects observed in our RNAi analysis in S2 cells, we have confirmed that at least 13 of the 14 known *DmelPex* genes are required for what are likely different aspects of peroxisome assembly. Moreover, we have shown that specific developmental abnormalities in the developing embryonic nervous system occur when the *DmelPex1* gene is mutated. Taken together, our findings make a compelling argument for the use of *Drosophila* as a valid and tractable model system with which to investigate the roles of peroxisomes and the effects of the PBDs on a multicellular organism's growth, development and response to the environment.

7 Perspectives

7.1 Synopsis

In conclusion, this thesis reports on the identification of a reticulon-peroxin complex that functions to regulate peroxisome biogenesis and proliferation by controlling the release of preperoxisomal vesicles from the ER in the budding yeast *Saccharomyces cerevisiae*. The reticulon-peroxin complex is composed of Pex30p, Pex29p, Rtn1p and Yop1p and these proteins associate dynamically with each other and, as a group, dynamically with peroxisomes. Pex30p and Pex29p are homologs and have orthologs in a diversity of Opisthokont lineages. The RNAi mediated knockdown of the *Drosophila* ortholog of Pex30p results in the dysregulation of peroxisome proliferation, confirming the conservation of this mechanism in Opisthokonts. We have also gained insight into the evolution of organelle inheritance in budding yeasts. Organelle inheritance is an emergent property in yeast, but shares a conserved evolutionary mechanism in the utilization of novel adaptor proteins to link myosin motors with their cargo. These observations have led to the proposal of the Widget Hypothesis, which states a propensity will exist for the emergence of evolutionarily novel adaptor proteins in cases where a cellular phenotype requires an interaction between conserved and essential cellular modules. Finally, we have learned of the utility of *Drosophila* as a model system for the study of ZS, the most prevalent form of PBD.

7.2 Future directions for studies on the reticulon-peroxin complex

Research on the function of the reticulon-peroxin complex is still in its infancy and many important questions regarding it and its regulation of peroxisome biogenesis and proliferation remain to be answered:

How is the reticulon-peroxin complex integrated into the growth cycle of the cell? Our studies have demonstrated that peroxisome proliferation relies on cues from the growth cycle of the cell as opposed to cell cycle cues. Presumably, the function of the reticulon-peroxin complex is integrated into, and receives signals from, the growth cycle of the cell. Pex30p from wild-type

whole cell lysates migrates as multiple bands in immunoblots, which may indicate that it is regulated by posttranslational modification (Figure 3-8). It would be interesting to identify posttranslational signaling mechanisms that exist for members of the reticulon-peroxin complex. In vitro, Pex30p is a target for Kss1p (Ptacek et al., 2005), a mitogen activated protein kinase that is involved in regulating filamentous growth (Cook et al., 1997). A global analysis of kinases and phosphatases identified Kss1p as a negative regulator of peroxisome proliferation (Saleem et al., 2008), consistent with a role for Kss1p in regulating Pex30p. Furthermore, the PI4P phosphatase Sac1p was also shown to be a negative regulator of peroxisome proliferation. Our immunoprecipitation experiments identified several linkages between Sac1p and the reticulon-peroxin complex. First, all four components interact with Dpm1p, which is required for Sac1p mediated regulation of cell secretion and growth by regulating PI4P levels at the ER (Faulhammer et al., 2005; 2007). The reticulon-peroxin complex also interacts with Scs2p, a component of the recently characterized ER-PM tether and an important regulator of Sac1p activity by transducing environmental cues from the PM to the ER (Manford et al., 2012; Stefan et al., 2013; 2011). Pex30p and Pex29p also interact with Tcb3, which is also a component of the ER-PM tether. It would be interesting to investigate how dysregulation of signaling events through the Kss1p signaling pathway, or through pathways involving Sac1p affect the function of the reticulon-peroxin complex.

Are there additional functions for the reticulon-peroxin complex? Our subcellular localization data indicate that Pex30p and Pex29p are ER-resident proteins that associate with peroxisome but are also distributed throughout the cell. This suggests that the reticulon-peroxin complex functions in other cellular processes, and this need not be mutually exclusive. One consideration is a role in the regulation of lipid metabolism. Rtn1p interacts with many components involved in lipid body biogenesis (Figure 3-9). This suggests that the reticulon-peroxin complex could be involved in integrating diverse cellular signals regulating the metabolism or storage of lipids in the cell.

Important metabolic connections between peroxisomes and lipid bodies have been demonstrated in the past (Binns et al., 2006; Goldberg et al., 2009).

The human ortholog of Pex30p has recently been implicated in autophagy (Chen et al., 2012) and this may suggest additional function for the reticulon-peroxin complex in autophagy or, more specifically, in pexophagy. Its position at the interface between peroxisomes and the ER suggests that the reticulon-peroxin complex could be regulating the entire life cycle of a peroxisome, from its birth to its death.

7.3 Future directions for studies of de novo peroxisome biogenesis

The major hurdle in the field of peroxisome biogenesis is understanding and identifying the molecular mechanisms and proteins involved in de novo peroxisome biogenesis. The identity of the reticulon-peroxin complex brings us a step closer in achieving those goals. Importantly, in our studies we did not address whether dysregulation of the reticulon-peroxin complex uncouples de novo biogenesis from the growth and division of existing peroxisomes. One way to address this question is by use of a switchable mCherry/GFP-tag (Hotz et al., 2012) and following the progression of Pex3p tagged with it. Wild-type yeast peroxisomes should have a mix of old and new Pex3p as they grow and divide (Menendez-Benito et al., 2013) and this can be compared to mutants of the reticulon-peroxin complex. Evidence in favor of uncoupling de novo biogenesis from growth and division of existing peroxisomes would be the presence of distinct red and green Pex3p foci in the cell.

In *Y. lipolytica* the requirement of a reticulon-peroxin complex may be more tightly coupled to de novo biogenesis. Cells lacking *PEX23* accumulate small non-functional peroxisomal vesicles and are unable to metabolize fatty acid carbon sources. In this yeast a well-orchestrated sequence of events begins with the fusion of two ER-derived preperoxisomal vesicle populations (Titorenko et al., 2000). These data therefore suggest that *PEX23* may function both in the negative regulation of

vesicle egress from the ER but also in the fusion of these preperoxisomal vesicles. Recent evidence suggests the presence of two preperoxisomal vesicle compartments also exist in *S. cerevisiae* (van der Zand et al., 2012). The metazoan protein dysferlin is involved in regulating vesicle production and vesicle fusion with the plasma membrane to assist in repairing damaged membranes. This may be a conserved function of proteins with dysferlin motifs irrespective of their location or molecular function.

How positive regulators are involved in de novo peroxisome biogenesis is also an outstanding question currently unresolved. New evidence is emerging that implicates members of the Pex11 family in de novo peroxisome biogenesis (Huber et al., 2012; Saraya et al., 2011; Tower et al., 2011) but the mechanism involved or how they integrate with the negative regulation of the reticulon-peroxin complex awaits further examination.

7.4 Future directions for the study of peroxisome evolution

With the emergence of a plethora of newly sequenced eukaryotic genomes the original evolutionary analyses of peroxisome evolution are outdated and need to be redone. A case in point is the evolution of the Pex23 family, which was previously concluded to be restricted to certain fungal lineages (Kiel et al., 2006; Schluter et al. 2006). Outstanding questions include: Are there Pex23 homologs outside of Opisthokonts? Was a Pex23 homolog present in the LECA? Where did the dysferlin domain come from and what was the ancestral function of that domain? Within the Saccharomycotina a large expansion, for a peroxin family, of the Pex23 and Pex24 families has occurred. This usually results in a divergence of functions that may also potentially divide the ancestral function amongst the new paralogs. What are the functions of Pex24p/Pex28p, Pex31p and Pex32p? Curiously, some of these proteins appear to be peroxisomal residents and therefore gene duplication has also brought about the evolution of targeting these genes from the ER to the peroxisome. This presents an opportunity for determining those targeting sequences through

comparative genomics and ancestral gene reconstruction, as has been demonstrated recently for the V_0 ATPase (Finnigan et al., 2011).

To address the origins of peroxisome, knowledge of the factors involved in preperoxisomal vesicle formation and scission at the ER will be essential for assigning a timeframe for the emergence of peroxisomes in eukaryotic lineages.

7.5 Future directions for study of the widget hypothesis

Currently, the widget hypothesis is primarily an observation of shared evolutionary novelty for a group of unrelated protein adaptors of class V myosin motors in Opisthokonts. To progress beyond this, functional characterization of cell biological mechanisms will need to proceed at a rapid enough pace to allow for the identification of additional applicable systems to look for these phenomena in. One potential area for exploration is autophagy, a mechanism that conceivably requires adaptors, or widgets, to bridge the cellular modules of organelle identity, cell cycle and autophagosome formation and maturation (Motley et al., 2012). These requirements for autophagy are akin to what was seen for organelle inheritance.

Another area of study is a better understanding of the origins of widget proteins, which may come from fast evolving proteins, or de novo gene birth. Recent evidence in yeast suggests that gene birth is more prevalent than previously proposed (Carvunis et al., 2012). But the mechanisms of both processes are far from being understood.

7.6 Future directions for studying Zellweger Syndrome in *Drosophila*

The demonstration that *Drosophila* is a tractable model system for the study of Zellweger Syndrome is an important stepping-stone into a better understanding of the etiology of this disease. The finding that, as in humans, developmental programs in *D. melanogaster* require functional peroxisomes was demonstrated by the gross scale malformations noted in the organization of the central and peripheral nervous systems. A previously unappreciated contribution to disease

appears to be the adverse regulation of gene expression for genes involved with innate immunity and mitotic regulations. Utilization of microarray analysis for monitoring systems level changes in gene expression is emerging as a useful way to monitor disease progression and as a way to verify efficacy of novel treatments for PBDs. Approaches to therapeutic intervention in the PBDs have been hampered due to the rarity of these diseases and because of the lack of a cost-effective, model organismal system. As a result, no large-scale assay of small molecules that could alleviate or reduce the developmental and physiological abnormalities associated with the PBDs has been conducted. In future studies, newly hatched mutant flies could be fed a library of small molecules to determine if a compound could be found that would alleviate the effects of mutation in a particular *Pex* gene that gives rise to a PBD. Classes of molecules that suppress the PBD phenotype in flies could be developed as potential new treatments for PBD patients.

7.7 Concluding remarks

Peroxisomes have never failed to surprise in their ability to do different things and to do things differently – their specialized metabolic pathways, their distinctive mechanisms of growth and division, their highly dynamic and flexible protein import machinery, and their ability to exchange and share biogenic and metabolic factors with the ER and mitochondria. The emerging view of peroxisomes as a stage or platform for orchestrating and organizing cellular responses to a variety of environmental challenges promises to provide a more nuanced appreciation of the complexity and diversity of function achievable by peroxisomes and, by extension, eukaryotic cells. Also, the nature of the interrelationship between peroxisomes, the ER and mitochondria promises new insights into the contribution of these organelles to cell physiology. The genetic tractability of model organisms, such as yeasts and fungi, have continued to facilitate the identification of several proteins involved in maintaining peroxisome populations. Discovery and characterization

peroxisomes in organisms outside of the classical model systems promises to shed further light onto their evolution and function.

8 References

Adames, N.R., J.R. Oberle, and J.A. Cooper. 2001. The surveillance mechanism of the spindle position checkpoint in yeast. *J Cell Biol.* 153:159–168.

Adams, A.E., D. Botstein, and D.G. Drubin. 1991. Requirement of yeast fimbrin for actin organization and morphogenesis in vivo. *Nature.* 354:404–408. doi:10.1038/354404a0.

Adams, M.D., S.E. Celniker, R.A. Holt, C.A. Evans, J.D. Gocayne, P.G. Amanatides, S.E. Scherer, P.W. Li, R.A. Hoskins, R.F. Galle, R.A. George, S.E. Lewis, S. Richards, M. Ashburner, S.N. Henderson, G.G. Sutton, J.R. Wortman, M.D. Yandell, Q. Zhang, L.X. Chen, R.C. Brandon, Y.H. Rogers, R.G. Blazej, M. Champe, B.D. Pfeiffer, K.H. Wan, C. Doyle, E.G. Baxter, G. Helt, C.R. Nelson, G.L. Gabor, J.F. Abril, A. Agbayani, H.J. An, C. Andrews-Pfannkoch, D. Baldwin, R.M. Ballew, A. Basu, J. Baxendale, L. Bayraktaroglu, E.M. Beasley, K.Y. Beeson, P.V. Benos, B.P. Berman, D. Bhandari, S. Bolshakov, D. Borkova, M.R. Botchan, J. Bouck, P. Brokstein, P. Brottier, K.C. Burtis, D.A. Busam, H. Butler, E. Cadieu, A. Center, I. Chandra, J.M. Cherry, S. Cawley, C. Dahlke, L.B. Davenport, P. Davies, B. de Pablos, A. Delcher, Z. Deng, A.D. Mays, I. Dew, S.M. Dietz, K. Dodson, L.E. Doup, M. Downes, S. Dugan-Rocha, B.C. Dunkov, P. Dunn, K.J. Durbin, C.C. Evangelista, C. Ferraz, S. Ferriera, W. Fleischmann, C. Fosler, A.E. Gabrielian, N.S. Garg, W.M. Gelbart, K. Glasser, A. Glodek, F. Gong, J.H. Gorrell, Z. Gu, P. Guan, M. Harris, N.L. Harris, D. Harvey, T.J. Heiman, J.R. Hernandez, J. Houck, D. Hostin, K.A. Houston, T.J. Howland, M.H. Wei, et al. 2000. The genome sequence of *Drosophila melanogaster*. *Science.* 287:2185–2195.

Adl, S.M., A.G.B. Simpson, C.E. Lane, J. Lukes, D. Bass, S.S. Bowser, M.W. Brown, F. Burki, M. Dunthorn, V. Hampl, A. Heiss, M. Hoppenrath, E. Lara, L. Le Gall, D.H. Lynn, H. McManus, E.A.D. Mitchell, S.E. Mozley-Stanridge, L.W. Parfrey, J. Pawlowski, S. Rueckert, L. Shadwick, C.L. Schoch, A. Smirnov, and F.W. Spiegel. 2012. The revised classification of eukaryotes. *J Eukaryot Microbiol.* 59:429–493. doi:10.1111/j.1550-7408.2012.00644.x.

Agne, B., N.M. Meindl, K. Niederhoff, H. Einwächter, P. Rehling, A. Sickmann, H.E. Meyer, W. Girzalsky, and W.H. Kunau. 2003. Pex8p: an intraperoxisomal organizer of the peroxisomal import machinery. *Mol Cell.* 11:635–646.

Agrawal, G., S. Joshi, and S. Subramani. 2011. Cell-free sorting of peroxisomal membrane proteins from the endoplasmic reticulum. *Proc Nat Acad Sci USA.* 108:9113–9118. doi:10.1073/pnas.1018749108.

Aitchison, J.D., M.P. Rout, M. Marelli, G. Blobel, and R.W. Wozniak. 1995. Two novel related yeast nucleoporins Nup170p and Nup157p: complementation with the vertebrate homologue Nup155p and functional interactions with the yeast nuclear pore-membrane protein Pom152p. *J Cell Biol.* 131:1133–1148. doi:10.1083/jcb.131.5.1133.

Akhmanova, A., and J.A. Hammer. 2010. Linking molecular motors to membrane cargo. *Curr Opin Cell Biol.* 22:479–487. doi:10.1016/j.ceb.2010.04.008.

Altschul, S.F., T.L. Madden, A.A. Schäffer, J. Zhang, Z. Zhang, W. Miller, and D.J. Lipman. 1997. Gapped BLAST and PSI-BLAST: a new generation of protein database search programs. *Nuc Acids Res.* 25:3389–3402.

Anderson, R.M., K.J. Bitterman, J.G. Wood, O. Medvedik, and D.A. Sinclair. 2003. Nicotinamide and *PNC1* govern lifespan extension by calorie restriction in *Saccharomyces cerevisiae*. *Nature.*

423:181–185. doi:10.1038/nature01578.

Andrade-Navarro, M.A., L. Sanchez-Pulido, and H.M. McBride. 2009. Mitochondrial vesicles: an ancient process providing new links to peroxisomes. *Curr Opin Cell Biol.* 21:560–567. doi:10.1016/j.ceb.2009.04.005.

Angermüller, S., M. Islinger, and A. Völkl. 2009. Peroxisomes and reactive oxygen species, a lasting challenge. *Histochem Cell Biol.* 131:459–463. doi:10.1007/s00418-009-0563-7.

Antonenkova, V.D., and J.K. Hiltunen. 2006. Peroxisomal membrane permeability and solute transfer. *Biochim Biophys Acta.* 1763:1697–1706. doi:10.1016/j.bbamcr.2006.08.044.

Aparicio, S., J. Chapman, E. Stupka, N. Putnam, J.-M. Chia, P. Dehal, A. Christoffels, S. Rash, S. Hoon, A. Smit, M.D.S. Gelpke, J. Roach, T. Oh, I.Y. Ho, M. Wong, C. Detter, F. Verhoef, P. Predki, A. Tay, S. Lucas, P. Richardson, S.F. Smith, M.S. Clark, Y.J.K. Edwards, N. Doggett, A. Zharkikh, S.V. Tavtigian, D. Pruss, M. Barnstead, C. Evans, H. Baden, J. Powell, G. Glusman, L. Rowen, L. Hood, Y.H. Tan, G. Elgar, T. Hawkins, B. Venkatesh, D. Rokhsar, and S. Brenner. 2002. Whole-genome shotgun assembly and analysis of the genome of *Fugu rubripes*. *Science.* 297:1301–1310. doi:10.1126/science.1072104.

Arai, S., Y. Noda, S. Kainuma, I. Wada, and K. Yoda. 2008. Ypt11 functions in bud-directed transport of the Golgi by linking Myo2 to the coatamer subunit Ret2. *Curr Biol.* 18:987–991. doi:10.1016/j.cub.2008.06.028.

Ausubel, F.J., R. Brent, R.E. Kingston, D.D. Moore, J.G. Seidman, J.A. Smith, and K. Struhl. 1989. Current Protocols in Molecular Biology. Greene Publishing Associates, New York, NY.

Baerends, R.J., S.W. Rasmussen, R.E. Hilbrands, M. van der Heide, K.N. Faber, P.T. Reuvekamp, J.A. Kiel, J.M. Cregg, I.J. van der Klei, and M. Veenhuis. 1996. The *Hansenula polymorpha* PER9 gene encodes a peroxisomal membrane protein essential for peroxisome assembly and integrity. *J Biol Chem.* 271:8887–8894.

Bankaitis, V.A., J.R. Aitken, A.E. Cleves, and W. Dowhan. 1990. An essential role for a phospholipid transfer protein in yeast Golgi function. *Nature.* 347:561–562. doi:10.1038/347561a0.

Barbrook, A.C., C.J. Howe, and S. Purton. 2006. Why are plastid genomes retained in non-photosynthetic organisms? *Trends Plant Sci.* 11:101–108. doi:10.1016/j.tplants.2005.12.004.

Bard, F., L. Casano, A. Mallabiabarrena, E. Wallace, K. Saito, H. Kitayama, G. Guizzunti, Y. Hu, F. Wendler, R. Dasgupta, N. Perrimon, and V. Malhotra. 2006. Functional genomics reveals genes involved in protein secretion and Golgi organization. *Nature.* 439:604–607. doi:10.1038/nature04377.

Barelle, C.J., M.L. Richard, C. Gaillardin, N.A.R. Gow, and A.J.P. Brown. 2006. *Candida albicans* VAC8 is required for vacuolar inheritance and normal hyphal branching. *Euk Cell.* 5:359–367. doi:10.1128/EC.5.2.359-367.2006.

Barlowe, C., L. Orci, T. Yeung, M. Hosobuchi, S. Hamamoto, N. Salama, M.F. Rexach, M. Ravazzola, M. Amherdt, and R. Schekman. 1994. COPII: a membrane coat formed by Sec proteins that drive vesicle budding from the endoplasmic reticulum. *Cell.* 77:895–907.

- Baudhuin, P., H. Beaufay, and C. de Duve. 1965. Combined biochemical and morphological study of particulate fractions from rat liver. Analysis of preparations enriched in lysosomes or in particles containing urate oxidase, D-amino acid oxidase, and catalase. *J Cell Biol.* 26:219–243.
- Beach, D.L., J. Thibodeaux, P. Maddox, E. Yeh, and K. Bloom. 2000. The role of the proteins Kar9 and Myo2 in orienting the mitotic spindle of budding yeast. *Curr Biol.* 10:1497–1506.
- Beard, M.E., and E. Holtzman. 1987. Peroxisomes in *wild-type* and *rosy* mutant *Drosophila melanogaster*. *Proc Natl Acad Sci USA.* 84:7433–7437.
- Bilen, J., and N.M. Bonini. 2005. *Drosophila* as a model for human neurodegenerative disease. *Annu. Rev. Genet.* 39:153–171. doi:10.1146/annurev.genet.39.110304.095804.
- Bindea, G., B. Mlecnik, H. Hackl, P. Charoentong, M. Tosolini, A. Kirilovsky, W.-H. Fridman, F. Pagès, Z. Trajanoski, and J. Galon. 2009. ClueGO: a Cytoscape plug-in to decipher functionally grouped gene ontology and pathway annotation networks. *Bioinformatics.* 25:1091–1093. doi:10.1093/bioinformatics/btp101.
- Binns, D., T. Januszewski, Y. Chen, J. Hill, V.S. Markin, Y. Zhao, C. Gilpin, K.D. Chapman, R.G.W. Anderson, and J.M. Goodman. 2006. An intimate collaboration between peroxisomes and lipid bodies. *J Cell Biol.* 173:719–731. doi:10.1083/jcb.200511125.
- Birschmann, I., A.K. Stroobants, M. van den Berg, A. Schäfer, K. Rosenkranz, W.-H. Kunau, and H.F. Tabak. 2003. Pex15p of *Saccharomyces cerevisiae* provides a molecular basis for recruitment of the AAA peroxin Pex6p to peroxisomal membranes. *Mol Biol Cell.* 14:2226–2236. doi:10.1091/mbc.E02-11-0752.
- Blobel, G. 1980. Intracellular protein topogenesis. *Proc Natl Acad Sci USA.* 77:1496–1500.
- Bock, J.B., H.T. Matern, A.A. Peden, and R.H. Scheller. 2001. A genomic perspective on membrane compartment organization. *Nature.* 409:839–841. doi:10.1038/35057024.
- Bodnar, A.G., and R.A. Rachubinski. 1991. Characterization of the integral membrane polypeptides of rat liver peroxisomes isolated from untreated and clofibrate-treated rats. *Biochem Cell Biol.* 69:499–508.
- Bolte, S., and F.P. Cordelières. 2006. A guided tour into subcellular colocalization analysis in light microscopy. *Journal of Microscopy.* 224:213–232. doi:10.1111/j.1365-2818.2006.01706.x.
- Bonifacino, J.S., and B.S. Glick. 2004. The mechanisms of vesicle budding and fusion. *Cell.* 116:153–166.
- Bork, P., T. Dandekar, Y. Diaz-Lazcoz, F. Eisenhaber, M. Huynen, and Y. Yuan. 1998. Predicting function: from genes to genomes and back. *J Mol Biol.* 283:707–725. doi:10.1006/jmbi.1998.2144.
- Boukh-Viner, T., T. Guo, A. Alexandrian, A. Cerracchio, C. Gregg, S. Haile, R. Kyskan, S. Milijevic, D. Oren, J. Solomon, V. Wong, J.-M. Nicaud, R.A. Rachubinski, A.M. English, and V.I. Titorenko. 2005. Dynamic ergosterol- and ceramide-rich domains in the peroxisomal membrane serve as an organizing platform for peroxisome fusion. *J Cell Biol.* 168:761–773. doi:10.1083/jcb.200409045.

Boveris, A., N. Oshino, and B. Chance. 1972. The cellular production of hydrogen peroxide. *Biochem J.* 128:617–630.

Böhl, F., C. Kruse, A. Frank, D. Ferring, and R.P. Jansen. 2000. She2p, a novel RNA-binding protein tethers *ASH1* mRNA to the Myo4p myosin motor via She3p. *EMBO J.* 19:5514–5524. doi:10.1093/emboj/19.20.5514.

Böhni, P.C., R.J. Deshaies, and R.W. Schekman. 1988. *SEC11* is required for signal peptide processing and yeast cell growth. *J Cell Biol.* 106:1035–1042.

Braakman, I., and N.J. Bulleid. 2011. Protein folding and modification in the mammalian endoplasmic reticulum. *Annu Rev Biochem.* 80:71–99. doi:10.1146/annurev-biochem-062209-093836.

Brade, A.M. 1992. Peroxisome Assembly in *Yarrowia lipolytica*. M.Sc. Thesis, McMaster University, Hamilton.

Bradford, M.M. 1976. A rapid and sensitive method for the quantification of microgram quantities of protein utilizing the principle of protein-dye binding. *Anal Biochem.* 72:248–254.

Bradford, B.U., C.B. Seed, J.A. Handler, D.T. Forman, and R.G. Thurman. 1993. Evidence that catalase is a major pathway of ethanol oxidation in vivo: dose-response studies in deer mice using methanol as a selective substrate. *Arch Biochem Biophys.* 303:172–176. doi:10.1006/abbi.1993.1269.

Bridges, C.B., and K.S. Brehme. 1944. The mutants of *Drosophila melanogaster*. *The mutants of Drosophila melanogaster*.

Brighouse, A., J.B. Dacks, and M.C. Field. 2010. Rab protein evolution and the history of the eukaryotic endomembrane system. *Cell Mol Life Sci.* 67:3449–3465. doi:10.1007/s00018-010-0436-1.

Brown, T.W., V.I. Titorenko, and R.A. Rachubinski. 2000. Mutants of the *Yarrowia lipolytica* *PEX23* gene encoding an integral peroxisomal membrane peroxin mislocalize matrix proteins and accumulate vesicles containing peroxisomal matrix and membrane proteins. *Mol Biol Cell.* 11:141–152.

Brul, S., E.A. Wiemer, A. Westerveld, A. Strijland, R.J. Wanders, A.W. Schram, H.S. Heymans, R.B. Schutgens, H. Van den Bosch, and J.M. Tager. 1988. Kinetics of the assembly of peroxisomes after fusion of complementary cell lines from patients with the cerebro-hepato-renal (Zellweger) syndrome and related disorders. *Biochem Biophys Res Commun.* 152:1083–1089.

Burnette, W.N. 1981. "Western Blotting": electrophoretic transfer of proteins from sodium dodecyl sulphate-polyacrylamide gels to unmodified nitrocellulose and radiographic detection with antibody and radioiodinated protein A. *Anal Biochem.* 112:195–203.

Byrne, K., and K. Wolfe. 2005. The Yeast Gene Order Browser: combining curated homology and syntenic context reveals gene fate in polyploid species. *Genome Res.* 15:1456.

C. elegans Sequencing Consortium. 1998. Genome sequence of the nematode *C. elegans*: a

platform for investigating biology. *Science*. 282:2012–2018.

Cai, H., K. Reinisch, and S. Ferro-Novick. 2007. Coats, tethers, Rab, and SNAREs work together to mediate the intracellular destination of a transport vesicle. *Dev Cell*. 12:671–682. doi:10.1016/j.devcel.2007.04.005.

Carvunis, A.-R., T. Rolland, I. Wapinski, M.A. Calderwood, M.A. Yildirim, N. Simonis, B. Charloteaux, C.A. Hidalgo, J. Barbette, B. Santhanam, G.A. Brar, J.S. Weissman, A. Regev, N. Thierry-Mieg, M.E. Cusick, and M. Vidal. 2012. Proto-genes and de novo gene birth. *Nature*. 487:370–374. doi:10.1038/nature11184.

Cauchi, R.J., and M. van den Heuvel. 2006. The fly as a model for neurodegenerative diseases: is it worth the jump? *Neurodegener Dis*. 3:338–356. doi:10.1159/000097303.

Cavalier-Smith, T. 1975. The origin of nuclei and of eukaryotic cells. *Nature*. 256:463–468.

Cavalier-Smith, T. 2010. Origin of the cell nucleus, mitosis and sex: roles of intracellular coevolution. *Biol. Direct*. 5:7. doi:10.1186/1745-6150-5-7.

Chacinska, A., C.M. Koehler, D. Milenkovic, T. Lithgow, and N. Pfanner. 2009. Importing mitochondrial proteins: machineries and mechanisms. *Cell*. 138:628–644. doi:10.1016/j.cell.2009.08.005.

Chadrin, A., B. Hess, M. San Roman, X. Gatti, B. Lombard, D. Loew, Y. Barral, B. Palancade, and V. Doye. 2010. Pom33, a novel transmembrane nucleoporin required for proper nuclear pore complex distribution. *J Cell Biol*. 189:795–811. doi:10.1083/jcb.200910043.

Chang, J., F.D. Mast, A. Fagarasanu, D.A. Rachubinski, G.A. Eitzen, J.B. Dacks, and R.A. Rachubinski. 2009. Pex3 peroxisome biogenesis proteins function in peroxisome inheritance as class V myosin receptors. *J Cell Biol*. 187:233–246. doi:10.1083/jcb.200902117.

Chen, D., W. Fan, Y. Lu, X. Ding, S. Chen, and Q. Zhong. 2012. A mammalian autophagosome maturation mechanism mediated by TECPR1 and the Atg12-Atg5 conjugate. *Mol Cell*. 45:629–641. doi:10.1016/j.molcel.2011.12.036.

Chen, H., Z. Liu, and X. Huang. 2010. Drosophila models of peroxisomal biogenesis disorder: peroxins are required for spermatogenesis and very-long-chain fatty acid metabolism. *Hum Mol Genet*. 19:494–505. doi:10.1093/hmg/ddp518.

Cherry, J.M., C. Adler, C. Ball, S.A. Chervitz, S.S. Dwight, E.T. Hester, Y. Jia, G. Juvik, T. Roe, M. Schroeder, S. Weng, and D. Botstein. 1998. SGD: Saccharomyces Genome Database. *Nucleic Acids Res*. 26:73–79.

Chung, S., and P.A. Takizawa. 2010. Multiple Myo4 motors enhance *ASH1* mRNA transport in *Saccharomyces cerevisiae*. *J Cell Biol*. 189:755–767. doi:10.1083/jcb.200912011.

Cook, J.G., L. Bardwell, and J. Thorner. 1997. Inhibitory and activating functions for MAPK Kss1 in the *S. cerevisiae* filamentous-growth signalling pathway. *Nature*. 390:85–88. doi:10.1038/36355.

Craig, R., and R.C. Beavis. 2004. TANDEM: matching proteins with tandem mass spectra.

Bioinformatics. 20:1466–1467. doi:10.1093/bioinformatics/bth092.

Cristea, I.M., R. Williams, B.T. Chait, and M.P. Rout. 2005. Fluorescent proteins as proteomic probes. *Mol Cell Proteomics*. 4:1933–1941. doi:10.1074/mcp.M500227-MCP200.

Curtis, B.A., G. Tanifuji, F. Burki, A. Gruber, M. Irimia, S. Maruyama, M.C. Arias, S.G. Ball, G.H. Gile, Y. Hirakawa, J.F. Hopkins, A. Kuo, S.A. Rensing, J. Schmutz, A. Symeonidi, M. Elias, R.J.M. Eveleigh, E.K. Herman, M.J. Klute, T. Nakayama, M. Oborník, A. Reyes-Prieto, E.V. Armbrust, S.J. Aves, R.G. Beiko, P. Coutinho, J.B. Dacks, D.G. Durnford, N.M. Fast, B.R. Green, C.J. Grisdale, F. Hempel, B. Henrissat, M.P. Höppner, K.-I. Ishida, E. Kim, L. Kořený, P.G. Kroth, Y. Liu, S.-B. Malik, U.G. Maier, D. McRose, T. Mock, J.A.D. Neilson, N.T. Onodera, A.M. Poole, E.J. Pritham, T.A. Richards, G. Rocap, S.W. Roy, C. Sarai, S. Schaack, S. Shirato, C.H. Slamovits, D.F. Spencer, S. Suzuki, A.Z. Worden, S. Zauner, K. Barry, C. Bell, A.K. Bharti, J.A. Crow, J. Grimwood, R. Kramer, E. Lindquist, S. Lucas, A. Salamov, G.I. McFadden, C.E. Lane, P.J. Keeling, M.W. Gray, I.V. Grigoriev, and J.M. Archibald. 2012. Algal genomes reveal evolutionary mosaicism and the fate of nucleomorphs. *Nature*. doi:10.1038/nature11681.

Dacks, J.B., A.A. Peden, and M.C. Field. 2009. Evolution of specificity in the eukaryotic endomembrane system. *Int J Biochem Cell Biol*. 41:330–340. doi:10.1016/j.biocel.2008.08.041.

Dacks, J.B., and M.C. Field. 2007. Evolution of the eukaryotic membrane-trafficking system: origin, tempo and mode. *J Cell Sci*. 120:2977–2985. doi:10.1242/jcs.013250.

Dacks, J.B., and W.F. Doolittle. 2001. ScienceDirect - Cell : Reconstructing/Deconstructing the Earliest Eukaryotes : How Comparative Genomics Can Help. *Cell*. 107:419–425.

Dacks, J.B., P.P. Poon, and M.C. Field. 2008. Phylogeny of endocytic components yields insight into the process of nonendosymbiotic organelle evolution. *Proc Nat Acad Sci USA*. 105:588–593. doi:10.1073/pnas.0707318105.

de Craene, J.-O., J. Coleman, P. Estrada de Martin, M. Pypaert, S. Anderson, J.R. Yates, S. Ferro-Novick, and P. Novick. 2006. Rtn1p is involved in structuring the cortical endoplasmic reticulum. *Mol Biol Cell*. 17:3009–3020. doi:10.1091/mbc.E06-01-0080.

de Duve, C. 2007. The origin of eukaryotes: a reappraisal. *Nat Rev Genet*. 8:395–403. doi:10.1038/nrg2071.

de Duve, C., and P. Baudhuin. 1966. Peroxisomes (microbodies and related particles). *Physiol Rev*. 46:323–357.

de Duve, C., and R. WATTIAUX. 1966. Functions of lysosomes. *Ann Rev Phys*. 28:435–492. doi:10.1146/annurev.ph.28.030166.002251.

de Duve, C., H. Beaufay, P. Jacques, Y. Rahman-Li, O.Z. Sellinger, R. Wattiaux, and S. de Coninck. 1960. Intracellular localization of catalase and of some oxidases in rat liver. *Biochim Biophys Acta*. 40:186–187.

de Schutter, K., Y.-C. Lin, P. Tiels, A. van Hecke, S. Glinka, J. Weber-Lehmann, P. Rouzé, Y. van de Peer, and N. Callewaert. 2009. Genome sequence of the recombinant protein production host *Pichia pastoris*. *Nat Biotechnol*. 27:561–566. doi:10.1038/nbt.1544.

De Souza, C.P.C., and S.A. Osmani. 2007. Mitosis, Not Just Open or Closed. *Euk Cell.* 6:1521–1527. doi:10.1128/EC.00178-07.

de Souza, W., A. Lanfredi-Rangel, and L. Campanati. 2004. Contribution of microscopy to a better knowledge of the biology of *Giardia lamblia*. *Microsc Microanal.* 10:513–527. doi:10.1017/S1431927604040954.

Devos, D., S. Dokudovskaya, F. Alber, R. Williams, B.T. Chait, A. Sali, and M.P. Rout. 2004. Components of coated vesicles and nuclear pore complexes share a common molecular architecture. *PLoS Biol.* 2:e380. doi:10.1371/journal.pbio.0020380.

Diekmann, Y., E. Seixas, M. Gouw, F. Tavares-Cadete, M.C. Seabra, and J.B. Pereira-Leal. 2011. Thousands of rab GTPases for the cell biologist. *PLoS Comput Biol.* 7:e1002217. doi:10.1371/journal.pcbi.1002217.

Dietrich, F.S., S. Voegeli, S. Brachat, A. Lerch, K. Gates, S. Steiner, C. Mohr, R. Pöhlmann, P. Luedi, S. Choi, R.A. Wing, A. Flavier, T.D. Gaffney, and P. Philippsen. 2004. The *Ashbya gossypii* genome as a tool for mapping the ancient *Saccharomyces cerevisiae* genome. *Science.* 304:304–307. doi:10.1126/science.1095781.

Dilworth, D. J., Suprpto, A., Padovan, J. C., Chait, B. T., Wozniak, R. W., Rout, M. P., & Aitchison, J. D. (2001). Nup2p dynamically associates with the distal regions of the yeast nuclear pore complex. *J Cell Biol.*, 153(7), 1465–1478. doi:10.1083/jcb.153.7.1465.

Dilworth, D.J., R.A. Saleem, R.S. Rogers, H. Mirzaei, J. Boyle, and J.D. Aitchison. 2010. QTIPS: a novel method of unsupervised determination of isotopic amino acid distribution in SILAC experiments. *J. Am. Soc. Mass Spectrom.* 21:1417–1422. doi:10.1016/j.jasms.2010.04.002.

Distel, B., R. Erdmann, S.J. Gould, G. Blobel, D.I. Crane, J.M. Cregg, G. Dodt, Y. Fujiki, J.M. Goodman, W.W. Just, J.A. Kiel, W.H. Kunau, P.B. Lazarow, G.P. Mannaerts, H.W. Moser, T. Osumi, R.A. Rachubinski, A. Roscher, S. Subramani, H.F. Tabak, T. Tsukamoto, D. Valle, I. van der Klei, P.P. van Veldhoven, and M. Veenhuis. 1996. A unified nomenclature for peroxisome biogenesis factors. *J Cell Biol.* 135:1–3.

Dixit, E., S. Boulant, Y. Zhang, A.S.Y. Lee, C. Odendall, B. Shum, N. Hacohen, Z.J. Chen, S.P. Whelan, M. Fransen, M.L. Nibert, G. Superti-Furga, and J.C. Kagan. 2010. Peroxisomes are signaling platforms for antiviral innate immunity. *Cell.* 141:668–681. doi:10.1016/j.cell.2010.04.018.

Doolittle, W.F. 1998. You are what you eat: a gene transfer ratchet could account for bacterial genes in eukaryotic nuclear genomes. *Trends Genet.* 14:307–311.

Doolittle, W.F., and E. Baptiste. 2007. Pattern pluralism and the Tree of Life hypothesis. *Proc Natl Acad Sci USA.* 104:2043–2049. doi:10.1073/pnas.0610699104.

Dranchak, P.K., E. Di Pietro, A. Snowden, N. Oesch, N.E. Braverman, S.J. Steinberg, and J.G. Hacia. 2010. Nonsense suppressor therapies rescue peroxisome lipid metabolism and assembly in cells from patients with specific PEX gene mutations. *J Cell Biochem.* doi:10.1002/jcb.22979.

Dujon, B., D. Sherman, G. Fischer, P. Durrens, S. Casaregola, I. Lafontaine, J. de Montigny, C. Marck, C. Neuvéglise, E. Talla, N. Goffard, L. Frangeul, M. Aigle, V. Anthouard, A. Babour, V.

Barbe, S. Barnay, S. Blanchin, J.-M. Beckerich, E. Beyne, C. Bleykasten, A. Boisramé, J. Boyer, L. Cattolico, F. Confanioleri, A. de Daruvar, L. Despons, E. Fabre, C. Fairhead, H. Ferry-Dumazet, A. Groppi, F. Hantraye, C. Hennequin, N. Jauniaux, P. Joyet, R. Kachouri, A. Kerrest, R. Koszul, M. Lemaire, I. Lesur, L. Ma, H. Muller, J.-M. Nicaud, M. Nikolski, S. Oztas, O. Ozier-Kalogeropoulos, S. Pellenz, S. Potier, G.-F. Richard, M.-L. Straub, A. Suleau, D. Swennen, F. Tekaiia, M. Wésolowski-Louvel, E. Westhof, B. Wirth, M. Zeniou-Meyer, I. Zivanovic, M. Bolotin-Fukuhara, A. Thierry, C. Bouchier, B. Caudron, C. Scarpelli, C. Gaillardin, J. Weissenbach, P. Wincker, and J.-L. Souciet. 2004. Genome evolution in yeasts. *Nature*. 430:35–44. doi:10.1038/nature02579.

Eddy, S.R. 1998. Profile hidden Markov models. *Bioinformatics*. 14:755–763.

Eddy, S.R. 2008. A probabilistic model of local sequence alignment that simplifies statistical significance estimation. *PLoS Comput Biol*. 4:e1000069. doi:10.1371/journal.pcbi.1000069.

Eddy, S.R. 2009. A new generation of homology search tools based on probabilistic inference. *Genome Inform*. 23:205–211.

Edgar, R.C. 2004. MUSCLE: multiple sequence alignment with high accuracy and high throughput. *Nucleic Acids Res*. 32:1792–1797. doi:10.1093/nar/gkh340.

Eichinger, L., J.A. Pachebat, G. Glöckner, M.-A. Rajandream, R. Sucgang, M. Berriman, J. Song, R. Olsen, K. Szafranski, Q. Xu, B. Tunggal, S. Kummerfeld, M. Madera, B.A. Konfortov, F. Rivero, A.T. Bankier, R. Lehmann, N. Hamlin, R. Davies, P. Gaudet, P. Fey, K. Pilcher, G. Chen, D. Saunders, E. Sodergren, P. Davis, A. Kerhornou, X. Nie, N. Hall, C. Anjard, L. Hemphill, N. Bason, P. Farbrother, B. Desany, E. Just, T. Morio, R. Rost, C. Churcher, J. Cooper, S. Haydock, N. van Driessche, A. Cronin, I. Goodhead, D. Muzny, T. Mourier, A. Pain, M. Lu, D. Harper, R. Lindsay, H. Hauser, K. James, M. Quiles, M. Madan Babu, T. Saito, C. Buchrieser, A. Wardroper, M. Felder, M. Thangavelu, D. Johnson, A. Knights, H. Loulseged, K. Mungall, K. Oliver, C. Price, M.A. Quail, H. Urushihara, J. Hernandez, E. Rabbino-witsch, D. Steffen, M. Sanders, J. Ma, Y. Kohara, S. Sharp, M. Simmonds, S. Spiegler, A. Tivey, S. Sugano, B. White, D. Walker, J. Woodward, T. Winckler, Y. Tanaka, G. Shaulsky, M. Schleicher, G. Weinstock, A. Rosenthal, E.C. Cox, R.L. Chisholm, R. Gibbs, W.F. Loomis, M. Platzer, R.R. Kay, J. Williams, P.H. Dear, A.A. Noegel, B. Barrell, and A. Kuspa. 2005. The genome of the social amoeba *Dictyostelium discoideum*. *Nature*. 435:43–57. doi:10.1038/nature03481.

Eitzen, G.A. An Analysis of Peroxisome Assembly Mutants of the Yeast *Yarrowia lipolytica*. 1997. Ph.D. Thesis, University of Alberta, Alberta.

Eitzen, G.A., R.K. Szilard, and R.A. Rachubinski. 1997. Enlarged peroxisomes are present in oleic acid-grown *Yarrowia lipolytica* overexpressing the *PEX16* gene encoding an intraperoxisomal peripheral membrane peroxin. *J Cell Biol*. 137:1265–1278. doi:10.1083/jcb.137.6.1265.

Elgersma, Y., L. Kwast, M. van den Berg, W.B. Snyder, B. Distel, S. Subramani, and H.F. Tabak. 1997. Overexpression of Pex15p, a phosphorylated peroxisomal integral membrane protein required for peroxisome assembly in *S. cerevisiae*, causes proliferation of the endoplasmic reticulum membrane. *EMBO J*. 16:7326–7341. doi:10.1093/emboj/16.24.7326.

Elias, M., A. Brighouse, C.G. Castello, M.C. Field, and J.B. Dacks. 2012. Sculpting the endomembrane system in deep time: High resolution phylogenetics of Rab GTPases. *J Cell Sci*.

doi:10.1242/jcs.101378.

Erdmann, R., and G. Blobel. 1995. Giant peroxisomes in oleic acid-induced *Saccharomyces cerevisiae* lacking the peroxisomal membrane protein Pmp27p. *J Cell Biol.* 128:509–523.

Erdmann, R., M. Veenhuis, D. Mertens, and W.H. Kunau. 1989. Isolation of peroxisome-deficient mutants of *Saccharomyces cerevisiae*. *Proc Natl Acad Sci USA.* 86:5419–5423.

Estrada, P., J. Kim, J. Coleman, L. Walker, B. Dunn, P. Takizawa, P. Novick, and S. Ferro-Novick. 2003. Myo4p and She3p are required for cortical ER inheritance in *Saccharomyces cerevisiae*. *J Cell Biol.* 163:1255–1266. doi:10.1083/jcb.200304030.

Fagarasanu, A., and R.A. Rachubinski. 2007. Orchestrating organelle inheritance in *Saccharomyces cerevisiae*. *Curr Opin Microbiol.* 10:528–538. doi:10.1016/j.mib.2007.10.002.

Fagarasanu, A., F.D. Mast, B. Knoblach, and R.A. Rachubinski. 2010. Molecular mechanisms of organelle inheritance: lessons from peroxisomes in yeast. *Nat Rev Mol Cell Biol.* 11:644–654. doi:10.1038/nrm2960.

Fagarasanu, A., F.D. Mast, B. Knoblach, Y. Jin, M.J. Brunner, M.R. Logan, J.N.M. Glover, G.A. Eitzen, J.D. Aitchison, L.S. Weisman, and R.A. Rachubinski. 2009. Myosin-driven peroxisome partitioning in *S. cerevisiae*. *J Cell Biol.* 186:541–554. doi:10.1083/jcb.200904050.

Fagarasanu, A., M. Fagarasanu, and R.A. Rachubinski. 2007. Maintaining peroxisome populations: a story of division and inheritance. *Annu Rev Cell Dev Biol.* 23:321–344. doi:10.1146/annurev.cellbio.23.090506.123456.

Fagarasanu, A., M. Fagarasanu, G.A. Eitzen, J.D. Aitchison, and R.A. Rachubinski. 2006. The peroxisomal membrane protein Inp2p is the peroxisome-specific receptor for the myosin V motor Myo2p of *Saccharomyces cerevisiae*. *Dev Cell.* 10:587–600. doi:10.1016/j.devcel.2006.04.012.

Fagarasanu, M., A. Fagarasanu, Y.Y.C. Tam, J.D. Aitchison, and R.A. Rachubinski. 2005. Inp1p is a peroxisomal membrane protein required for peroxisome inheritance in *Saccharomyces cerevisiae*. *J Cell Biol.* 169:765–775. doi:10.1083/jcb.200503083.

Fang, Y., J.C. Morrell, J.M. Jones, and S.J. Gould. 2004. PEX3 functions as a PEX19 docking factor in the import of class I peroxisomal membrane proteins. *J Cell Biol.* 164:863–875. doi:10.1083/jcb.200311131.

Faulhammer, F., G. Konrad, B. Brankatschk, S. Tahirovic, A. Knödler, and P. Mayinger. 2005. Cell growth-dependent coordination of lipid signaling and glycosylation is mediated by interactions between Sac1p and Dpm1p. *J Cell Biol.* 168:185–191. doi:10.1083/jcb.200407118.

Faulhammer, F., S. Kanjilal-Kolar, A. Knödler, J. Lo, Y. Lee, G. Konrad, and P. Mayinger. 2007. Growth control of Golgi phosphoinositides by reciprocal localization of sac1 lipid phosphatase and pik1 4-kinase. *Traffic.* 8:1554–1567. doi:10.1111/j.1600-0854.2007.00632.x.

Ferdinandusse, S., S. Denis, P.L. Faust, and R.J.A. Wanders. 2009. Bile acids: the role of peroxisomes. *J Lipid Res.* 50:2139–2147. doi:10.1194/jlr.R900009-JLR200.

Field, M.C., A. Sali, and M.P. Rout. 2011. Evolution: On a bender--BARs, ESCRTs, COPs, and finally getting your coat. *J Cell Biol.* 193:963–972. doi:10.1083/jcb.201102042.

Field, M.C., and J.B. Dacks. 2009. First and last ancestors: reconstructing evolution of the endomembrane system with ESCRTs, vesicle coat proteins, and nuclear pore complexes. *Curr Opin Cell Biol.* 21:4–13. doi:10.1016/j.ceb.2008.12.004.

Finnigan, G.C., V. Hanson-Smith, B.D. Houser, H.J. Park, and T.H. Stevens. 2011. The reconstructed ancestral subunit a functions as both V-ATPase isoforms Vph1p and Stv1p in *Saccharomyces cerevisiae*. *Mol Biol Cell.* 22:3176–3191. doi:10.1091/mbc.E11-03-0244.

Fleckenstein, D., M. Rohde, D.J. Klionsky, and M. Rüdiger. 1998. Yel013p (Vac8p), an armadillo repeat protein related to plakoglobin and importin alpha is associated with the yeast vacuole membrane. *J Cell Sci.* 111 (Pt 20):3109–3118.

Foley, E., and P.H. O'Farrell. 2004. Functional dissection of an innate immune response by a genome-wide RNAi screen. *PLoS Biol.* 2:E203. doi:10.1371/journal.pbio.0020203.

Fraser, F., C.G. Corstorphine, N.T. Price, and V.A. Zammit. 1999. Evidence that carnitine palmitoyltransferase I (CPT I) is expressed in microsomes and peroxisomes of rat liver. Distinct immunoreactivity of the N-terminal domain of the microsomal protein. *FEBS Lett.* 446:69–74.

Freeman, M.R., and J. Doherty. 2006. Glial cell biology in *Drosophila* and vertebrates. *Trends Neurosci.* 29:82–90. doi:10.1016/j.tins.2005.12.002.

Freitag, J., J. Ast, and M. Böcker. 2012. Cryptic peroxisomal targeting via alternative splicing and stop codon read-through in fungi. *Nature.* 485:522–525. doi:10.1038/nature11051.

Fujiki, Y., and P.B. Lazarow. 1985. Post-translational import of fatty acyl-CoA oxidase and catalase into peroxisomes of rat liver in vitro. *J Biol Chem.* 260:5603–5609.

Fujiki, Y., R.A. Rachubinski, and P.B. Lazarow. 1984. Synthesis of a major integral membrane polypeptide of rat liver peroxisomes on free polysomes. *Proc Natl Acad Sci USA.* 81:7127–7131.

Fujiki, Y., R.A. Rachubinski, R.M. Mortensen, and P.B. Lazarow. 1985. Synthesis of 3-ketoacyl-CoA thiolase of rat liver peroxisomes on free polyribosomes as a larger precursor. Induction of thiolase mRNA activity by clofibrate. *Biochem J.* 226:697–704.

Fujiki, Y., S. Fowler, H. Shio, A.L. Hubbard, and P.B. Lazarow. 1982. Polypeptide and phospholipid composition of the membrane of rat liver peroxisomes: comparison with endoplasmic reticulum and mitochondrial membranes. *J Cell Biol.* 93:103–110.

Fujiki, Y., Y. Matsuzono, T. Matsuzaki, and M. Fransen. 2006. Import of peroxisomal membrane proteins: the interplay of Pex3p- and Pex19p-mediated interactions. *Biochim Biophys Acta.* 1763:1639–1646. doi:10.1016/j.bbamcr.2006.09.030.

Gabaldón, T. 2010. Peroxisome diversity and evolution. *Philos. Trans. R. Soc. Lond., B, Biol. Sci.* 365:765–773. doi:10.1098/rstb.2009.0240.

Gabaldón, T., and S. Capella-Gutiérrez. 2010. Lack of phylogenetic support for a supposed

actinobacterial origin of peroxisomes. *Gene*. 465:61–65. doi:10.1016/j.gene.2010.06.004.

Gabalón, T., B. Snel, F. van Zimmeren, W. Hemrika, H. Tabak, and M.A. Huynen. 2006. Origin and evolution of the peroxisomal proteome. *Biol. Direct.* 1:8. doi:10.1186/1745-6150-1-8.

Galagan, J.E., S.E. Calvo, C. Cuomo, L.-J. Ma, J.R. Wortman, S. Batzoglou, S.-I. Lee, M. Baştürkmen, C.C. Spevak, J. Clutterbuck, V. Kapitonov, J. Jurka, C. Scazzocchio, M. Farman, J. Butler, S. Purcell, S. Harris, G.H. Braus, O. Draht, S. Busch, C. D'Enfert, C. Bouchier, G.H. Goldman, D. Bell-Pedersen, S. Griffiths-Jones, J.H. Doonan, J. Yu, K. Vienken, A. Pain, M. Freitag, E.U. Selker, D.B. Archer, M.A. Peñalva, B.R. Oakley, M. Momany, T. Tanaka, T. Kumagai, K. Asai, M. Machida, W.C. Nierman, D.W. Denning, M. Caddick, M. Hynes, M. Paoletti, R. Fischer, B. Miller, P. Dyer, M.S. Sachs, S.A. Osmani, and B.W. Birren. 2005. Sequencing of *Aspergillus nidulans* and comparative analysis with *A. fumigatus* and *A. oryzae*. *Nature*. 438:1105–1115. doi:10.1038/nature04341.

Galagan, J.E., S.E. Calvo, K.A. Borkovich, E.U. Selker, N.D. Read, D. Jaffe, W. FitzHugh, L.-J. Ma, S. Smirnov, S. Purcell, B. Rehman, T. Elkins, R. Engels, S. Wang, C.B. Nielsen, J. Butler, M. Endrizzi, D. Qui, P. Ianakiev, D. Bell-Pedersen, M.A. Nelson, M. Werner-Washburne, C.P. Selitrennikoff, J.A. Kinsey, E.L. Braun, A. Zelter, U. Schulte, G.O. Kothe, G. Jedd, W. Mewes, C. Staben, E. Marcotte, D. Greenberg, A. Roy, K. Foley, J. Naylor, N. Stange-Thomann, R. Barrett, S. Gnerre, M. Kamal, M. Kamvysselis, E. Mauceli, C. Bielke, S. Rudd, D. Frishman, S. Krystofova, C. Rasmussen, R.L. Metzenberg, D.D. Perkins, S. Kroken, C. Cogoni, G. Macino, D. Catcheside, W. Li, R.J. Pratt, S.A. Osmani, C.P.C. DeSouza, L. Glass, M.J. Orbach, J.A. Berglund, R. Voelker, O. Yarden, M. Plamann, S. Seiler, J. Dunlap, A. Radford, R. Aramayo, D.O. Natvig, L.A. Alex, G. Mannhaupt, D.J. Ebbole, M. Freitag, I. Paulsen, M.S. Sachs, E.S. Lander, C. Nusbaum, and B. Birren. 2003. The genome sequence of the filamentous fungus *Neurospora crassa*. *Nature*. 422:859–868. doi:10.1038/nature01554.

Gari, E., L. Piedrafita, M. Aldea, and E. Herrero. 1997. A set of vectors with a tetracycline-regulatable promoter system for modulated gene expression in *Saccharomyces cerevisiae*. *Yeast*. 13:837–848. doi:10.1002/(SICI)1097-0061(199707)13:9<837::AID-YEA145>3.0.CO;2-T.

Geuze, H.J., J.L. Murk, A.K. Stroobants, J.M. Griffith, M.J. Kleijmeer, A.J. Koster, A.J. Verkleij, B. Distel, and H.F. Tabak. 2003. Involvement of the endoplasmic reticulum in peroxisome formation. *Mol Biol Cell*. 14:2900–2907. doi:10.1091/mbc.E02-11-0734.

Giaever, G., A.M. Chu, L. Ni, C. Connelly, L. Riles, S. Véronneau, S. Dow, A. Lucau-Danila, K. Anderson, B. André, A.P. Arkin, A. Astromoff, M. El-Bakkoury, R. Bangham, R. Benito, S. Brachat, S. Campanaro, M. Curtiss, K. Davis, A. Deutschbauer, K. Entian, P. Flaherty, F. Foury, D.J. Garfinkel, M. Gerstein, D. Gotte, U. Güldener, J.H. Hegemann, S. Hempel, Z. Herman, D.F. Jaramillo, D.E. Kelly, S.L. Kelly, P. Kötter, D. LaBonte, D.C. Lamb, N. Lan, H. Liang, H. Liao, L. Liu, C. Luo, M. Lussier, R. Mao, P. Menard, S.L. Ooi, J.L. Revuelta, C.J. Roberts, M. Rose, P. Ross-Macdonald, B. Scherens, G. Schimmack, B. Shafer, D.D. Shoemaker, S. Sookai-Mahadeo, R.K. Storms, J.N. Strathern, G. Valle, M. Voet, G. Volckaert, C. Wang, T.R. Ward, J. Wilhelmy, E.A. Winzeler, Y. Yang, G. Yen, E. Youngman, K. Yu, H. Bussey, J.D. Boeke, M. Snyder, P. Philippsen, R.W. Davis, and M. Johnston. (2002). Functional profiling of the *Saccharomyces cerevisiae* genome. *Nature*, 418:387–391. doi:10.1038/nature00935.

Gietz, R.D. and R.A. Woods. 2002. Transformation of yeast by lithium acetate/single-stranded carrier DNA/polyethylene glycol method. *Methods Enzymol.* 350:87–96.

- Girzalsky, W., D. Saffian, and R. Erdmann. 2010. Peroxisomal protein translocation. *Biochim Biophys Acta*. 1803:724–731. doi:10.1016/j.bbamcr.2010.01.002.
- Glassman, E., and H.K. Mitchell. 1959. Mutants of *Drosophila melanogaster* Deficient in Xanthine Dehydrogenase. *Genetics*. 44:153–162.
- Glover, J.R., D.W. Andrews, and R.A. Rachubinski. 1994. *Saccharomyces cerevisiae* peroxisomal thiolase is imported as a dimer. *Proc Natl Acad Sci USA*. 91:10541–10545.
- Goffeau, A., B.G. Barrell, H. Bussey, R.W. Davis, B. Dujon, H. Feldmann, F. Galibert, J.D. Hoheisel, C. Jacq, M. Johnston, E.J. Louis, H.W. Mewes, Y. Murakami, P. Philippsen, H. Tettelin, and S.G. Oliver. 1996. Life with 6000 genes. *Science*. 274:546, 563–7.
- Goldberg, A.A., S.D. Bourque, P. Kyryakov, T. Boukh-Viner, C. Gregg, A. Beach, M.T. Burstein, G. Machkalyan, V. Richard, S. Rampersad, and V.I. Titorenko. 2009. A novel function of lipid droplets in regulating longevity. *Biochem Soc Trans*. 37:1050–1055. doi:10.1042/BST0371050.
- Goldfischer, S., C.L. Moore, A.B. Johnson, A.J. Spiro, M.P. Valsamis, H.K. Wisniewski, R.H. Ritch, W.T. Norton, I. Rapin, and L.M. Gartner. 1973. Peroxisomal and mitochondrial defects in the cerebro-hepato-renal syndrome. *Science*. 182:62–64.
- Goldman, B.M., and G. Blobel. 1978. Biogenesis of peroxisomes: intracellular site of synthesis of catalase and uricase. *Proc Natl Acad Sci USA*. 75:5066–5070.
- Goto, S., S. Mano, C. Nakamori, and M. Nishimura. 2011. *Arabidopsis* ABERRANT PEROXISOME MORPHOLOGY9 Is a Peroxin That Recruits the PEX1-PEX6 Complex to Peroxisomes. *Plant Cell*. doi:10.1105/tpc.110.080770.
- Gould, S.B., R.F. Waller, and G.I. McFadden. 2008. Plastid evolution. *Annu Rev Plant Biol*. 59:491–517. doi:10.1146/annurev.arplant.59.032607.092915.
- Gould, S.G., G.A. Keller, and S. Subramani. 1987. Identification of a peroxisomal targeting signal at the carboxy terminus of firefly luciferase. *J Cell Biol*. 105:2923–2931.
- Gould, S.J., G.A. Keller, N. Hosken, J. Wilkinson, and S. Subramani. 1989. A conserved tripeptide sorts proteins to peroxisomes. *J Cell Biol*. 108:1657–1664.
- Govindan, B., R. Bowser, and P. Novick. 1995. The role of Myo2, a yeast class V myosin, in vesicular transport. *J Cell Biol*. 128:1055–1068.
- Götte, K., W. Girzalsky, M. Linkert, E. Baumgart, S. Kammerer, W.H. Kunau, and R. Erdmann. 1998. Pex19p, a farnesylated protein essential for peroxisome biogenesis. *Mol Cell Biol*. 18:616–628.
- Gray, M.W., and W.F. Doolittle. 1982. Has the endosymbiont hypothesis been proven? *Microbiol. Rev*. 46:1–42.
- Gribaldo, S., and P. Cammarano. 1998. The root of the universal tree of life inferred from anciently duplicated genes encoding components of the protein-targeting machinery. *J Mol Evol*. 47:508–516.

- Groesch, M.E., G. Rossi, S. Ferro-Novick. 1992. Reconstitution of endoplasmic reticulum to Golgi transport in yeast: in vitro assay to characterize secretory mutants and functional transport vesicles. *Meth Enzymol.* 219:137–152.
- Grosshans, B.L., D. Ortiz, and P. Novick. 2006. Rabs and their effectors: achieving specificity in membrane traffic. *Proc Natl Acad Sci USA.* 103:11821–11827. doi:10.1073/pnas.0601617103.
- Grunau, S., W. Schliebs, R. Linnepe, C. Neufeld, C. Cizmowski, B. Reinartz, H.E. Meyer, B. Warscheid, W. Girzalsky, and R. Erdmann. 2009. Peroxisomal targeting of PTS2 pre-import complexes in the yeast *Saccharomyces cerevisiae*. *Traffic.* 10:451–460. doi:10.1111/j.1600-0854.2009.00876.x.
- Guindon, S., and O. Gascuel. 2003. A simple, fast, and accurate algorithm to estimate large phylogenies by maximum likelihood. *Syst Biol.* 52:696–704.
- Guo, T., C. Gregg, T. Boukh-Viner, P. Kyryakov, A. Goldberg, S. Bourque, F. Banu, S. Haile, S. Milijevic, K.H.Y. San, J. Solomon, V. Wong, and V.I. Titorenko. 2007. A signal from inside the peroxisome initiates its division by promoting the remodeling of the peroxisomal membrane. *J Cell Biol.* 177:289–303. doi:10.1083/jcb.200609072.
- Guo, T., Y.Y. Kit, J.-M. Nicaud, M.-T. Le Dall, S.K. Sears, H. Vali, H. Chan, R.A. Rachubinski, and V.I. Titorenko. 2003. Peroxisome division in the yeast *Yarrowia lipolytica* is regulated by a signal from inside the peroxisome. *J Cell Biol.* 162:1255–1266. doi:10.1083/jcb.200305055.
- Gurvitz, A., and H. Rottensteiner. 2006. The biochemistry of oleate induction: transcriptional upregulation and peroxisome proliferation. *Biochim Biophys Acta.* 1763:1392–1402. doi:10.1016/j.bbamcr.2006.07.011.
- Hagemann, R. The reception of the Schimper-Mereschkowsky endosymbiont hypothesis on the origin of plastids—between 1883 and 1960—many negative, but a few relevant. 2007. *Managing Editor Volker Wissemann Justus-Liebig-*
- Halbach, A., R. Rucktäschel, H. Rottensteiner, and R. Erdmann. 2009. The N-domain of Pex22p can functionally replace the Pex3p N-domain in targeting and peroxisome formation. *J Biol Chem.* 284:3906–3916. doi:10.1074/jbc.M806950200.
- Halbach, A., S. Lorenzen, C. Landgraf, R. Volkmer-Engert, R. Erdmann, and H. Rottensteiner. 2005. Function of the *PEX19*-binding site of human adrenoleukodystrophy protein as targeting motif in man and yeast. PMP targeting is evolutionarily conserved. *J Biol Chem.* 280:21176–21182. doi:10.1074/jbc.M501750200.
- Hammond, A.T., and B.S. Glick. 2000. Raising the speed limits for 4D fluorescence microscopy. *Traffic.* 1:935–940.
- Han, D.K., J. Eng, H. Zhou, and R. Aebersold. 2001. Quantitative profiling of differentiation-induced microsomal proteins using isotope-coded affinity tags and mass spectrometry. *Nat Biotechnol.* 19:946–951. doi:10.1038/nbt1001-946.
- Harlow E., and D. Lane. 1988. Antibodies: a laboratory manual. Cold Spring Harbor Laboratory Press, Cold Spring Harbor, NY. 63–70.

Hartwell, L.H., J.J. Hopfield, S. Leibler, and A.W. Murray. 1999. From molecular to modular cell biology. *Nature*. 402:C47–52. doi:10.1038/35011540.

Hayashi, M., and M. Nishimura. 2006. *Arabidopsis thaliana*--a model organism to study plant peroxisomes. *Biochim Biophys Acta*. 1763:1382–1391. doi:10.1016/j.bbamcr.2006.08.014.

Heiland, I., and R. Erdmann. 2005. Biogenesis of peroxisomes. Topogenesis of the peroxisomal membrane and matrix proteins. *FEBS J.* 272:2362–2372. doi:10.1111/j.1742-4658.2005.04690.x.

Heinemann, P., and W.W. Just. 1992. Peroxisomal protein import. In vivo evidence for a novel translocation competent compartment. *FEBS Lett.* 300:179–182.

Herman, P.K. 2002. Stationary phase in yeast. *Curr Opin Microbiol.* 5:602–607. doi:10.1016/S1369-5274(02)00377-6.

Hermann, G.J., and J.M. Shaw. 1998. Mitochondrial dynamics in yeast. *Annu Rev Cell Dev Biol.* 14:265–303. doi:10.1146/annurev.cellbio.14.1.265.

Hermann, G.J., J.W. Thatcher, J.P. Mills, K.G. Hales, M.T. Fuller, J. Nunnari, and J.M. Shaw. 1998. Mitochondrial fusion in yeast requires the transmembrane GTPase Fzo1p. *J Cell Biol.* 143:359–373.

Herold, A., R. Truant, H. Wiegand, and B.R. Cullen. 1998. Determination of the functional domain organization of the importin alpha nuclear import factor. *J Cell Biol.* 143:309–318.

Hettema, E.H., and A.M. Motley. 2009. How peroxisomes multiply. *J Cell Sci.* 122:2331–2336. doi:10.1242/jcs.034363.

Hettema, E.H., W. Girzalsky, M. van den Berg, R. Erdmann, and B. Distel. 2000. *Saccharomyces cerevisiae* Pex3p and Pex19p are required for proper localization and stability of peroxisomal membrane proteins. *EMBO J.* 19:223–233. doi:10.1093/emboj/19.2.223.

Heuck, A., I. Fetka, D. Brewer, D. Hüls, M. Munson, R. Jansen, and D. Niessing. 2010. The structure of the Myo4p globular tail and its function in *ASH1* mRNA localization. *J Cell Biol.* 189:497.

Hirst, J., L.D. Barlow, G.C. Francisco, D.A. Sahlender, M.N.J. Seaman, J.B. Dacks, and M.S. Robinson. 2011. The fifth adaptor protein complex. *PLoS Biol.* 9:e1001170. doi:10.1371/journal.pbio.1001170.

Hoepfner, D., D. Schildknecht, I. Braakman, P. Philippsen, and H.F. Tabak. 2005. Contribution of the endoplasmic reticulum to peroxisome formation. *Cell.* 122:85–95. doi:10.1016/j.cell.2005.04.025.

Hoepfner, D., M. van den Berg, P. Philippsen, H.F. Tabak, and E.H. Hettema. 2001. A role for Vps1p, actin, and the Myo2p motor in peroxisome abundance and inheritance in *Saccharomyces cerevisiae*. *J Cell Biol.* 155:979–990. doi:10.1083/jcb.200107028.

Hotz, M., C. Leisner, D. Chen, C. Manatschal, T. Wegleiter, J. Ouellet, D. Lindstrom, D.E. Gottschling, J. Vogel, and Y. Barral. 2012. Spindle pole bodies exploit the mitotic exit network in metaphase to drive their age-dependent segregation. *Cell.* 148:958–972. doi:10.1016/j.cell.2012.01.041.

- Hsieh, E.J., M.R. Hoopmann, B. MacLean, and M.J. MacCoss. 2010. Comparison of database search strategies for high precursor mass accuracy MS/MS data. *J Proteome Res.* 9:1138–1143. doi:10.1021/pr900816a.
- Hu, J., Y. Shibata, C. Voss, T. Shemesh, Z. Li, M. Coughlin, M.M. Kozlov, T.A. Rapoport, and W.A. Prinz. 2008. Membrane proteins of the endoplasmic reticulum induce high-curvature tubules. *Science.* 319:1247–1250. doi:10.1126/science.1153634.
- Hu, J., Y. Shibata, P.-P. Zhu, C. Voss, N. Rismanchi, W.A. Prinz, T.A. Rapoport, and C. Blackstone. 2009. A class of dynamin-like GTPases involved in the generation of the tubular ER network. *Cell.* 138:549–561. doi:10.1016/j.cell.2009.05.025.
- Huang, D.W., B.T. Sherman, and R.A. Lempicki. 2009. Systematic and integrative analysis of large gene lists using DAVID bioinformatics resources. *Nat Protoc.* 4:44–57. doi:10.1038/nprot.2008.211.
- Huber, A., J. Koch, F. Kragler, C. Brocard, and A. Hartig. 2012. A subtle interplay between three Pex11 proteins shapes de novo formation and fission of peroxisomes. *Traffic.* 13:157–167. doi:10.1111/j.1600-0854.2011.01290.x.
- Huber, A.H., W.J. Nelson, and W.I. Weis. 1997. Three-dimensional structure of the armadillo repeat region of beta-catenin. *Cell.* 90:871–882.
- Hughes, T.R., M.J. Marton, A.R. Jones, C.J. Roberts, R. Stoughton, C.D. Armour, H.A. Bennett, E. Coffey, H. Dai, Y.D. He, M.J. Kidd, A.M. King, M.R. Meyer, D. Slade, P.Y. Lum, S.B. Stepaniants, D.D. Shoemaker, D. Gachotte, K. Chakraborty, J. Simon, M. Bard, and S.H. Friend. 2000. Functional discovery via a compendium of expression profiles. *Cell.* 102:109–126.
- Huh, W.-K., J.V. Falvo, L.C. Gerke, A.S. Carroll, R.W. Howson, J.S. Weissman, and E.K. O'Shea. 2003. Global analysis of protein localization in budding yeast. *Nature.* 425:686–691. doi:10.1038/nature02026.
- Huynh, T.V., R.A. Young, and R.W. Davis. 1985. DNA cloning: A Practical Approach. IRL Press, Oxford.
- Imanaka, T., Y. Shiina, T. Takano, T. Hashimoto, and T. Osumi. 1996. Insertion of the 70-kDa peroxisomal membrane protein into peroxisomal membranes in vivo and in vitro. *J Biol Chem.* 271:3706–3713.
- Innis, M.A., and D.H. Gelfand. 1990. Optimization of PCRs. In *PCR Protocols: A Guide to Methods and Applications*. M.A. Innis, D.H. Gelfand, J.J. Sninsky, and T.J. White, editors. Academic Press, San Diego, 3–12.
- International Chicken Genome Sequencing Consortium. 2004. Sequence and comparative analysis of the chicken genome provide unique perspectives on vertebrate evolution. *Nature.* 432:695–716. doi:10.1038/nature03154.
- Itoh, T., A. Toh-E, and Y. Matsui. 2004. Mmr1p is a mitochondrial factor for Myo2p-dependent inheritance of mitochondria in the budding yeast. *EMBO J.* 23:2520–2530. doi:10.1038/sj.emboj.7600271.

Iwabe, N., K. Kuma, M. Hasegawa, S. Osawa, and T. Miyata. 1989. Evolutionary relationship of archaeobacteria, eubacteria, and eukaryotes inferred from phylogenetic trees of duplicated genes. *Proc Natl Acad Sci USA*. 86:9355–9359.

James, T.Y., F. Kauff, C.L. Schoch, P.B. Matheny, V. Hofstetter, C.J. Cox, G. Celio, C. Gueidan, E. Fraker, J. Miadlikowska, H.T. Lumbsch, A. Rauhut, V. Reeb, A.E. Arnold, A. Amtoft, J.E. Stajich, K. Hosaka, G.-H. Sung, D. Johnson, B. O'Rourke, M. Crockett, M. Binder, J.M. Curtis, J.C. Slot, Z. Wang, A.W. Wilson, A. Schüssler, J.E. Longcore, K. O'Donnell, S. Mozley-Standridge, D. Porter, P.M. Letcher, M.J. Powell, J.W. Taylor, M.M. White, G.W. Griffith, D.R. Davies, R.A. Humber, J.B. Morton, J. Sugiyama, A.Y. Rossman, J.D. Rogers, D.H. Pfister, D. Hewitt, K. Hansen, S. Hambleton, R.A. Shoemaker, J. Kohlmeyer, B. Volkmann-Kohlmeyer, R.A. Spotts, M. Serdani, P.W. Crous, K.W. Hughes, K. Matsuura, E. Langer, G. Langer, W.A. Untereiner, R. Lücking, B. Büdel, D.M. Geiser, A. Aptroot, P. Diederich, I. Schmitt, M. Schultz, R. Yahr, D.S. Hibbett, F. Lutzoni, D.J. McLaughlin, J.W. Spatafora, and R. Vilgalys. 2006. Reconstructing the early evolution of Fungi using a six-gene phylogeny. *Nature*. 443:818–822. doi:10.1038/nature05110.

Janssen, G., S. Toppet, and G. Parmentier. 1982. Structure of the side chain of the C29 dicarboxylic bile acid occurring in infants with coprostanic acidemia. *J Lipid Res*. 23:456–465.

Javaux, E.J., A.H. Knoll, and M.R. Walter. 2001. Morphological and ecological complexity in early eukaryotic ecosystems. *Nature*. 412:66–69. doi:10.1038/35083562.

Jeffries, T.W., I.V. Grigoriev, J. Grimwood, J.M. Laplaza, A. Aerts, A. Salamov, J. Schmutz, E. Lindquist, P. Dehal, H. Shapiro, Y.-S. Jin, V. Passoth, and P.M. Richardson. 2007. Genome sequence of the lignocellulose-bioconverting and xylose-fermenting yeast *Pichia stipitis*. *Nat Biotechnol*. 25:319–326. doi:10.1038/nbt1290.

Johnston, G.C., J.R. Pringle, and L.H. Hartwell. 1977. Coordination of growth with cell division in the yeast *Saccharomyces cerevisiae*. *Exp Cell Res*. 105:79–98.

Jones, J.M., J.C. Morrell, and S.J. Gould. 2004a. *PEX19* is a predominantly cytosolic chaperone and import receptor for class I peroxisomal membrane proteins. *J Cell Biol*. 164:57–67. doi:10.1083/jcb.200304111.

Jones, T., N.A. Federspiel, H. Chibana, J. Dungan, S. Kalman, B.B. Magee, G. Newport, Y.R. Thorstenson, N. Agabian, P.T. Magee, R.W. Davis, and S. Scherer. 2004b. The diploid genome sequence of *Candida albicans*. *Proc Natl Acad Sci USA*. 101:7329–7334. doi:10.1073/pnas.0401648101.

Jung, S., M. Marelli, R. Rachubinski, D. Goodlett, and J. Aitchison. 2010. Dynamic changes in the subcellular distribution of Gpd1p in response to cell stress. *J Biol Chem*. 285: 6739–6749.

Kamiryo, T., M. Abe, K. Okazaki, S. Kato, and N. Shimamoto. 1982. Absence of DNA in peroxisomes of *Candida tropicalis*. *J Bacteriol*. 152:269–274.

Karnati, S., and E. Baumgart-Vogt. 2009. Peroxisomes in airway epithelia and future prospects of these organelles for pulmonary cell biology. *Histochem Cell Biol*. 131:447–454. doi:10.1007/s00418-009-0566-4.

Kassmann, C.M., C. Lappe-Siefke, M. Baes, B. Brügger, A. Mildner, H.B. Werner, O. Natt, T.

Michaelis, M. Prinz, J. Frahm, and K.-A. Nave. 2007. Axonal loss and neuroinflammation caused by peroxisome-deficient oligodendrocytes. *Nat Genet.* 39:969–976. doi:10.1038/ng2070.

Katinka, M.D., S. Duprat, E. Cornillot, G. Méténier, F. Thomarat, G. Prensier, V. Barbe, E. Peyretaillade, P. Brottier, P. Wincker, F. Delbac, H. el Alaoui, P. Peyret, W. Saurin, M. Gouy, J. Weissenbach, and C.P. Vivarès. 2001. Genome sequence and gene compaction of the eukaryote parasite *Encephalitozoon cuniculi*. *Nature.* 414:450–453. doi:10.1038/35106579.

Kämper, J., R. Kahmann, M. Bölker, L.-J. Ma, T. Brefort, B.J. Saville, F. Banuett, J.W. Kronstad, S.E. Gold, O. Müller, M.H. Perlin, H.A.B. Wösten, R. de Vries, J. Ruiz-Herrera, C.G. Reynaga-Peña, K. Snetselaar, M. McCann, J. Pérez-Martín, M. Feldbrügge, C.W. Basse, G. Steinberg, J.I. Ibeas, W. Holloman, P. Guzman, M. Farman, J.E. Stajich, R. Sentandreu, J.M. González-Prieto, J.C. Kennell, L. Molina, J. Schirawski, A. Mendoza-Mendoza, D. Greilinger, K. Münch, N. Rössel, M. Scherer, M. Vranes, O. Ladendorf, V. Vincon, U. Fuchs, B. Sandrock, S. Meng, E.C.H. Ho, M.J. Cahill, K.J. Boyce, J. Klose, S.J. Klosterman, H.J. Deelstra, L. Ortiz-Castellanos, W. Li, P. Sanchez-Alonso, P.H. Schreier, I. Häuser-Hahn, M. Vaupel, E. Koopmann, G. Friedrich, H. Voss, T. Schlüter, J. Margolis, D. Platt, C. Swimmer, A. Gnirke, F. Chen, V. Vysotskaia, G. Mannhaupt, U. Güldener, M. Münsterkötter, D. Haase, M. Oesterheld, H.-W. Mewes, E.W. Mauceli, D. DeCaprio, C.M. Wade, J. Butler, S. Young, D.B. Jaffe, S. Calvo, C. Nusbaum, J. Galagan, and B.W. Birren. 2006. Insights from the genome of the biotrophic fungal plant pathogen *Ustilago maydis*. *Nature.* 444:97–101. doi:10.1038/nature05248.

Keeling, P.J. 2010. The endosymbiotic origin, diversification and fate of plastids. *Philos. Trans. R. Soc. Lond., B, Biol. Sci.* 365:729–748. doi:10.1098/rstb.2009.0103.

Keeling, P.J., and J.D. Palmer. 2008. Horizontal gene transfer in eukaryotic evolution. *Nat Rev Genet.* 9:605–618. doi:10.1038/nrg2386.

Keeling, P.J., and J.M. Archibald. 2008. Organelle evolution: what's in a name? *Curr Biol.* 18:R345–7. doi:10.1016/j.cub.2008.02.065.

Keller, A., A.I. Nesvizhskii, E. Kolker, and R. Aebersold. 2002. Empirical statistical model to estimate the accuracy of peptide identifications made by MS/MS and database search. *Anal. Chem.* 74:5383–5392.

Keller, A., J. Eng, N. Zhang, X.-J. Li, and R. Aebersold. 2005. A uniform proteomics MS/MS analysis platform utilizing open XML file formats. *Mol Syst Biol.* 1:2005.0017. doi:10.1038/msb4100024.

Kiel, J.A.K.W., M. Veenhuis, and I.J. van der Klei. 2006. PEX genes in fungal genomes: common, rare or redundant. *Traffic.* 7:1291–1303. doi:10.1111/j.1600-0854.2006.00479.x.

Kim, P.K., R.T. Mullen, U. Schumann, and J. Lippincott-Schwartz. 2006. The origin and maintenance of mammalian peroxisomes involves a de novo *PEX16*-dependent pathway from the ER. *J Cell Biol.* 173:521–532. doi:10.1083/jcb.200601036.

King, N., M.J. Westbrook, S.L. Young, A. Kuo, M. Abedin, J. Chapman, S. Fairclough, U. Hellsten, Y. Isogai, I. Letunic, M. Marr, D. Pincus, N. Putnam, A. Rokas, K.J. Wright, R. Zuzow, W. Dirks, M. Good, D. Goodstein, D. Lemons, W. Li, J.B. Lyons, A. Morris, S. Nichols, D.J. Richter, A. Salamov, J.G.I. Sequencing, P. Bork, W.A. Lim, G. Manning, W.T. Miller, W. McGinnis, H. Shapiro, R. Tjian,

I.V. Grigoriev, and D. Rokhsar. 2008. The genome of the choanoflagellate *Monosiga brevicollis* and the origin of metazoans. *Nature*. 451:783–788. doi:10.1038/nature06617.

Klämbt, C., L. Glazer, and B.Z. Shilo. 1992. *breathless*, a *Drosophila* FGF receptor homolog, is essential for migration of tracheal and specific midline glial cells. *Genes Dev*.

Koch, A., M. Thiemann, M. Grabenbauer, Y. Yoon, M.A. McNiven, and M. Schrader. 2003. Dynamin-like protein I is involved in peroxisomal fission. *J Biol Chem*. 278:8597–8605. doi:10.1074/jbc.M211761200.

Koch, A., Y. Yoon, N.A. Bonekamp, M.A. McNiven, and M. Schrader. 2005. A role for FisI in both mitochondrial and peroxisomal fission in mammalian cells. *Mol Biol Cell*. 16:5077–5086. doi:10.1091/mbc.E05-02-0159.

Koch, J., K. Pranjic, A. Huber, A. Ellinger, A. Hartig, F. Kragler, and C. Brocard. 2010. *PEX11* family members are membrane elongation factors that coordinate peroxisome proliferation and maintenance. *J Cell Sci*. 123:3389–3400. doi:10.1242/jcs.064907.

Koonin, E.V. 2010. Preview. The incredible expanding ancestor of eukaryotes. *Cell*. 140:606–608. doi:10.1016/j.cell.2010.02.022.

Kornmann, B., E. Currie, S. Collins, M. Schuldiner, J. Nunnari, J. Weissman, and P. Walter. 2009. An ER-Mitochondria Tethering Complex Revealed by a Synthetic Biology Screen. *Science*. doi:10.1126/science.1175088.

Kovacs, W.J., J.E. Shackelford, K.N. Tape, M.J. Richards, P.L. Faust, S.J. Fliesler, and S.K. Krisans. 2004. Disturbed cholesterol homeostasis in a peroxisome-deficient *PEX2* knockout mouse model. *Mol Cell Biol*. 24:1–13.

Kovacs, W.J., K.N. Tape, J.E. Shackelford, T.M. Wikander, M.J. Richards, S.J. Fliesler, S.K. Krisans, and P.L. Faust. 2009. Peroxisome deficiency causes a complex phenotype because of hepatic SREBP/Insig dysregulation associated with endoplasmic reticulum stress. *J Biol Chem*. 284:7232–7245. doi:10.1074/jbc.M809064200.

Kragt, A., T. Voorn-Brouwer, M. van den Berg, and B. Distel. 2005. Endoplasmic reticulum-directed Pex3p routes to peroxisomes and restores peroxisome formation in a *Saccharomyces cerevisiae* pex3Delta strain. *J Biol Chem*. 280:34350–34357. doi:10.1074/jbc.M505432200.

Krogan, N.J., G. Cagney, H. Yu, G. Zhong, X. Guo, A. Ignatchenko, J. Li, S. Pu, N. Datta, A.P. Tikuisis, T. Punna, J.M. Peregrín-Alvarez, M. Shales, X. Zhang, M. Davey, M.D. Robinson, A. Paccarano, J.E. Bray, A. Sheung, B. Beattie, D.P. Richards, V. Canadien, A. Lalev, F. Mena, P. Wong, A. Starostine, M.M. Canete, J. Vlasblom, S. Wu, C. Orsi, S.R. Collins, S. Chandran, R. Haw, J.J. Rilstone, K. Gandi, N.J. Thompson, G. Musso, P. St Onge, S. Ghanny, M.H.Y. Lam, G. Butland, A.M. Altaf-Ul, S. Kanaya, A. Shilatifard, E. O'Shea, J.S. Weissman, C.J. Ingles, T.R. Hughes, J. Parkinson, M. Gerstein, S.J. Wodak, A. Emili, and J.F. Greenblatt. 2006. Global landscape of protein complexes in the yeast *Saccharomyces cerevisiae*. *Nature*, 440:637–643. doi:10.1038/nature04670

Kural, C., H. Kim, S. Syed, G. Goshima, V.I. Gelfand, and P.R. Selvin. 2005. Kinesin and dynein move a peroxisome in vivo: a tug-of-war or coordinated movement? *Science*. 308:1469–1472.

doi:10.1126/science.1108408.

Kuravi, K., S. Nagotu, A.M. Krikken, K. Sjollem, M. Deckers, R. Erdmann, M. Veenhuis, and I.J. van der Klei. 2006. Dynamin-related proteins Vps1p and Dnm1p control peroxisome abundance in *Saccharomyces cerevisiae*. *J Cell Sci.* 119:3994–4001. doi:10.1242/jcs.03166.

Lam, S.K., N. Yoda, and R. Schekman. 2010. A vesicle carrier that mediates peroxisome protein traffic from the endoplasmic reticulum. *Proc Nat Acad Sci USA.* 107:21523–21528. doi:10.1073/pnas.1013397107.

Lam, S.K., N. Yoda, and R. Schekman. 2011. A vesicle carrier that mediates peroxisome protein traffic from the endoplasmic reticulum. *Proc Nat Acad Sci USA.* 108:E51–2. doi:10.1073/pnas.1103526108.

Lambkin, G.R., and R.A. Rachubinski. 2001. *Yarrowia lipolytica* cells mutant for the peroxisomal peroxin Pex19p contain structures resembling wild-type peroxisomes. *Mol Biol Cell.* 12:3353–3364.

Lander, E.S., L.M. Linton, B. Birren, C. Nusbaum, M.C. Zody, J. Baldwin, K. Devon, K. Dewar, M. Doyle, W. FitzHugh, R. Funke, D. Gage, K. Harris, A. Heaford, J. Howland, L. Kann, J. Lehoczy, R. LeVine, P. McEwan, K. McKernan, J. Meldrim, J.P. Mesirov, C. Miranda, W. Morris, J. Naylor, C. Raymond, M. Rosetti, R. Santos, A. Sheridan, C. Sougnez, N. Stange-Thomann, N. Stojanovic, A. Subramanian, D. Wyman, J. Rogers, J. Sulston, R. Ainscough, S. Beck, D. Bentley, J. Burton, C. Clee, N. Carter, A. Coulson, R. Deadman, P. Deloukas, A. Dunham, I. Dunham, R. Durbin, L. French, D. Grafham, S. Gregory, T. Hubbard, S. Humphray, A. Hunt, M. Jones, C. Lloyd, A. McMurray, L. Matthews, S. Mercer, S. Milne, J.C. Mullikin, A. Mungall, R. Plumb, M. Ross, R. Shownkeen, S. Sims, R.H. Waterston, R.K. Wilson, L.W. Hillier, J.D. McPherson, M.A. Marra, E.R. Mardis, L.A. Fulton, A.T. Chinwalla, K.H. Pepin, W.R. Gish, S.L. Chisoe, M.C. Wendl, K.D. Delehaunty, T.L. Miner, A. Delehaunty, J.B. Kramer, L.L. Cook, R.S. Fulton, D.L. Johnson, P.J. Minx, S.W. Clifton, T. Hawkins, E. Branscomb, P. Predki, P. Richardson, S. Wenning, T. Slezak, N. Doggett, J.F. Cheng, A. Olsen, S. Lucas, C. Elkin, E. Uberbacher, et al. 2001. Initial sequencing and analysis of the human genome. *Nature.* 409:860–921. doi:10.1038/35057062.

Lay, D., B. L. Grosshans, H. Heid, K. Gorgas, and W.W. Just. 2005. Binding and functions of ADP-ribosylation factor on mammalian and yeast peroxisomes. *J Biol Chem.* 280:34489–34499. doi:10.1074/jbc.M503497200.

Lazarow, P.B. 2003. Peroxisome biogenesis: advances and conundrums. *Curr Opin Cell Biol.* 15:489–497.

Lazarow, P.B. 2006. The import receptor Pex7p and the PTS2 targeting sequence. *Biochim Biophys Acta.* 1763:1599–1604. doi:10.1016/j.bbamcr.2006.08.011.

Lazarow, P.B., and Y. Fujiki. 1985. Biogenesis of peroxisomes. *Annu Rev Cell Biol.* 1:489–530. doi:10.1146/annurev.cb.01.110185.002421.

Lek, A., F.J. Evesson, R.B. Sutton, K.N. North, and S.T. Cooper. 2012. Ferlins: regulators of vesicle fusion for auditory neurotransmission, receptor trafficking and membrane repair. *Traffic.* 13:185–194. doi:10.1111/j.1600-0854.2011.01267.x.

Lek, A., M. Lek, K.N. North, and S.T. Cooper. 2010. Phylogenetic analysis of ferlin genes reveals

ancient eukaryotic origins. *BMC Evol Biol.* 10:231. doi:10.1186/1471-2148-10-231.

Léon, S., L. Zhang, W.H. McDonald, J. Yates, J.M. Cregg, and S. Subramani. 2006. Dynamics of the peroxisomal import cycle of PpPex20p: ubiquitin-dependent localization and regulation. *J Cell Biol.* 172:67–78. doi:10.1083/jcb.200508096.

Li, Q., A. Lau, T.J. Morris, L. Guo, C.B. Fordyce, and E.F. Stanley. 2004. A syntaxin 1, Galpha(o), and N-type calcium channel complex at a presynaptic nerve terminal: analysis by quantitative immunocolocalization. *J Neurosci.* 24:4070–4081. doi:10.1523/JNEUROSCI.0346-04.2004.

Li, X., and S.J. Gould. 2002. *PEX11* promotes peroxisome division independently of peroxisome metabolism. *J Cell Biol.* 156:643–651. doi:10.1083/jcb.200112028.

Li, X., E. Baumgart, J.C. Morrell, G. Jimenez-Sanchez, D. Valle, and S.J. Gould. 2002. *PEX11* beta deficiency is lethal and impairs neuronal migration but does not abrogate peroxisome function. *Mol Cell Biol.* 22:4358–4365.

Lillie, S.H., and S.S. Brown. 1987. Artifactual immunofluorescent labelling in yeast, demonstrated by affinity purification of antibody. *Yeast.* 3:63–70. doi:10.1002/yea.320030202.

Lipatova, Z., A.A. Tokarev, Y. Jin, J. Mulholland, L.S. Weisman, and N. Segev. 2008. Direct interaction between a myosin V motor and the Rab GTPases Ypt31/32 is required for polarized secretion. *Mol Biol Cell.* 19:4177–4187. doi:10.1091/mbc.E08-02-0220.

Lister, D.L., J.M. Bateman, S. Purton, and C.J. Howe. 2003. DNA transfer from chloroplast to nucleus is much rarer in *Chlamydomonas* than in tobacco. *Gene.* 316:33–38.

Liti, G., D.M. Carter, A.M. Moses, J. Warringer, L. Parts, S.A. James, R.P. Davey, I.N. Roberts, A. Burt, V. Koufopanou, I.J. Tsai, C.M. Bergman, D. Bensasson, M.J.T. O'Kelly, A. van Oudenaarden, D.B.H. Barton, E. Bailes, A.N. Nguyen, M. Jones, M.A. Quail, I. Goodhead, S. Sims, F. Smith, A. Blomberg, R. Durbin, and E.J. Louis. 2009. Population genomics of domestic and wild yeasts. *Nature.* 458:337–341. doi:10.1038/nature07743.

Liu, F., S.K. Ng, Y. Lu, W. Low, J. Lai, and G. Jedd. 2008. Making two organelles from one: Woronin body biogenesis by peroxisomal protein sorting. *J Cell Biol.* 180:325–339. doi:10.1083/jcb.200705049.

Liu, Y., J.W. Leigh, H. Brinkmann, M.T. Cushion, N. Rodriguez-Ezpeleta, H. Philippe, and B.F. Lang. 2009. Phylogenomic analyses support the monophyly of Taphrinomycotina, including *Schizosaccharomyces* fission yeasts. *Mol Biol Evol.* 26:27–34. doi:10.1093/molbev/msn221.

Longabaugh, W.J.R. 2012. Combing the hairball with BioFabric: a new approach for visualization of large networks. *BMC bioinformatics*, 13:275. doi:10.1186/1471-2105-13-275

Longtine, M. S., A. McKenzie, D.J. Demarini, N.G. Shah, A. Wach, A. Brachat, P. Philippsen, and J.R. Pringle. 1998. Additional modules for versatile and economical PCR-based gene deletion and modification in *Saccharomyces cerevisiae*. *Yeast*, 14(10), 953–961. doi:10.1002/(SICI)1097-0061(199807)14:10<953::AID-YEA293>3.0.CO;2-U

Lowry, O.H., N.J. Rosebrough, A.L. Farr, and R.J. Randall. 1951. Protein measurement with the

Folin phenol reagent. *J Biol Chem.* 193:265–275.

Löytynoja, A., and N. Goldman. 2008. Phylogeny-aware gap placement prevents errors in sequence alignment and evolutionary analysis. *Science.* 320:1632–1635. doi:10.1126/science.1158395.

Lukes, J., J.M. Archibald, P.J. Keeling, W.F. Doolittle, and M.W. Gray. 2011. How a neutral evolutionary ratchet can build cellular complexity. *IUBMB Life.* 63:528–537. doi:10.1002/iub.489.

Ma, C., and S. Subramani. 2009. Peroxisome matrix and membrane protein biogenesis. *IUBMB Life.* 61:713–722. doi:10.1002/iub.196.

Ma, C., G. Agrawal, and S. Subramani. 2011. Peroxisome assembly: matrix and membrane protein biogenesis. *J Cell Biol.* 193:7–16. doi:10.1083/jcb.201010022.

Ma, L.-J., A.S. Ibrahim, C. Skory, M.G. Grabherr, G. Burger, M. Butler, M. Elias, A. Idnurm, B.F. Lang, T. Sone, A. Abe, S.E. Calvo, L.M. Corrochano, R. Engels, J. Fu, W. Hansberg, J.-M. Kim, C.D. Kodira, M.J. Koehrsen, B. Liu, D. Miranda-Saavedra, S. O'Leary, L. Ortiz-Castellanos, R. Poulter, J. Rodriguez-Romero, J. Ruiz-Herrera, Y.-Q. Shen, Q. Zeng, J. Galagan, B.W. Birren, C.A. Cuomo, and B.L. Wickes. 2009. Genomic analysis of the basal lineage fungus *Rhizopus oryzae* reveals a whole-genome duplication. *PLoS Genet.* 5:e1000549. doi:10.1371/journal.pgen.1000549.

MacLean, B., J.K. Eng, R.C. Beavis, and M. McIntosh. 2006. General framework for developing and evaluating database scoring algorithms using the TANDEM search engine. *Bioinformatics.* 22:2830–2832. doi:10.1093/bioinformatics/btl379.

Maitra, U., N. Singh, L. Gan, L. Ringwood, and L. Li. 2009. IRAK-1 contributes to lipopolysaccharide-induced reactive oxygen species generation in macrophages by inducing NOX-1 transcription and Rac1 activation and suppressing the expression of antioxidative enzymes. *J Biol Chem.* 284:35403–35411. doi:10.1074/jbc.M109.059501.

Manders, E.M., J. Stap, G.J. Brakenhoff, R. van Driel, and J.A. Aten. 1992. Dynamics of three-dimensional replication patterns during the S-phase, analysed by double labelling of DNA and confocal microscopy. *J Cell Sci.* 103 (Pt 3):857–862.

Manford, A.G., C.J. Stefan, H.L. Yuan, J.A. Macgurn, and S.D. Emr. 2012. ER-to-plasma membrane tethering proteins regulate cell signaling and ER morphology. *Dev Cell.* 23:1129–1140. doi:10.1016/j.devcel.2012.11.004.

Maniatis, T., E.F. Fritsch, and J. Sambrook. 1982. Molecular Cloning: A Laboratory Manual. Cold Spring Harbor Laboratory, Cold Spring Harbor.

Manjithaya, R. S. Jain, Farré, and S. Subramani. 2010. A yeast MAPK cascade regulates pexophagy but not other autophagy pathways. *J Cell Biol.* 189:303–310. doi:10.1083/jcb.200909154.

Manjithaya, R., C. Anjard, W.F. Loomis, and S. Subramani. 2010a. Unconventional secretion of *Pichia pastoris* Acb1 is dependent on GRASP protein, peroxisomal functions, and autophagosome formation. *J Cell Biol.* 188:537–546. doi:10.1083/jcb.200911149.

Manjithaya, R., T.Y. Nazarko, J.-C. Farré, and S. Subramani. 2010b. Molecular mechanism and

physiological role of pexophagy. *FEBS Lett.* 584:1367–1373. doi:10.1016/j.febslet.2010.01.019.

Marelli, M., J.J. Smith, S. Jung, E. Yi, A.I. Nesvizhskii, R.H. Christmas, R.A. Saleem, Y.Y.C. Tam, A. Fagarasanu, D.R. Goodlett, R. Aebersold, R.A. Rachubinski, and J.D. Aitchison. 2004. Quantitative mass spectrometry reveals a role for the GTPase Rho1p in actin organization on the peroxisome membrane. *J Cell Biol.* 167:1099–1112. doi:10.1083/jcb.200404119.

Marin, B., E.C.M. Nowack, and M. Melkonian. 2005. A plastid in the making: evidence for a second primary endosymbiosis. *Protist.* 156:425–432. doi:10.1016/j.protis.2005.09.001.

Marshall, P.A., J.M. Dyer, M.E. Quick, and J.M. Goodman. 1996. Redox-sensitive homodimerization of Pex11p: a proposed mechanism to regulate peroxisomal division. *J Cell Biol.* 135:123–137.

Martin, F., A. Aerts, D. Ahrén, A. Brun, E.G.J. Danchin, F. Duchaussoy, J. Gibon, A. Kohler, E. Lindquist, V. Pereda, A. Salamov, H.J. Shapiro, J. Wuyts, D. Blaudez, M. Buée, P. Brokstein, B. Canbäck, D. Cohen, P.E. Courty, P.M. Coutinho, C. Delaruelle, J.C. Detter, A. Deveau, S. DiFazio, S. Duplessis, L. Fraissinet-Tachet, E. Lucic, P. Frey-Klett, C. Fourrey, I. Feussner, G. Gay, J. Grimwood, P.J. Hoegger, P. Jain, S. Kilaru, J. Labbé, Y.C. Lin, V. Legué, F. Le Tacon, R. Marmeisse, D. Melayah, B. Montanini, M. Muratet, U. Nehls, H. Niculita-Hirzel, M.P. Oudot-Le Secq, M. Peter, H. Quesneville, B. Rajashekar, M. Reich, N. Rouhier, J. Schmutz, T. Yin, M. Chalot, B. Henrissat, U. Kües, S. Lucas, Y. van de Peer, G.K. Podila, A. Polle, P.J. Pukkila, P.M. Richardson, P. Rouzé, I.R. Sanders, J.E. Stajich, A. Tunlid, G. Tuskan, and I.V. Grigoriev. 2008. The genome of *Laccaria bicolor* provides insights into mycorrhizal symbiosis. *Nature.* 452:88–92. doi:10.1038/nature06556.

Martin, W., T. Rujan, E. Richly, A. Hansen, S. Cornelsen, T. Lins, D. Leister, B. Stoebe, M. Hasegawa, and D. Penny. 2002. Evolutionary analysis of *Arabidopsis*, cyanobacterial, and chloroplast genomes reveals plastid phylogeny and thousands of cyanobacterial genes in the nucleus. *Proc Natl Acad Sci USA.* 99:12246–12251. doi:10.1073/pnas.182432999.

Marzioch, M., R. Erdmann, M. Veenhuis, and W.H. Kunau. 1994. PAS7 encodes a novel yeast member of the WD-40 protein family essential for import of 3-oxoacyl-CoA thiolase, a PTS2-containing protein, into peroxisomes. *EMBO J.* 13:4908–4918.

Matsumoto, N., S. Tamura, and Y. Fujiki. 2003. The pathogenic peroxin Pex26p recruits the Pex1p-Pex6p AAA ATPase complexes to peroxisomes. *Nat Cell Biol.* 5:454–460. doi:10.1038/ncb982.

Matsuzaki, T., and Y. Fujiki. 2008. The peroxisomal membrane protein import receptor Pex3p is directly transported to peroxisomes by a novel Pex19p- and Pex16p-dependent pathway. *J Cell Biol.* 183:1275–1286. doi:10.1083/jcb.200806062.

Matsuzono, Y., N. Kinoshita, S. Tamura, N. Shimozawa, M. Hamasaki, K. Ghaedi, R.J. Wanders, Y. Suzuki, N. Kondo, and Y. Fujiki. 1999. Human *PEX19*: cDNA cloning by functional complementation, mutation analysis in a patient with Zellweger syndrome, and potential role in peroxisomal membrane assembly. *Proc Natl Acad Sci USA.* 96:2116–2121.

Meinecke, M. 2010. The peroxisomal importomer constitutes a large and highly dynamic pore. *Nat Cell Biol.* 12:273–277.

Menendez-Benito, V., S.J. van Deventer, V. Jimenez-Garcia, M. Roy-Luzarraga, F. van Leeuwen, and J. Neefjes. 2013. Spatiotemporal analysis of organelle and macromolecular complex inheritance. *Proc Nat Acad Sci USA*. 110:175–180. doi:10.1073/pnas.1207424110.

Michels, P.A.M., F. Bringaud, M. Herman, and V. Hannaert. 2006. Metabolic functions of glycosomes in trypanosomatids. *Biochim Biophys Acta*. 1763:1463–1477. doi:10.1016/j.bbamcr.2006.08.019.

Mnaimneh, S., A.P. Davierwala, J. Haynes, J. Moffat, W.-T. Peng, W. Zhang, X. Yang, J. Pootoolal, G. Chua, A. Lopez, M. Trocheset, D. Morse, N.J. Krogan, S.L. Hiley, Z. Li, Q. Morris, J. Grigull, N. Mitsakakis, C.J. Roberts, J.F. Greenblatt, C. Boone, C.A. Kaiser, B.J. Andrews, and T.R. Hughes. 2004. Exploration of essential gene functions via titratable promoter alleles. *Cell*. 118:31–44. doi:10.1016/j.cell.2004.06.013.

Moore, C.E., and J.M. Archibald. 2009. Nucleomorph genomes. *Annu. Rev. Genet.* 43:251–264. doi:10.1146/annurev-genet-102108-134809.

Moser, A.B., M. Rasmussen, S. Naidu, P.A. Watkins, M. McGuinness, A.K. Hajra, G. Chen, G. Raymond, A. Liu, and D. Gordon. 1995. Phenotype of patients with peroxisomal disorders subdivided into sixteen complementation groups. *J. Pediatr.* 127:13–22.

Motley, A.M., and E.H. Hettema. 2007. Yeast peroxisomes multiply by growth and division. *J Cell Biol.* 178:399–410. doi:10.1083/jcb.200702167.

Motley, A.M., G.P. Ward, and E.H. Hettema. 2008. Dnm1p-dependent peroxisome fission requires Caf4p, Mdv1p and Fis1p. *J Cell Sci.* 121:1633–1640. doi:10.1242/jcs.026344.

Motley, A.M., J.M. Nuttall, and E.H. Hettema. 2012. Atg36: the *Saccharomyces cerevisiae* receptor for pexophagy. *Autophagy*. 8:1680–1681. doi:10.4161/auto.21485.

Mouse Genome Sequencing Consortium, R.H. Waterston, K. Lindblad-Toh, E. Birney, J. Rogers, J.F. Abril, P. Agarwal, R. Agarwala, R. Ainscough, M. Alexandersson, P. An, S.E. Antonarakis, J. Attwood, R. Baertsch, J. Bailey, K. Barlow, S. Beck, E. Berry, B. Birren, T. Bloom, P. Bork, M. Botcherby, N. Bray, M.R. Brent, D.G. Brown, S.D. Brown, C. Bult, J. Burton, J. Butler, R.D. Campbell, P. Carninci, S. Cawley, F. Chiaromonte, A.T. Chinwalla, D.M. Church, M. Clamp, C. Clee, F.S. Collins, L.L. Cook, R.R. Copley, A. Coulson, O. Couronne, J. Cuff, V. Curwen, T. Cutts, M. Daly, R. David, J. Davies, K.D. Delehaunty, J. Deri, E.T. Dermitzakis, C. Dewey, N.J. Dickens, M. Diekhans, S. Dodge, I. Dubchak, D.M. Dunn, S.R. Eddy, L. Elnitski, R.D. Emes, P. Eswara, E. Eyra, A. Felsenfeld, G.A. Fewell, P. Flicek, K. Foley, W.N. Frankel, L.A. Fulton, R.S. Fulton, T.S. Furey, D. Gage, R.A. Gibbs, G. Glusman, S. Gnerre, N. Goldman, L. Goodstadt, D. Grafham, T.A. Graves, E.D. Green, S. Gregory, R. Guigó, M. Guyer, R.C. Hardison, D. Haussler, Y. Hayashizaki, L.W. Hillier, A. Hinrichs, W. Hlavina, T. Holzer, F. Hsu, A. Hua, T. Hubbard, A. Hunt, I. Jackson, D.B. Jaffe, L.S. Johnson, M. Jones, T.A. Jones, A. Joy, et al. 2002. Initial sequencing and comparative analysis of the mouse genome. *Nature*. 420:520–562. doi:10.1038/nature01262.

Müller, M., M. Mentel, J.J. van Hellemond, K. Henze, C. Woehle, S.B. Gould, R.-Y. Yu, M. van der Giezen, A.G.M. Tielens, and W.F. Martin. 2012. Biochemistry and evolution of anaerobic energy metabolism in eukaryotes. *Microbiol Mol Biol Rev.* 76:444–495. doi:10.1128/MMBR.05024-11.

Münchow, S., C. Sauter, and R.P. Jansen. 1999. Association of the class V myosin Myo4p with a

localised messenger RNA in budding yeast depends on She proteins. *J Cell Sci.* 112 (Pt 10):1511–1518.

Nagotu, S., R. Saraya, M. Otzen, M. Veenhuis, and I.J. van der Klei. 2008. Peroxisome proliferation in *Hansenula polymorpha* requires Dnm1p which mediates fission but not de novo formation. *Biochim Biophys Acta.* 1783:760–769. doi:10.1016/j.bbamcr.2007.10.018.

Neafsey, D.E., B.M. Barker, T.J. Sharpton, J.E. Stajich, D.J. Park, E. Whiston, C.-Y. Hung, C. McMahan, J. White, S. Sykes, D. Heiman, S. Young, Q. Zeng, A. Abouelleil, L. Aftuck, D. Bessette, A. Brown, M. FitzGerald, A. Lui, J.P. Macdonald, M. Priest, M.J. Orbach, J.N. Galgiani, T.N. Kirkland, G.T. Cole, B.W. Birren, M.R. Henn, J.W. Taylor, and S.D. Rounsley. 2010. Population genomic sequencing of *Coccidioides* fungi reveals recent hybridization and transposon control. *Genome Res.* 20:938–946. doi:10.1101/gr.103911.109.

Nenicu, A., G.H. Lüers, W. Kovacs, M. David, A. Zimmer, M. Bergmann, and E. Baumgart-Vogt. 2007. Peroxisomes in human and mouse testis: differential expression of peroxisomal proteins in germ cells and distinct somatic cell types of the testis. *Biol Reprod.* 77:1060–1072. doi:10.1095/biolreprod.107.061242.

Neuspiel, M., A.C. Schauss, E. Braschi, R. Zunino, P. Rippstein, R.A. Rachubinski, M.A. Andrade-Navarro, and H.M. McBride. 2008. Cargo-selected transport from the mitochondria to peroxisomes is mediated by vesicular carriers. *Curr Biol.* 18:102–108. doi:10.1016/j.cub.2007.12.038.

Ng, D.T., J.D. Brown, and P. Walter. 1996. Signal sequences specify the targeting route to the endoplasmic reticulum membrane. *J Cell Biol.* 134:269–278.

Novick, P., S. Ferro, and R. Schekman. 1981. Order of events in the yeast secretory pathway. *Cell.* 25:461–469.

Nuttall, J.M., A. Motley, and E.H. Hetttema. 2011. Peroxisome biogenesis: recent advances. *Curr Opin Cell Biol.* doi:10.1016/j.ceb.2011.05.005.

Oeffinger, M., K.E. Wei, R. Rogers, J.A. DeGrasse, B.T. Chait, J.D. Aitchison, and M.P. Rout. 2007. Comprehensive analysis of diverse ribonucleoprotein complexes. *Nat Methods.* 4:951–956. doi:10.1038/nmeth1101.

Oertle, T., M. Klinger, C.A.O. Stuermer, and M.E. Schwab. 2003. A reticular rhapsody: phylogenic evolution and nomenclature of the *RTN/Nogo* gene family. *FASEB J.* 17:1238–1247. doi:10.1096/fj.02-1166hyp.

Okamoto, N., and I. Inouye. 2005. A secondary symbiosis in progress? *Science.* 310:287. doi:10.1126/science.1116125.

Orellana, M., R. Rodrigo, and E. Valdés. 1998. Peroxisomal and microsomal fatty acid oxidation in liver of rats after chronic ethanol consumption. *Gen Pharmacol.* 31:817–820.

Orso, G., D. Pendin, S. Liu, J. Tassetto, T.J. Moss, J.E. Faust, M. Micaroni, A. Egorova, A. Martinuzzi, J.A. McNew, and A. Daga. 2009. Homotypic fusion of ER membranes requires the dynamin-like GTPase Atlastin. *Nature.* 460:978–983. doi:10.1038/nature08280.

Otzen, M., A.M. Krikken, P.Z. Ozimek, E. Kurbatova, S. Nagotu, M. Veenhuis, and I.J. van der Klei. 2006. In the yeast *Hansenula polymorpha*, peroxisome formation from the ER is independent of Pex19p, but involves the function of p24 proteins. *FEMS Yeast Res.* 6:1157–1166. doi:10.1111/j.1567-1364.2006.00102.x.

Palmer, J.D. 2003. The symbiotic birth and spread of plastids: how many times and whodunit? *Journal of Phycology.* 39:4–12.

Pan, X., and D.S. Goldfarb. 1998. YEB3/VAC8 encodes a myristylated armadillo protein of the *Saccharomyces cerevisiae* vacuolar membrane that functions in vacuole fusion and inheritance. *J Cell Sci.* 111 (Pt 15):2137–2147.

Park, H.-O., and E. Bi. 2007. Central roles of small GTPases in the development of cell polarity in yeast and beyond. *Microbiol Mol Biol Rev.* 71:48–96. doi:10.1128/MMBR.00028-06.

Parmentier, G.G., G.A. Janssen, E.A. Eggermont, and H.J. Eyssen. 1979. C27 bile acids in infants with coprostanic acidemia and occurrence of a 3 alpha,7 alpha,12 alpha-trihydroxy-5 beta-C29 dicarboxylic bile acid as a major component in their serum. *Eur J Biochem.* 102:173–183.

Pashkova, N., Y. Jin, S. Ramaswamy, and L.S. Weisman. 2006. Structural basis for myosin V discrimination between distinct cargoes. *EMBO J.* 25:693–700. doi:10.1038/sj.emboj.7600965.

Passreiter, M., M. Anton, D. Lay, R. Frank, C. Harter, F.T. Wieland, K. Gorgas, and W.W. Just. 1998. Peroxisome biogenesis: involvement of ARF and coatomer. *J Cell Biol.* 141:373–383.

Pawley, J.B. ed. 2006. Handbook Of Biological Confocal Microscopy. Third. Springer Science+Business Media, LLC, 233 Spring Street, New York, NY 10013, USA, Madison, Wisconsin. 1 pp.

Penny, D., and A. Poole. 1999. The nature of the last universal common ancestor. *Curr. Opin. Genet. Dev.* 9:672–677.

Pereira-Leal, J.B. 2008. The Ypt/Rab family and the evolution of trafficking in fungi. *Traffic.* 9:27–38. doi:10.1111/j.1600-0854.2007.00667.x.

Pereira-Leal, J.B., and M.C. Seabra. 2001. Evolution of the Rab family of small GTP-binding proteins. *J Mol Biol.* 313:889–901. doi:10.1006/jmbi.2001.5072.

Perry, R.J., F.D. Mast, and R.A. Rachubinski. 2009. Endoplasmic reticulum-associated secretory proteins Sec20p, Sec39p, and Dsl1p are involved in peroxisome biogenesis. *Eukaryotic Cell.* 8:830–843. doi:10.1128/EC.00024-09.

Peterson, G.L. 1977. A simplification of the protein assay method of Lowry et al. which is more generally applicable. *Anal Biochem.* 83:346–356.

Petriv, O.I., D.B. Pilgrim, R.A. Rachubinski, and V.I. Titorenko. 2002. RNA interference of peroxisome-related genes in *C. elegans*: a new model for human peroxisomal disorders. *Physiol Genomics.* 10:79–91. doi:10.1152/physiolgenomics.00044.2002.

Pinto, M.P., C.P. Grou, I.S. Alencastre, M.E. Oliveira, C. Sá-Miranda, M. Fransen, and J.E. Azevedo.

2006. The import competence of a peroxisomal membrane protein is determined by Pex19p before the docking step. *J Biol Chem.* 281:34492–34502. doi:10.1074/jbc.M607183200.

Platta, H.W., and R. Erdmann. 2007. Peroxisomal dynamics. *Trends Cell Biol.* 17:474–484. doi:10.1016/j.tcb.2007.06.009.

Platta, H.W., F. el Magraoui, D. Schlee, S. Grunau, W. Girzalsky, and R. Erdmann. 2007. Ubiquitination of the peroxisomal import receptor Pex5p is required for its recycling. *J Cell Biol.* 177:197–204. doi:10.1083/jcb.200611012.

Platta, H.W., S. Grunau, K. Rosenkranz, W. Girzalsky, and R. Erdmann. 2005. Functional role of the AAA peroxins in dislocation of the cycling PTS1 receptor back to the cytosol. *Nat Cell Biol.* 7:817–822. doi:10.1038/ncb1281.

Poirier, Y., V.D. Antonenkov, T. Glumoff, and J.K. Hiltunen. 2006. Peroxisomal beta-oxidation—a metabolic pathway with multiple functions. *Biochim Biophys Acta.* 1763:1413–1426. doi:10.1016/j.bbamcr.2006.08.034.

Powers, J.M., H.W. Moser, A.B. Moser, J.K. Upshur, B.F. Bradford, S.G. Pai, P.H. Kohn, J. Frias, and C. Tiffany. 1985. Fetal cerebrohepatorenal (Zellweger) syndrome: dysmorphic, radiologic, biochemical, and pathologic findings in four affected fetuses. *Hum. Pathol.* 16:610–620.

Pringle J.R., Adams, A.E., Drubin, D.G., and B.K. Haarer. 1991. Immunofluorescence methods for yeast. *Methods Enzymol.* 194:565–602.

Provance, D.W., T.L. James, and J.A. Mercer. 2002. Melanophilin, the product of the *leaden* locus, is required for targeting of myosin-Va to melanosomes. *Traffic.* 3:124–132.

Pruyne, D., A. Legesse-Miller, L. Gao, Y. Dong, and A. Bretscher. 2004. Mechanisms of polarized growth and organelle segregation in yeast. *Annu Rev Cell Dev Biol.* 20:559–591. doi:10.1146/annurev.cellbio.20.010403.103108.

Ptacek, J., G. Devgan, G. Michaud, H. Zhu, X. Zhu, J. Fasolo, H. Guo, G. Jona, A. Breitkreutz, R. Sopko, R.R. McCartney, M.C. Schmidt, N. Rachidi, S.-J. Lee, A.S. Mah, L. Meng, M.J.R. Stark, D.F. Stern, C. De Virgilio, M. Tyers, B. Andrews, M. Gerstein, B. Schweitzer, P.F. Predki, and M. Snyder. 2005. Global analysis of protein phosphorylation in yeast. *Nature.* 438:679–684. doi:10.1038/nature04187.

Putnam, N.H., M. Srivastava, U. Hellsten, B. Dirks, J. Chapman, A. Salamov, A. Terry, H. Shapiro, E. Lindquist, V.V. Kapitonov, J. Jurka, G. Genikhovich, I.V. Grigoriev, S.M. Lucas, R.E. Steele, J.R. Finnerty, U. Technau, M.Q. Martindale, and D.S. Rokhsar. 2007. Sea anemone genome reveals ancestral eumetazoan gene repertoire and genomic organization. *Science.* 317:86–94. doi:10.1126/science.1139158.

Putnam, N.H., T. Butts, D.E.K. Ferrier, R.F. Furlong, U. Hellsten, T. Kawashima, M. Robinson-Rechavi, E. Shoguchi, A. Terry, J.-K. Yu, E.L. Benito-Gutiérrez, I. Dubchak, J. Garcia-Fernández, J.J. Gibson-Brown, I.V. Grigoriev, A.C. Horton, P.J. de Jong, J. Jurka, V.V. Kapitonov, Y. Kohara, Y. Kuroki, E. Lindquist, S. Lucas, K. Osoegawa, L.A. Pennacchio, A.A. Salamov, Y. Satou, T. Sauka-Spengler, J. Schmutz, T. Shin-I, A. Toyoda, M. Bronner-Fraser, A. Fujiyama, L.Z. Holland, P.W.H. Holland, N. Satoh, and D.S. Rokhsar. 2008. The amphioxus genome and the evolution of the

chordate karyotype. *Nature*. 453:1064–1071. doi:10.1038/nature06967.

Rachubinski, R.A., and S. Subramani. 1995. How proteins penetrate peroxisomes. *Cell*. 83:525–528.

Rachubinski, R.A., Y. Fujiki, R.M. Mortensen, and P.B. Lazarow. 1984. Acyl-CoA oxidase and hydratase-dehydrogenase, two enzymes of the peroxisomal beta-oxidation system, are synthesized on free polysomes of clofibrate-treated rat liver. *J Cell Biol*. 99:2241–2246.

Ramadas, R., and M. Thattai. 2013. New organelles by gene duplication in a biophysical model of eukaryote endomembrane evolution. *Biophys J*. 104:2553–2563. doi:10.1016/j.bpj.2013.03.066.

Rapoport, T.A. 2007. Protein translocation across the eukaryotic endoplasmic reticulum and bacterial plasma membranes. *Nature*. 450:663–669. doi:10.1038/nature06384.

Raychaudhuri, S., and W.A. Prinz. 2008. Nonvesicular phospholipid transfer between peroxisomes and the endoplasmic reticulum. *Proc Nat Acad Sci USA*. 105:15785–15790. doi:10.1073/pnas.0808321105.

Raymond, F.L., and P. Tarpey. 2006. The genetics of mental retardation. *Hum Mol Genet*. 15 Spec No 2:R110–6. doi:10.1093/hmg/ddl189.

Rehling, P., M. Marzioch, F. Niesen, E. Wittke, M. Veenhuis, and W.H. Kunau. 1996. The import receptor for the peroxisomal targeting signal 2 (PTS2) in *Saccharomyces cerevisiae* is encoded by the *PAS7* gene. *EMBO J*. 15:2901–2913.

Reiter, L.T., L. Potocki, S. Chien, M. Gribskov, and E. Bier. 2001. A systematic analysis of human disease-associated gene sequences in *Drosophila melanogaster*. *Genome Res*. 11:1114–1125. doi:10.1101/gr.169101.

Reuber, B.E., E. Germain-Lee, C.S. Collins, J.C. Morrell, R. Ameritunga, H.W. Moser, D. Valle, and S.J. Gould. 1997. Mutations in *PEX1* are the most common cause of peroxisome biogenesis disorders. *Nat Genet*. 17:445–448. doi:10.1038/ng1297-445.

Richards, T.A., and T. Cavalier-Smith. 2005. Myosin domain evolution and the primary divergence of eukaryotes. *Nature*. 436:1113–1118. doi:10.1038/nature03949.

Richards, T.A., J.B. Dacks, J.M. Jenkinson, C.R. Thornton, and N.J. Talbot. 2006. Evolution of filamentous plant pathogens: gene exchange across eukaryotic kingdoms. *Curr Biol*. 16:1857–1864. doi:10.1016/j.cub.2006.07.052.

Roberg, K.J., N. Rowley, and C.A. Kaiser. 1997. Physiological regulation of membrane protein sorting late in the secretory pathway of *Saccharomyces cerevisiae*. *J Cell Biol*. 137:1469–1482.

Robinson, M.S. 2004. Adaptable adaptors for coated vesicles. *Trends Cell Biol*. 14:167–174. doi:10.1016/j.tcb.2004.02.002.

Roger, A. 1999. Reconstructing Early Events in Eukaryotic Evolution. *Am. Nat*. 154:S146–S163. doi:10.1086/303290.

- Ronquist, F., and J.P. Huelsenbeck. 2003. MrBayes 3: Bayesian phylogenetic inference under mixed models. *Bioinformatics*. 19:1572–1574.
- Rose, M.D., F. Winston, and P. Heiter. 1988. Laboratory Course Manual for Methods in Yeast Genetics. Cold Spring Harbor Laboratory, Cold Spring Harbor.
- Roscher, A.A., S. Hoefler, G. Hoefler, E. Paschke, F. Paltauf, A. Moser, and H. Moser. 1989. Genetic and phenotypic heterogeneity in disorders of peroxisome biogenesis--a complementation study involving cell lines from 19 patients. *Pediatr. Res.* 26:67–72.
- Rose, M.D., L.M. Misra, and J.P. Vogel. 1989. *KAR2*, a karyogamy gene, is the yeast homolog of the mammalian *BiP/GRP78* gene. *Cell*. 57:1211–1221. doi:10.1016/0092-8674(89)90058-5.
- Rossanese, O.W., C.A. Reinke, B.J. Bevis, A.T. Hammond, I.B. Sears, J. O'Connor, and B.S. Glick. 2001. A role for actin, Cdc1p, and Myo2p in the inheritance of late Golgi elements in *Saccharomyces cerevisiae*. *J Cell Biol.* 153:47–62.
- Rottensteiner, H., A. Kramer, S. Lorenzen, K. Stein, C. Landgraf, R. Volkmer-Engert, and R. Erdmann. 2004. Peroxisomal membrane proteins contain common Pex19p-binding sites that are an integral part of their targeting signals. *Mol Biol Cell*. 15:3406–3417. doi:10.1091/mbc.E04-03-0188.
- Rottensteiner, H., K. Stein, E. Sonnenhol, and R. Erdmann. 2003. Conserved function of Pex11p and the novel pex25p and pex27p in peroxisome biogenesis. *Mol Biol Cell*. 14:4316–4328. doi:10.1091/mbc.E03-03-0153.
- Rout, M.P., G. Blobel, and J.D. Aitchison. 1997. A distinct nuclear import pathway used by ribosomal proteins. *Cell*. 89:715–725.
- Sacksteder, K.A., J.C. Morrell, R.J. Wanders, R. Matalon, and S.J. Gould. 1999. *MCD* encodes peroxisomal and cytoplasmic forms of malonyl-CoA decarboxylase and is mutated in malonyl-CoA decarboxylase deficiency. *J Biol Chem*. 274:24461–24468.
- Sacksteder, K.A., J.M. Jones, S.T. South, X. Li, Y. Liu, and S.J. Gould. 2000. *PEX19* binds multiple peroxisomal membrane proteins, is predominantly cytoplasmic, and is required for peroxisome membrane synthesis. *J Cell Biol.* 148:931–944.
- Sagan, L. 1967. On the origin of mitosing cells. *J. Theor. Biol.* 14:255–274.
- Saiki, R.K. 1990. Amplification of genomic DNA. In *PCR Protocols: A guide to Methods and Applications*. M.A. Innis, D.H. Gelfand, J.J. Sninsky, and T.J. White, editors. Academic Press, San Diego. 13–21.
- Saleem, R.A., B. Knoblach, F.D. Mast, J.J. Smith, J. Boyle, C.M. Dobson, R. Long-O'Donnell, R.A. Rachubinski, and J.D. Aitchison. 2008. Genome-wide analysis of signaling networks regulating fatty acid-induced gene expression and organelle biogenesis. *J Cell Biol.* 181:281–292. doi:10.1083/jcb.200710009.
- Saleem, R.A., J.J. Smith, and J.D. Aitchison. 2006. Proteomics of the peroxisome. *Biochim Biophys Acta*. 1763:1541–1551. doi:10.1016/j.bbamcr.2006.09.005.

Sanger, F., S. Nicklen, and A.R. Coulson. 1977. DNA sequencing with chain-terminating inhibitors. *Proc Natl Acad Sci USA*. 74:5463–5467.

Santiago-Tirado, F.H., A. Legesse-Miller, D. Schott, and A. Bretscher. 2011. PI4P and Rab inputs collaborate in myosin-V-dependent transport of secretory compartments in yeast. *Dev Cell*. 20:47–59. doi:10.1016/j.devcel.2010.11.006.

Saraya, R., A.M. Krikken, M. Veenhuis, and I.J. van der Klei. 2011. Peroxisome reintroduction in *Hansenula polymorpha* requires Pex25 and Rho1. *J Cell Biol*. 193:885–900. doi:10.1083/jcb.201012083.

Sánchez-Martínez, A., N. Luo, P. Clemente, C. Adán, R. Hernández-Sierra, P. Ochoa, M.A. Fernández-Moreno, L.S. Kaguni, and R. Garesse. 2006. Modeling human mitochondrial diseases in flies. *Biochim Biophys Acta*. 1757:1190–1198. doi:10.1016/j.bbabi.2006.05.008.

Scannell, D.R., K.P. Byrne, J.L. Gordon, S. Wong, and K.H. Wolfe. 2006. Multiple rounds of speciation associated with reciprocal gene loss in polyploid yeasts. *Nature*. 440:341–345. doi:10.1038/nature04562.

Schäffer, A.A., L. Aravind, T.L. Madden, S. Shavirin, J.L. Spouge, Y.I. Wolf, E.V. Koonin, and S.F. Altschul. 2001. Improving the accuracy of PSI-BLAST protein database searches with composition-based statistics and other refinements. *Nucleic Acids Res*. 29:2994–3005.

Schekman, R. 2005. Peroxisomes: another branch of the secretory pathway? *Cell*. 122:1–2. doi:10.1016/j.cell.2005.06.033.

Schluter, A., S. Fourcade, R. Ripp, J.L. Mandel, O. Poch, and A. Pujol. 2006. The Evolutionary Origin of Peroxisomes: An ER-Peroxisome Connection. *Mol Biol Evol*. 23:838–845. doi:10.1093/molbev/msj103.

Schneper, L., K. Düvel, and J.R. Broach. 2004. Sense and sensibility: nutritional response and signal integration in yeast. *Curr Opin Microbiol*. 7:624–630. doi:10.1016/j.mib.2004.10.002.

Schopf, J.W. 1999. Deep divisions in the Tree of Life--what does the fossil record reveal? *Biol. Bull.* 196:351–3– discussion 354–5.

Schrader, M. 2006. Shared components of mitochondrial and peroxisomal division. *Biochim Biophys Acta*. 1763:531–541. doi:10.1016/j.bbamcr.2006.01.004.

Schrader, M., and H.D. Fahimi. 2006. Peroxisomes and oxidative stress. *Biochim Biophys Acta*. 1763:1755–1766. doi:10.1016/j.bbamcr.2006.09.006.

Schrader, M., and H.D. Fahimi. 2008. The peroxisome: still a mysterious organelle. *Histochem Cell Biol*. 129:421–440. doi:10.1007/s00418-008-0396-9.

Schrader, M., E. Baumgart, A. Völkl, and H.D. Fahimi. 1994. Heterogeneity of peroxisomes in human hepatoblastoma cell line HepG2. Evidence of distinct subpopulations. *Eur J Cell Biol*. 64:281–294.

Schuldiner, M., J. Metz, V. Schmid, V. Denic, M. Rakwalska, H.D. Schmitt, B. Schwappach, and J.S.

Weissman. 2008. The GET complex mediates insertion of tail-anchored proteins into the ER membrane. *Cell*. 134:634–645. doi:10.1016/j.cell.2008.06.025.

Schwartz, K., K. Richards, and D. Botstein. 1997. *BIM1* encodes a microtubule-binding protein in yeast. *Mol Biol Cell*. 8:2677–2691.

Sea Urchin Genome Sequencing Consortium, E. Sodergren, G.M. Weinstock, E.H. Davidson, R.A. Cameron, R.A. Gibbs, R.C. Angerer, L.M. Angerer, M.I. Arnone, D.R. Burgess, R.D. Burke, J.A. Coffman, M. Dean, M.R. Elphick, C.A. Ettensohn, K.R. Foltz, A. Hamdoun, R.O. Hynes, W.H. Klein, W. Marzluff, D.R. McClay, R.L. Morris, A. Mushegian, J.P. Rast, L.C. Smith, M.C. Thorndyke, V.D. Vacquier, G.M. Wessel, G. Wray, L. Zhang, C.G. Elsik, O. Ermolaeva, W. Hlavina, G. Hofmann, P. Kitts, M.J. Landrum, A.J. Mackey, D. Maglott, G. Panopoulou, A.J. Poustka, K. Pruitt, V. Sapojnikov, X. Song, A. Souvorov, V. Solovyev, Z. Wei, C.A. Whittaker, K. Worley, K.J. Durbin, Y. Shen, O. Fedrigo, D. Garfield, R. Haygood, A. Primus, R. Satija, T. Severson, M.L. Gonzalez-Garay, A.R. Jackson, A. Milosavljevic, M. Tong, C.E. Killian, B.T. Livingston, F.H. Wilt, N. Adams, R. Bellé, S. Carbonneau, R. Cheung, P. Cormier, B. Cosson, J. Croce, A. Fernandez-Guerra, A.-M. Genevière, M. Goel, H. Kelkar, J. Morales, O. Mulner-Lorillon, A.J. Robertson, J.V. Goldstone, B. Cole, D. Epel, B. Gold, M.E. Hahn, M. Howard-Ashby, M. Scally, J.J. Stegeman, E.L. Allgood, J. Cool, K.M. Judkins, S.S. McCafferty, A.M. Musante, R.A. Obar, A.P. Rawson, B.J. Rossetti, I.R. Gibbons, M.P. Hoffman, A. Leone, S. Istrail, S.C. Materna, M.P. Samanta, et al. 2006. The genome of the sea urchin *Strongylocentrotus purpuratus*. *Science*. 314:941–952. doi:10.1126/science.1133609.

Shaner, N. C., Campbell, R. E., Steinbach, P. A., Giepmans, B. N. G., Palmer, A. E., & Tsien, R. Y. (2004). Improved monomeric red, orange and yellow fluorescent proteins derived from *Discosoma* sp. red fluorescent protein. *Nature biotechnology*, 22(12), 1567–1572. doi:10.1038/nbt1037.

Shevchenko, A., H. Tomas, J. Havlis, J.V. Olsen, and M. Mann. 2006. In-gel digestion for mass spectrometric characterization of proteins and proteomes. *Nature protocols*, 1:2856–2860. doi:10.1038/nprot.2006.468.

Shimozawa, N. 2011. Molecular and clinical findings and diagnostic flowchart of peroxisomal diseases. *Brain Dev*. doi:10.1016/j.braindev.2011.03.004.

Shimozawa, N., T. Nagase, Y. Takemoto, M. Funato, N. Kondo, and Y. Suzuki. 2005. Molecular and neurologic findings of peroxisome biogenesis disorders. *J. Child Neurol*. 20:326–329.

Shimozawa, N., Y. Suzuki, Z. Zhang, A. Imamura, N. Kondo, N. Kinoshita, Y. Fujiki, T. Tsukamoto, T. Osumi, T. Imanaka, T. Orii, F. Beemer, P. Mooijer, C. Dekker, and R.J. Wanders. 1998. Genetic basis of peroxisome-assembly mutants of humans, Chinese hamster ovary cells, and yeast: identification of a new complementation group of peroxisome-biogenesis disorders apparently lacking peroxisomal-membrane ghosts. *Am J Hum Genet*. 63:1898–1903. doi:10.1086/302142.

Slot, J.C., and A. Rokas. 2011. Horizontal transfer of a large and highly toxic secondary metabolic gene cluster between fungi. *Curr Biol*. 21:134–139. doi:10.1016/j.cub.2010.12.020.

Smith, D.R., K. Crosby, and R.W. Lee. 2011. Correlation between nuclear plastid DNA abundance and plastid number supports the limited transfer window hypothesis. *Genome Biol Evol*. 3:365–371. doi:10.1093/gbe/evr001.

Smith, J.J., M. Marelli, R.H. Christmas, F.J. Vizeacoumar, D.J. Dilworth, T. Ideker, T. Galitski, K. Dimitrov, R.A. Rachubinski, and J.D. Aitchison. 2002. Transcriptome profiling to identify genes involved in peroxisome assembly and function. *J Cell Biol.* 158:259–271. doi:10.1083/jcb.200204059.

Smith, J.J., Y. Sydorsky, M. Marelli, D. Hwang, H. Bolouri, R.A. Rachubinski, and J.D. Aitchison. 2006. Expression and functional profiling reveal distinct gene classes involved in fatty acid metabolism. *Mol Syst Biol.* 2:–. doi:10.1038/msb4100051.

South, S.T., and S.J. Gould. 1999. Peroxisome synthesis in the absence of preexisting peroxisomes. *J Cell Biol.* 144:255–266.

South, S.T., E. Baumgart, and S.J. Gould. 2001. Inactivation of the endoplasmic reticulum protein translocation factor, Sec61p, or its homolog, Ssh1p, does not affect peroxisome biogenesis. *Proc Natl Acad Sci USA.* 98:12027–12031. doi:10.1073/pnas.221289498.

South, S.T., K.A. Sacksteder, X. Li, Y. Liu, and S.J. Gould. 2000. Inhibitors of COPI and COPII do not block PEX3-mediated peroxisome synthesis. *J Cell Biol.* 149:1345–1360.

Srivastava, M., E. Begovic, J. Chapman, N.H. Putnam, U. Hellsten, T. Kawashima, A. Kuo, T. Mitros, A. Salamov, M.L. Carpenter, A.Y. Signorovitch, M.A. Moreno, K. Kamm, J. Grimwood, J. Schmutz, H. Shapiro, I.V. Grigoriev, L.W. Buss, B. Schierwater, S.L. Dellaporta, and D.S. Rokhsar. 2008. The *Trichoplax* genome and the nature of placozoans. *Nature.* 454:955–960. doi:10.1038/nature07191.

Stajich, J.E., M.L. Berbee, M. Blackwell, D.S. Hibbett, T.Y. James, J.W. Spatafora, and J.W. Taylor. 2009. The fungi. *Curr Biol.* 19:R840–5. doi:10.1016/j.cub.2009.07.004.

Stajich, J.E., S.K. Wilke, D. Ahrén, C.H. Au, B.W. Birren, M. Borodovsky, C. Burns, B. Canbäck, L.A. Casselton, C.K. Cheng, J. Deng, F.S. Dietrich, D.C. Fargo, M.L. Farman, A.C. Gathman, J. Goldberg, R. Guigó, P.J. Hoegger, J.B. Hooker, A. Huggins, T.Y. James, T. Kamada, S. Kilaru, C. Kodira, U. Kües, D. Kupfer, H.S. Kwan, A. Lomsadze, W. Li, W.W. Lilly, L.-J. Ma, A.J. Mackey, G. Manning, F. Martin, H. Muraguchi, D.O. Natvig, H. Palmerini, M.A. Ramesh, C.J. Rehmer, B.A. Roe, N. Shenoy, M. Stanke, V. Ter-Hovhannisyan, A. Tunlid, R. Velagapudi, T.J. Vision, Q. Zeng, M.E. Zolan, and P.J. Pukkila. 2010. Insights into evolution of multicellular fungi from the assembled chromosomes of the mushroom *Coprinopsis cinerea* (*Coprinus cinereus*). *Proc Nat Acad Sci USA.* 107:11889–11894. doi:10.1073/pnas.1003391107.

Stamatakis, A. 2006. RAxML-VI-HPC: maximum likelihood-based phylogenetic analyses with thousands of taxa and mixed models. *Bioinformatics.* 22:2688–2690. doi:10.1093/bioinformatics/btl446.

Stefan, C.J., A.G. Manford, and S.D. Emr. 2013. ER-PM connections: sites of information transfer and inter-organelle communication. *Curr Opin Cell Biol.* doi:10.1016/j.ceb.2013.02.020.

Stefan, C.J., A.G. Manford, D. Baird, J. Yamada-Hanff, Y. Mao, and S.D. Emr. 2011. Osh proteins regulate phosphoinositide metabolism at ER-plasma membrane contact sites. *Cell.* 144:389–401. doi:10.1016/j.cell.2010.12.034.

Steinberg, S.J., G. Dodt, G.V. Raymond, N.E. Braverman, A.B. Moser, and H.W. Moser. 2006. Peroxisome biogenesis disorders. *Biochim Biophys Acta.* 1763:1733–1748.

doi:10.1016/j.bbamcr.2006.09.010.

Stirling, C.J., J. Rothblatt, M. Hosobuchi, R. Deshaies, and R. Schekman. 1992. Protein translocation mutants defective in the insertion of integral membrane proteins into the endoplasmic reticulum. *Mol Biol Cell*. 3:129–142.

Stoltzfus, A. 1999. On the possibility of constructive neutral evolution. *J Mol Evol*. 49:169–181.

Subramani, S. 1993. Protein import into peroxisomes and biogenesis of the organelle. *Annu Rev Cell Biol*. 9:445–478. doi:10.1146/annurev.cb.09.110193.002305.

Sucgang, R., A. Kuo, X. Tian, W. Salerno, A. Parikh, C.L. Feasley, E. Dalin, H. Tu, E. Huang, K. Barry, E. Lindquist, H. Shapiro, D. Bruce, J. Schmutz, A. Salamov, P. Fey, P. Gaudet, C. Anjard, M.M. Babu, S. Basu, Y. Bushmanova, H. van der Wel, M. Katoh-Kurasawa, C. Dinh, P.M. Coutinho, T. Saito, M. Elias, P. Schaap, R.R. Kay, B. Henrissat, L. Eichinger, F. Rivero, N.H. Putnam, C.M. West, W.F. Loomis, R.L. Chisholm, G. Shaulsky, J.E. Strassmann, D.C. Queller, A. Kuspa, and I.V. Grigoriev. 2011. Comparative genomics of the social amoebae *Dictyostelium discoideum* and *Dictyostelium purpureum*. *Genome Biol*. 12:R20. doi:10.1186/gb-2011-12-2-r20.

Swinkels, B.W., S.J. Gould, A.G. Bodnar, R.A. Rachubinski, and S. Subramani. 1991. A novel, cleavable peroxisomal targeting signal at the amino-terminus of the rat 3-ketoacyl-CoA thiolase. *EMBO J*. 10:3255–3262.

Szilard, R.K. 2000. Identification and Characterization of YIPex5p, a Component of the Peroxisomal Translocation Machinery of *Yarrowia lipolytica*. Ph.D. Thesis, University of Alberta, Alberta.

Tackett, A.J., D.J. Dilworth, M.J. Davey, M. O'Donnell, J.D. Aitchison, M.P. Rout, and B.T. Chait. 2005a. Proteomic and genomic characterization of chromatin complexes at a boundary. *J Cell Biol*. 169:35–47. doi:10.1083/jcb.200502104.

Tackett, A.J., J.A. DeGrasse, M.D. Sekedat, M. Oeffinger, M.P. Rout, and B.T. Chait. 2005b. I-DIRT, a general method for distinguishing between specific and nonspecific protein interactions. *J Proteome Res*. 4:1752–1756. doi:10.1021/pr050225e.

Tam, Y.Y.C., A. Fagarasanu, M. Fagarasanu, and R.A. Rachubinski. 2005. Pex3p initiates the formation of a preperoxisomal compartment from a subdomain of the endoplasmic reticulum in *Saccharomyces cerevisiae*. *J Biol Chem*. 280:34933–34939. doi:10.1074/jbc.M506208200.

Tam, Y.Y.C., J.C. Torres-Guzman, F.J. Vizeacoumar, J.J. Smith, M. Marelli, J.D. Aitchison, and R.A. Rachubinski. 2003. Pex11-related proteins in peroxisome dynamics: a role for the novel peroxin Pex27p in controlling peroxisome size and number in *Saccharomyces cerevisiae*. *Mol Biol Cell*. 14:4089–4102. doi:10.1091/mbc.E03-03-0150.

Tang, F., E.J. Kauffman, J.L. Novak, J.J. Nau, N.L. Catlett, and L.S. Weisman. 2003. Regulated degradation of a class V myosin receptor directs movement of the yeast vacuole. *Nature*. 422:87–92. doi:10.1038/nature01453.

Tatusov, R.L., E.V. Koonin, and D.J. Lipman. 1997. A genomic perspective on protein families. *Science*. 278:631–637.

- Terlecky, S.R., W.M. Nuttley, D. McCollum, E. Sock, and S. Subramani. 1995. The *Pichia pastoris* peroxisomal protein PAS8p is the receptor for the C-terminal tripeptide peroxisomal targeting signal. *EMBO J.* 14:3627–3634.
- Thompson, J.R., E. Register, J. Curotto, M. Kurtz, and R. Kelly. 1998. An improved protocol for the preparation of yeast cells for transformation by electroporation. *Yeast.* 14:565–571.
- Thoms, S., I. Harms, K.-U. Kalies, and J. Gärtner. 2012. Peroxisome formation requires the endoplasmic reticulum channel protein Sec61. *Traffic.* 13:599–609. doi:10.1111/j.1600-0854.2011.01324.x.
- Thoms, S., M.O. Debelyy, K. Nau, H.E. Meyer, and R. Erdmann. 2008. Lpx1p is a peroxisomal lipase required for normal peroxisome morphology. *FEBS J.* 275:504–514. doi:10.1111/j.1742-4658.2007.06217.x.
- Thurman, R.G., and W.R. McKenna. 1975. Pathways of ethanol metabolism in perfused rat liver. *Adv Exp Med Biol.* 56:57–76.
- Titorenko, V.I., and R.A. Rachubinski. 1998. Mutants of the yeast *Yarrowia lipolytica* defective in protein exit from the endoplasmic reticulum are also defective in peroxisome biogenesis. *Mol Cell Biol.* 18:2789–2803.
- Titorenko, V.I., and R.A. Rachubinski. 2009. Spatiotemporal dynamics of the ER-derived peroxisomal endomembrane system. *Int Rev Cell Mol Biol.* 272:191–244. doi:10.1016/S1937-6448(08)01605-5.
- Titorenko, V.I., D.M. Ogrydziak, and R.A. Rachubinski. 1997. Four distinct secretory pathways serve protein secretion, cell surface growth, and peroxisome biogenesis in the yeast *Yarrowia lipolytica*. *Mol Cell Biol.* 17:5210–5226.
- Titorenko, V.I., H. Chan, and R.A. Rachubinski. 2000. Fusion of small peroxisomal vesicles in vitro reconstructs an early step in the in vivo multistep peroxisome assembly pathway of *Yarrowia lipolytica*. *J Cell Biol.* 148:29–44.
- Towbin, H., T. Staehelin, and J. Gordon. 1979. Electrophoretic transfer of proteins from polyacrylamide gels to nitrocellulose sheets: procedure and some applications. *Proc Natl Acad Sci USA.* 76:4350–4354.
- Tower, R.J., A. Fagarasanu, J.D. Aitchison, and R.A. Rachubinski. 2011. The Peroxin Pex34p Functions with the Pex11 Family of Peroxisomal Divisional Proteins to Regulate the Peroxisome Population in Yeast. *Mol Biol Cell.* doi:10.1091/mbc.E11-01-0084.
- van Dam, T.J.P., M.J. Townsend, M. Turk, A. Schlessinger, A. Sali, M.C. Field, and M.A. Huynen. 2013. Evolution of modular intraflagellar transport from a coatomer-like progenitor. *Proc Nat Acad Sci.* 110:6943–6948. doi:10.1073/pnas.1221011110.
- van der Klei, I.J., and M. Veenhuis. 2006. PTS1-independent sorting of peroxisomal matrix proteins by Pex5p. *Biochim Biophys Acta.* 1763:1794–1800. doi:10.1016/j.bbamcr.2006.08.013.
- van der Zand, A., I. Braakman, and H.F. Tabak. 2010. Peroxisomal membrane proteins insert into

the endoplasmic reticulum. *Mol Biol Cell*. 21:2057–2065. doi:10.1091/mbc.E10-02-0082.

van der Zand, A., J. Gent, I. Braakman, and H.F. Tabak. 2012. Biochemically distinct vesicles from the endoplasmic reticulum fuse to form peroxisomes. *Cell*. 149:397–409. doi:10.1016/j.cell.2012.01.054.

van Roermund, C.W., H.F. Tabak, M. van den Berg, R.J. Wanders, and E.H. Hettema. 2000. Pex11p plays a primary role in medium-chain fatty acid oxidation, a process that affects peroxisome number and size in *Saccharomyces cerevisiae*. *J Cell Biol*. 150:489–498.

van Steensel, B., E.P. van Binnendijk, C.D. Hornsby, H.T. van der Voort, Z.S. Krozowski, E.R. de Kloet, and R. van Driel. 1996. Partial colocalization of glucocorticoid and mineralocorticoid receptors in discrete compartments in nuclei of rat hippocampus neurons. *J Cell Sci*. 109 (Pt 4):787–792.

van Veldhoven, P.P., G. Vanhove, S. Assselberghs, H.J. Eyssen, and G.P. Mannaerts. 1992. Substrate specificities of rat liver peroxisomal acyl-CoA oxidases: palmitoyl-CoA oxidase (inducible acyl-CoA oxidase), pristanoyl-CoA oxidase (non-inducible acyl-CoA oxidase), and trihydroxycoprostanoyl-CoA oxidase. *J Biol Chem*. 267:20065–20074.

Vastiau, I.M.K., E.A. Anthonio, M. Brams, C. Brees, S.G. Young, S. van de Velde, R.J.A. Wanders, G.P. Mannaerts, M. Baes, P.P. van Veldhoven, and M. Fransen. 2006. Farnesylation of Pex19p is not essential for peroxisome biogenesis in yeast and mammalian cells. *Cell Mol Life Sci*. 63:1686–1699. doi:10.1007/s00018-006-6110-y.

Veenhuis, M., M. Mateblowski, W.H. Kunau, and W. Harder. 1987. Proliferation of microbodies in *Saccharomyces cerevisiae*. *Yeast*. 3:77–84. doi:10.1002/yea.320030204.

Venter, J.C., M.D. Adams, E.W. Myers, P.W. Li, R.J. Mural, G.G. Sutton, H.O. Smith, M. Yandell, C.A. Evans, R.A. Holt, J.D. Gocayne, P. Amanatides, R.M. Ballew, D.H. Huson, J.R. Wortman, Q. Zhang, C.D. Kodira, X.H. Zheng, L. Chen, M. Skupski, G. Subramanian, P.D. Thomas, J. Zhang, G.L. Gabor Miklos, C. Nelson, S. Broder, A.G. Clark, J. Nadeau, V.A. McKusick, N. Zinder, A.J. Levine, R.J. Roberts, M. Simon, C. Slayman, M. Hunkapiller, R. Bolanos, A. Delcher, I. Dew, D. Fasulo, M. Flanagan, L. Florea, A. Halpern, S. Hannenhalli, S. Kravitz, S. Levy, C. Mobarry, K. Reinert, K. Remington, J. Abu-Threideh, E. Beasley, K. Biddick, V. Bonazzi, R. Brandon, M. Cargill, I. Chandramouliswaran, R. Charlab, K. Chaturvedi, Z. Deng, V. Di Francesco, P. Dunn, K. Eilbeck, C. Evangelista, A.E. Gabrielian, W. Gan, W. Ge, F. Gong, Z. Gu, P. Guan, T.J. Heiman, M.E. Higgins, R.R. Ji, Z. Ke, K.A. Ketchum, Z. Lai, Y. Lei, Z. Li, J. Li, Y. Liang, X. Lin, F. Lu, G.V. Merkulov, N. Milshina, H.M. Moore, A.K. Naik, V.A. Narayan, B. Neelam, D. Nusskern, D.B. Rusch, S. Salzberg, W. Shao, B. Shue, J. Sun, Z. Wang, A. Wang, X. Wang, J. Wang, M. Wei, R. Wides, C. Xiao, et al. 2001. The sequence of the human genome. *Science*. 291:1304–1351. doi:10.1126/science.1058040.

Vizeacoumar, F.J., J.C. Torres-Guzman, D. Bouard, J.D. Aitchison, and R.A. Rachubinski. 2004. Pex30p, Pex31p, and Pex32p form a family of peroxisomal integral membrane proteins regulating peroxisome size and number in *Saccharomyces cerevisiae*. *Mol Biol Cell*. 15:665–677. doi:10.1091/mbc.E03-09-0681.

Vizeacoumar, F.J., J.C. Torres-Guzman, Y.Y.C. Tam, J.D. Aitchison, and R.A. Rachubinski. 2003.

YHR150w and YDR479c encode peroxisomal integral membrane proteins involved in the regulation of peroxisome number, size, and distribution in *Saccharomyces cerevisiae*. *J Cell Biol.* 161:321–332. doi:10.1083/jcb.200210130.

Vizeacoumar, F.J., W.N. Vreden, M. Fagarasanu, G.A. Eitzen, J.D. Aitchison, and R.A. Rachubinski. 2006. The dynamin-like protein Vps1p of the yeast *Saccharomyces cerevisiae* associates with peroxisomes in a Pex19p-dependent manner. *J Biol Chem.* 281:12817–12823. doi:10.1074/jbc.M600365200.

Voeltz, G.K., W.A. Prinz, Y. Shibata, J.M. Rist, and T.A. Rapoport. 2006. A class of membrane proteins shaping the tubular endoplasmic reticulum. *Cell.* 124:573–586. doi:10.1016/j.cell.2005.11.047.

Voorn-Brouwer, T., A. Kragt, H.F. Tabak, and B. Distel. 2001. Peroxisomal membrane proteins are properly targeted to peroxisomes in the absence of COPI- and COPII-mediated vesicular transport. *J Cell Sci.* 114:2199–2204.

Walker, G., R.G. Dorrell, A. Schlacht, and J.B. Dacks. 2011. Eukaryotic systematics: a user's guide for cell biologists and parasitologists. *Parasitology.* 1–26. doi:10.1017/S0031182010001708.

Wanders, B.J., S.W. Denis, and G. Dacremont. 1993. Studies on the substrate specificity of the inducible and non-inducible acyl-CoA oxidases from rat kidney peroxisomes. *J Biochem.* 113:577–582.

Wanders, R.J.A., and H.R. Waterham. 2006. Biochemistry of mammalian peroxisomes revisited. *Annu Rev Biochem.* 75:295–332. doi:10.1146/annurev.biochem.74.082803.133329.

Wanders, R.J.A., S. Ferdinandusse, P. Brites, and S. Kemp. 2010. Peroxisomes, lipid metabolism and lipotoxicity. *Biochim Biophys Acta.* 1801:272–280. doi:10.1016/j.bbalip.2010.01.001.

Wang, Y.X., N.L. Catlett, and L.S. Weisman. 1998. Vac8p, a vacuolar protein with armadillo repeats, functions in both vacuole inheritance and protein targeting from the cytoplasm to vacuole. *J Cell Biol.* 140:1063–1074.

Waterham, H.R., J. Koster, C.W.T. van Roermund, P.A.W. Mooyer, R.J.A. Wanders, and J.V. Leonard. 2007. A lethal defect of mitochondrial and peroxisomal fission. *N Engl J Med.* 356:1736–1741. doi:10.1056/NEJMoa064436.

Weisman, L.S. 2006. Organelles on the move: insights from yeast vacuole inheritance. *Nat Rev Mol Cell Biol.* 7:243–252. doi:10.1038/nrm1892.

Wickstead, B., K. Gull, and T.A. Richards. 2010. Patterns of kinesin evolution reveal a complex ancestral eukaryote with a multifunctional cytoskeleton. *BMC Evol Biol.* 10:110. doi:10.1186/1471-2148-10-110.

Wiese, S., T. Gronemeyer, R. Ofman, M. Kunze, C.P. Grou, J.A. Almeida, M. Eisenacher, C. Stephan, H. Hayen, L. Schollenberger, T. Korosec, H.R. Waterham, W. Schliebs, R. Erdmann, J. Berger, H.E. Meyer, W. Just, J.E. Azevedo, R.J.A. Wanders, and B. Warscheid. 2007. Proteomics characterization of mouse kidney peroxisomes by tandem mass spectrometry and protein correlation profiling. *Mol Cell Proteomics.* 6:2045–2057. doi:10.1074/mcp.M700169-MCP200.

Wilcke, M., K. Hultenby, and S.E. Alexson. 1995. Novel peroxisomal populations in subcellular fractions from rat liver. Implications for peroxisome structure and biogenesis. *J Biol Chem.* 270:6949–6958.

Wishart, J.A., A. Hayes, L. Wardleworth, N. Zhang, and S.G. Oliver. 2005. Doxycycline, the drug used to control the tet-regulatable promoter system, has no effect on global gene expression in *Saccharomyces cerevisiae*. *Yeast.* 22:565–569. doi:10.1002/yea.1225.

Wood, V., R. Gwilliam, M.-A. Rajandream, M. Lyne, R. Lyne, A. Stewart, J. Sgouros, N. Peat, J. Hayles, S. Baker, D. Basham, S. Bowman, K. Brooks, D. Brown, S. Brown, T. Chillingworth, C. Churcher, M. Collins, R. Connor, A. Cronin, P. Davis, T. Feltwell, A. Fraser, S. Gentles, A. Goble, N. Hamlin, D. Harris, J. Hidalgo, G. Hodgson, S. Holroyd, T. Hornsby, S. Howarth, E.J. Huckle, S. Hunt, K. Jagels, K. James, L. Jones, M. Jones, S. Leather, S. McDonald, J. McLean, P. Mooney, S. Moule, K. Mungall, L. Murphy, D. Niblett, C. Odell, K. Oliver, S. O'Neil, D. Pearson, M.A. Quail, E. Rabinowitsch, K. Rutherford, S. Rutter, D. Saunders, K. Seeger, S. Sharp, J. Skelton, M. Simmonds, R. Squares, S. Squares, K. Stevens, K. Taylor, R.G. Taylor, A. Tivey, S. Walsh, T. Warren, S. Whitehead, J. Woodward, G. Volckaert, R. Aert, J. Robben, B. Grymonprez, I. Weltjens, E. Vanstreels, M. Rieger, M. Schäfer, S. Müller-Auer, C. Gabel, M. Fuchs, A. Düsterhöft, C. Fritz, E. Holzer, D. Moestl, H. Hilbert, K. Borzym, I. Langer, A. Beck, H. Lehrach, R. Reinhardt, T.M. Pohl, P. Eger, W. Zimmermann, H. Wedler, R. Wambutt, B. Purnelle, A. Goffeau, E. Cadieu, S. Dréano, et al. 2002. The genome sequence of *Schizosaccharomyces pombe*. *Nature.* 415:871–880. doi:10.1038/nature724.

Yan, M., D.A. Rachubinski, S. Joshi, R.A. Rachubinski, and S. Subramani. 2008. Dysferlin domain-containing proteins, Pex30p and Pex31p, localized to two compartments, control the number and size of oleate-induced peroxisomes in *Pichia pastoris*. *Mol Biol Cell.* 19:885–898. doi:10.1091/mbc.E07-10-1042.

Yang, X., P.E. Purdue, and P.B. Lazarow. 2001. Eci1p uses a PTS1 to enter peroxisomes: either its own or that of a partner, Dci1p. *Eur J Cell Biol.* 80:126–138.

Yin, H., D. Pruyne, T.C. Huffaker, and A. Bretscher. 2000. Myosin V orientates the mitotic spindle in yeast. *Nature.* 406:1013–1015. doi:10.1038/35023024.

Zhang, J.W., and P.B. Lazarow. 1996. Peb1p (Pas7p) is an intraperoxisomal receptor for the NH₂-terminal, type 2, peroxisomal targeting sequence of thiolase: Peb1p itself is targeted to peroxisomes by an NH₂-terminal peptide. *J Cell Biol.* 132:325–334.

Zhang, R., L. Chen, S. Jiralerspong, A. Snowden, S. Steinberg, and N. Braverman. 2010. Recovery of PEX1-Gly843Asp peroxisome dysfunction by small-molecule compounds. *Proc Nat Acad Sci USA.* 107:5569–5574. doi:10.1073/pnas.0914960107.

Zmijewski, J.W., E. Lorne, X. Zhao, Y. Tsuruta, Y. Sha, G. Liu, and E. Abraham. 2009. Antiinflammatory effects of hydrogen peroxide in neutrophil activation and acute lung injury. *Am J Respir Crit Care Med.* 179:694–704. doi:10.1164/rccm.200806-851OC.